Doctoral Dissertation
Doctoral Program in Energy Engineering (35th Cycle)

Refined zigzag models for the response of general multilayered composite and sandwich structures: numerical and experimental investigations

Matteo Sorrenti

******

Supervisor
Prof. Marco Gherlone

Doctoral Examination Committee:
Prof. Mehmet Dorduncu, Referee, Erciyes University
Prof. Vescovini Lorenzo, Referee, Politecnico di Milano

Politecnico di Torino
July, 2023

Declaration

I hereby declare that the contents and organization of this dissertation constitute my own original work and do not compromise in any way the rights of third parties, including those relating to the security of personal data.

Matteo Sorrenti

Turin, July, 2023

* This dissertation is presented in partial fulfillment of the requirements for **Ph.D. degree** in the Graduate School of Politecnico di Torino (ScuDo).

"La ciencia siempre vale la
pena porque sus descubrimientos,
tarde o temprano, siempre se aplican"
(Severo Ochoa de Albornoz)

Acknowledgements

Firstly, I would like to express my sincere and best acknowledgements and gratitude to my supervisors, Prof. Marco Gherlone and Prof. Di Sciuva, who supervised my research activity at different moments during my PhD. Thanks to their guidance, experience and knowledge, they encouraged me to face the research activity's difficulties and joys during these years. I am grateful that I had the opportunity to have both of them and at the same time to grow as a researcher and as a person.

Secondly, I would like to thank Prof. Xavier Martinez for hosting me at his research group at the Centre Internacional de Mètodes Numèrics a l'Enginyeria (CIMNE), Barcelona and all his research group, Fermin, Alex, Francesc, Raul, Irene, Montserrat, Jose, Pablo and Miquel. A special thanks go to all of them for welcoming me warmly and having had the opportunity to broaden my horizons with an experience that changed me and made me grow, especially in the Spanish language.

I am also grateful to the cooperation with the Department of Science and Aerospace Technology of Politecnico di Milano, in particular Prof. Bettini and Dr. Rigamonti to improve my knowledge in sandwich beam manufacturing.

I would like to thank my colleagues here in Politecnico di Torino, Ing. Mattone, Dr. Esposito, Giulia and Filippo, who gave me a hand with the experimental part of my research activity and their advice and suggestions.

A very special thanks go to my partner, Davide, who has supported and encouraged me every day during these months while I was writing this Thesis. I want to dedicate to him this special acknowledgement for the courage he showed in being close to me, even in the most difficult moments.

Finally, a thanks go to my family. To my mum Cristina, my father Francesco and my brother Davide who, over the years, have always been able to encourage and support me in every choice I have made.

Lastly, I would like to thank all my friends for their support during these years.

Contents

List of Figures

List of Tables

Summary

In recent decades, multilayered composites and sandwich structures have been widely used in various engineering fields (aerospace, automotive, naval, defence, and civil). These structures exhibit a high stiffness-to-weight ratio if compared with their metallic counterparts. Moreover, their tailoring capabilities make them interesting in design optimization. On the other hand, their intrinsic complex transverse material properties description requires an accurate structural model able to predict their structural response. Three-dimensional high-fidelity finite element models could be considered to evaluate the multilayered structural response; however, it is common to find industrial applications in which many layers are involved. Consequently, the computational cost of three-dimensional finite elements becomes prohibitive even for simple analysis. It becomes necessary to pursue another way to reach an affordable solution, even for more complex structures. In the framework of theories developed in recent years by researchers, the zigzag models represent a new class of models to investigate the structural response of multilayered composites and sandwich structures. These models, originally formulated by Prof. Di Sciuva, inspired many researchers, among them Prof. Gherlone, to put their efforts into contributing to developing accurate, efficient and computationally attractive zigzag theories.

In this context, this research aims to enhance the available refined zigzag models to investigate more general structures that exhibit a pronounced transverse anisotropy, including the effect of transverse normal deformation and non-linearities of displacement components typically present in thick multilayered structures and sandwich structures.

Chapter 1 presents a general overview of the most used structural theories available in the current literature, with particular attention to the zigzag models and variational formulations.

In Chapter 2, the enhanced Refined Zigzag Theory is formulated to analyse general multilayered structures in which the transverse shear coupling due to the

material anisotropy is present. The formulation of the enhanced zigzag functions, the derivation of governing equations, and consistent boundary conditions are presented in detail.

Chapter 3 is devoted to the formulation of a new higher-order mixed model based on the en-RZT that takes into account a finer description of the transverse shear and normal stresses. The new model formulation, named en-$\text{RZT}^{(m)}_{\{3,2\}}$, implements the Hellinger-Reissner variational principle, considering a new set of independent strain variables. A penalty term guarantees the compatibility conditions on the strain quantities in the governing functional. The governing equation and consistent boundary conditions are obtained to analyse anisotropic and cross-ply multilayered composite and sandwich plates.

In Chapter 4, the new mixed model is simplified to beam analysis. The beam governing equations and consistent boundary conditions of the B-$\text{RZT}^{(m)}_{\{3,2\}}$ are derived using the previous mixed variational statement. Then, two mixed finite elements are formulated to analyse cross-ply and sandwich beam structures.

In Chapters 5 and 6, the numerical and experimental results are presented. In Chapter 5, the newly formulated models are numerically assessed to evaluate the predictivity responses for linear bending, buckling and free vibration problems. The experimental campaign on three- and four-point bending tests and free vibration analysis of sandwich structures is conducted, and the results are compared with the new beam models. The activity proposed, supported by the numerical and experimental results, wants to offer a more general and complete methodology based on the refined zigzag models to investigate multilayered composite and sandwich structures. In particular, the newly formulated models could be used to analyse structures in which the material transverse anisotropy is not negligible. Moreover, the mixed formulation of the new models could be used to investigate even thick multilayered structures. The formulated elements make these new mixed models appealing in their predictivity capabilities and affordable low computational cost compared to other available models.

During the PhD research activity, the aspects concerning model development, finite element formulations, and numerical and experimental assessment constitute the basis of this thesis work. In addition, other aspects of PhD research activity not explicitly considered in this thesis cover numerical analysis of functionally graded structures, approximate solutions using the higher-order Haar-Wavelet method and advanced aspects of finite element modelling, some of them

during the period spent abroad at CIMNE, Barcelona. These interesting aspects and worthy of being mentioned for the sake of the conciseness of this dissertation, are not included in the presented models.

Here follows a list of the published articles and participations in International congresses.

Journal publications:

Di Sciuva M, Sorrenti M. A Family of C^0 Quadrilateral Plate Elements Based on the Refined Zigzag Theory for the Analysis of Thin and Thick Laminated Composite and Sandwich Plates. Journal of Composites Science 2019;3:1–31. https://doi.org/10.3390/jcs3040100.

Sorrenti M, Di Sciuva M, Tessler A. A robust four-node quadrilateral element for laminated composite and sandwich plates based on Refined Zigzag Theory. Computers & Structures 2021;242:1–22. https://doi.org/10.1016/j.compstruc.2020.106369.

Sorrenti M, Di Sciuva M, Majak J, Auriemma F. Static Response and Buckling Loads of Multilayered Composite Beams Using the Refined Zigzag Theory and Higher-Order Haar Wavelet Method. Mech Compos Mater 2021;57:1–18. https://doi.org/10.1007/s11029-021-09929-2.

Di Sciuva M, Sorrenti M. Bending and free vibration analysis of functionally graded sandwich plates: An assessment of the Refined Zigzag Theory. Journal of Sandwich Structures & Materials 2019:1–43. https://doi.org/10.1177/1099636219843970.

Di Sciuva M, Sorrenti M. Bending, free vibration and buckling of functionally graded carbon nanotube-reinforced sandwich plates, using the extended Refined Zigzag Theory. Composite Structures 2019;227:1–20. https://doi.org/10.1016/j.compstruct.2019.111324.

Sorrenti M, Di Sciuva M. An enhancement of the warping shear functions of Refined Zigzag Theory. Journal of Applied Mechanics 2021;88:7. https://doi.org/10.1115/1.4050908.

Sorrenti M, Gherlone M, Di Sciuva M. Buckling analysis of angle-ply multilayered and sandwich plates using the enhanced Refined Zigzag Theory. PEAS 2022;71:84. https://doi.org/10.3176/proc.2022.1.08.

Sorrenti M, Gherlone M. A new mixed model based on the enhanced-Refined Zigzag Theory for the analysis of thick multilayered composite plates. Composite Structures 2023;311:116787. https://doi.org/10.1016/j.compstruct.2023.116787.

International conferences presentations:

Sorrenti, M.; Di Sciuva, M.; Tessler, A.; Development of a locking-free quadrilateral element for laminated composite and sandwich plates based on refined zigzag theory. CIVIL-COMP 2019, Riva del Garda (Italy), September 16 - 19, 2019.

Sorrenti, M.; Gherlone, M.; Di Sciuva, M.; Free vibration analysis of angle-ply laminated and sandwich plates using enhanced Refined Zigzag Theory. In 19th International Conference of Numerical Analysis and Applied Mechanics (ICNAAM 2021), Rhodes (Greece), September 20 – 26, 2021.

Sorrenti, M.; Gherlone, M.; Dynamic analysis of sandwich beams with adhesive layers using the mixed Refined Zigzag Theory. In 19th International Conference of Numerical Analysis and Applied Mechanics (ICNAAM 2021), Rhodes (Greece), September 20 – 26, 2021.

Sorrenti, M.; Gherlone, M.; A new mixed model based on the enhanced-Refined Zigzag Theory for the analysis of thick multilayered composite plates. In 25th International Conference on Composite Structures (ICCS25), Porto (Portugal), July 19 - 22, 2022.

Preliminaries

This preliminary Section introduces some notions related to the three-dimensional linear elasticity that are abundantly used in this thesis work. The interested reader is referred to Reddy's book [1] for the omitted details.

Displacements

A solid deformable body of known geometry, material constituent, loads and boundary conditions is considered.

As shown in Figure , each material point P of the body, indicated by a volume V and an edge surface S, is referred to a Cartesian coordinate system $\mathbf{X} = \{x_1, x_2, x_3\}$.

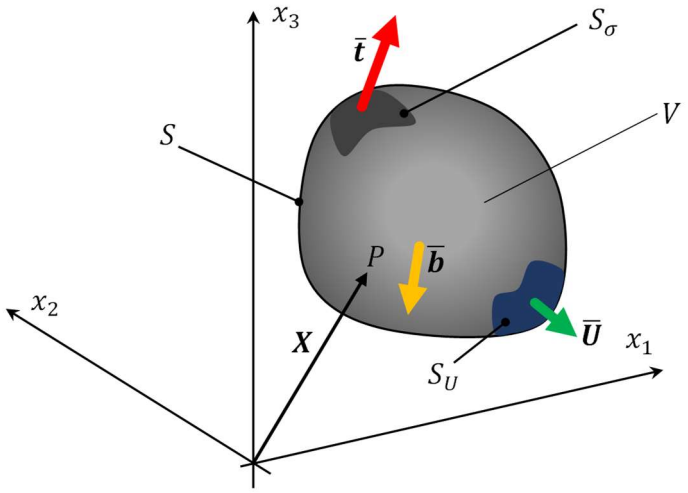

Figure 1: Coordinate reference system, deformable body representation and notations.

When the body is under the action of external forces and boundary conditions, the material particles of the body move towards a new configuration, identified by the position of the point $\mathbf{X}^{c1}$.

The displacement vector of the particle is given by

$$\mathbf{U} = \mathbf{X}^{c1} - \mathbf{X} \tag{0.1}$$

where $\mathbf{U} = \{U_i\}$, $i = 1,2,3$ is the vector of orthogonal Cartesian components of displacement.

Moreover, in Figure are shown: the vector of the applied body forces $\bar{\mathbf{b}} = \{\bar{b}_1, \bar{b}_2, \bar{b}_3\}$; the portion of the external surface, S_σ, on which is imposed (or prescribed) the traction vector $\bar{\mathbf{t}} = \{\bar{t}_1, \bar{t}_2, \bar{t}_3\}$; and the portion of the external surface, S_U, on which is imposed the displacement vector $\bar{\mathbf{U}}$.

Strain-displacement relations

According to Ref. [1], the strain-displacement relations are given using the most common strain measure in solid mechanics, i.e. the Green-Lagrange (G-L) strain tensor $\mathbf{E}$. The expression of G-L strain tensor as function of the displacement gradients reads as follows:

$$\mathbf{E} = \frac{1}{2}\left[\nabla\mathbf{U} + (\nabla\mathbf{U})^T + \nabla\mathbf{U}\cdot(\nabla\mathbf{U})^T\right] \tag{0.2}$$

If the displacement gradients are small, i.e. $|\nabla\mathbf{U}| \ll 1$, the G-L strain tensor can be reduced to the infinitesimal strain tensor $\mathbf{e} = \frac{1}{2}\left[\nabla\mathbf{U} + (\nabla\mathbf{U})^T\right]$. In components it reads $e_{ij} = \frac{1}{2}\left(\frac{\partial U_i}{\partial x_j} + \frac{\partial U_j}{\partial x_i}\right)$, $i, j = 1,2,3$, where $\partial(\bullet)/\partial x_i$ is the derivative of the quantity $(\bullet)$ along the coordinate x_i. The infinitesimal strain tensor can also be denoted using the engineering expressions as follows:

$$\varepsilon_{11}=\frac{\partial U_1}{\partial x_1};\quad \varepsilon_{22}=\frac{\partial U_2}{\partial x_2};\quad \varepsilon_{33}=\frac{\partial U_3}{\partial x_3};$$
$$\gamma_{12}=\frac{\partial U_1}{\partial x_2}+\frac{\partial U_2}{\partial x_1};\quad \gamma_{13}=\frac{\partial U_1}{\partial x_3}+\frac{\partial U_3}{\partial x_1};\qquad (0.3)$$
$$\gamma_{23}=\frac{\partial U_2}{\partial x_3}+\frac{\partial U_3}{\partial x_2}$$

In this thesis work, the infinitesimal strain tensor, according to the engineering notation, is used.

Constitutive material law

The constitutive equations of the linear elasticity in the case of infinitesimal deformation are shown in this Section. Introducing the vector of the stress components, as reported in Reddy's book [1], the generalized Hooke's law for an orthotropic material in its material system coordinate $\mathbf{X}^m=\left\{x_1^m,x_2^m,x_3^m\right\}$ has the following expression:

$$\boldsymbol{\sigma}^m=\begin{Bmatrix}\sigma_{11}\\ \sigma_{22}\\ \sigma_{33}\\ \tau_{13}\\ \tau_{23}\\ \tau_{12}\end{Bmatrix}^m=\begin{bmatrix}C_{11} & C_{12} & C_{13} & 0 & 0 & 0\\ & C_{22} & C_{23} & 0 & 0 & 0\\ & & C_{33} & 0 & 0 & 0\\ & & & C_{44} & 0 & 0\\ & & & & C_{55} & 0\\ & & & & & C_{66}\end{bmatrix}\begin{Bmatrix}\varepsilon_{11}\\ \varepsilon_{22}\\ \varepsilon_{33}\\ \gamma_{13}\\ \gamma_{23}\\ \gamma_{12}\end{Bmatrix}^m=\mathbf{C}\boldsymbol{\varepsilon}^m \qquad (0.4)$$

where $\boldsymbol{\sigma}^m$ and $\boldsymbol{\varepsilon}^m$ are the vector of the stress and strain components in material axes, respectively, and $\mathbf{C}$ is the stiffness tensor written according to the Voigt-Kelvin notation. The stress-strain relation, i.e. Eq. (0.4), can be inverted in a more convenient form highlighting the orthotropic material mechanical constants. It results in $\boldsymbol{\varepsilon}^m=\mathbf{C}^{-1}\boldsymbol{\sigma}^m=\mathbf{S}\boldsymbol{\sigma}^m$, where the compliance matrix is defined as follows:

$$\begin{bmatrix} \frac{1}{E_1} & -\frac{\nu_{12}}{E_1} & -\frac{\nu_{13}}{E_1} & 0 & 0 & 0 \\ & \frac{1}{E_2} & -\frac{\nu_{23}}{E_2} & 0 & 0 & 0 \\ & & \frac{1}{E_3} & 0 & 0 & 0 \\ & & & \frac{1}{G_{13}} & 0 & 0 \\ & \textit{sym.} & & & \frac{1}{G_{23}} & 0 \\ & & & & & \frac{1}{G_{12}} \end{bmatrix} \tag{0.5}$$

where E_1, E_2, E_3 are Young's moduli in x_1^m, x_2^m and x_3^m material directions, respectively; ν_{12}, ν_{13} and ν_{23} are the Poisson's ratios and G_{12}, G_{13}, G_{23} are the shear moduli in 1-2, 1-3 and 2-3 planes, respectively. Furthermore, the relation between Poisson's ratios and Young's moduli is also valid, i.e. $\nu_{ij}/E_i = \nu_{ji}/E_j$ $i,j = 1,2,3$.

Generally, in multilayered composite structures, the material coordinate system $\mathbf{X}^m$ could not coincide with the structure coordinate system $\mathbf{X}$. However, it is commonly considered that the transverse coordinate in flat structures like plates and beams x_3 coincides with the material laminate transverse coordinate x_3^m. The orientation angle of a general k^{th} layer $\mathrm{Y}^{(k)}$, between the material x_1^m and x_1 axes (see Figure 2) is defined as positive in the counter-clockwise direction. Thus, the generalized Hooke's law written in the structure reference system is:

$$\boldsymbol{\sigma} = \tilde{\mathbf{C}}\boldsymbol{\varepsilon} \tag{0.6}$$

where $\boldsymbol{\sigma}^T = \lfloor \sigma_{11} \quad \sigma_{22} \quad \sigma_{33} \quad \tau_{13} \quad \tau_{23} \quad \tau_{12} \rfloor$ and $\boldsymbol{\varepsilon}^T = \lfloor \varepsilon_{11} \quad \varepsilon_{22} \quad \varepsilon_{33} \quad \gamma_{13} \quad \gamma_{23} \quad \gamma_{12} \rfloor$ are, respectively, the stress and strain components in the global structure reference system, and $\tilde{\mathbf{C}}$ is the transformed stiffness matrix in the global coordinate.

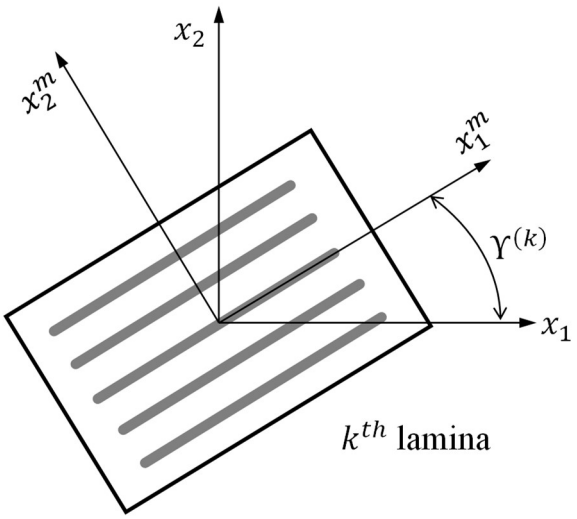

Figure 2: Laminate material coordinate system and structure reference axes.

The relationship between $\tilde{\mathbf{C}}$ and $\mathbf{C}$ is given by the rotation matrix, i.e. $\mathbf{R}^{(k)}$ function of the laminate rotation angle $\Upsilon^{(k)}$. It reads:

$$\tilde{\mathbf{C}} = \mathbf{R}\mathbf{C}\mathbf{R}^{T} \tag{0.7}$$

with

$$\mathbf{R} = \begin{bmatrix} \cos^2\left(\Upsilon^{(k)}\right) & \sin^2\left(\Upsilon^{(k)}\right) & 0 & 0 & 0 & -2\sin\left(\Upsilon^{(k)}\right)\cos\left(\Upsilon^{(k)}\right) \\ \sin^2\left(\Upsilon^{(k)}\right) & \cos^2\left(\Upsilon^{(k)}\right) & 0 & 0 & 0 & 2\sin\left(\Upsilon^{(k)}\right)\cos\left(\Upsilon^{(k)}\right) \\ 0 & 0 & 1 & 0 & 0 & 0 \\ 0 & 0 & 0 & \cos\left(\Upsilon^{(k)}\right) & -\sin\left(\Upsilon^{(k)}\right) & 0 \\ 0 & 0 & 0 & \sin\left(\Upsilon^{(k)}\right) & \cos\left(\Upsilon^{(k)}\right) & 0 \\ \sin\left(\Upsilon^{(k)}\right)\cos\left(\Upsilon^{(k)}\right) & -\sin\left(\Upsilon^{(k)}\right)\cos\left(\Upsilon^{(k)}\right) & 0 & 0 & 0 & \cos^2\left(\Upsilon^{(k)}\right)-\sin^2\left(\Upsilon^{(k)}\right) \end{bmatrix} \tag{0.8}$$

In plate models, the constitutive material law for an arbitrarily oriented lamina, under the plane stress hypothesis in which $\sigma_{33} = 0$, is rewritten as follows:

$$\begin{Bmatrix}\sigma_{11}\\ \sigma_{22}\\ \tau_{13}\\ \tau_{23}\\ \tau_{12}\end{Bmatrix}=\begin{bmatrix}\breve{C}_{11} & \breve{C}_{12} & 0 & 0 & \breve{C}_{16}\\ & \breve{C}_{22} & 0 & 0 & \breve{C}_{26}\\ & & \breve{C}_{44} & \breve{C}_{45} & 0\\ & & & \breve{C}_{55} & 0\\ sym. & & & & \breve{C}_{66}\end{bmatrix}\begin{Bmatrix}\varepsilon_{11}\\ \varepsilon_{22}\\ \gamma_{13}\\ \gamma_{23}\\ \gamma_{12}\end{Bmatrix} \tag{0.9}$$

where $\breve{C}_{ij}\ i,j=1,2,6$ are the in-plane reduced stiffness components, and $\breve{C}_{ij}=\tilde{C}_{ij}\ i,j=4,5$ are the transverse shear transformed stiffness. It is worth noting that the plane stress assumption does not affect the transverse shear stress. The reduced in-plane stiffness components read:

$$\breve{C}_{ij}=\tilde{C}_{ij}-\frac{\tilde{C}_{i3}\tilde{C}_{j3}}{\tilde{C}_{33}} \qquad i,j=1,2,6 \tag{0.10}$$

A mixed form of the constitutive material relations for the generic oriented lamina, helpful to the formulation of the mixed models developed in this thesis, reads as:

$$\begin{Bmatrix}\sigma_{11}\\ \sigma_{22}\\ \varepsilon_{33}\\ \tau_{13}\\ \tau_{23}\\ \tau_{12}\end{Bmatrix}=\begin{bmatrix}\breve{C}_{11} & \breve{C}_{12} & R_{13} & 0 & 0 & \breve{C}_{16}\\ \breve{C}_{12} & \breve{C}_{22} & R_{23} & 0 & 0 & \breve{C}_{26}\\ -R_{13} & -R_{23} & \tilde{S}_{33} & 0 & 0 & -R_{63}\\ 0 & 0 & 0 & \breve{C}_{44} & \breve{C}_{45} & 0\\ 0 & 0 & 0 & \breve{C}_{45} & \breve{C}_{55} & 0\\ \breve{C}_{16} & \breve{C}_{26} & R_{63} & 0 & 0 & \breve{C}_{66}\end{bmatrix}\begin{Bmatrix}\varepsilon_{11}\\ \varepsilon_{22}\\ \sigma_{33}\\ \gamma_{13}\\ \gamma_{23}\\ \gamma_{12}\end{Bmatrix} \tag{0.11}$$

where $\tilde{S}_{33}=1/\tilde{C}_{33}$ and $R_{i3}=\tilde{S}_{33}\tilde{C}_{i3}\ i=1,2,6$.

Cauchy's equations

The local three-dimensional equilibrium equations or Cauchy's equations in the absence of body forces that govern the structural behaviour, read as follows:

$$\begin{aligned}\sigma_{11,1}+\tau_{12,2}+\tau_{13,3}&=0\\ \tau_{12,1}+\sigma_{22,2}+\tau_{23,3}&=0\\ \tau_{13,1}+\tau_{23,2}+\sigma_{33,3}&=0\end{aligned} \tag{0.12}$$

General plate notation

In this Section, the solid general problem is specialized for the plate notation useful in this thesis work.

It is considered a multilayered flat plate made of a finite number N of perfectly bonded layers, as shown in Figure 3. Assuming as V the plate volume, h is the thickness, $S=S_U\cup S_\sigma$ the total cylindrical edge surface, comprised of S_U, the portion on which displacement restraints are imposed (or prescribed), and S_σ, the portion on which a traction vector (force per unit length), $\overline{\mathbf{F}}=\left\{\overline{F}_i\right\}\ (i=1,2,3)$, is prescribed. Moreover, let $\overline{\mathbf{p}}_{(\mathrm{B})}=\left\{\overline{p}_{i(\mathrm{B})}\right\}$ and $\overline{\mathbf{p}}_{(\mathrm{T})}=\left\{\overline{p}_{i(\mathrm{T})}\right\}\ (i=1,2,3)$ be the vectors of the prescribed tractions (force per unit surface) on the plate's bottom (B) and top (T) bounding surfaces along the coordinate axis x_i, see Figure 3. The prescribed quantities are indicated with an overbar. If not otherwise specified, the Einsteinian summation convention over repeated indices is adopted, with Latin indices ranging from 1 to 3 and Greek indices ranging from 1 to 2.

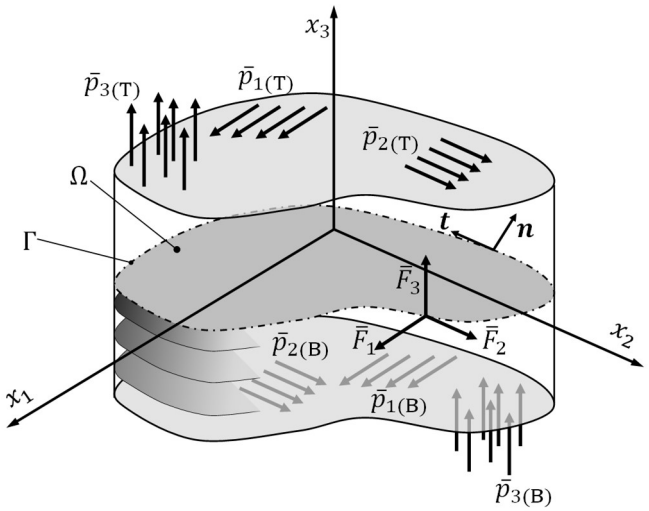

Figure 3: General plate notation: plate geometry, applied loads and coordinate system.

The thickness of each layer, as well as of the whole plate, is assumed to be constant in each direction. The points of the plate are referred to an orthogonal Cartesian coordinate system defined by the vector $\mathbf{X}=\{x_i\}$ $(i=1,2,3)$, where the vector $\mathbf{x}=\{x_\alpha\}$ $(\alpha=1,2)$ is the set of in-plane coordinates on the reference surface. Normally, if not otherwise specified, the reference surface is chosen to be the middle plane of the plate, and x_3 being the coordinate normal to the reference plane (see Figure 4), so that $x_3 \in \left[x_{3(B)}, x_{3(T)}\right] \equiv \left[-h/2, +h/2\right]$. Furthermore, Ω represents the set of points given by the intersection of the plate with the plane $x_3 = 0$ and $\Gamma = S \cap \Omega = \Gamma_U \cup \Gamma_\sigma$ $(\Gamma_U \cap \Gamma_\sigma = \varnothing)$ its contour line, with $\Gamma_U = S_U \cap \Omega$ and $\Gamma_\sigma = S_\sigma \cap \Omega$. Moreover, $(\mathbf{t}, \mathbf{n})$ are the tangential and normal axes with the point belonging to the contour line Γ.

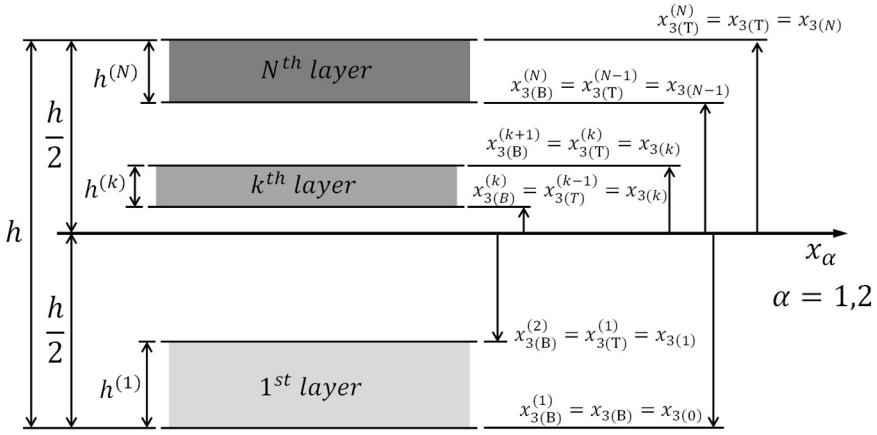

Figure 4: Layer numbering and notation.

If not otherwise stated, the superscript $(.)^{(k)}$ is used to indicate quantities corresponding to the k^{th} layer (k=1,…,N), whereas the subscript $(.)_{(k)}$ (k=1,…,N-1) stands for the quantity (.) valued at $x_3 = x_{3(k)}$, i.e. at the k^{th} interface (k=1,…,N-1) between the k^{th} and the $(k+1)^{\text{th}}$ layer. In addition, subscripts (B) and (T) indicate the bottom and top surfaces of a single layer/whole plate, respectively. Specifically, as it is reported in Figure 4, $x^{(1)}_{3(\mathrm{B})} = x_{3(\mathrm{B})}$ and $x^{(N)}_{3(\mathrm{T})} = x_{3(\mathrm{T})}$ denote the transverse coordinates of the bottom and top surfaces of the whole plate; thus,

$h = x_{3(\mathrm{T})} - x_{3(\mathrm{B})}$ is the total plate thickness and $h^{(k)} = x_{3(k)} - x_{3(k-1)} = x_{3(\mathrm{T})}^{(k)} - x_{3(\mathrm{B})}^{(k)}$ $(k = 1,2,...,N)$, the thickness of the k^{th} layer.

Finally, the material of each layer is assumed to be linear elastic orthotropic with a plane of elastic symmetry parallel to the reference surface. However, its principal orthotropy directions (material axes) are arbitrarily oriented with an angle $\Upsilon^{(k)}$ according to the scheme provided in Figure 2.

Chapter 1

Introduction

Multilayered composite and sandwich structures have been widely used in engineering fields (aerospace, marine, automotive, military, civil and energy) due to their exceptional mechanical properties over traditional metallic structures. As a matter of fact, they are to be preferred thanks to their high specific flexural stiffness and specific strength [2]. Moreover, they exhibit good fatigue behaviour, and their tailoring capabilities allow the design of performant and optimized structures. On the other hand, such structures typically exhibit a transverse anisotropy and transverse shear deformability higher than their metallic counterpart. The abrupt change in the transverse direction of the mechanical material properties generates stress concentrations at the interfaces that can cause the failure of the structure, such as delamination and debonding. Furthermore, in sandwich structures, the transverse applied loads could cause irreversible compressions of the core material and, consequently, the failure of the structure.

It is necessary to design these structures accurately to prevent failures and guarantee the highest level of safety during their operative life. It becomes important offering to the engineers accurate and efficient mathematical models to pursue those objectives during the design process. The structural theories formulated in recent decades represent a key role in this process.

In this Chapter, an overview of the existing structural theories is presented on the analysis of multilayered composite and sandwich structures. Their basic hypothesis, advantages and limitations are highlighted. Furthermore, the most

relevant variational methods used in the elasticity theory are presented to obtain the governing equations and the consistent boundary conditions.

1.1 State of the art on existing structural theories

In the design process of multilayered composite and sandwich structures, the mathematical model used to describe these structures should be able to describe the behaviour of these structures under the applied loads in conjunction with the applied boundary conditions. By solving three-dimensional equilibrium equations that describe linear elasticity, the actual stress field of the structure under the applied loads can be reconstructed.

In the literature framework, some studies on the exact elasticity solutions of multilayered composite and sandwich structures are available. An exact solution has been proposed in Pagano's works [3,4] for the cylindrical bending of simply-supported composite cross-ply laminates and sandwich beams and plates. Moreover, Pagano [5] investigated the static response of anisotropic general multilayered laminates under cylindrical bending assumptions, revealing the not negligible effect of transverse shear coupling in the displacement and stress responses.

Pagano and Wang [6] extended the previous method, obtaining an exact three-dimensional static solution for bending multilayered and sandwich simply-supported plates under distributed and concentrated loads. Then, Pagano and Hatfield [6] implemented an exact static solution for the three-dimensional elasticity of multilayered, bi-directional composites with several layers. Starting from Pagano and Hatfield's work, Zenkour [7] provided an alternative three-dimensional exact solution for uniformly loaded cross-ply laminates and sandwich plates. Later, Srinivas and co-authors [8–10] developed and successfully applied an exact three-dimensional solutions for bending, stability and free vibrations of simply-supported thick laminated plates.

A more general and comprehensive formulation of homogeneous and laminated orthotropic plates has been reported by Srinivas and Rao [11]. Among the exact solutions obtained for antisymmetric laminated plates, Noor and Burton [12] have implemented a mixed formulation for stress and free vibration problems of anisotropic multilayered plates. Later, Savoia and Reddy [13] obtained a solution for the three-dimensional static bending problem of rectangular antisymmetric angle-ply multilayered plates with simply-supported edges. It has

been revealed that Pagano's three-dimensional solution is a particular case of Savoia and Reddy's approach. Ye [15] recently investigated the free-vibrations of cross-ply laminated rectangular plates with clamped boundaries by implementing a recursive method. Finally, Brischetto [14,15] provided a general exact three-dimensional elasticity solution for the static analysis of multilayered composite and sandwich plates/shells using orthogonal curvilinear coordinates under transverse normal pressure and simply-supported boundary conditions.

The proposed literature overview shows that three-dimensional solutions can be applied only to a limited number of cases, i.e. simple geometry, applied loads and boundary conditions. In fact, most of them are related to beams or rectangular plates under sinusoidal or bi-sinusoidal transverse pressure and simply-supported boundary conditions.

As stated by many researchers, these solutions are often used as benchmark tests for new theories, model validations or finite element formulations. As a matter of fact, such types of loads and boundary conditions are rarely found in industrial applications. Without using high-fidelity 3D finite element models for complex structures, since they are affected by prohibitive computational costs, some alternative models to achieve a reliable and accurate solution must be developed.

Due to the difficulty of obtaining an exact solution for the three-dimensional elasticity problem, an approximate model should be considered. A two-dimension model, commonly named plate/shell, can be used if the structure has two dimensions greater than the third one. Otherwise, if only one dimension is greater with respect to the others, it is preferable to model the structure as a beam.

In the open literature, the simplified models can be further classified based on the assumption of the primary variables. For example, in displacement-based theories, the primary or master field is represented by displacements; whereas the strain field is derived from the displacement one and by using the strain-stress constitutive relations, the stress field can be evaluated. In such theories, since the strain and stress fields are derived from the master-displacements field, they are typically called slave fields. A second class of theories are the mixed models, wherein the displacement, the strain and the stress fields can be assumed independently, i.e. there is more than one master field.

An appropriate variational statement [18] should be used in both classifications to obtain the beam/plate/shell governing equations and the consistent boundary conditions.

A further classification noticeable in the literature is related to the assumptions on the displacement field. Such models are generally grouped into two macro-areas: Equivalent Single Layer (ESL) and Layer-wise (LW) theories. In the formers, the displacement field is assumed to be a smoothly continuous distribution across the entire laminate thickness. These models are sufficiently accurate in predicting global quantities such as maximum displacements, natural frequencies and buckling loads, but they are poor in the stress descriptions. In fact, according to the assumptions on the displacement field and by using the material constitutive relations, it is impossible to obtain a through-the-thickness transverse shear stress continuous distribution, i.e., the interlaminar stress continuity is not satisfied. A typical procedure to reconstruct a continuous distribution of the transverse shear stresses is the a-posteriori integration of the indefinite equilibrium Cauchy's equations. However, since these theories use a limited number of variables, they are very computationally attractive.

The LW theories assume, for each layer, an independent displacement field. The number of unknown variables assumed for each layer is then reduced by enforcing the continuity of the displacements at the layer interfaces. As a result, these models are more accurate than the ESL ones since they can predict a displacement distribution closer to those typically represented for a multilayered structure, i.e., changes of slopes in its distributions across the interface. However, unless it is considered a mixed model, the continuity of the transverse stresses is still not enforced, and the a-posteriori integration of the indefinite equilibrium equations should be used. Furthermore, a negative aspect of the LW models is the prohibitive computational cost when applied to analyse structures with several layers.

In the last decades, a new group of structural theories faced among the previous ones. i.e. the ZigZag Theories (ZZT). These theories exhibit some advantageous characteristics of both ESL and LW theories. For example, they are based on kinematic assumptions different for each layer, which is typical of a LW theory, but the total number of variables is fixed and independent of the number of layers, which is typical of an ESL model.

The generally adopted procedure starts from a general ESL theory that can describe the laminate's global behaviour. Then, the global displacement field is enriched by a local contribution, i.e. the zigzag functions that introduce the changes in the slopes of the displacement distributions across the laminate interfaces due to the variation of the lamina material properties. The zigzag contribution in the displacement field is generally defined by enforcing the displacement and transverse stress continuity at the interfaces. This procedure can make them dependent on only a limited number of variables.

In the next Section, some of the canonical functionals of linear elasticity are introduced to give an overview of the most important variational statements that can be used to obtain the governing beam/plate/shell governing equation and consistent boundary condition.

1.2 Canonical functionals of the linear elasticity

In this Section, according to the book of Washizu [16], some of the most important variational principles in elasticity are briefly enounced and assessed. The hypotheses and assumptions behind these principles are the keys to understanding the choices, advantages and limitations of our developed models. Moreover, these variational statements are practically used to derive the governing equations and the consistent boundary conditions of generally formulated models. Based on the assumed field number, they can be classified into single-field functionals (such as the displacement-based model) or mixed-field functionals. Hereafter, the quantity indicated with a suffix represents the quantity’s master field from which it has been derived. For the sake of conciseness, the interested reader is referred to the book of Washizu [16] and the other provided references for a full detailed explanation of the proposed functionals.

1.2.1 Hu-Washizu functional

The Hu-Washizu (HW) principle is a mixed-field functional that allows, at the same time, three independent variations of displacements, strains and stresses. As stated in the book of Washizu [16], this functional, due to the assumption of the master fields, can be considered the most general canonical functional in the

elasticity. Consequently, the other variational principles could be derived by the Hu-Washizu functional by using the available field equations (or strong relations):

- Strain-displacement relations or kinematic equations
- Strain-stress relations or constitutive material equations
- Internal equilibrium equations or Cauchy's equations

The Hu-Washizu principle, according to the notation of the three-dimensional elasticity, reads:

$$\begin{aligned}\delta\Pi^{HW} = &\int_V \left[\delta\boldsymbol{\sigma}^T\left(\boldsymbol{\varepsilon}^U-\boldsymbol{\varepsilon}\right)+\delta\boldsymbol{\varepsilon}^T\left(\boldsymbol{\sigma}^e-\boldsymbol{\sigma}\right)+\delta\boldsymbol{\varepsilon}^{UT}\boldsymbol{\sigma}-\delta\mathbf{U}^T\bar{\mathbf{b}}\right]dV + \\ &-\int_{S_\sigma}\delta\mathbf{U}^T\bar{\mathbf{t}}dS-\int_{S_U}\left[\delta\boldsymbol{\sigma}^T\left(\mathbf{U}-\bar{\mathbf{U}}\right)+\delta\mathbf{U}^T\boldsymbol{\sigma}\right]dS=0\end{aligned} \tag{1.1}$$

where $\mathbf{U}$, $\boldsymbol{\varepsilon}$, $\boldsymbol{\sigma}$ are the independent displacement, strain and stress master fields, respectively. Thus, the total number of unknown variables represented by the three fields is fifteen. Moreover, $\boldsymbol{\varepsilon}^U$ is the strain field derived from the displacement field, $\boldsymbol{\sigma}^e$ is the stress field obtained from the strain master field using the material constitutive relations.

It is worth noting that some of the terms expressed in Eq. (1.1) are expressions of the compatibility relations that ensure the consistency of the field variables. More specifically, the term $\int_V \delta\boldsymbol{\sigma}^T\left(\boldsymbol{\varepsilon}^U-\boldsymbol{\varepsilon}\right)dV$ guarantees in a weak form the compatibility between the strains coming from the displacements field (using the well-known strains-displacements relations) and the strains variables assumed as independent variables. Furthermore, the term $\int_V \delta\boldsymbol{\varepsilon}^T\left(\boldsymbol{\sigma}^e-\boldsymbol{\sigma}\right)dV$ guarantees, in a weak form, the compatibility between the assumed stress variables and those obtained from the strain field using the strain-stress relations, i.e. the constitutive material relations.

The main advantage of this functional is the independent assumption on the three fields and their weak connections that allow to formulate very accurate models as those in Refs. [17–22], although the degree of complexity behind the model formulation and field distributions is high.

1.2.1 Hellinger – Reissner (HR) and the Reissner's Mixed Variational Theorem (RMVT)

The Hellinger – Reissner (HR) principle is a mixed variational statement that allows at the same time two independent fields, i.e. the displacements and the stresses [16,23]. According to the previous notation, the two derived fields are $\boldsymbol{\varepsilon}^U$, the strains obtained from the displacement field (according to the strain-displacement relations) and $\boldsymbol{\varepsilon}^\sigma$, the strains obtained from the stress field using the constitutive material relations (strain-stress relations).

In formula, the Hellinger – Reissner principle reads:

$$\begin{aligned}\delta\Pi^{HR} = &\int_V \left[\delta\boldsymbol{\sigma}^T\left(\boldsymbol{\varepsilon}^u - \boldsymbol{\varepsilon}^\sigma\right) + \delta\boldsymbol{\varepsilon}^{UT}\boldsymbol{\sigma} - \delta\mathbf{U}^T\bar{\mathbf{b}}\right]dV \\ &- \int_{S_\sigma} \delta\mathbf{U}^T\bar{\mathbf{t}}dS - \int_{S_U}\left[\delta\boldsymbol{\sigma}^T\left(\mathbf{U}-\bar{\mathbf{U}}\right) + \delta\mathbf{U}^T\boldsymbol{\sigma}\right]dS = 0\end{aligned} \tag{1.2}$$

It should be noted that the variational statement described by Eq. (1.2) can be obtained from the HW functional, i.e. Eq. (1.1), by enforcing the strong relation $\boldsymbol{\varepsilon} = \mathbf{S}\boldsymbol{\sigma}$. Moreover, in Eq. (1.2) the term $\int_V \delta\boldsymbol{\sigma}^T\left(\boldsymbol{\varepsilon}^U - \boldsymbol{\varepsilon}^\sigma\right)dV$ weakly enforces the compatibility between the two derived strain fields.

The HR functional involves only three displacements and six stresses as unknown variables, making it computationally more attractive than the HW functional.

It has been demonstrated by Reissner [24,25] that the HR functional can be simplified by assuming only the transverse shear and normal stresses as independent stress variables, which are directly used to enforce the interlaminar equilibrium between adjacent layers. The researchers named this theorem Reissner's Mixed Variational Theorem (RMVT). According to the RMVT, Eq. (1.2) is simplified leading:

$$\begin{aligned}\delta\Pi^{RMVT} = &\int_V \left[\begin{array}{l}\delta\boldsymbol{\tau}_t^T\left(\boldsymbol{\gamma}_t^U - \boldsymbol{\gamma}_t^\tau\right) + \delta\sigma_{33}\left(\varepsilon_{33}^U - \varepsilon_{33}{}^\sigma\right) + \\ + \delta\boldsymbol{\varepsilon}_m^{UT}\boldsymbol{\sigma}_m^U + \delta\boldsymbol{\gamma}_t^{UT}\boldsymbol{\tau}_t + \delta\varepsilon_{33}^U\sigma_{33} - \delta\mathbf{U}^T\bar{\mathbf{b}}\end{array}\right]dV + \\ &- \int_{S_\sigma}\delta\mathbf{U}^T\bar{\mathbf{t}}dS - \int_{S_U}\left[\delta\boldsymbol{\sigma}^T\left(\mathbf{U}-\bar{\mathbf{U}}\right) + \delta\mathbf{U}^T\boldsymbol{\sigma}\right]dS = 0\end{aligned} \tag{1.3}$$

where $\boldsymbol{\tau}_t$ and σ_{33} are the assumed transverse shear and normal stresses, respectively; $\boldsymbol{\gamma}_t^U$ are the transverse shear strain using the strain-displacement relations, and $\boldsymbol{\gamma}_t^\tau$ those from the assumed transverse shear stress field. Moreover, ${\varepsilon_{33}}^U$ and ${\varepsilon_{33}}^\sigma$ are the transverse normal strain from the displacement field and those from the assumed one, respectively. Finally, the vector of strains $\boldsymbol{\varepsilon}_m^U$ and the stresses $\boldsymbol{\sigma}_m^U$ are obtained from the displacement field using the strain displacement and the constitutive material relations, respectively. It is worth noting that the number of total variables in the RMVT is reduced to six unknowns.

Among the various application of the RMVT to structural models in the literature framework, Auricchio and Sacco have provided an interesting example [26]. From a mathematical point of view, the transverse shear and normal strain compatibilities in the functional of Eq. (1.3), correspond as single weak variational statements in which the assumed stress fields play the role of Lagrangian multipliers. Thus, enforcing this condition before obtaining the governing equations is possible. In formula, it reads:

$$\delta\Pi^{RMVT} = \begin{cases} \int_V \delta\sigma_{33}\left({\varepsilon_{33}}^U - {\varepsilon_{33}}^\sigma\right)dV = 0 \\ \int_V \delta{\boldsymbol{\tau}_t}^T\left(\boldsymbol{\gamma}_t^U - \boldsymbol{\gamma}_t^\tau\right)dV = 0 \\ \int_V \left[\delta{\boldsymbol{\varepsilon}_m^u}^T\boldsymbol{\sigma}_m^U + \delta\boldsymbol{\gamma}_t^{UT}\boldsymbol{\tau}_t + \delta\varepsilon_{33}^U\sigma_{33} - \delta\mathbf{U}^T\bar{\mathbf{b}}\right]dV + \\ -\int_{S_\sigma}\delta\mathbf{U}^T\bar{\mathbf{t}}dS - \int_{S_U}\left[\delta\boldsymbol{\sigma}^T\left(\mathbf{U}-\bar{\mathbf{U}}\right) + \delta\mathbf{U}^T\boldsymbol{\sigma}\right]dS = 0 \end{cases} \tag{1.4}$$

Solving the first two relations of Eq. (1.4), the assumed stress variables are connected to the displacement field variable, reducing the number of governing equations.

It should be paid attention to when RMVT is used in conjunction with low-order theories since some drawbacks arise in the transverse shear stress descriptions. It can be seen that the second weak relation of Eq. (1.4) corresponds to the definition of the complementary constitutive relation for the transverse shear energy. As highlighted by Auricchio and Sacco [26], some inconsistencies in transverse stress distributions arise when the previous condition is enforced with low-order models. In such cases, the transverse strain distributions from the displacement field are typically poorly described, whereas the description of the

transverse shear stress profile assumed a priori involves a large number of variables. This further aspect and the compatibility condition, i.e. the second expression of Eq. (1.4), try to make the assumed strain distribution similar to the derived one, resulting in a worse representation of the transverse shear stresses.

1.2.2 Principle of Virtual Displacements (PVDs)

Among the variational principles in linear elasticity, the most used and simplest is the Principle of Virtual Displacements (PVDs). This functional involves only the displacement field as primary unknowns, whereas the strains and stresses are derived using the strain-displacement and the strain-stress relations, respectively.

The PVDs can be obtained directly from the HR functional by enforcing kinematic relations or the strain-displacement equations in a strong manner. Its expression follows:

$$\begin{aligned}\delta\Pi^{PVD} = &\int_V \left[\delta\boldsymbol{\varepsilon}^{UT}\boldsymbol{\sigma}^U - \delta\mathbf{U}^T\bar{\mathbf{b}}\right]dV + \\ &-\int_{S_\sigma}\delta\mathbf{U}^T\bar{\mathbf{t}}dS - \int_{S_U}\left[\delta\boldsymbol{\sigma}^T\left(\mathbf{U}-\bar{\mathbf{U}}\right)+\delta\mathbf{U}^T\boldsymbol{\sigma}\right]dS = 0\end{aligned} \tag{1.5}$$

where $\boldsymbol{\varepsilon}^U$ and $\boldsymbol{\sigma}^U$ are the strain and stress vectors, respectively, functions of the variables of the displacement field. The major advantage of this functional is its limited number of unknowns making him appealing with respect to the other functionals. However, its drawback relies on the description of displacement field that often is not able to represent the strains and stresses correctly.

1.3 The structural theories: a historical and conceptual overview

In this Section, the widely used structural theories are briefly recalled. Their hypotheses and their validity range are addressed to understand better the advantages and limitations of analysing multilayered composite and sandwich structures.

In the next paragraphs, the classification of the considered theories starts from the displacement-based assumptions. In addition, for some relevant models are also presented the corresponding mixed versions.

1.3.1 Equivalent Single Layer (ESL) models

In the Equivalent Single Layers (ESL) theories, as briefly introduced before, the displacement field is assumed through a continuous function of the transverse coordinate. The distribution is unrelated to the investigated structure's material or lamination scheme. Generally, they can be expressed as follows:

$$\begin{aligned} U_1(\mathbf{x},x_3;t) &= \sum_{p=1}^{P} f^{(p)}(x_3)u_1^{(p)}(\mathbf{x};t) \\ U_2(\mathbf{x},x_3;t) &= \sum_{q=1}^{Q} f^{(q)}(x_3)u_2^{(q)}(\mathbf{x};t) \\ U_3(\mathbf{x},x_3;t) &= \sum_{r=1}^{R} f^{(r)}(x_3)u_3^{(r)}(\mathbf{x};t) \end{aligned} \tag{1.6}$$

where $f^{(i)}(x_3)$ $(i = p,q,r)$ are appropriate through-the-thickness continuous functions of the transverse coordinate x_3, typically $f^{(i)}(x_3) = x_3^i$ $(i = p,q,r)$; P,Q and R are the order of expansion and $u_\alpha^{(i)}(\mathbf{x};t)$ $(i = p,q,r)$ $\alpha = 1,2,3$ are the kinematic unknowns. Moreover, $\mathbf{x} = \{x_1, x_3\}$. Commonly some kinematic hypotheses are enforced to the assumed displacement field to limit or reduce the number of unknowns, making the ESL models attractive from a computational point of view.

It can be seen from Eq. (1.6), that the strains are also continuous through-the-thickness continuous with no changes in their slopes at the layer interfaces. However, differences in slopes and discontinuities across the layer interfaces are expected in the stress distributions due to the constitutive material relations.

According to the three-dimensional elasticity, the in-plane stresses σ_{11},σ_{22} and τ_{12} could be discontinuous across the laminate, but the transverse shear stresses τ_{13},τ_{23} and the transverse normal stress σ_{33} have to be continuous at the interfaces in virtue of Cauchy's equilibrium equations. In addition, the transverse shear and normal deformation are typically present in sandwich structures, making ESL models less useful for studying them.

Despite these effects, the ESL theories are widely used since they are the simplest, computationally attractive and generally provide good results if the hypotheses behind their formulation are respected.

In the last decades, many authors have put their effort into formulating accurate and simple ESL theories. It follows a brief overview of the most famous models. For a more detailed and comprehensive overview of existing ESL models, the interested reader is referred to the works of Di Sciuva and Abrate [27] and Sayyad and Ghugal [28].

1.3.1.1 Classical Laminated Plate Theory

The simplest ESL plate theory is the Classical Laminated Plate Theory (CLT). Originally developed as an extension of the Kirchhoff plate theory, the CLT is applied to the analysis of laminated composite structures. The displacement field reads:

$$\begin{aligned} \widehat{\mathbf{U}}\left(\mathbf{x},x_3;t\right) &= \mathbf{u}\left(\mathbf{x};t\right) - x_3\partial\mathbf{w}\left(\mathbf{x};t\right) \\ U_3\left(\mathbf{x},x_3;t\right) &= u_3\left(\mathbf{x};t\right) \end{aligned} \tag{1.7}$$

where $\widehat{\mathbf{U}}^T = \lfloor U_1 \quad U_2 \rfloor$ are the in-plane displacements, $\mathbf{u}^T = \lfloor u_1 \quad u_2 \rfloor$ are the uniform part of the in-plane displacements corresponding to the in-plane displacements of the reference plane, when $x_3 = 0$; $\partial\mathbf{w}^T = \lfloor u_{3,1} \quad u_{3,2} \rfloor$ are the derivatives of the transverse displacement u_3 with respect to the axis x_1 and x_2. Moreover, $u_i\left(\mathbf{x};t\right)$ $i = 1,2,3$ are the in-plane and transverse displacement components of a point referred to the reference plane of the plate along the coordinate system $\left(x_1,x_2,x_3\right)$. The assumed displacement field is coherent with the kinematic assumptions of Kirchhoff's plate theory:

- the transverse normal deformability is neglected, i.e. $\varepsilon_{33} = 0$;
- line segments perpendicular to the reference surface remain straight after the deformation, i.e. in-plane displacements are a linear function of the transverse coordinate x_3;
- line segments normal to the reference surface remain perpendicular to that surface after deformation, i.e. $\gamma_{13} = \gamma_{23} = 0$;

Obviously, these hypotheses are strong simplifications of the real behaviour of a composite multilayered plate, as demonstrated by Pagano [4]. It has been shown in Ref. [4] that neglecting the transverse shear deformability in the model leads to errors in displacements and stress evaluations for span-to-thickness ratios below to 50 (for isotropic plates, this value could be lower till 20). Moreover, neglecting the transverse normal deformability limits the range of applicability of the CLT to sandwich structures. Clearly, the effect of transverse shear deformability can be recovered a-posteriori by integrating in-plane stresses in Cauchy's equilibrium equations.

The presence of $\partial \mathbf{w}(\mathbf{x};t)$ term makes the CLT less attractive in the finite element formulation since it is necessary to satisfy the C^1-continuity of the shape functions that approximate the kinematic variables. Thus, higher-order shape functions and more integration points are required, increasing the computational cost.

1.3.1.2 First-order Shear Deformation Theory

The assumption in the CLT on the transverse shear strains is too restrictive for the analysis of multilayered composites and sandwich plates; thus, a more complex model should be considered. The First-order Shear Deformation Theory (FSDT) relaxes the previous assumption by allowing the transverse shear deformation of the plate. The FSDT is the general extension of the Reissner-Mindlin plate theory originally developed for isotropic plates to multilayered structures. The displacement field of FSDT reads:

$$\begin{aligned} \widehat{\mathbf{U}}(\mathbf{x},x_3;t) &= \mathbf{u}(\mathbf{x};t) + x_3\boldsymbol{\theta}(\mathbf{x};t) \\ U_3(\mathbf{x},x_3;t) &= u_3(\mathbf{x};t) \end{aligned} \tag{1.8}$$

where $\boldsymbol{\theta}^T = \lfloor \theta_1 \quad \theta_2 \rfloor$ are the bending rotations around the negative direction of x_2 and the positive direction of x_1, respectively.

In the FSDT, the transverse shear deformability is included. In fact, starting from the displacement field of Eq. (1.8), the transverse shear strains are through-the-thickness constant functions, whereas the corresponding transverse shear stresses are constant with discontinuities in their distributions across the layer interfaces.

These distributions clearly do not represent the three-dimensional elasticity solution since the continuity of the transverse shear stress at the layer interfaces and the null stress conditions at the top and bottom external surfaces are not satisfied. Furthermore, comparing the results of the FSDT with the exact three-dimensional ones, the latters exhibit a pronounced shear flexibility. In fact, the elasticity solution provides a parabolic distribution of the transverse shear stresses for a single-layer structure, whereas the FSDT gives a constant and higher value across the plate thickness. Therefore, a solution provided by the researchers has been to apply to the material constitutive relations a Shear Correction Factor (SCF) for the shear stiffnesses. The purpose of this factor is to correct by matching the transverse shear strain energies caused by the different through-the-thickness distributions.

Various authors have formulated an SCF in the open literature that better captures the transverse shear behaviour. Some of them are worthy of mentioning, such as Reissner [29], Cowper [30], Whitney [31], Hutchinson [32], Raman [33] and Oñate [34]. In particular, the method developed by Madabhusi-Raman and Davalos [33] and later by Oñate [34] gives a general expression for the SCF (also valid for the multilayered sandwich plates) that includes the effect of lamination schemes (such as the number of layers, lamina orientations, mechanical properties and thickness).

Generally, the FSDT using an appropriate SCF provides accurate results regarding maximum deflections, natural frequencies and buckling loads for plates with span-to-thickness ratios greater than 20. The in-plane displacement and stress distributions are also good if compared with the exact results; however, the through-the-thickness distributions of shear stresses are poorly described unless obtained by a-posteriori integration of Cauchy's equations. Clearly, the discrepancies with respect to the three-dimensional behaviour increase for low values of the span-to-thickness ratio due to the effect of transverse anisotropy that becomes relevant in the structural predictions.

However, an interesting aspect of the FSDT is that it requires only the C^0-continuity in the finite element formulations to approximate the kinematic variables, making it appealing for the low computational cost.

As a matter of fact, the majority of the commercial finite element codes implement this formulation. However, the shear-locking phenomenon is one main drawbacks associated with C^0-continuous shear deformable elements. Such

elements overly stiff the response prediction of modelled thin structures. As shown in Pagano [4], the transverse shear deformability in thin structures could be neglected, but this condition cannot be reached from a numerical point of view. It results in the finite element application that the shear stiffness is over-estimated with respect to the bending contribution.

In the open literature, many approaches have been used to remedy this issue. Among them, reduced integration has been widely used [35–38] using a low-order Gauss integration to compute the transverse shear stiffness contribution. The reduced integration strategy has been demonstrated to be computationally valid, although extra zero energy modes may appear that require appropriate stabilization techniques to correct the provided solutions [39,40]. Other methodologies include the Discrete Kirchhoff Theory (DKT) [41,42], where the zero transverse shear strains are enforced in some discrete points in the element formulation. For shell element formulation, a common procedure is the Mixed Interpolation of the Tensorial Components (MITC) [43–46], where the element stiffness matrix assumes a different interpolation scheme for bending and shear effects. For further consideration of MITC elements, the interested reader is referred to the book of Bathe [45]. The Assumed Natural Strain (ASN) method [47] introduces a mixed-field formulation for an independent strain evaluation. Finally, the anisoparametric interpolation strategy, in combination with an element correction factor, has been proposed by Tessler and co-workers [48–52] to formulate variationally consistent locking-free finite elements.

Implementing a mixed formulation could increase the predictivity capabilities of the FSDT model. As highlighted in the previous section, Reissner [24] has formulated a mixed formulation based on the Hellinger-Reissner functional for transverse shear deformability. In another example in the open literature, Auricchio and Sacco [53,26] have formulated different refined mixed models based on FSTD kinematics to improve the predictions of transverse shear stresses.

1.3.1.3 Third-order Shear Deformation Theory

As expected from the three-dimensional elasticity, the typical distribution of the transverse shear strains is parabolic for a single-layer structure. Thus, assumptions of through-the-thickness linear displacements are no longer valid. Consequently, a cubic expansion of the in-plane displacements should be considered to follow the correct three-dimensional behaviour. By neglecting the transverse normal deformability, the displacement field of a third-order model reads:

$$\begin{aligned}\widehat{\mathbf{U}}\left(\mathbf{x},x_3;t\right)&=\mathbf{u}\left(\mathbf{x};t\right)+x_3\boldsymbol{\theta}\left(\mathbf{x};t\right)+x_3^{\,2}\boldsymbol{\omega}\left(\mathbf{x};t\right)+x_3^{\,3}\boldsymbol{\chi}\left(\mathbf{x};t\right)\\ U_3\left(\mathbf{x},x_3;t\right)&=u_3\left(\mathbf{x};t\right)\end{aligned} \tag{1.9}$$

where $\boldsymbol{\omega}^T=\lfloor\omega_1 \quad \omega_2\rfloor$, $\boldsymbol{\chi}^T=\lfloor\chi_1 \quad \chi_2\rfloor$ are the new kinematic unknowns related to the parabolic and cubic part of the in-plane displacements. This kinematic field involves nine variables, resulting in a set of nine second-order partial differential equations that should be solved. The procedure adopted by Reddy [1,54,55] is to enforce the traction-free boundary condition on the laminate's top and bottom external surfaces, i.e. $\tau_{13}\left(x_3=\pm h/2\right)=\tau_{23}\left(x_3=\pm h/2\right)=0$.

According to this assumption, the displacement field expressed by Eq. (1.9) is rewritten as follows:

$$\begin{aligned}\widehat{\mathbf{U}}\left(\mathbf{x},x_3;t\right)&=\mathbf{u}\left(\mathbf{x};t\right)+x_3\boldsymbol{\theta}\left(\mathbf{x};t\right)-\frac{4}{3h^2}x_3^{\,3}\left(\boldsymbol{\theta}\left(\mathbf{x};t\right)+\partial\mathbf{w}\left(\mathbf{x};t\right)\right)\\ U_3\left(\mathbf{x},x_3;t\right)&=u_3\left(\mathbf{x};t\right)\end{aligned} \tag{1.10}$$

The quantities defined in Eq. (1.10) can be recalled from the FSDT and the CLT. Hereafter, the displacement model identified by Eq. (1.10) is referred to as Third-order Shear Deformation Theory (TSDT). Although its parabolic distribution for the transverse shear strain, the transverse shear stress continuity at the layer interfaces is not satisfied in this model for multilayered structures. However, it is accurate enough in global quantities predictions and through-the-thickness in-plane and stresses distributions. Moreover, the TSDT does not require any shear correction factor due to the more accurate distribution of the transverse shear stresses.

Although the TSDT is more accurate than the FSDT in displacements, frequencies, buckling loads and through-the-thickness stresses, some inconsistencies arise when this model is applied to structures with clamped edges [56]. In such cases, due to the boundary conditions on the kinematic variables, both the bending rotations, i.e. $\boldsymbol{\theta}$, and both the first derivatives of the transverse displacements, i.e. $\partial\mathbf{w}$, need to be null. As a result, null transverse shear stress distributions and null shear forces are obtained at the clamped edges. This result is clearly inaccurate and limits this model's application range. Furthermore, the presence in the displacement field of the first derivative of the transverse

displacements requires C^1-continuity to approximate the transverse displacement in finite element formulations.

A final consideration on general Third-order Shear Deformation models has been given by Di Sciuva [57], where the author has demonstrated that a class of polynomial TDSTs are kinematically equivalent since they can produce the same numerical results for the displacements and global quantities, such as frequencies and buckling loads.

1.3.1.4 Higher Order Shear Deformation Theories and non-polynomial theories

Among the other ESL theories available and used in literature are the Higher-order Shear Deformation Theories (HSDTs) and the non-polynomial theories.

Higher-order theories have been formulated in order to take into account the transverse shear and transverse normal deformability. Based on Eq. (1.6) many authors in literature have formulated their theories. In the open literature, it is common to find the nomenclature of $\{m,n\}$-order theories where m is the maximum order of expansion of the in-plane displacements and n is the maximum order of expansion of the transverse displacement.

Recently, many authors have combined the typical displacement fields seen before with non-polynomial functions to account for the transverse shear deformability. The non-polynomial models can be distinguished based on the assumed functions. In the literature framework are worthy of being cited, the sinusoidal functions of Touratier [58], the hyperbolic functions of Soldatos [59], the exponential functions used by Karama et al. [60] and the functions of Sarangan and Singh [61].

The literature provided just wants to overview the existing ESL models, and the reader is referred to the Di Sciuva and Abrate review work [27].

1.3.2 Layer-Wise (LW) models

This paragraph presents an overview of the existing Layer-Wise (LW) models, with particular attention to the displacement-based formulation.

The Layer-Wise models (LW) have often been used to analyse multilayered composite and sandwich structures. For these structures from the three-dimensional elasticity, the through-the-thickness distributions of the

displacements are typically non-linear zigzag continuous functions. This effect is related to the transverse shear and normal mechanical properties that generate a remarkable effect in the deformation under the applied loads in thick multilayered composite structures. However, as seen before, the ESL theories' kinematic cannot reproduce this zigzag effect in the displacement distributions. Moreover, less accurate displacement fields cannot describe transverse shear and normal stresses with the stress continuity satisfied at the layer interfaces.

Due to their independent kinematic assumptions for each layer, the LW models could reproduce the different effects of different materials that form the multilayered structure. Generally, the same theory could be applied for each layer using independent variables. According to this assumption, the general displacement field for an arbitrary k^{th} layer of an LW model reads:

$$U_i^{(k)}\left(\mathbf{x}, x_3; t\right) = \sum_{p=1}^{P_i} f_k^{(p)}(x_3) u_i^{k(p)}(\mathbf{x}; t) \quad i = 1,2,3 \tag{1.11}$$

where N is the total number of layers, P_i is the maximum order of expansion for the i^{th} component of the displacement vector, $f_k^{(p)}(x_3)$ is the p^{th} assumed through-the-thickness function valid for the k^{th} layer

The most simple LW theory assumes a linear through-the-thickness variation of the displacements in each layer. Once each layer's kinematics is chosen, the displacement continuity is enforced at each interface. Generally, the transverse shear and normal stresses might still be discontinuous; however, their continuity could be enforced in the LW formulations to increase further the model's accuracy.

In the literature framework, Carrera [62] has formulated an LW model that can be applied to finite element formulations by involving a hierarchical scheme. The Carrera Unified Formulation (CUF) has been used by many authors [63–70] to investigate the structural behaviour of multilayered composite and sandwich beams/plates and shells. In the framework of CUF, Demasi [71–73] has further generalized the CUF formulating the Generalized Unified Formulation (GUF) in which each displacement variable has a different order of expansion by enabling more importance to some variables than others. For a more detailed overview of the CUF and other developed LW models, the interested reader is referred to the book of Petrolo et al. [74]. Furthermore, other interesting and more general works

related to the LW theories are assessed in Reddy's book [1], Abrate and Di Sciuva's book chapter [75] and Li's review article [76].

Generally, these models are often more accurate than the ESL ones due to the layer-wise approach that is able to accurately describe a more complex distribution of the displacement in laminated structures. However, the main obstacle of these models is related to the strong dependency of the total number of kinematic variables on the number of layers. When the number of layers is high, the computational cost of these models becomes prohibitive, and the advantages of other solutions are lost.

1.3.3 Zigzag models

Historically, the first attempt to develop a simple but accurate model without involving the layerwise theories in which the effect of the lamination scheme is assumed a-priori in the transverse shear stresses has done by Ambartsumyan [77] and later by Whitney [78]. Both authors started assuming an a-priori appropriate function for transverse shear stress distributions inspired by the three-dimensional elasticity solution. The unknown coefficients are obtained by enforcing the stress continuity at the layer interfaces and the continuity of the displacements.

Even if the proposed models [77,78] have been revealed to be accurate enough to the global quantity predictions, the assumed transverse shear stress distributions have been demonstrated inaccurately predict the three-dimensional solution. Moreover, the dependency of the displacement field from these inaccurate distributions is clearly undesirable for describing the laminate behaviour correctly.

Based on the previous idea of having only a few functions that can represent the layerwise displacement description and maintain at the same time the model simplicity, a new group of structural theories has been proposed in recent years. The ZigZag Theories (ZZTs) take some of the best properties of the ESL and LW models. Generally, these theories are formulated using a limited number of unknown kinematic variables, such as the ESL theories, but the displacement field is enriched with a finer layerwise description given by the "zigzag" functions.

The assumed displacement field of a zigzag model can be seen as a superposition of two main contributions: the first is a coarse representation of the global laminate behaviour, and the second is a local (layer-scale) refinement represented by the zigzag functions. The zigzag functions are only dependent on

the transverse thickness coordinate, whereas the dependency of the other directions has given by the zigzag amplitudes or zigzag rotations. A typical representation of the displacement field of a ZZT in which the transverse displacement, for the sake of simplicity, is assumed to be constant, is represented as follows:

$$\begin{aligned}&\widehat{\mathbf{U}}^{(k)}\left(\mathbf{x},x_3;t\right)=\mathbf{u}_G\left(\mathbf{x},x_3;t\right)+\mathbf{u}_L^{(k)}\left(\mathbf{x},x_3;t\right)\qquad k=1,...,N\\&U_3^{(k)}\left(\mathbf{x},x_3;t\right)=u_3\left(\mathbf{x};t\right)\end{aligned}\tag{1.12}$$

where $\mathbf{u}_L^{(k)}\left(\mathbf{x},x_3;t\right)=\mathbf{f}^{(k)}(x_3)\boldsymbol{\psi}\left(\mathbf{x};t\right)\ k=1,...,N$ is the definition of the local displacement refinement. Moreover, $\mathbf{f}^{(k)}(x_3)$ are the zigzag functions and $\boldsymbol{\psi}\left(\mathbf{x};t\right)$ the zigzag amplitudes or zigzag rotations.

The selection of the zigzag functions is important to represent the multilayered structure's response better. Therefore, the developed model could be more or less accurate depending on the hypothesis or the assumptions behind the zigzag functions formulation.

In the following paragraphs, some of the most important zigzag theories available in the current literature are recalled.

1.3.3.1 Di Sciuva's Zigzag Theory (ZZT)

Chronologically, Di Sciuva proposed the first zigzag model able to investigate the behaviour of multilayered composite and sandwich structures. In the middle of the '80s, he proposed a new displacement model [79–82] in which a first-order kinematic has been superposed with a through-the-thickness piecewise continuous function, i.e. the zigzag functions. By assuming as the reference plane the bottom external surface of the laminate and neglecting the transverse normal deformability, the assumed kinematic field of Di Sciuva's ZZT reads:

$$\begin{aligned}&\widehat{\mathbf{U}}^{(k)}\left(\mathbf{x},x_3;t\right)=\mathbf{u}\left(\mathbf{x};t\right)+x_3\boldsymbol{\theta}\left(\mathbf{x};t\right)+\sum_{i=1}^{k-1}\left(x_3-x_{3k}\right)\boldsymbol{\psi}_k\left(\mathbf{x};t\right)H_k(x_3)\ \ k=1,...,N\\&U_3^{(k)}\left(\mathbf{x},x_3;t\right)=u_3\left(\mathbf{x};t\right)\end{aligned}\tag{1.13}$$

where H_k is the Heaviside unit function and $\boldsymbol{\psi}_k\left(\mathbf{x};t\right)=\mathbf{a}_k\left(\boldsymbol{\theta}\left(\mathbf{x};t\right)+\partial\mathbf{w}\left(\mathbf{x};t\right)\right)$. The constant matrix $\mathbf{a}_k$ is obtained by enforcing two conditions: the former is related to the transverse shear stress continuity that is ensured at each layer interface across the whole laminate thickness; the latter condition assumes that the

zigzag functions are null across the entire bottom layer. These two sets of conditions can fully define the zigzag functions.

A typical example of one of Di Sciuva's zigzag functions $\left(\phi_{DZZ}^{(k)}(x_3)=\sum_{i=1}^{k-1}(x_3-x_{3k})a_{11k}H_k(x_3)\right)$ for three-layered structures is represented in Figure 5.

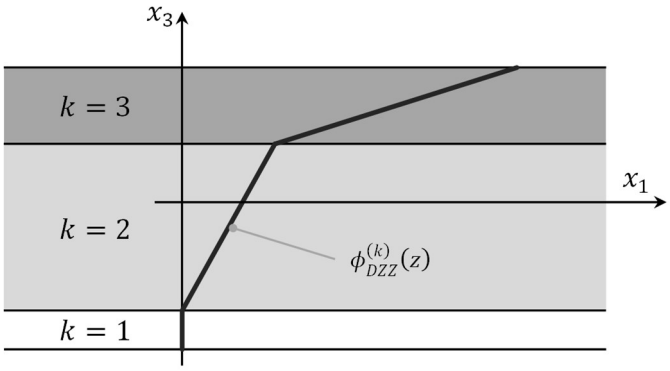

Figure 5: Local through-the-thickness displacement contributions using Di Sciuva's zigzag function for a general three-layered beam structure.

Due to the kinematic field and zigzag function formulations, the in-plane displacements are able to reproduce the typical "zigzag" distribution of multilayered structures by involving only five unknown variables (the same number of the FSDT). Moreover, the through-the-thickness transverse shear stresses continuity is guaranteed, although the transverse shear stress functions are constant across the whole thickness, unable to satisfy the null values at the bottom and top surfaces. It has been demonstrated in Refs. [83,84] that the transverse shear stresses obtained from integrating local equilibrium equations are more accurate than the other ESL theories.

The kinematic field of Eq. (1.13) has been further extended by Cho and Parmerter [85,86] and Di Sciuva [87], considering a through-the-thickness cubic variation of the in-plane displacements. In Ref. [88], the ZZT has been extended and applied to shell structures. Furthermore, Di Sciuva [89] has generalized his ZZT, including the in-plane nonlinear elastodynamic behaviour of multilayered anisotropic plates with the possibility of considering interlayer slips. Finally, it

has been remarked in Ref. [89] that the previous models could be considered a particular case of the last general one.

Based on Di Sciuva's zigzag model, Icardi [90,91] has further increased the complexity of the previous kinematics to investigate the three-dimensional behaviour of thick structures, including the transverse normal deformability. By adding higher-order terms in global and local contributions for the in-plane and transverse displacements and enforcing the transverse and normal stress continuities, the formulated model has demonstrated to reproduce the behaviour of multilayered composite thick structures accurately.

It is important to remark that the zigzag functions chosen in these models can satisfy the continuity of the transverse shear stresses and, at the same time, the transverse normal stress continuity. As a matter of fact, the coefficients that define the zigzag functions are strongly related to the transverse material properties, which is an important effect in such structures.

One drawback of Di Sciuva's ZZ model is easily noted by looking at the in-plane displacements in Eq. (1.13). It appears the first derivatives of the transverse displacement with respect to the in-plane axes; thus, in finite element formulation, a C^1-continuity, such as CLT-based elements, is required for the shape functions that interpolate the transverse displacement. Moreover, this model suffers from the same inconsistencies as the TSDT, i.e. the inability of the model to correctly predict the transverse shear stress distributions and the shear force resultants at the clamped edges.

1.3.3.2 Murakami Zigzag Theory

Similarly, Murakami [92] has proposed a new laminated plate theory that includes linear zigzag functions as local contributions of the in-plane kinematics.

In Murakami's model, the zigzag functions have a linear piecewise distribution with changes in the sign of their slopes across the layer interfaces. To simplify the zigzag slopes definitions, they are not dependent on the material properties. In fact, their values alternatively vary from -1 to +1.

According to Ref. [92], the displacement field reads:

$$\begin{aligned}\widehat{\mathbf{U}}^{(k)}\left(\mathbf{x},x_3;t\right)&=\mathbf{u}\left(\mathbf{x};t\right)+x_3\boldsymbol{\theta}\left(\mathbf{x};t\right)+\left[\left(-1\right)^k\xi^{(k)}(x_3)\right]\boldsymbol{\psi}\left(\mathbf{x};t\right)\quad k=1,...,N\\ U_3^{(k)}\left(\mathbf{x},x_3;t\right)&=u_3\left(\mathbf{x};t\right)\end{aligned}\tag{1.14}$$

where the zigzag function is represented by the term $\phi_{MZZ}^{(k)} = \left[(-1)^k \xi^{(k)}(x_3)\right]$, in which $\xi^{(k)}(x_3) = \dfrac{2x_{3k}}{h^{(k)}}$ is the local layer transverse coordinate. Figure 6 reports a typical Murakami's zigzag function.

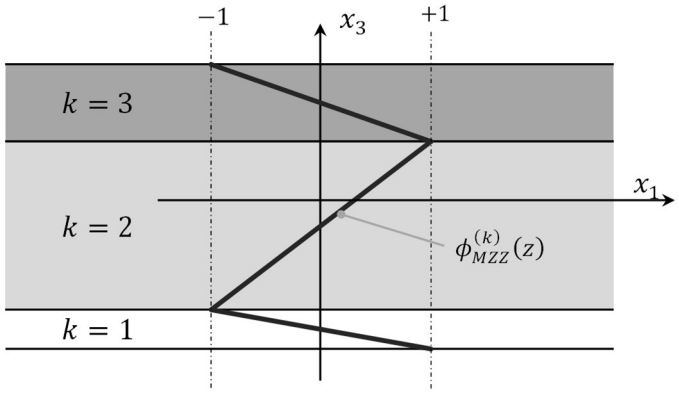

Figure 6: Through-the-thickness representation of Murakami's zigzag function, $\phi_{MZZ}^{(k)}(x_3)$, for a three-layered beam structure.

A further enhancement is developed later by Toledano and Murakami [93] involving the RMVT. This model has demonstrated to accurately describe the kinematics of periodic laminated structures with respect to the three-dimensional elasticity solution. However, some inconsistencies and inaccuracies arise when these models are applied to structures with non-periodical laminations, as Gherlone shows in Ref. [94]. As a matter of fact, Di Sciuva's zigzag functions are physically consistent since they are formulated by enforcing the transverse shear stress continuity at the layer interface and the conditions on the in-plane displacements in the first layer. Instead, Murakami's zigzag functions are periodic functions, insensible to the changes in the transverse material properties, which is an important effect in the transverse shear stress continuity when the kinematic model is applied to more general lamination schemes.

1.3.3.3 Other zigzag theories

In the current literature, other zigzag models have been formulated to investigate the structural behaviour of multilayered composites and sandwich structures. In Averill's zigzag model [95] to the first order kinematics, it has been superposed a zigzag contribution in the in-plane displacements. The zigzag functions are obtained by a partial through-the-thickness continuity of the

transverse shear stresses at the layer interfaces. In order to enforce the total continuity of the transverse shear stresses in a limiting sense, a penalty term has been added in the governing functional. With respect to Di Sciuva's Zigzag model, Averill's model [96,97] requires only the C^0-continuity of the shape functions that interpolate the quantities since the first derivatives of the transverse displacement are not involved in the in-plane displacements. Moreover, the penalty term added in the functional could be seen as an alternative condition that respects Di Sciuva's ZZT enforcement of assuming the first layer as the reference for the transverse shear stiffness. However, the same physical inconsistencies arise in clamped boundary conditions, i.e. all the unknown variables vanish, and both shear stress and strains are null, whereas the shear force is expected not to be null.

In the CUF/GUF models framework, Murakami's zigzag functions have been added [98–101] to improve the prediction capabilities without increasing the complexity. However, the improvements are shown to be less accurate in multilayered structures in which the lamination schemes do not satisfy the periodicity prescribed by Murakami.

Among the model derived by Di Sciuva's original kinematics, in Icardi and Sola's model [98,99], the effect of zigzag representation is adapted to the solution thanks to a reformulation in which appropriate variables substitute the quantities derived. Using symbolic calculus and an energy-based method, the author achieves high-order quality solutions for analysing thick multilayered composite plates. The proposed model named adaptive-zigzag (AZZ) [100] has been further extended by Icardi and Urraci [20,101,21,22] using the mixed formulations, i.e. Hu-Washizu and Hellinger-Reissner functionals. Even if these last models have been demonstrated to be very accurate for some applications, due to their complexity and computational cost are not considered in this thesis. The interested reader is addressed to the theses of Sola [100] and Urraci [22] for a more comprehensive dissertation on these models.

1.3.3.3 The Refined Zigzag Theory (RZT)

In the early years of the 21st century, Tessler and co-workers [102,103] formulated a new zigzag model that takes into account the Di Sciuva and Averill inconsistencies and has been able to study the behaviour of multilayered composite and sandwich beams/plates. The new Refined Zigzag Theory (RZT) starts from the assumption of first-order kinematics for the global contribution of the displacement field. The local contribution for the in-plane displacements is

given by appropriate piecewise through-the-thickness continuous linear functions with the constraint of being null at the top and bottom external surfaces. According to the formulation of RZT [104], the zigzag slopes are obtained by partially fulfilling the transverse shear stress continuity at the layer interfaces. According to these hypotheses, the displacement field reads:

$$\begin{aligned}\widehat{\mathbf{U}}^{(k)}\left(\mathbf{x},x_3;t\right)&=\mathbf{u}\left(\mathbf{x};t\right)+x_3\boldsymbol{\theta}\left(\mathbf{x};t\right)+\boldsymbol{\varphi}^{(k)}(x_3)\boldsymbol{\psi}\left(\mathbf{x};t\right)\quad k=1,...,N\\ U_3^{(k)}\left(\mathbf{x},x_3;t\right)&=u_3\left(\mathbf{x};t\right)\end{aligned}\tag{1.15}$$

where

$$\boldsymbol{\varphi}^{(k)}(x_3)=\begin{bmatrix}\phi_1^{(k)}(x_3) & 0\\ 0 & \phi_2^{(k)}(x_3)\end{bmatrix}\tag{1.16}$$

with $\phi_\alpha^{(k)}(x_3)=(x_3-x_{3(B)}^{(k)})\beta_\alpha^{(k)}+\sum_{q=1}^{k}h^{(q)}\left(\beta_\alpha^{(q)}-\beta_\alpha^{(k)}\right)$ and $\beta_1^{(k)}=\frac{\breve{C}_{44}^{(k)}}{G_1}-1$ and $\beta_2^{(k)}=\frac{\breve{C}_{55}^{(k)}}{G_2}-1$. G_1 and G_2 are the weighted-average transverse shear moduli computed according to Ref. [104].

A typical through-the-thickness representation of one of the refined zigzag functions is shown in Figure 7. More specifically, it is reported $\phi_{RZT}^{(k)}(x_3)=\phi_1^{(k)}(x_3)$.

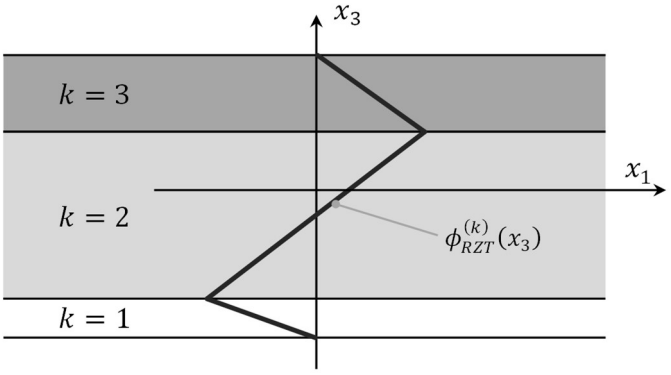

Figure 7: Through-the-thickness representation of the refined zigzag function, $\phi_{RZT}^{(k)}(x_3)$, for a three-layered beam structure.

The potentiality of RZT relies on its zigzag functions, as demonstrated by Tessler et al. [105]. The authors have applied the RZT kinematics in analysing a homogenous plate without using any shear correction factor. Using an appropriate through-the-thickness small parabolic variation of the transverse shear moduli, the RZT has reproduced the parabolic shear strain and stress distributions consistent with the three-dimensional elasticity. Similarly, Iurlaro et al. [106] has applied the RZT to the functionally graded structures demonstrating great accuracy in displacement predictions and through-the-thickness stress distributions, buckling loads and natural frequencies of plates under different boundary conditions.

As stated before, for Murakami's zigzag model, Gherlone [94] has deeply investigated the role of the zigzag functions in the kinematics of RZT. It has been pointed out that the zigzag functions formulated according to the RZT formulation could significantly improve the displacement and stress predictions since they consider the variation of the shear laminate properties. On the contrary, the Murakami model does not include this effect in its zigzag functions. Moreover, in Ref. [94], the effect of external weak layers (EWL) has also been studied in order to improve the zigzag performances and the predictability of the RZT.

Since the RZT formulation requires only C^0-continuity in the governing functional, it is possible to formulate simple but accurate finite elements. The interested reader is referred to Gherlone and co-workers [107,108] and Oñate [34,109] for beam elements, to Ejio et al. [110] and Versino et al. [111,112] for plate/shell elements.

The RZT has also been used in conjunction with the peridynamic differential operator to solve the equilibrium equation by the effect of possible discontinuities in the structure domain. As a result, Dorduncu [113] has obtained an accurate model for highly heterogeneous beam structures. Based on the results for beam structures reported in Ref. [114], the procedure has been extended to sandwich structures with functionally graded cores, revealing a good accuracy in the static predicting response.

One of the main advantages of the RZT is the accuracy without introducing a shear correction factor. Like the FSDT, the RZT presents a through-the-thickness piecewise transverse shear stress distribution. It is evident that by integrating the local equilibrium equations, continuous distributions of shear stresses could be

obtained, but those computed by the RZT are closer than the others with respect to the three-dimensional solution.

In the framework of the RZT-based model, the RMVT has also been applied to derive the governing equations of RZT beams and plates. In Tessler's first work [115], the mixed-RZT ($RZT^{(m)}$) has been formulated for beam multilayered structures. According to Ref. [115], the $RZT^{(m)}$ assumes a-priori a trough-the-thickness distribution of the transverse shear stresses. The assumed functions derive directly by integrating the local Chauchy's equilibrium equations using the in-plane RZT stresses under the hypothesis of cylindrical bending. Implicitly valid for beam structures, this condition is necessary for plates, as pointed out in Iurlaro et al. [116]; otherwise, the mixed model has been demonstrated to be less accurate. In fact, the main issue relies on the governing functional, specifically in the compatibility condition between the transverse shear strains from the displacement field and those obtained from the assumed stresses. This condition tries to enforce the congruence between a through-the-thickness piecewise continuous parabolic function and a piece-wise, not continuous one, which is impossible. If more stress variables in the transverse stress functions are considered, more inaccuracies arise due to the mathematical over-fitting problem. Thus, the cylindrical bending condition has been chosen as the best compromise to achieve a good transverse shear stress representation with a limited number of terms in the assumed functions. One of the main advantage of the $RZT^{(m)}$ is that the governing equations are exactly the same of the RZT via PVDs. Moreover, the same formulated finite elements could be used to investigate the structural responses of beams/plates/shells.

Using the $RZT^{(m)}$, Gherlone [117] has investigated the role of the adhesive layer in the static response of sandwich beams, respectively. Moreover, Gherlone [118] has formulated a class of efficient tree-node and four-node plate finite elements for the elastodynamic analysis of multilayered composite and sandwich structures. In Ref. [127], the RZT flat elements have been enhanced with two more degrees of freedom to study shell structures not included in the displacement formulation, i.e., the drilling rotation and drilling zigzag rotation. Similarly, Kefal et al. [119] have implemented a beam element based on the $RZT^{(m)}$ in conjunction with the iso-geometric analysis.

Based on the Hellinger-Reissner functional, Kutlu and co-workers [120,121] have presented a novel mixed-RZT analysing multilayered beams and plates. Despite the higher number of variables used in Kutlu's models [120,121] than the

RZT$^{(m)}$, the high accuracy in stress predictions has been shown even for laminates with several layers and loading conditions.

Groh et al. [122] have applied the RZT to investigate the effect of delamination in laminate composite by introducing a fictitious layer with quasi-null mechanical properties. Later, Groh and Tessler [123] successfully applied the RZT$^{(m)}$ to analyse multilayered composite and sandwich beams with delamination in the lamination stacking sequence.

In sandwich structures, the effect of transverse normal deformability should not be neglected. The effect of transverse normal deformability has not been considered in the previously proposed formulations, focusing more on a better representation of the transverse shear deformability. Barut et al. [124] presented a further enhancement of the RZT in which a quadratic through-the-thickness variation has represented the in-plane and transverse kinematics, while the effect of transverse normal stress has been assumed as a smeared cubic variation in the thickness coordinate. The kinematic variables have been linked to the stress unknowns in the transverse normal distribution using the least-square statement. Then according to the PVDs, the governing equations have been obtained. It results in a simple but accurate model that is able to include in the RZT the transverse normal deformability. The same authors later made a further comparison using triangular finite elements based on the previous higher-order RZT model [125], revealing its accuracy in displacements and stress predictions. Dorduncu et al. [126] have used the {2,2}-RZT in the dynamic analysis of free and forced vibrations of laminate plates.

By using a higher-order kinematics applied to the RZT, Groh and Weaver [127–129] have formulated a mixed model based on the Hellinger-Reissner functional. The assumed transverse shear stress functions are assumed directly from integrating local equilibrium equations without involving the cylindrical bending assumption. In Groh and Weaver's model, the interesting aspect is the derivation of the transverse normal stress field directly by the assumed transverse shear stress by integrating Cauchy's transverse equilibrium equation, but in the displacement field, the transverse displacement component is still through-the-thickness constant.

Recently, Iurlaro and co-workers [130] have proposed a mixed cubic model based on the RZT incorporating transverse normal deformability. The zigzag contribution is superposed to third-order in-plane kinematics, while the transverse

displacement is a smeared parabolic function that interpolates top, bottom and average transverse displacement values. The transverse normal deformability assumes a-priori as a cubic function that satisfies the top and bottom stress tractions, and the transverse shear stress distributions are a-priori functions obtained by integrating Cauchy's equations under the cylindrical bending assumptions. Using the RMVT, the variables of the new stress fields are related to the primary kinematic variables and the governing equations and consistent boundary conditions are obtained. This model, named $RZT^{(m)}_{\{3,2\}}$, has demonstrated to accurately describe the static behaviour of thick multilayered composite and sandwich structures [131,132]. Moreover, its formulation requires only C^0-continuity, and the limited number of kinematic variables makes it computationally less expensive. For a more detailed discussion on the $RZT_{\{3,2\}}^{(m)}$ outcomes, the reader is referred to Iurlaro's thesis [132]

Despite these positive aspects of the RZT model, some negative aspects are encountered. The first one has been highlighted by Krejia and Sabik [133], i.e. the inability of the RZT to investigate a class of laminates characterized by the same absolute value of the lamination angle for all the layers. These laminates, often called angle-ply, are quite used in the aerospace industry. The authors highlighted that the RZT or $RZT^{(m)}$, as it has been formulated, cannot investigate the behaviour of angle-ply multilayered plates since both zigzag functions are through-the-thickness null.

As Tessler et al. [143] showed in quasi-isotropic and angle-ply laminates, the weighted-average transverse shear stiffness coefficients are the same as the transformed transverse shear stiffness coefficients. More specifically, $G_1 \to \tilde{C}_{44}^{(k)}$, $G_2 \to \tilde{C}_{55}^{(k)}$ $(k = 1,...,N)$; thus, also the zigzag functions are required to vanish.

Obviously, this unlikely and undesirable effect is obtained for homogeneous monolayer plates, but in this case, it can be easily managed to adopt the strategy suggested by Tessler et al. [134] by using an appropriate variation of transverse shear properties. Other cases are multilayered symmetric $\left[+\mathrm{Y}/-\mathrm{Y}/+\mathrm{Y}\right]$ and anti-symmetric $\left[+\mathrm{Y}/-\mathrm{Y}\right]$ angle-ply laminated plates. Kreja and Sabik [144] found that this entails the singularity of the stiffness matrix, regardless of the solution method adopted (Navier-type solutions, approximate Ritz and Finite element method).

Moreover, it is clear from the three-dimensional solutions, see Ref. [13], that the zigzag effect is still present for these laminates. In order to overcome this issue, Krejia and Sabik [133] have slightly modified the lamination angle to use the RZT formulation and provide a solution. However, if this aspect could provide a solution for global values like displacements and frequencies, it cannot correctly describe the trough-the-thickness distributions of shear stress. Moreover, the assumption of cylindrical bending, as it has been used to formulate the RZT-mixed model to avoid the inconsistencies of transverse shear stress distributions, is no longer valid for angle-ply laminates. In fact, Pagano's work [5] has shown the strong influence of transverse shear coupling in anisotropic multilayered structures, such as symmetric and anti-symmetric laminates.

1.4 The novelty of this work

In this context, this thesis aims to provide an accurate and complete mathematical zigzag model that can overcome the issues encountered in the previously cited models. The work has been conducted according to the following steps: model formulations, numerical assessments and experimental investigations. More specifically, the main objectives of this research work are:

a. to extend the Refined Zigzag Theory to the analysis of more general structures, including angle-ply and general lamination schemes that in previous formulations are not considered due to the incapacity of computing the zigzag functions. For this problem, Kreja et al. [133] provided a partial solution, numerically valid; however, it is intended in this dissertation to enhance and provide a more complete and variationally consistent approach to this problem;

b. to include the transverse normal deformability, generally included only in a limited number of zigzag models and with expensive computational costs. Moreover, to increase the through-the-thickness predictions of the transverse shear stresses in multilayered structures with a general lamination scheme via a mixed model that overcomes the limitations related to the cylindrical bending assumptions;

c. to formulate accurate and simple finite elements for the static and dynamic analysis of sandwich beam structures, including the new variational formulation for the transverse normal and transverse shear stress distributions;

d. to validate the previous models experimentally and provide new results for static and dynamic analysis of sandwich beams which are barely reported in the current literature.

Chapter 2

The enhanced Refined Zigzag Theory

As highlighted in the previous chapter, the Refined Zigzag Theory (RZT), formulated both by using the PVDs [135] and the RMVT [131], has been demonstrated to be unable to investigate general laminate structures such as multilayered angle-ply laminated structures. It is worth noting that the RZT and RZT$^{(m)}$ have been used by Kreja and Sabik [133] to investigate the bending of simply-supported multilayered plates, with particular attention on the analysis of angle-ply antisymmetric multilayered plates. The approach proposed in Ref. [133] is to perturb the orientations slightly, thus allowing the classical RZT to model angle-ply laminates. Notwithstanding that the method provided by the author is numerically admissible, this thesis intends to provide a more coherent and variationally consistent structural model according to the three-dimensional elasticity solution for these general lamination schemes.

In this Chapter, a new enhanced model based on the Refined Zigzag kinematics is formulated to analyse composite multilayered composites and sandwich plates with more general lamination schemes. In the next Sections, the theoretical background to understand the motivation of this new formulation is presented. The new displacement field is presented in detail, and the enhanced zigzag functions are formulated according to the RZT procedure. Moreover, the governing equations and the consistent boundary conditions of the newly developed model, the enhanced Refined Zigzag Theory (en-RZT), are derived

using the dynamic version of the Principle of Virtual Displacements, i.e. the D'Alembert equations.

This new model can consider the effect of transverse shear coupling by the new set of enhanced zigzag functions in the zigzag kinematics.

Some of this Chapter's contents have been subject to publication in International Journals or presented at International Conferences. More specifically, the formulation of the enhanced Refined Zigzag Theory (en-RZT) and the numerical assessment for the linear static behaviour has been done in Ref. [136]. Furthermore, the extension of the enhanced-RZT to the free-vibration study of multilayered composite has been presented to the 19th International Conference of Numerical Analysis and Applied Mathematics (ICNAAM 2021), and the stability analysis using the Ritz-Method has been reported in Ref. [137].

2.1 Theoretical background

In the literature framework, the effect of transverse shear coupling in multilayered angle-ply structures has been studied by Pagano [5] by providing an exact three-dimensional solution for the static cylindrical bending of these laminates. It has been shown in such cases that the effect of the transverse load is able to influence the structural response also in the other in-plane transverse direction, not only in the longitudinal one.

This coupling effect has been studied since the late 50s by Ambartsumyan [77] in the static analysis of anisotropic multilayered plates. In Ambartsumyan's model, a refinement of the Classical Plate Theory with the inclusion of the transverse shear deformability, the effect of different material anisotropy has been considered. By assuming a-priori, a transverse shear stress distribution for each component, i.e. τ_{13}, τ_{23}, the corresponding transverse shear strains, γ_{13}, γ_{23} are coupled due to the material anisotropy effect. The in-plane displacements are then obtained by integrating the transverse shear strains in which the coupling effect is present. However, as highlighted in Chapter 1, Ambartsumyan's model suffers inaccuracies due to the a-priori parabolic through-the-thickness transverse shear stress functions.

Later, in Di Sciuva's Zigzag Theory (ZZT), the effect of transverse shear coupling in anisotropic multilayered structures was observed differently. As reported in Ref. [81] and in Chapter 1, the zigzag contribution in the displacement

field of Di Sciuva's ZZT is characterized by the satisfaction of transverse shear stress continuities at the layer interfaces. In general, for a multilayered anisotropic laminate with arbitrarily oriented layers, the displacement field can be expressed as follows:

$$\begin{aligned} U_1(\mathbf{x},x_3) &= u(\mathbf{x}) + x_3\left(\gamma_{13}(\mathbf{x}) - w_{,3}(\mathbf{x})\right) + \sum_{k=1}^{N-1}\left(a_k\gamma_{13} + c_k\gamma_{23}\right)\left(x_3 - x_{3B}^{(k)}\right)H\left(x_3 - x_{3B}^{(k)}\right) \\ U_2(\mathbf{x},x_3) &= v(\mathbf{x}) + x_3\left(\gamma_{23}(\mathbf{x}) - w_{,3}(\mathbf{x})\right) + \sum_{k=1}^{N-1}\left(d_k\gamma_{13} + b_k\gamma_{23}\right)\left(x_3 - x_{3B}^{(k)}\right)H\left(x_3 - x_{3B}^{(k)}\right) \\ U_3(\mathbf{x},x_3) &= w(\mathbf{x}) \end{aligned} \tag{2.1}$$

where a_k, b_k, c_k, d_k are constant depending only on the mechanical properties of the various layer. It is worth noting in Eq. (2.1) the explicit dependence of the in-plane displacements by the transverse shear strains. Moreover, the effect of transverse shear stress coupling in enforcing the transverse shear stress continuity is clearly evident from the c_k, d_k coefficients. The superiority prediction regarding through-the-thickness displacements and stresses, fundamental frequencies and buckling loads of the ZZT, especially for the multilayered anisotropic multilayered plates, has been demonstrated by works of the same author [80,84,87,138].

Similarly, Cho and Parmerter [85,86] have reached the same conclusions as Di Sciuva's model in the transverse shear coupling effect described in the in-plane displacements due to the transverse shear anisotropy.

Moreover, Shu and Soldatos [139] have investigated the cylindrical bending of angle-ply laminates with different boundary conditions. Starting from a similar kinematics of a ZZT and under the cylindrical bending hypotheses, the displacement field, as reported in Ref. [139], reads:

$$\begin{aligned} U_1(x_1,x_3) &= u(x_1) - x_3 w_{,3}(x_1) + \varphi_1(x_3)u_1(x_1) \\ U_2(x_1,x_3) &= v(x_1) + \varphi_2(x_3)u_2(x_1) \\ U_3(x_1,x_3) &= w(x_1) \end{aligned} \tag{2.2}$$

where the functions $\varphi_1(x_3)$ and $\varphi_2(x_3)$ are derived by the three-dimensional local equilibrium equations. Notwithstanding the good results provided in Ref. [139], the solution of Shu and Soldatos can be obtained only under the hypothesis of cylindrical bending of the structure, which is not applicable to more general

cases. A further generalization to the plates structures has been made by Messina and Soldatos [140], where the effect of transverse shear coupling has been guaranteed by two conditions: the inclusion of two more global shape functions which are determined a-posteriori satisfying the transverse shear stress continuity, and the coupling of the in-plane displacements using two related unknown variables. The proposed model in Ref. [142] involves the same number of variables and continuity conditions of Di Sciuva's ZZT to define the global shape functions. The work of Kim and Cho represents another example in the literature framework regarding the transverse shear coupling [141] in which the first-order kinematic has been enhanced with third-order zigzag functions, similar to the higher-order zigzag model of Ref. [89]. The accuracy of the first-order model has been increased in a least square sense with the three-dimensional theory.

In Loredo's model [142], a new set of through-the-thickness functions, named warping shear functions, has been formulated to predict both the transverse shear deformability and the transverse shear coupling typical of anisotropic plates. These functions are formulated using an energetic variational approach without any a-priori assumption on their shapes. However, they provided a system of partial differential equations that is able to compute the warping faction only for very few cases. Based on these considerations, Loredo and Castel [145] have reformulated the previous model to provide an accurate solution for more general lamination cases. Loredo and co-workers have dedicated many efforts to the warping functions definitions, relative assessments and comparisons, attested by the published works [143–145]. It is highlighted that the model's accuracy is inherent to the warping function definitions, not only in the model's kinematics.

It is, therefore, evident how the role of appropriate through-the-thickness shape or warping functions plays in the correct evaluation of the transverse shear coupling in the multilayered laminate response when anisotropic materials are considered in the lamination. Moreover, Di Sciuva's Zigzag model has been considered an inspiration since it can provide the necessary information regarding how to enhance the zigzag contribution of the Refined Zigzag Theory to consider the transverse shear coupling.

Based on the generalization of the original Di Sciuva's ZZT in conjunction with the formulation of the zigzag functions of RZT, a new set of warping shear functions for the RZT kinematics is defined in the following.

2.2 Geometrical preliminaries, displacement field, strains and stresses

2.2.1 Plate notation

In this paragraph, some basic notations related to the zigzag plate model are recalled. It is considered a multilayered flat plate of N perfectly bonded orthotropic layers. The coordinate system is taken as reference where the thickness coordinate x_3 ranges from $-h/2$ to $+h/2$. In Figure 8, Ω is the middle reference surface and Γ is its perimeter. Moreover, in Figure 8 the kinematic variables and their positive verse are also reported according to the Cartesian coordinate system. Finally, the reader is referred to the preliminary section for a more detailed overview of the other quantities (geometry, loads and layer notations).

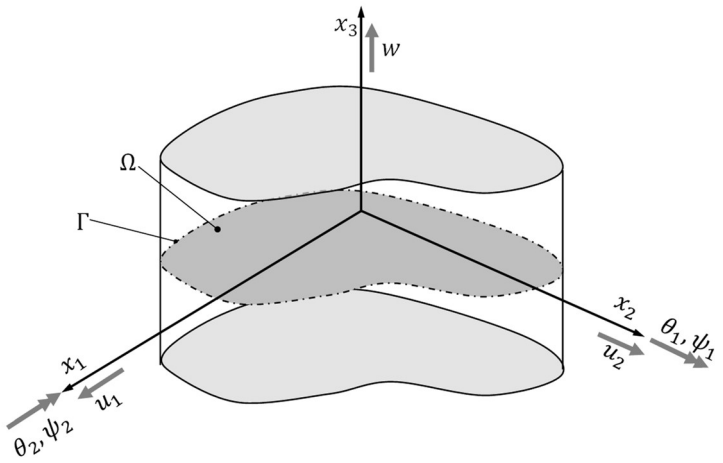

Figure 8: Plate coordinate system and kinematic variable representation.

2.2.2 Kinematic assumptions of the enhanced Refined Zigzag Theory

The enhanced Refined Zigzag Theory (en-RZT), following the standard RZT kinematics [135], is based on the superposition of a Global (G) first-order kinematics and a Local (L) layer-wise correction of the in-plane displacements. The global contribution is a through-the-thickness linear function that does not depend on the laminate properties. The local contribution is a through-the-

thickness piecewise linear function of the transverse coordinate x_3 with jumps in the first derivatives across the interfaces between two adjacent layers.

Such as done in the standard RZT model, the transverse normal deformability is neglected in enhanced Refined Zigzag Theory, i.e. $\varepsilon_{33}=0$; thus, the transverse deflection is considered uniform along the whole laminate thickness.

According to these assumptions, the enhanced RZT displacement field reads:

$$\begin{aligned}\widehat{\mathbf{U}}^{(k)}(\mathbf{X};t) &= \tilde{\mathbf{u}}^{G}(\mathbf{X};t)+\tilde{\mathbf{u}}^{L(k)}(\mathbf{X};t)\\ U_3^{(k)}(\mathbf{X};t) &= w(\mathbf{x};t)\end{aligned} \tag{2.3}$$

where,

$$\begin{aligned}\tilde{\mathbf{u}}^{G}(\mathbf{X};t) &= \mathbf{u}(\mathbf{x};t)+x_3\boldsymbol{\theta}(\mathbf{x};t)\\ \tilde{\mathbf{u}}^{L(k)}(\mathbf{X};t) &= \boldsymbol{\varphi}^{(k)}(x_3)\boldsymbol{\psi}(\mathbf{x};t)\end{aligned} \tag{2.4}$$

Furthermore, in Eq. (2.4) the expressions of the various contributions read:

$$\tilde{\mathbf{u}}^{(k)}(\mathbf{X};t)=\begin{Bmatrix}\tilde{u}_1(\mathbf{X};t)\\ \tilde{u}_2(\mathbf{X};t)\end{Bmatrix}^{(k)};\ \mathbf{u}(\mathbf{x};t)=\begin{Bmatrix}u_1(\mathbf{x};t)\\ u_2(\mathbf{x};t)\end{Bmatrix};\ \boldsymbol{\theta}(\mathbf{x};t)=\begin{Bmatrix}\theta_1(\mathbf{x};t)\\ \theta_2(\mathbf{x};t)\end{Bmatrix} \tag{2.5}$$

$$\boldsymbol{\varphi}^{(k)}(x_3)=\begin{bmatrix}\phi_{11}^{(k)}(x_3) & \phi_{12}^{(k)}(x_3)\\ \phi_{21}^{(k)}(x_3) & \phi_{22}^{(k)}(x_3)\end{bmatrix};\ \boldsymbol{\psi}(\mathbf{x};t)=\begin{Bmatrix}\psi_1(\mathbf{x};t)\\ \psi_2(\mathbf{x};t)\end{Bmatrix} \tag{2.6}$$

In Eq. (2.5) $\mathbf{u}(\mathbf{x};t)$ and $\boldsymbol{\theta}(\mathbf{x};t)$ are the global in-plane uniform displacements and rotations of the normal to the reference plane about the positive x_2 and the negative x_1 directions, respectively; $w(\mathbf{x};t)$ is the uniform transverse displacements; $\boldsymbol{\psi}(\mathbf{x};t)$ denotes the matrix of the unknown zigzag rotations of the $\boldsymbol{\varphi}^{(k)}(x_3)$ zigzag functions, these last being assumed piecewise linear functions through-the-thickness, vanishing on the top and bottom surfaces of the plate, i.e. $\boldsymbol{\varphi}^{(1)}(-h/2)=\boldsymbol{\varphi}^{(N)}(+h/2)=\mathbf{0}$.

The kinematic field of the en-RZT involves only seven kinematic variables, like the standard RZT, but it involves two more zigzag functions that should be considered in the zigzag formulation.

The en-RZT differs from the RZT in the $\boldsymbol{\varphi}^{(k)}(x_3)$ matrix expressed in Eq. (2.6), in the off-diagonal terms. In the en-RZT, since the transverse shear coupling is included in the model, the in-plane local displacement contributions due to the zigzag rotation are coupled. For the sake of clarity, it is here reported the same $\boldsymbol{\varphi}^{(k)}(x_3)$ matrix, according to the standard RZT kinematics:

$$\boldsymbol{\varphi}^{(k)}(x_3)=\begin{bmatrix}\phi_1^{(k)}(x_3) & 0\\ 0 & \phi_2^{(k)}(x_3)\end{bmatrix} \tag{2.7}$$

Moreover, the first derivatives of the enhanced zigzag functions from Eq. (2.6), i.e. the zigzag slopes, according to the RZT notation, read:

$$\boldsymbol{\beta}^{(k)}(x_3)=\frac{\partial\boldsymbol{\varphi}^{(k)}(x_3)}{\partial x_3}=\begin{bmatrix}\beta_{11}^{(k)} & \beta_{12}^{(k)}\\ \beta_{21}^{(k)} & \beta_{22}^{(k)}\end{bmatrix} \tag{2.8}$$

It is obvious that due to the zigzag function definition, Eq. (2.8) , the through-the-thickness zigzag slopes are piecewise constant functions with jumps at the interfaces. Therefore, the zigzag slopes are defined in the next section according to the RZT procedure.

2.2.3 Strains and stresses relations

Consistent with the linear strain-displacement relations introduced in the preliminaries, the en-RZT strain components read:

$$\begin{aligned}\boldsymbol{\varepsilon}_p^{(k)}\left(\mathbf{x},x_3;t\right)&=\begin{Bmatrix}U_{1,1}^{(k)}\left(\mathbf{x},x_3;t\right)\\ U_{2,2}^{(k)}\left(\mathbf{x},x_3;t\right)\\ U_{1,2}^{(k)}\left(\mathbf{x},x_3;t\right)+U_{2,1}^{(k)}\left(\mathbf{x},x_3;t\right)\end{Bmatrix}=\begin{Bmatrix}\varepsilon_{11}^{(k)}\left(\mathbf{x},x_3;t\right)\\ \varepsilon_{22}^{(k)}\left(\mathbf{x},x_3;t\right)\\ \gamma_{12}^{(k)}\left(\mathbf{x},x_3;t\right)\end{Bmatrix}\\ \boldsymbol{\gamma}_t^{(k)}\left(\mathbf{x},x_3;t\right)&=\begin{Bmatrix}U_{1,3}^{(k)}\left(\mathbf{x},x_3;t\right)+U_{3,1}\left(\mathbf{x},x_3;t\right)\\ U_{2,3}^{(k)}\left(\mathbf{x},x_3;t\right)+U_{3,2}\left(\mathbf{x},x_3;t\right)\end{Bmatrix}=\begin{Bmatrix}\gamma_{13}^{(k)}\left(\mathbf{x},x_3;t\right)\\ \gamma_{23}^{(k)}\left(\mathbf{x},x_3;t\right)\end{Bmatrix}\end{aligned} \tag{2.9}$$

By taking into account the enhanced RZT kinematics, i.e. Eqs. (2.3)-(2.6), Eq. (2.9) can be rewritten:

$$\begin{aligned}\boldsymbol{\varepsilon}_{\mathrm{p}}^{(k)}\left(\mathbf{x},x_3;t\right)&=\boldsymbol{\varepsilon}_m\left(\mathbf{x};t\right)+x_3\boldsymbol{\varepsilon}_\theta\left(\mathbf{x};t\right)+\boldsymbol{\Phi}^{(k)}(x_3)\boldsymbol{\varepsilon}_\psi\left(\mathbf{x};t\right)\\ \boldsymbol{\gamma}_t^{(k)}\left(\mathbf{x},x_3;t\right)&=\boldsymbol{\gamma}^{(0)}\left(\mathbf{x};t\right)+\boldsymbol{\beta}^{(k)}(x_3)\boldsymbol{\psi}\left(\mathbf{x};t\right)\end{aligned} \tag{2.10}$$

where

$$\begin{aligned}\boldsymbol{\varepsilon}_m^T(\mathbf{x};t) &= \lfloor u_{1,1}(\mathbf{x};t) \quad u_{2,2}(\mathbf{x};t) \quad u_{1,2}(\mathbf{x};t)+u_{2,1}(\mathbf{x};t) \rfloor \\ \boldsymbol{\varepsilon}_\theta^T(\mathbf{x};t) &= \lfloor \theta_{1,1}(\mathbf{x};t) \quad \theta_{2,2}(\mathbf{x};t) \quad \theta_{1,2}(\mathbf{x};t)+\theta_{2,1}(\mathbf{x};t) \rfloor\end{aligned} \tag{2.11}$$

$$\begin{aligned}\boldsymbol{\varepsilon}_\psi^T(\mathbf{x};t) &= \lfloor \psi_{1,1}(\mathbf{x};t) \quad \psi_{2,2}(\mathbf{x};t) \quad \psi_{1,2}(\mathbf{x};t) \quad \psi_{2,1}(\mathbf{x};t) \rfloor \\ \boldsymbol{\Phi}^{(k)}(x_3) &= \begin{bmatrix} \phi_{11}^{(k)}(x_3) & 0 & 0 & \phi_{12}^{(k)}(x_3) \\ 0 & \phi_{22}^{(k)}(x_3) & \phi_{21}^{(k)}(x_3) & 0 \\ \phi_{21}^{(k)}(x_3) & \phi_{12}^{(k)}(x_3) & \phi_{11}^{(k)}(x_3) & \phi_{22}^{(k)}(x_3) \end{bmatrix}\end{aligned} \tag{2.12}$$

$$\boldsymbol{\gamma}^{(0)}(\mathbf{x};t) = \begin{Bmatrix} \gamma_1^{(0)}(\mathbf{x};t) \\ \gamma_2^{(0)}(\mathbf{x};t) \end{Bmatrix} = \begin{Bmatrix} \theta_1(\mathbf{x};t)+w_{,1}(\mathbf{x};t) \\ \theta_2(\mathbf{x};t)+w_{,2}(\mathbf{x};t) \end{Bmatrix} = \boldsymbol{\theta}(\mathbf{x};t)+\partial\mathbf{w}(\mathbf{x};t) \tag{2.13}$$

and $\partial\mathbf{w}^T(\mathbf{x};t) = \lfloor w_{,1}(\mathbf{x};t) \quad w_{,2}(\mathbf{x};t) \rfloor$.

As usual in plate theories applied to thin and moderately thick structures, the transverse normal stress is neglected, i.e. $\sigma_{33} = 0$. According to this assumption, the linear elastic constitutive relations are written as follows:

$$\begin{aligned}\boldsymbol{\sigma}_p^{(k)}(\mathbf{x},x_3;t) &= \breve{\mathbf{C}}_p^{(k)}\boldsymbol{\varepsilon}^{(k)}(\mathbf{x},x_3;t) \\ \boldsymbol{\tau}_t^{(k)}(\mathbf{x},x_3;t) &= \breve{\mathbf{C}}_t^{(k)}\boldsymbol{\gamma}_t^{(k)}(\mathbf{x},x_3;t)\end{aligned} \tag{2.14}$$

where

$$\begin{aligned}\boldsymbol{\sigma}_p^{(k)}(\mathbf{x},x_3;t) &= \begin{Bmatrix} \sigma_{11}^{(k)}(\mathbf{x},x_3;t) \\ \sigma_{22}^{(k)}(\mathbf{x},x_3;t) \\ \tau_{12}^{(k)}(\mathbf{x},x_3;t) \end{Bmatrix} \\ \boldsymbol{\tau}_t^{(k)}(\mathbf{x},x_3;t) &= \begin{Bmatrix} \tau_{13}^{(k)}(\mathbf{x},x_3;t) \\ \tau_{23}^{(k)}(\mathbf{x},x_3;t) \end{Bmatrix}\end{aligned} \tag{2.15}$$

are the in-plane and the transverse shear stresses, respectively. Moreover,

$$\breve{\mathbf{C}}_p^{(k)} = \begin{bmatrix} \breve{C}_{11} & \breve{C}_{12} & \breve{C}_{16} \\ \breve{C}_{12} & \breve{C}_{22} & \breve{C}_{26} \\ \breve{C}_{16} & \breve{C}_{26} & \breve{C}_{66} \end{bmatrix}^{(k)} \tag{2.16}$$

$$\breve{\mathbf{C}}_t^{(k)} = \begin{bmatrix} \breve{C}_{44} & \breve{C}_{45} \\ \breve{C}_{45} & \breve{C}_{55} \end{bmatrix}^{(k)} \tag{2.17}$$

As highlighted in the preliminary section, Eqs. (2.16) and (2.17) are, respectively, the in-plane reduced and transverse shear elastic stiffness coefficients of the k^{th} layer expressed in the plate axes.

2.2.4 Derivation of the enhanced zigzag functions

In the following, the enhanced zigzag functions are constructed using the typical procedure adopted by the standard RTZ but applied to the new set of functions.

The ingredients of the zigzag formulations involve the expression of the transverse shear strains and stresses. For the sake of clarity, they are here briefly recalled in a simplified version:

$$\begin{aligned} \boldsymbol{\gamma}_t^{(k)} &= \boldsymbol{\gamma}^{(0)} + \boldsymbol{\beta}^{(k)} \boldsymbol{\psi} \\ \boldsymbol{\tau}_t^{(k)} &= \breve{\mathbf{C}}_t^{(k)} \boldsymbol{\gamma}_t^{(k)} \end{aligned} \tag{2.18}$$

According to the standard RZT, the auxiliary strain measure vector is introduced here:

$$\boldsymbol{\eta}(\mathbf{x};t) = \boldsymbol{\gamma}^{(0)}(\mathbf{x};t) - \boldsymbol{\psi}(\mathbf{x};t) \tag{2.19}$$

where $\boldsymbol{\eta}^T(\mathbf{x};t) = \lfloor \eta_1(\mathbf{x};t) \quad \eta_2(\mathbf{x};t) \rfloor$.

By substituting Eq. (2.19) into the expression of the transverse shear strains, see Eq. (2.18), it is possible to rewrite it in terms of the auxiliary strain measures and the zigzag rotations:

$$\boldsymbol{\gamma}_t^{(k)}(\mathbf{x};t) = \boldsymbol{\eta}(\mathbf{x};t) + \left(\mathbf{I} + \boldsymbol{\beta}^{(k)}\right)\boldsymbol{\psi}(\mathbf{x};t) \tag{2.20}$$

where $\mathbf{I}$ stands for the identity matrix.

Substituting Eq. (2.20) into the second Eq. (2.18), the transverse shear stresses read:

$$\begin{aligned}\boldsymbol{\tau}_t^{(k)}\left(\mathbf{x};t\right) &= \breve{\mathbf{C}}_t^{(k)}\left[\boldsymbol{\eta}\left(\mathbf{x};t\right)+\left(\mathbf{I}+\boldsymbol{\beta}^{(k)}\right)\boldsymbol{\psi}\left(\mathbf{x};t\right)\right]= \\ &= \breve{\mathbf{C}}_t^{(k)}\boldsymbol{\eta}\left(\mathbf{x};t\right)+\breve{\mathbf{C}}_t^{(k)}\left(\mathbf{I}+\boldsymbol{\beta}^{(k)}\right)\boldsymbol{\psi}\left(\mathbf{x};t\right)\end{aligned} \tag{2.21}$$

In Eq. (2.21), two main contributions can be seen: the first is related to the auxiliary strain measure, and the second is related only to the zigzag rotations. Since the auxiliary strain measure is only dependent on the in-plane coordinate, it is a trough-the-thickness constant value; thus, the first contribution of the transverse shear stresses is a through-the-thickness constant and not continuous function, with jumps at the interfaces due to the transverse material anisotropy. The second term depends on the zigzag slopes, which are not yet defined. Although, according to the RZT, the interlaminar transverse shear continuity has been only partially satisfied [135], with the reference of Eq. (2.21) , only the second term is enforced to be continuous at the layer interfaces. It should be noted that if the auxiliary strain measure is enforced to be null, i.e. $\boldsymbol{\eta}=\mathbf{0}$ $\boldsymbol{\psi}(\mathbf{x};t)=\boldsymbol{\gamma}^{(0)}(\mathbf{x};t)$, the zigzag functions of the original ZZT are re-obtained since the transverse shear stress continuity is satisfied across the entire laminate thickness.

Based on these considerations, Eq. (2.21) can be rewritten, highlighting the two contributions:

$$\begin{aligned}\boldsymbol{\tau}_t^{(k)}\left(\mathbf{x};t\right) &= \breve{\mathbf{C}}_t^{(k)}\boldsymbol{\eta}\left(\mathbf{x};t\right)+\breve{\mathbf{C}}_t^{(k)}\left(\mathbf{I}+\boldsymbol{\beta}^{(k)}\right)\boldsymbol{\psi}\left(\mathbf{x};t\right)= \\ &= \boldsymbol{\tau}_t^{D(k)}\left(\mathbf{x},x_3;t\right)+\boldsymbol{\tau}_t^{C(k)}\left(\mathbf{x},x_3;t\right)\end{aligned} \tag{2.22}$$

where $\boldsymbol{\tau}_t^{C(k)}\left(\mathbf{x},x_3;t\right)=\breve{\mathbf{C}}_t^{(k)}\left(\mathbf{I}+\boldsymbol{\beta}^{(k)}\right)\boldsymbol{\psi}\left(\mathbf{x};t\right)$ is the through-the-thickness continuous term.

Enforcing the continuity conditions on $\boldsymbol{\tau}_t^{C(k)}$ contribution at each layer interface, i.e. $\boldsymbol{\tau}_t^{C(k)}\left(x_{3(T)}^{(k)}\right)=\boldsymbol{\tau}_t^{C(k+1)}\left(x_{3(B)}^{(k+1)}\right)$, and recalling the expression of the continuous part, it reads:

$$\breve{\mathbf{C}}_t^{(k)}\left(\mathbf{I}+\boldsymbol{\beta}^{(k)}\right)\boldsymbol{\psi}\left(\mathbf{x};t\right)=\breve{\mathbf{C}}_t^{(k+1)}\left(\mathbf{I}+\boldsymbol{\beta}^{(k+1)}\right)\boldsymbol{\psi}\left(\mathbf{x};t\right)=\mathbf{G}\boldsymbol{\psi}\left(\mathbf{x};t\right) \tag{2.23}$$

where $\mathbf{G}$ is a (2x2) matrix of the zigzag weighted-average transverse shear moduli of the whole plate. These values are independent of the layer, and the

matrix is not diagonal for a general lamination scheme in which the coupling transverse shear effect is present.

By solving Eq. (2.23) for $\boldsymbol{\beta}^{(k)}$ of the k^{th} layer, the expression of the enhanced zigzag slopes matrix reads:

$$\boldsymbol{\beta}^{(k)} = \mathbf{S}_t^{(k)}\mathbf{G} - \mathbf{I} \tag{2.24}$$

where $\mathbf{S}_t^{(k)} = \left(\breve{\mathbf{C}}_t^{(k)}\right)^{-1}$ is the symmetric matrix of the transverse shear compliance coefficients of the k^{th} layer.

Integrating Eq. (2.24) over the whole laminate thickness yields

$$\int_{x_{3(\text{B})}}^{x_{3(\text{T})}} \boldsymbol{\beta}^{(k)} dx_3 = \boldsymbol{\varphi}^{(N)}(x_{3(\text{T})}) - \boldsymbol{\varphi}^{(1)}(x_{3(\text{B})}) \tag{2.25}$$

Eq. (2.25) shows that only two free additional conditions are necessary to determine the zigzag functions uniquely. As in the standard RZT, we exploit this freedom by adding the condition that the local contribution is zero on the top and bottom surfaces of the whole plate, i.e.,

$$\tilde{\mathbf{u}}^{L(1)}(x_{3(B)}) = \tilde{\mathbf{u}}^{L(N)}(x_{3(T)}) = \mathbf{0} \tag{2.26}$$

from which (see, Eqs. (2.4) and (2.6))

$$\boldsymbol{\varphi}^{(N)}(x_{3(\text{T})}) - \boldsymbol{\varphi}^{(1)}(x_{3(\text{B})}) = \mathbf{0} \tag{2.27}$$

and, as a consequence,

$$\int_{x_{3(\text{B})}}^{x_{3(\text{T})}} \boldsymbol{\beta}^{(k)} dx_3 = \mathbf{0} \tag{2.28}$$

By considering the expression of the enhanced zigzag slopes, i.e. Eq. (2.24) and substituting it into Eq. (2.28), yields

$$\int_{x_{3(\text{B})}}^{x_{3(\text{T})}} \left(\mathbf{S}_{\text{t}}^{(k)}\mathbf{G} - \mathbf{I}\right) dx_3 = \mathbf{0} \;\Rightarrow\; \left(\sum_{k=1}^{N} \int_{x_{3(\text{B})}^{(k)}}^{x_{3(\text{T})}^{(k)}} \mathbf{S}_{\text{t}}^{(k)} dx_3\right)\mathbf{G} = \int_{x_{(\text{B})}}^{x_{3(\text{T})}} \mathbf{I} dx_3 \tag{2.29}$$

From which

$$\mathbf{G} = \left(x_{3(\text{T})} - x_{3(\text{B})}\right)\left(\sum_{k=1}^{N} (x_{3(\text{T})}^{(k)} - x_{3(\text{B})}^{(k)})\mathbf{S}_{\text{t}}^{(k)}\right)^{-1} = h\left(\sum_{k=1}^{N} h^{(k)}\mathbf{S}_{\text{t}}^{(k)}\right)^{-1} \tag{2.30}$$

Substituting Eq. (2.30) into Eq. (2.24), integrating over the thickness yields

$$\boldsymbol{\varphi}^{(k)}(x_3)-\boldsymbol{\varphi}^{(k)}\left(x_{3(\mathrm{B})}^{(k)}\right)=\left(x_3-x_{3(\mathrm{B})}^{(k)}\right)\left(\mathbf{S}_{\mathrm{t}}^{(k)}\mathbf{G}-\mathbf{I}\right)\quad\left(x_{3(B)}^{(k)}\le x_3\le x_{3(T)}^{(k)}\right)\tag{2.31}$$

with

$$x_{3(B)}^{(k)}=x_{3(B)}+\sum_{q=1}^{k-1}(x_{3(T)}^{(q)}-x_{3(B)}^{(q)})=x_{3(B)}+\sum_{q=1}^{k-1}h^{(q)}\qquad k=2,3,...,N\tag{2.32}$$

It is easy to show that Eq. (2.31) can be cast in the following recursive formula

$$\begin{aligned}\boldsymbol{\varphi}^{(k)}(x_3)&=\left(x_3-x_{3(\mathrm{B})}\right)\left(\mathbf{S}_{\mathrm{t}}^{(k)}\mathbf{G}-\mathbf{I}\right)+\sum_{q=1}^{k}h^{(q)}\left(\mathbf{S}_{\mathrm{t}}^{(q)}-\mathbf{S}_{\mathrm{t}}^{(k)}\right)\mathbf{G}\\&=\left(x_3-x_{3(\mathrm{B})}\right)\boldsymbol{\beta}^{(k)}+\sum_{q=1}^{k}h^{(q)}\left(\boldsymbol{\beta}^{(q)}-\boldsymbol{\beta}^{(k)}\right)\qquad(k=1,...,N)\end{aligned}\tag{2.33}$$

2.3 Governing equations and boundary conditions

The governing equations and the variationally consistent boundary conditions are derived here using the dynamic version of the principle of virtual work (D'Alembert principle).

The principle can be stated as follows (here δ stands for the variational operator):

$$\delta W_{\mathrm{int}}-\delta W_{\mathrm{ext}}+\delta W_{\mathrm{inp}}=\delta W_{\mathrm{in}}\tag{2.34}$$

where

$$\delta W_{\mathrm{int}}=\int_V\left(\boldsymbol{\sigma}_p^{(k)T}\delta\boldsymbol{\varepsilon}_p^{(k)}+\boldsymbol{\tau}_t^{(k)T}\delta\boldsymbol{\gamma}_t^{(k)}\right)dV\tag{2.35}$$

is the virtual variation of the internal work given by the stresses;

$$\delta W_{\mathrm{in}}=-\int_\Omega\left\langle\rho^{(k)}(x_3)\delta\mathbf{U}^T\ddot{\mathbf{U}}\right\rangle d\Omega\tag{2.36}$$

is the virtual variation of the work done by the inertia forces. In Eq. (2.36), $\rho^{(k)}(x_3)$ is the material mass density; the overdot indicates differentiation with respect to the time. Moreover,

$$\delta W_{\text{inp}} = \int_{\Omega} \left(\overline{P}_{11} w_{,1} \boldsymbol{\delta} w_{,1} + \overline{P}_{22} w_{,2} \boldsymbol{\delta} w_{,2} + \overline{P}_{12} w_{,1} \boldsymbol{\delta} w_{,2} + \overline{P}_{12} w_{,2} \boldsymbol{\delta} w_{,1} \right) d\Omega \tag{2.37}$$

is the virtual variation of the work done by the in-plane applied loads in the buckling mode (linearized stability equations). It is assumed that the plate is loaded by uniformly distributed in-plane normal loads for unit length, which vary neither in magnitude nor direction during buckling.

Normally, it is known that for general lamination plates, there is bending and stretching coupling [2]; thus, the plate will not remain flat in the pre-buckling state. However, as explained in Refs. [146–148], the antisymmetric multilayered plates remain flat for in-plane compressive loads and under the edges constraints corresponding to simply-supported and clamped cases.

Furthermore, δW_{ext} is the virtual variation of the work done by the applied loads

$$\delta W_{\text{ext}} = \int_{\Omega} \left(\overline{\mathbf{p}}_{(\text{B})}^{T} \boldsymbol{\delta} \mathbf{U}_{(\text{B})} + \overline{\mathbf{p}}_{(\text{T})}^{T} \delta \mathbf{U}_{(\text{T})} \right) d\Omega + \int_{\Gamma_{\sigma}} \left\langle \overline{\mathbf{F}}^{T} \delta \mathbf{U} \right\rangle d\Gamma \tag{2.38}$$

where

$$\begin{aligned} \overline{\mathbf{p}}_{(\text{B})}^{T}(\mathbf{x};t) &= \lfloor \, \overline{p}_{1(\text{B})}(\mathbf{x};t) \quad \overline{p}_{2(\text{B})}(\mathbf{x};t) \quad \overline{p}_{3(\text{B})}(\mathbf{x};t) \, \rfloor \\ \overline{\mathbf{p}}_{(\text{T})}^{T}(\mathbf{x};t) &= \lfloor \, \overline{p}_{1(\text{T})}(\mathbf{x};t) \quad \overline{p}_{2(\text{T})}(\mathbf{x};t) \quad \overline{p}_{3(\text{T})}(\mathbf{x};t) \, \rfloor \end{aligned} \tag{2.39}$$

are the applied surface loads on the bottom (B) and on the top (T) surfaces of the plate; $\mathbf{U}_{(\text{B})}$ and $\mathbf{U}_{(\text{T})}$ are the displacements at bottom and top external surfaces, respectively, and

$$\overline{\mathbf{F}}^{T}(\mathbf{x};t) = \lfloor \, \overline{F}_1(\mathbf{x};t) \quad \overline{F}_2(\mathbf{x};t) \quad \overline{F}_3(\mathbf{x};t) \, \rfloor \tag{2.40}$$

For the sake of simplicity, it is assumed that only the transverse load is acting on the plate. Since the effect of transverse normal deformability is neglected, it is irrelevant if the transverse applied load is acting on the top or the bottom external

surface; the resultant value is considered as follows: $\overline{p}_3 = \overline{p}_{3(\mathrm{T})} + \overline{p}_{3(\mathrm{B})}$. In addition, the integration along the thickness direction shown in the previous formulas can be performed according to the following expression $\langle \bullet \rangle = \sum_{k=1}^{N} \int_{x_3^{(k-1)}}^{x_3^{(k)}} (\bullet) dx_3 = \sum_{k=1}^{N} \int_{x_{3(\mathrm{B})}^{(k)}}^{x_{3(\mathrm{T})}^{(k)}} (\bullet) dx_3$.

Substituting the expression of the in-plane and transverse shear stresses (2.14) and strain relations (2.10) into Eq. (2.35) and integrating along the thickness direction, yields

$$\delta W_{\mathrm{int}} = \int_{\Omega} \left(\mathbf{N}^T \delta \boldsymbol{\varepsilon}_m + \mathbf{M}^T \delta \boldsymbol{\varepsilon}_\theta + \mathbf{M}^{\phi T} \delta \boldsymbol{\varepsilon}_\psi + \mathbf{Q}^T \boldsymbol{\gamma}^{(0)} + \mathbf{Q}^{\phi T} \boldsymbol{\psi} \right) d\Omega \tag{2.41}$$

In Eq. (2.41) , the following force and moment stress resultants for unit length have been introduced

$$\left(\mathbf{N}, \mathbf{M}, \mathbf{M}^{\boldsymbol{\phi}} \right) = \left(\begin{Bmatrix} N_{11} \\ N_{22} \\ N_{12} \end{Bmatrix}, \begin{Bmatrix} M_{11} \\ M_{22} \\ M_{12} \end{Bmatrix}, \begin{Bmatrix} M_{11}^{\boldsymbol{\phi}} \\ M_{22}^{\boldsymbol{\phi}} \\ M_{12}^{\boldsymbol{\phi}} \\ M_{21}^{\boldsymbol{\phi}} \end{Bmatrix} \right) = \left\langle \left(1, x_3, \boldsymbol{\varphi}^{(k)T} \right) \boldsymbol{\sigma}_{\mathrm{p}}^{(k)} \right\rangle \tag{2.42}$$

$$\left(\mathbf{Q}, \mathbf{Q}^{\boldsymbol{\phi}} \right) = \left(\begin{Bmatrix} Q_1 \\ Q_2 \end{Bmatrix}, \begin{Bmatrix} Q_1^{\boldsymbol{\phi}} \\ Q_2^{\boldsymbol{\phi}} \end{Bmatrix} \right) = \left\langle \left(1, \boldsymbol{\beta}^{(k)} \right) \boldsymbol{\tau}_t^{(k)} \right\rangle \tag{2.43}$$

Regarding the virtual work done by inertia forces, substituting Eq. (2.3) into Eq. (2.36), yields

$$\delta W_{\mathrm{in}} = -\int_{\Omega} \begin{bmatrix} \delta \mathbf{u}^T \mathbf{m}^{(0)} \ddot{\mathbf{u}} + \delta \mathbf{u}^T \mathbf{m}^{(1)} \ddot{\boldsymbol{\theta}} + \delta \mathbf{u}^T \mathbf{m}_\phi^{(0)} \ddot{\boldsymbol{\psi}} + \\ + \delta \boldsymbol{\theta}^T \mathbf{m}^{(1)} \ddot{\mathbf{u}} + \delta \boldsymbol{\theta}^T \mathbf{m}^{(2)} \ddot{\boldsymbol{\theta}} + \delta \boldsymbol{\theta}^T \mathbf{m}_\phi^{(1)} \ddot{\boldsymbol{\psi}} + \\ + \delta \boldsymbol{\psi}^T \mathbf{m}_\phi^{(0)T} \ddot{\mathbf{u}} + \delta \boldsymbol{\psi}^T \mathbf{m}_\phi^{(1)T} \ddot{\boldsymbol{\theta}} + \delta \boldsymbol{\psi}^T \mathbf{m}_\phi^{(2)} \ddot{\boldsymbol{\psi}} + \delta w m^{(0)} \ddot{w} \end{bmatrix} d\Omega \tag{2.44}$$

where the inertia resultants are defined as follows:

$$\begin{aligned} & m^{(0)} = \left\langle \rho^{(k)} \right\rangle; \quad \left(\mathbf{m}^{(0)}, \mathbf{m}^{(1)}, \mathbf{m}^{(0)} \right) = \left\langle \rho^{(k)} (1, x_3, x_3^2) \right\rangle \mathbf{I}; \\ & \left(\mathbf{m}_\phi^{(0)}, \mathbf{m}_\phi^{(1)}, \mathbf{m}_\phi^{(2)} \right) = \left\langle \rho^{(k)} (\mathbf{I}, x_3 \mathbf{I}, \boldsymbol{\varphi}^{(k)T}) \boldsymbol{\varphi}^{(k)} \right\rangle \end{aligned} \tag{2.45}$$

Finally,

$$\delta W_{\text{ext}} = \int_{\Omega} \left(\overline{p}_i \, \delta u_i + \overline{m}_\alpha \delta \theta_\alpha \right) d\Omega + \int_{\Gamma_\sigma} \left\langle \overline{F}_i \delta U_i^{(k)} \right\rangle d\Gamma \tag{2.46}$$

with

$$\overline{p}_i = \overline{p}_{i(B)} + \overline{p}_{i(T)} \;\; i = 1,2,3 \qquad \overline{m}_\alpha = x_{3(B)} \overline{p}_{\alpha(B)} + x_{3(T)} \overline{p}_{\alpha(T)} \;\; \alpha = 1,2 \tag{2.47}$$

Integrating by parts the governing functional, Eq. (2.34), and its contributions, Eqs. (2.35)-(2.44), the governing equations in terms of the kinematic unknowns are obtained.

2.3.1 Static response

The equilibrium equations for the static response of the plate can be obtained by considering, in the governing functional, only the virtual variation of the internal energy and the work done by the external forces. Thus, the equilibrium equations of the en-RZT expressed in terms of the resultant forces and moments read as [136]

$$\begin{aligned}
&\delta u_1 : \quad N_{11,1} + N_{12,2} + \overline{p}_1 = 0 \\
&\delta u_2 : \quad N_{12,1} + N_{22,2} + \overline{p}_2 = 0 \\
&\delta w : \quad Q_{1,1} + Q_{2,2} + \overline{p}_3 = 0 \\
&\delta \theta_1 : \quad M_{11,1} + M_{12,1} - Q_1 + \overline{m}_1 = 0 \\
&\delta \theta_2 : \quad M_{12,1} + M_{22,1} - Q_2 + \overline{m}_2 = 0 \\
&\delta \psi_1 : \quad M^{\phi}_{11,1} + M^{\phi}_{12,2} - Q^{\phi}_1 = 0 \\
&\delta \psi_2 : \quad M^{\phi}_{21,1} + M^{\phi}_{22,2} - Q^{\phi}_2 = 0
\end{aligned} \tag{2.48}$$

2.3.2 Buckling problem

The governing equations for the buckling problems are obtained by neglecting the inertial terms and the work done by the applied loads. Thus, they read as follows [137]:

$$
\begin{aligned}
&\delta u_1: \quad N_{11,1}+N_{12,2}=0\\
&\delta u_2: \quad N_{12,1}+N_{22,2}=0\\
&\delta w: \quad Q_{1,1}+Q_{2,2}+\overline{P}_{11}w_{,11}+\overline{P}_{22}w_{,22}+2\overline{P}_{12}w_{,12}=0\\
&\delta\theta_1: \quad M_{11,1}+M_{12,1}-Q_1=0\\
&\delta\theta_2: \quad M_{12,1}+M_{22,1}-Q_2=0\\
&\delta\psi_1: \quad M^{\phi}_{11,1}+M^{\phi}_{12,2}-Q^{\phi}_1=0\\
&\delta\psi_2: \quad M^{\phi}_{21,1}+M^{\phi}_{22,2}-Q^{\phi}_2=0
\end{aligned}
\tag{2.49}
$$

It should be noted that Eq. (2.49) are referred to the pre-buckling state in which the plate is assumed to remain flat.

2.3.3 Free vibration problem

By neglecting the applied external loads or buckling loads, the governing equations for the free vibration problem read

$$
\begin{aligned}
&\delta u_1: \quad N_{11,1}+N_{12,2}=m^{(0)}\ddot{u}_1+m^{(1)}\ddot{\theta}_1+m^{(0)}_{\phi 11}\ddot{\psi}_1+m^{(0)}_{\phi 12}\ddot{\psi}_2\\
&\delta u_2: \quad N_{12,1}+N_{22,2}=m^{(0)}\ddot{u}_2+m^{(1)}\ddot{\theta}_2+m^{(0)}_{\phi 21}\ddot{\psi}_1+m^{(0)}_{\phi 22}\ddot{\psi}_2\\
&\delta w: \quad Q_{1,1}+Q_{2,2}=m^{(0)}\ddot{u}_3\\
&\delta\theta_1: \quad M_{11,1}+M_{12,1}-Q_1=m^{(1)}\ddot{u}_1+m^{(2)}\ddot{\theta}_1+m^{(1)}_{\phi 11}\ddot{\psi}_1+m^{(1)}_{\phi 12}\ddot{\psi}_2\\
&\delta\theta_2: \quad M_{12,1}+M_{22,1}-Q_2=m^{(1)}\ddot{u}_2+m^{(2)}\ddot{\theta}_2+m^{(1)}_{\phi 21}\ddot{\psi}_1+m^{(1)}_{\phi 22}\ddot{\psi}_2\\
&\delta\psi_1: \quad M^{\phi}_{11,1}+M^{\phi}_{12,2}-Q^{\phi}_1=m^{(0)}_{\phi 11}\ddot{u}_1+m^{(0)}_{\phi 21}\ddot{u}_2+m^{(1)}_{\phi 11}\ddot{\theta}_1+m^{(1)}_{\phi 12}\ddot{\theta}_2+\\
&\qquad\qquad +m^{(2)}_{\phi 11}\ddot{\psi}_1+m^{(2)}_{\phi 12}\ddot{\psi}_2\\
&\delta\psi_2: \quad M^{\phi}_{21,1}+M^{\phi}_{22,2}-Q^{\phi}_2=m^{(0)}_{\phi 12}\ddot{u}_1+m^{(0)}_{\phi 22}\ddot{u}_2+m^{(1)}_{\phi 12}\ddot{\theta}_1+m^{(1)}_{\phi 22}\ddot{\theta}_2+\\
&\qquad\qquad +m^{(2)}_{\phi 21}\ddot{\psi}_1+m^{(2)}_{\phi 22}\ddot{\psi}_2
\end{aligned}
\tag{2.50}
$$

Generally, the governing equations, i.e. Eqs. (2.48), (2.49) and (2.50), are completed with a consistent set of boundary conditions

$$
\begin{array}{llll}
u_1 = \bar{u}_1 & \text{on } \Gamma_U & \vee & \bar{N}_{11}n_1 + \bar{N}_{12}n_2 \quad \text{on } \Gamma_\sigma \\
u_2 = \bar{u}_2 & \text{on } \Gamma_U & \vee & \bar{N}_{12}n_1 + \bar{N}_{22}n_2 \quad \text{on } \Gamma_\sigma \\
w = \bar{w} & \text{on } \Gamma_U & \vee & \bar{Q}_1 n_1 + \bar{Q}_2 n_2 \quad \text{on } \Gamma_\sigma \\
\theta_1 = \bar{\theta}_1 & \text{on } \Gamma_U & \vee & \bar{M}_{11}n_1 + \bar{M}_{12}n_2 \quad \text{on } \Gamma_\sigma \\
\theta_2 = \bar{\theta}_2 & \text{on } \Gamma_U & \vee & \bar{M}_{12}n_1 + \bar{M}_{22}n_2 \quad \text{on } \Gamma_\sigma \\
\psi_1 = \bar{\psi}_1 & \text{on } \Gamma_U & \vee & \bar{M}^{\phi}_{11}n_1 + \bar{M}^{\phi}_{12}n_2 \quad \text{on } \Gamma_\sigma \\
\psi_2 = \bar{\psi}_2 & \text{on } \Gamma_U & \vee & \bar{M}^{\phi}_{21}n_1 + \bar{M}^{\phi}_{22}n_2 \quad \text{on } \Gamma_\sigma
\end{array}
\tag{2.51}
$$

In Eq. (2.51) $n_\alpha = \cos(x_\alpha, n)$ are the direction cosines of the outward unit normal $\mathbf{n}$ to Γ with respect to the $\alpha-$axis, and $\mathbf{t}$ the unit vector tangent to Γ, the boundary of Ω, and oriented in such a way the $(\mathbf{n}, \mathbf{t}, x_3)$ form a right-handed coordinate system, see Figure 3.

Using the definition of en-RZT stresses, i.e. Eq. (2.18), the en-RZT constitutive relations are expressed as follows:

$$
\begin{aligned}
&\mathbf{N} = \mathbf{A}\boldsymbol{\varepsilon}_m + \mathbf{B}\boldsymbol{\varepsilon}_\theta + \mathbf{A}^\phi\boldsymbol{\varepsilon}_\theta \\
&\mathbf{M} = \mathbf{B}\boldsymbol{\varepsilon}_m + \mathbf{D}\boldsymbol{\varepsilon}_\theta + \mathbf{B}^\phi\boldsymbol{\varepsilon}_\theta \\
&\mathbf{M}^\phi = \mathbf{A}^{\phi T}\boldsymbol{\varepsilon}_m + \mathbf{B}^{\phi T}\boldsymbol{\varepsilon}_\theta + \mathbf{D}^\phi\boldsymbol{\varepsilon}_\theta \\
&\mathbf{Q} = \mathbf{A}_t\boldsymbol{\gamma}^{(0)} + \mathbf{B}_t\boldsymbol{\psi} \\
&\mathbf{Q}^\phi = \mathbf{B}_t{}^T\boldsymbol{\gamma}^{(0)} + \mathbf{D}_t\boldsymbol{\psi}
\end{aligned}
\tag{2.52}
$$

where the matrices of the constitutive relations are expressed as follows:

$$
\begin{aligned}
&\left(\mathbf{A}, \mathbf{B}, \mathbf{A}^\phi\right) = \left\langle \breve{\mathbf{C}}_p^{(k)}\left(1, x_3, \boldsymbol{\varphi}^{(k)}\right)\right\rangle; \\
&\left(\mathbf{B}^\phi, \mathbf{D}^\phi\right) = \left\langle x_3\breve{\mathbf{C}}_p^{(k)}\boldsymbol{\varphi}^{(k)}, \boldsymbol{\varphi}^{(k)T}\breve{\mathbf{C}}_p^{(k)}\boldsymbol{\varphi}^{(k)}\right\rangle; \\
&\left(\mathbf{A}_t, \mathbf{B}_t\right) = \left\langle \breve{\mathbf{C}}_t^{(k)}\left(1, \boldsymbol{\beta}^{(k)}\right)\right\rangle; \qquad \mathbf{D}_t = \left\langle \boldsymbol{\beta}^{(k)T}\breve{\mathbf{C}}_t^{(k)}\boldsymbol{\beta}^{(k)}\right\rangle
\end{aligned}
\tag{2.53}
$$

2.4 The Ritz method for the en-RZT

In this Section, the approximated Ritz method is proposed to solve the linearized governing equations of the en-RZT plate model. Due to the

mathematical difficulty of solving the governing equations analytically when general lamination schemes, constraint conditions or applied loads are considered, an approximated solution that transforms the differential problem into an algebraical one is formulated here. The starting point is the D'Alembert principle introduced by Eq. (2.34), in which the following functions approximate the kinematic variables:

$$\hat{f}\left(x_1,x_2\right)=\sum_{m=1}^{M_f} C_m^{(f)} f_m^{(f)}\left(x_1,x_2\right)=\mathbf{g}^{(f)T}\left(x_1,x_2\right)\mathbf{C}^{(f)} \tag{2.54}$$

where $\hat{f}\left(x_1,x_2\right)$ denotes the general unknown kinematic variable, i.e. u_1, u_2, w, θ_1, θ_2, ψ_1 and ψ_2. In Eq. (2.54), $C_m^{(f)}$ are the m unknown generalized constant that multiplies the corresponding $f_m^{(f)}\left(x_1,x_2\right)$ approximating function. In the Ritz method, the admissible functions must be a complete set of at least linearly independent and able to satisfy the geometric boundary conditions. In this work, the admissible functions are the Gram-Schmidt orthogonal polynomials. In the following expressions, the symbol $\mathbf{C}_{GS}$ denotes the vector of the unknowns coefficients of the Gram-Schmidt polynomials used to approximate the kinematic variables.

Introducing the vector of the unknown kinematic variables, i.e. $\hat{\mathbf{d}}^T=\lfloor u_1 \quad u_2 \quad \theta_1 \quad \theta_2 \quad \psi_1 \quad \psi_2 \quad w \rfloor$, and taking into account Eq. (2.54), it yields the following expression:

$$\hat{\mathbf{d}}=\begin{bmatrix} \mathbf{g}^{u_1T} & \mathbf{0} & \mathbf{0} & \mathbf{0} & \mathbf{0} & \mathbf{0} & \mathbf{0} \\ & \mathbf{g}^{u_2T} & \mathbf{0} & \mathbf{0} & \mathbf{0} & \mathbf{0} & \mathbf{0} \\ & & \mathbf{g}^{\theta_1T} & \mathbf{0} & \mathbf{0} & \mathbf{0} & \mathbf{0} \\ & & & \mathbf{g}^{\theta_2T} & \mathbf{0} & \mathbf{0} & \mathbf{0} \\ & & & & \mathbf{g}^{\psi_1T} & \mathbf{0} & \mathbf{0} \\ & sym. & & & & \mathbf{g}^{\psi_2T} & \mathbf{0} \\ & & & & & & \mathbf{g}^{wT} \end{bmatrix} \begin{Bmatrix} \mathbf{C}^{u_1} \\ \mathbf{C}^{u_2} \\ \mathbf{C}^{\theta_1} \\ \mathbf{C}^{\theta_2} \\ \mathbf{C}^{\psi_1} \\ \mathbf{C}^{\psi_2} \\ \mathbf{C}^{w} \end{Bmatrix} \tag{2.55}$$

Substituting Eq. (2.55) into Eq. (2.18), the strain quantities are expressed as follows:

$$\hat{\mathbf{e}} = \begin{Bmatrix} \boldsymbol{\varepsilon}_m \\ \boldsymbol{\varepsilon}_\theta \\ \boldsymbol{\varepsilon}_\psi \\ \boldsymbol{\gamma}^{(0)} \\ \boldsymbol{\psi} \end{Bmatrix} = \begin{bmatrix} \mathbf{g}_{,1}^{u_1 T} & \mathbf{0} & \mathbf{0} & \mathbf{0} & \mathbf{0} & \mathbf{0} & \mathbf{0} \\ \mathbf{0} & \mathbf{g}_{,2}^{u_2 T} & \mathbf{0} & \mathbf{0} & \mathbf{0} & \mathbf{0} & \mathbf{0} \\ \mathbf{g}_{,2}^{u_2 T} & \mathbf{g}_{,1}^{u_1 T} & \mathbf{0} & \mathbf{0} & \mathbf{0} & \mathbf{0} & \mathbf{0} \\ \mathbf{0} & \mathbf{0} & \mathbf{g}_{,1}^{\theta_1 T} & \mathbf{0} & \mathbf{0} & \mathbf{0} & \mathbf{0} \\ \mathbf{0} & \mathbf{0} & \mathbf{0} & \mathbf{g}_{,2}^{\theta_2 T} & \mathbf{0} & \mathbf{0} & \mathbf{0} \\ \mathbf{0} & \mathbf{0} & \mathbf{g}_{,2}^{\theta_1 T} & \mathbf{g}_{,1}^{\theta_2 T} & \mathbf{0} & \mathbf{0} & \mathbf{0} \\ \mathbf{0} & \mathbf{0} & \mathbf{0} & \mathbf{0} & \mathbf{g}_{,1}^{\psi_1 T} & \mathbf{0} & \mathbf{0} \\ \mathbf{0} & \mathbf{0} & \mathbf{0} & \mathbf{0} & \mathbf{0} & \mathbf{g}_{,1}^{\psi_2 T} & \mathbf{0} \\ \mathbf{0} & \mathbf{0} & \mathbf{0} & \mathbf{0} & \mathbf{g}_{,2}^{\psi_1 T} & \mathbf{0} & \mathbf{0} \\ \mathbf{0} & \mathbf{0} & \mathbf{0} & \mathbf{0} & \mathbf{0} & \mathbf{g}_{,2}^{\psi_2 T} & \mathbf{0} \\ \mathbf{0} & \mathbf{0} & \mathbf{g}^{\theta_1 T} & \mathbf{0} & \mathbf{0} & \mathbf{0} & \mathbf{g}_{,1}^{w T} \\ \mathbf{0} & \mathbf{0} & \mathbf{0} & \mathbf{g}^{\theta_2 T} & \mathbf{0} & \mathbf{0} & \mathbf{g}_{,2}^{w T} \\ \mathbf{0} & \mathbf{0} & \mathbf{0} & \mathbf{0} & \mathbf{g}^{\psi_1 T} & \mathbf{0} & \mathbf{0} \\ \mathbf{0} & \mathbf{0} & \mathbf{0} & \mathbf{0} & \mathbf{0} & \mathbf{g}^{\psi_2 T} & \mathbf{0} \end{bmatrix} \begin{Bmatrix} \mathbf{C}^{u_1} \\ \mathbf{C}^{u_2} \\ \mathbf{C}^{\theta_1} \\ \mathbf{C}^{\theta_2} \\ \mathbf{C}^{\psi_1} \\ \mathbf{C}^{\psi_2} \\ \mathbf{C}^{w} \end{Bmatrix} \tag{2.56}$$

In a more useful matrix form

$$\begin{aligned} \hat{\mathbf{d}} &= \mathbf{G}_d \mathbf{C}_{GS} \\ \hat{\mathbf{e}} &= \mathbf{G}_\nabla \mathbf{C}_{GS} \end{aligned} \tag{2.57}$$

By substituting Eq. (2.57) into Eq. (2.34), and taking into account that the virtual variations are arbitrarily independent, yields the following approximated discretized governing equations:

$$\mathbf{M}\ddot{\mathbf{C}}_{GS} + \left(\mathbf{K} + \lambda \mathbf{K}_G\right)\mathbf{C}_{GS} = \mathbf{P} \tag{2.58}$$

where

$$\mathbf{K} = \int_\Omega \mathbf{G}_\nabla^T \begin{bmatrix} \mathbf{A} & \mathbf{B} & \mathbf{A}^\phi & \mathbf{0} & \mathbf{0} \\ \mathbf{B} & \mathbf{D} & \mathbf{B}^\phi & \mathbf{0} & \mathbf{0} \\ \mathbf{A}^{\phi T} & \mathbf{B}^{\phi T} & \mathbf{D}^\phi & \mathbf{0} & \mathbf{0} \\ \mathbf{0} & \mathbf{0} & \mathbf{0} & \mathbf{A}_t & \mathbf{B}_t \\ \mathbf{0} & \mathbf{0} & \mathbf{0} & \mathbf{B}_t^T & \mathbf{D}_t \end{bmatrix} \mathbf{G}_\nabla d\Omega \tag{2.59}$$

is the stiffness matrix;

$$\mathbf{K}_G = \begin{bmatrix} \mathbf{0} & \mathbf{0} & \mathbf{0} & \mathbf{0} & \mathbf{0} & \mathbf{0} & \mathbf{0} \\ \mathbf{0} & \mathbf{0} & \mathbf{0} & \mathbf{0} & \mathbf{0} & \mathbf{0} & \mathbf{0} \\ \mathbf{0} & \mathbf{0} & \mathbf{0} & \mathbf{0} & \mathbf{0} & \mathbf{0} & \mathbf{0} \\ \mathbf{0} & \mathbf{0} & \mathbf{0} & \mathbf{0} & \mathbf{0} & \mathbf{0} & \mathbf{0} \\ \mathbf{0} & \mathbf{0} & \mathbf{0} & \mathbf{0} & \mathbf{0} & \mathbf{0} & \mathbf{0} \\ \mathbf{0} & \mathbf{0} & \mathbf{0} & \mathbf{0} & \mathbf{0} & \mathbf{0} & \mathbf{0} \\ \mathbf{0} & \mathbf{0} & \mathbf{0} & \mathbf{0} & \mathbf{0} & \mathbf{0} & \mathbf{k}_G \end{bmatrix}$$
$$\text{with } \mathbf{k}_G = \int_\Omega \begin{Bmatrix} \mathbf{g}_{,1}^w \\ \mathbf{g}_{,2}^w \end{Bmatrix}^T \begin{bmatrix} 1 & r_{12} \\ r_{12} & r_{11} \end{bmatrix} \begin{Bmatrix} \mathbf{g}_{,1}^w \\ \mathbf{g}_{,2}^w \end{Bmatrix} d\Omega \tag{2.60}$$

is the geometric stiffness matric and $\lambda = \overline{P}_{11}$, $r_{11} = \dfrac{\overline{P}_{22}}{\overline{P}_{11}}$, $r_{12} = \dfrac{\overline{P}_{12}}{\overline{P}_{11}}$ the buckling load parameter;

$$\mathbf{M} = \int_\Omega \mathbf{G}_d^T \begin{bmatrix} m^{(0)} & 0 & m^{(1)} & 0 & m_{11\phi}^{(0)} & m_{12\phi}^{(0)} & 0 \\ 0 & m^{(0)} & 0 & 0 & m_{21\phi}^{(0)} & m_{22\phi}^{(0)} & 0 \\ m^{(1)} & 0 & m^{(2)} & 0 & m_{11\phi}^{(1)} & m_{12\phi}^{(2)} & 0 \\ 0 & m^{(1)} & 0 & m^{(2)} & m_{21\phi}^{(1)} & m_{22\phi}^{(1)} & 0 \\ m_{11\phi}^{(0)} & m_{21\phi}^{(0)} & m_{11\phi}^{(1)} & m_{21\phi}^{(1)} & m_{11\phi}^{(2)} & m_{12\phi}^{(2)} & 0 \\ m_{12\phi}^{(0)} & m_{22\phi}^{(0)} & m_{12\phi}^{(2)} & m_{22\phi}^{(1)} & m_{21\phi}^{(2)} & m_{22\phi}^{(2)} & 0 \\ 0 & 0 & 0 & 0 & 0 & 0 & m^{(0)} \end{bmatrix} \mathbf{G}_d d\Omega \tag{2.61}$$

is the mass matrix and

$$\mathbf{P}^T = \int_\Omega \begin{bmatrix} \overline{p}_1 & \overline{p}_2 & \overline{m}_1 & \overline{m}_2 & 0 & 0 & \overline{p}_3 \end{bmatrix} \mathbf{G}_d d\Omega + \\ + \int_{\Gamma_\sigma} \begin{bmatrix} \overline{F}_1 & \overline{F}_2 & 0 & 0 & 0 & 0 & \overline{F}_3 \end{bmatrix} \mathbf{G}_d d\Gamma \tag{2.62}$$

is the load vector.

The discretized governing equations, i.e. Eq. (2.58), could be specialized for free vibration $\mathbf{P} = \mathbf{0}$ and $\mathbf{K_G} = \mathbf{0}$, for bending analysis $\mathbf{K}_G = \mathbf{0}$ and $\mathbf{M} = \mathbf{0}$, for buckling analysis $\mathbf{P} = \mathbf{0}$ and $\mathbf{M} = \mathbf{0}$.

Chapter 3

The mixed {3,2}-enhanced Refined Zigzag Theory

In thick multilayered composite and sandwich structures, the role of transverse normal deformability, typically neglected in most plate models, needs to be included to guarantee an accurate prediction of stresses. Moreover, as highlighted by three-dimensional solutions, the trough-the-thickness displacements across the laminate section are no longer piecewise linear, but they assume higher-order patterns.

As reported in Chapter 1, many authors have put their efforts into including higher-order terms in their theories to represent the through-the-thickness profiles of thick laminated structures accurately. Among the existing literature, some examples related to how to include the transverse normal deformability in current models are briefly recalled in the next Section. Furthermore, the use of mixed formulations, despite introducing new variables, leads to a more accurate representation of the stress patterns with respect to the models formulated according to the Principle of Virtual Displacements (PVDs).

In this Chapter, a new mixed higher-order model is proposed starting from the enhanced Refined Zigzag Theory and extended for thick multilayered composite and sandwich structures. The involved kinematics is assumed cubic for the in-plane displacements and parabolic for the transverse one. The number of kinematic variables is then reduced thanks to a partial constraint condition on the

transverse shear stresses at the laminate's top and bottom external surfaces. This procedure provides a new set of higher-order enhanced zigzag functions. Furthermore, the transverse normal stress is assumed a-priori as a smeared cubic function across the entire laminate thickness. The transverse shear stresses are through-the-thickness assumed distributions derived from integrating Cauchy's equations in which a new set of strain variables has been used. The variational principle used to derive the governing equations involves the Hellinger-Reissner functional and a new penalty term for strains' compatibility.

The present formulation has been proposed at the 25th International Conference on Composite Structures (ICCS25) in Porto (Portugal) [149] and published in the Composite Structures Journal [150].

3.1 Theoretical background

In this Section, a brief theoretical background is presented to give an overview of higher-order models and mixed formulations useful to understand this new model's assumptions better.

In the literature background, Tessler and co-workers [151–153] have presented the *{m,n}*-th model in which the in-plane displacements and the transverse displacements are expanded as Taylor's series of the transverse coordinate of order *m* and *n*, respectively. In Refs. [151–153], the transverse shear strains and transverse normal stress are also assumed as through-the-thickness parabolic and cubic smeared functions, assumed independently from the displacement field. Moreover, the assumed transverse shear stress functions are able to satisfy the traction-free conditions at the top and bottom surfaces. Whereas, according to the last Cauchy's equation, the assumed transverse normal stress has its first derivative null on the external laminate surfaces. A least-square compatibility constraint is enforced between the strains derived by the two assumed fields to reduce the number of unknown variables. Although its simplicity, the presented model is quite inaccurate in displacements and stresses predictions.

In Di Sciuva's ZZT [89], the in-plane contribution of the displacement field has been enriched with a higher-order term. A further enhancement in the zigzag model can be found in Di Sciuva and Gherlone [154,155], where the authors enriched the zigzag plate theory with third-order Hermitian functions to include

the cubic variation of the in-plane displacements. One of the advantages of the proposed model, as reported in Refs. [154,155], have represented the possibility of including damaged interfaces and transverse normal deformability. Furthermore, the Hermitian zigzag model [156] has also been extended, including the sub-laminate approach to increase the predictivity capabilities of the model to investigate the static and dynamic response of damaged and undamaged sandwich beams. Finally, the Hermitian zigzag model and the sub-laminate approach have been combined in a mixed version using the RMVT by Gherlone and Di Sciuva [157,158] for the thermos-mechanical analysis, revealing the great accuracy in displacement, stress and strain through-the-thickness predictions with a limited number of variables. Furthermore, the contributions of Icardi and co-workers [90,91,98,101] are worthy to be cited where both in the displacement and stresses predictions by using mixed formulations with the aim of the Hellinger-Reissner and Hu-Washizu formulations.

In the framework of Refined Zigzag Theory models, among the existing attempts to include higher-order effects and transverse normal deformability to assess the structural behaviour of thick laminated structures, is worthy of mentioning Barut et al. [124,125] where it has been used a quadratic through-the-thickness variation of the in-plane and transverse displacements. The normal stress is then considered as in the Tessler's *{m,n}*-models as a smeared cubic function of the transverse coordinate. A least-square statement links the new stress variables to ensure the transverse normal strain compatibility condition.

Later, Iurlaro and co-workers [131,132] enriched the RZT kinematics with a set of piecewise cubic and continuous zigzag functions for the in-plane displacements and for the transverse one with a smeared distribution which depends on the top, bottom and average displacements. In his model, Iurlarlo [132], such as done in Barut et al. [124], has included the same cubic assumption of the transverse normal stress distribution that satisfies the outer surfaces' stress conditions on the prescribed tractions. The transverse shear stresses are then assumed as continuous functions by integrating Cauchy's equations. The RMVT is then used to enforce in a weak manner the transverse shear and transverse normal strains compatibilities in order to link the variables of the assumed stress fields to the variables of the displacement field. According to the Auricchio and Sacco recommendations [26], related to the use of the RMVT with low-order theories, the cylindrical bending assumption has been used in the Iurlaro's {3,2}-RZT$^{(m)}$ model since problems of over-fitting for the assumed transverse shear stresses distributions could arise.

Similarly, Groh and Weaver [127] developed a mixed model for static analysis of highly heterogeneous laminates and sandwich beams, in which the linear RZT has been used in combination with the Hellinger-Reissner functional. For the stress field, the assumed transverse shear and transverse normal stress distribution are formulated by integration of Cauchy's equations. It has been revealed in Ref. [127] that the HR functional can provide an accurate description of both in-plane and transverse stress fields with more accuracy than the corresponding RMVT. A further extension of Groh and Weaver's mixed model has been done for multilayered plate structures [128,129] and curved anisotropic beams [159]. Moreover, in the literature, Köpple and Wagner [162] and Tringh et al. [163] are further examples of the success due to the mixed formulation using HR functional and RZT for a more accurate prediction of stresses.

As enounced by Iurlaro et al. [116], in the mixed formulation of the RZT using the RMVT, introducing the cylindrical bending hypothesis in Cauchy's equations is necessary to obtain the assumed transverse shear stress functions. The fundamental reason for this assumption relies on the transverse shear strain compatibility part of the RMVT, as highlighted by Auricchio and Sacco [26]. If the assumed stresses, obtained from the integration of in-plane stresses using Cauchuy's equations, are described, including the in-plane shear contribution, the transverse shear compatibility tends to be enforced in a strong manner. However, the transverse shear strains coming from the displacement field are not generally accurate, even for the third-order RZT model. As a consequence, inaccuracy and inconsistencies in the through-the-thickness transverse shear distributions are detectable even for cross-ply and sandwich plates. The strategy is to adopt fewer unknown stress variables to describe the transverse shear stresses to prevent this undesirable effect. In context, the cylindrical bending assumption intends to pursue this aim. This strong but effective simplification is clearly valid for cross-ply and sandwich plates, according to the three-dimensional behaviour. However, for anisotropic multilayered plates in which the effect of transverse shear coupling is not negligible leads to an erroneous description of the laminate response. It should be noted that this problem does not arise when the Hellinger-Reissner functional is considered, as testified by Auricchio and Sacco [26] for FSDT and Groh and Weaver [128] for RZT.

Starting from the models that Auricchio and Sacco [26] presented for First Order kinematics, one could be used to achieve a simple but accurate model that considers both a higher-order variation of the displacements and transverse shear and normal stresses. The variational statement uses the Hellinger-Reissner

principle, where the transverse shear stresses are functions of a new set of strain variables. A penalty term in the governing functional has been added to ensure the compatibility between the new in-plane strain variables and those derived from the displacement field. In addition, the penalty functional includes a penalty parameter used to enforce the compatibility condition in a stronger/weaker manner. The results provided by Auricchio and Sacco [26] for the transverse shear stresses by using the FSDT for an antisymmetric angle-ply plate are encouraging to apply this method to a higher-order version of the enhanced-RZT.

In the following Sections, a new higher-order zigzag model is presented. First, the enhanced higher-order zigzag functions are obtained following the standard RZT procedure that prescribes the partial enforcement of the transverse shear stress continuity at the layer interfaces. The number of kinematic variables is then reduced by enforcing a null value for the continuous part of transverse shear stress at the top and bottom external surfaces. Moreover, in the formulated model, the effect of the transverse normal stress is considered by assuming an a-priori through-the-thickness cubic variation that satisfies the top and bottom normal traction conditions. Furthermore, the transverse shear stresses are derived from integrating Cauchy's equations without using any simplification related to the cylindrical bending assumption. Finally, the governing equations and the consistent boundary conditions according to the mixed variational formulation are obtained and specialized for bending and free vibration problems.

3.2 Geometrical preliminaries, displacement field, strains, stresses and higher-order zigzag functions

3.2.1 Kinematic field, strains and stresses

The kinematic field assumption of the en-RZT$^{(m)}_{\{3,2\}}$ considers the en-RZT displacement field for the in-plane displacements with the superposition of second- and third-order power-series terms of the thickness coordinate. A second-order power-series expansion in the thickness coordinate approximates the transverse displacement. The complete kinematic field can be represented as follows:

$$\begin{aligned}\widehat{\mathbf{U}}^{(k)}\left(\mathbf{X};t\right)&=\breve{\mathbf{u}}_G(\mathbf{X};t)+\breve{\mathbf{u}}_L^{(k)}(\mathbf{X};t)\\ U_3\left(\mathbf{X};t\right)&=w^{(0)}\left(\mathbf{x};t\right)+x_3w^{(1)}\left(\mathbf{x};t\right)+x_3^2w^{(2)}\left(\mathbf{x};t\right)\end{aligned}\tag{3.1}$$

where

$$\begin{aligned}\breve{\mathbf{u}}_G\left(\mathbf{X};t\right)&=\mathbf{u}(\mathbf{x};t)+x_3\boldsymbol{\theta}(\mathbf{x};t)+x_3^2\boldsymbol{\chi}(\mathbf{x};t)+x_3^3\boldsymbol{\omega}(\mathbf{x};t)\\ \breve{\mathbf{u}}_L^{(k)}\left(\mathbf{X};t\right)&=\boldsymbol{\varphi}^{(k)}(x_3)\boldsymbol{\psi}(\mathbf{x};t)\end{aligned}\tag{3.2}$$

$$\begin{aligned}&\widehat{\mathbf{U}}^{(k)}\left(\mathbf{X};t\right)=\begin{Bmatrix}U_1^{(k)}\left(\mathbf{X};t\right)\\ U_2^{(k)}\left(\mathbf{X};t\right)\end{Bmatrix};\\ &\mathbf{u}\left(\mathbf{x};t\right)=\begin{Bmatrix}u_1\left(\mathbf{x};t\right)\\ u_2\left(\mathbf{x};t\right)\end{Bmatrix};\quad \boldsymbol{\theta}\left(\mathbf{x};t\right)=\begin{Bmatrix}\theta_1\left(\mathbf{x};t\right)\\ \theta_2\left(\mathbf{x};t\right)\end{Bmatrix};\\ &\boldsymbol{\chi}\left(\mathbf{x};t\right)=\begin{Bmatrix}\chi_1\left(\mathbf{x};t\right)\\ \chi_2\left(\mathbf{x};t\right)\end{Bmatrix};\quad \boldsymbol{\omega}\left(\mathbf{x};t\right)=\begin{Bmatrix}\omega_1\left(\mathbf{x};t\right)\\ \omega_2\left(\mathbf{x};t\right)\end{Bmatrix};\\ &\boldsymbol{\varphi}^{(k)}(x_3)=\begin{bmatrix}\phi_{11}^{(k)}(x_3) & \phi_{12}^{(k)}(x_3)\\ \phi_{21}^{(k)}(x_3) & \phi_{22}^{(k)}(x_3)\end{bmatrix};\quad \boldsymbol{\psi}\left(\mathbf{x};t\right)=\begin{Bmatrix}\psi_1\left(\mathbf{x};t\right)\\ \psi_2\left(\mathbf{x};t\right)\end{Bmatrix}\end{aligned}\tag{3.3}$$

where $\mathbf{u}\left(\mathbf{x};t\right)$ and $\boldsymbol{\theta}\left(\mathbf{x};t\right)$ are the global uniform displacements and rotations of the normal to the reference plane about the positive x_2 and the negative x_1 directions, respectively; $\boldsymbol{\psi}\left(\mathbf{x};t\right)$ are the zigzag rotations, whereas $\boldsymbol{\chi}\left(\mathbf{x};t\right)$, $\boldsymbol{\omega}\left(\mathbf{x};t\right)$, $w^{(1)}\left(\mathbf{x};t\right)$ and $w^{(2)}\left(\mathbf{x};t\right)$ are the additional kinematic unknowns that take into account the effect of the non-linear distribution of in-plane and transverse displacements along the thickness direction.

Moreover, in Eq. (3.3) the expression of the linear zigzag functions (such as in Ref. [136]) reads:

$$\boldsymbol{\varphi}^{(k)}(x_3)=\left(x_3-x_{3(B)}^{(k)}\right)\boldsymbol{\beta}^{(k)}+\sum_{q=1}^{k}h^{(q)}\left(\boldsymbol{\beta}^{(q)}-\boldsymbol{\beta}^{(k)}\right)\qquad(k=1,...,N)\tag{3.4}$$

where $\boldsymbol{\beta}^{(k)}=\begin{bmatrix}\beta_{11} & \beta_{12}\\ \beta_{21} & \beta_{22}\end{bmatrix}^{(k)}$ is the matrix of zigzag slopes, i.e. $\boldsymbol{\beta}^{(k)}(x_3)=\boldsymbol{\varphi}_{,3}^{(k)}(x_3)$.

The kinematics shown in Eq. (3.1)-(3.3) involves thirteen unknown variables independent of the number of layers. The procedure described by Iurlaro et al. [131] to reduce the number of variables is here adopted to condense some of the global unknowns, thus introducing a new set of higher-order zigzag functions expected to be piecewise cubic along the thickness direction. In the following section, the procedure enounced in Iurlaro et al. [131] is applied here in a general way to the enhanced zigzag functions.

The final reduced kinematic can be expressed as follows:

$$\begin{aligned}\widehat{\mathbf{U}}^{(k)}\left(\mathbf{x},x_3;t\right)&=\mathbf{u}_G\left(\mathbf{x},x_3;t\right)+\mathbf{u}_L^{(k)}\left(\mathbf{x},x_3;t\right)\\ U_3\left(\mathbf{x},x_3;t\right)&=w^{(0)}\left(\mathbf{x};t\right)+x_3w^{(1)}\left(\mathbf{x};t\right)+x_3^2w^{(2)}\left(\mathbf{x};t\right)\end{aligned} \tag{3.5}$$

where

$$\begin{aligned}\mathbf{u}_G\left(\mathbf{x},x_3;t\right)&=\mathbf{u}\left(\mathbf{x};t\right)+x_3\boldsymbol{\theta}\left(\mathbf{x};t\right)\\ \mathbf{u}_L^{(k)}\left(\mathbf{x},x_3;t\right)&=\boldsymbol{\mu}^{(k)}(x_3)\boldsymbol{\psi}\left(\mathbf{x};t\right)\end{aligned} \tag{3.6}$$

and

$$\boldsymbol{\mu}^{(k)}(x_3)=\begin{bmatrix}\mu_{11}^{(k)}(x_3) & \mu_{12}^{(k)}(x_3)\\ \mu_{21}^{(k)}(x_3) & \mu_{22}^{(k)}(x_3)\end{bmatrix} \tag{3.7}$$

is the new set of higher-order, piecewise cubic zigzag functions that satisfy the null condition at the top and bottom external surfaces and the displacement continuity at the layer interfaces.

It should be noted that the coupling extra-diagonal terms in Eq. (3.7), i.e. $\mu_{12}^{(k)}(x_3)$ and $\mu_{21}^{(k)}(x_3)$, are null for cross-ply multilayered and orthotropic sandwich plates. In fact, the expressions $\mu_{11}^{(k)}(x_3)$ and $\mu_{22}^{(k)}(x_3)$ obtained by Iurlaro [132] are a particular case of this general formulation.

According to the displacement field defined in Eq. (3.5), the strain quantities can be defined as follows:

$$\boldsymbol{\varepsilon}_p^{(k)}\left(\mathbf{x},x_3;t\right)=\begin{Bmatrix}\varepsilon_{11}^{(k)}\left(\mathbf{x},x_3;t\right)\\ \varepsilon_{22}^{(k)}\left(\mathbf{x},x_3;t\right)\\ \gamma_{12}^{(k)}\left(\mathbf{x},x_3;t\right)\end{Bmatrix}=\boldsymbol{\varepsilon}_m\left(\mathbf{x};t\right)+z\boldsymbol{\varepsilon}_\theta\left(\mathbf{x};t\right)+\mathbf{M}^{(k)}(x_3)\boldsymbol{\varepsilon}_\psi\left(\mathbf{x};t\right)$$

$$\varepsilon_{33}\left(\mathbf{x},x_3;t\right)=\begin{bmatrix}0 & 1 & 2x_3\end{bmatrix}\begin{Bmatrix}w^{(0)}\left(\mathbf{x};t\right)\\ w^{(1)}\left(\mathbf{x};t\right)\\ w^{(2)}\left(\mathbf{x};t\right)\end{Bmatrix}=\mathbf{H}_{,3}^{z}(x_3)\mathbf{w}\left(\mathbf{x};t\right) \tag{3.8}$$

$$\boldsymbol{\gamma}_t^{(k)}\left(\mathbf{x},x_3;t\right)=\mathbf{H}^{z}(x_3)\partial\mathbf{w}\left(\mathbf{x};t\right)+\frac{\partial\boldsymbol{\mu}^{(k)}(x_3)}{\partial x_3}\boldsymbol{\psi}\left(\mathbf{x};t\right)$$

where $\mathbf{H}^{z}(x_3)=\begin{bmatrix}\widehat{\mathbf{H}}^{z}(x_3) & \mathbf{0}\\ \mathbf{0} & \widehat{\mathbf{H}}^{z}(x_3)\end{bmatrix}$, $\widehat{\mathbf{H}}^{z}(x_3)=\begin{bmatrix}1 & x_3 & x_3^2\end{bmatrix}$, $\partial\mathbf{w}(\mathbf{x};t)^T=\begin{bmatrix}w_{,1}^{(0)} & w_{,1}^{(1)} & w_{,1}^{(2)} & w_{,2}^{(0)} & w_{,2}^{(1)} & w_{,2}^{(2)}\end{bmatrix}$ and

$$\mathbf{M}^{(k)}(x_3)=\begin{bmatrix}\mu_{11}(x_3) & 0 & 0 & \mu_{12}(x_3)\\ 0 & \mu_{22}(x_3) & \mu_{21}(x_3) & 0\\ \mu_{21}(x_3) & \mu_{12}(x_3) & \mu_{11}(x_3) & \mu_{22}(x_3)\end{bmatrix}^{(k)}.$$

Moreover, $\boldsymbol{\varepsilon}_m{}^T=\begin{bmatrix}u_{1,1} & u_{2,2} & u_{1,2}+u_{2,1}\end{bmatrix}$, $\boldsymbol{\varepsilon}_\theta{}^T=\begin{bmatrix}\theta_{1,1} & \theta_{2,2} & \theta_{1,2}+\theta_{2,1}\end{bmatrix}$ and $\boldsymbol{\varepsilon}_\psi{}^T=\begin{bmatrix}\psi_{1,1} & \psi_{2,2} & \psi_{1,2} & \psi_{2,1}\end{bmatrix}$.

3.2.2 Enhanced higher-order zigzag functions

The derivation of the enhanced higher-order zigzag functions follows the procedure described by Iurlaro [132]. It is here extended to the case of more general lamination schemes that include the effect of transverse shear coupling. For the sake of clarity, the time dependency of the unknown variables is not reported here.

The expression of transverse shear strains is written as follows:

$$\begin{aligned}\gamma_{13}^{(k)}(\mathbf{x},x_3) &= U_{3,1}(\mathbf{x},x_3)+\theta_1(\mathbf{x})+\\ &\quad +2x_3\chi_1(\mathbf{x})+3x_3^2\omega_1(\mathbf{x})+\beta_{11}^{(k)}\psi_1(\mathbf{x})+\beta_{12}^{(k)}\psi_2(\mathbf{x})\\ \gamma_{23}^{(k)}(\mathbf{x},x_3) &= U_{3,2}(\mathbf{x},x_3)+\theta_2(\mathbf{x})+\\ &\quad +2x_3\chi_2(\mathbf{x})+3x_3^2\omega_2(\mathbf{x})+\beta_{21}^{(k)}\psi_1(\mathbf{x})+\beta_{22}^{(k)}\psi_2(\mathbf{x})\end{aligned} \tag{3.9}$$

The auxiliary strain measures η_1,η_2 [103] are introduced:

$$\begin{aligned}\theta_1(\mathbf{x})+U_{3,1}(\mathbf{x},x_3)-\psi_1 &= \gamma_1(\mathbf{x})-\psi_1(\mathbf{x})=\eta_1(\mathbf{x},x_3)\\ \theta_2(\mathbf{x})+U_{3,2}(\mathbf{x},x_3)-\psi_2 &= \gamma_2(\mathbf{x})-\psi_2(\mathbf{x})=\eta_2(\mathbf{x},x_3)\end{aligned} \tag{3.10}$$

Moreover, substituting (3.10) into Eq. (3.9), we rewrite :

$$\begin{aligned}\gamma_{13}^{(k)}(\mathbf{x},x_3) &= \eta_1(\mathbf{x},x_3)+2z\chi_1(\mathbf{x})+3x_3^2\omega_1(\mathbf{x})+\left(\beta_{11}^{(k)}+1\right)\psi_1(\mathbf{x})+\beta_{12}^{(k)}\psi_2(\mathbf{x})\\ \gamma_{23}^{(k)}(\mathbf{x},x_3) &= \eta_2(\mathbf{x},x_3)+2z\chi_2(\mathbf{x})+3x_3^2\omega_2(\mathbf{x})+\beta_{21}^{(k)}\psi_1(\mathbf{x})+\left(\beta_{22}^{(k)}+1\right)\psi_2(\mathbf{x})\end{aligned} \tag{3.11}$$

In a more convenient matrix form,

$$\begin{aligned}\begin{Bmatrix}\gamma_{13}^{(k)}(\mathbf{x},x_3)\\ \gamma_{13}^{(k)}(\mathbf{x},x_3)\end{Bmatrix} = \boldsymbol{\gamma}_t^{(k)}(\mathbf{x},x_3) &= \boldsymbol{\eta}(\mathbf{x},x_3)+2x_3\boldsymbol{\chi}(\mathbf{x})+\\ &\quad +3x_3^2\boldsymbol{\omega}(\mathbf{x})+\left(\boldsymbol{\beta}^{(k)}(x_3)+\mathbf{I}\right)\boldsymbol{\psi}(\mathbf{x})\end{aligned} \tag{3.12}$$

The transverse shear stresses, using the constitutive material relation, can be expressed as follows:

$$\begin{aligned}\boldsymbol{\tau}_t^{(k)}(\mathbf{x},x_3) &= \breve{\mathbf{C}}_t^{(k)}\left[\boldsymbol{\eta}(\mathbf{x},z)+2x_3\boldsymbol{\chi}(\mathbf{x})+3x_3^2\boldsymbol{\omega}(\mathbf{x})+\left(\boldsymbol{\beta}^{(k)}(x_3)+\mathbf{I}\right)\boldsymbol{\psi}(\mathbf{x})\right]=\\ &= \breve{\mathbf{C}}_t^{(k)}\boldsymbol{\eta}(\mathbf{x},x_3)+\breve{\mathbf{C}}_t^{(k)}\left[2x_3\boldsymbol{\chi}(\mathbf{x})+3x_3^2\boldsymbol{\omega}(\mathbf{x})+\left(\boldsymbol{\beta}^{(k)}(x_3)+\mathbf{I}\right)\boldsymbol{\psi}(\mathbf{x})\right]=\\ &= \boldsymbol{\tau}_t^{D(k)}(\mathbf{x},x_3)+\boldsymbol{\tau}_t^{C(k)}(\mathbf{x},x_3)\end{aligned} \tag{3.13}$$

with

$$\begin{aligned}\boldsymbol{\tau}_t^{D(k)}(\mathbf{x},x_3) &= \breve{\mathbf{C}}_t^{(k)}\boldsymbol{\eta}(\mathbf{x},x_3)\\ \boldsymbol{\tau}_t^{C(k)}(\mathbf{x},x_3) &= \breve{\mathbf{C}}_t^{(k)}\left[2x_3\boldsymbol{\chi}(\mathbf{x})+3x_3^2\boldsymbol{\omega}(\mathbf{x})+\left(\boldsymbol{\beta}^{(k)}(x_3)+\mathbf{I}\right)\boldsymbol{\psi}(\mathbf{x})\right]\end{aligned} \tag{3.14}$$

The continuity of the transverse shear stress, as defined by Eqs. (3.13) and (3.14) is limited to $\boldsymbol{\tau}_t^{C(k)}(\mathbf{x},x_3)$, as typical in the RZT formulation. Thus, the continuity conditions at the *N-1* interfaces read as follows:

$$\begin{aligned}&\breve{\mathbf{C}}_t^{(k)}\left[2x_{3(k)}\boldsymbol{\chi}(\mathbf{x})+3x_{3(k)}^2\boldsymbol{\omega}(\mathbf{x})+\left(\boldsymbol{\beta}^{(k)}+\mathbf{I}\right)\boldsymbol{\psi}(\mathbf{x})\right]=\\&=\breve{\mathbf{C}}_t^{(k+1)}\left[2x_{3(k)}\boldsymbol{\chi}(\mathbf{x})+3x_{3(k)}^2\boldsymbol{\omega}(\mathbf{x})+\left(\boldsymbol{\beta}^{(k+1)}+\mathbf{I}\right)\boldsymbol{\psi}(\mathbf{x})\right]\end{aligned} \tag{3.15}$$

The number of kinematic variables can be reduced by enforcing the vanishing condition on the top and bottom external surfaces only on the continuous part of the transverse shear stresses. If applied on the external top and bottom plate surface, the discontinuous term ensures the in-plane tractions equilibrium with the transverse shear stresses. However, since the transverse shear stresses considered in this model are those assumed from integrating the local equilibrium equations, the traction conditions are satisfied by that contribution.

In formula, the vanishing condition reads:

$$\tau_{13}^{C(k)}(\mathbf{x},x_3)\Big|_{x_3=\pm h/2}=0;\quad \tau_{23}^{C(k)}(\mathbf{x},x_3)\Big|_{x_3=\pm h/2}=0 \tag{3.16}$$

Developing Eq. (3.16):

$$\begin{aligned}&\breve{\mathbf{C}}_t^{(1)}\left[-h\boldsymbol{\chi}(\mathbf{x})+\frac{3}{4}h^2\boldsymbol{\omega}(\mathbf{x})+\left(\boldsymbol{\beta}^{(1)}+\mathbf{I}\right)\boldsymbol{\psi}(\mathbf{x})\right]=\mathbf{0}\\&\breve{\mathbf{C}}_t^{(N)}\left[h\boldsymbol{\chi}(\mathbf{x})+\frac{3}{4}h^2\boldsymbol{\omega}(\mathbf{x})+\left(\boldsymbol{\beta}^{(N)}+\mathbf{I}\right)\boldsymbol{\psi}(\mathbf{x})\right]=\mathbf{0}\end{aligned} \tag{3.17}$$

After some mathematical manipulations, the following relations are obtained:

$$\begin{aligned}\boldsymbol{\omega}(\mathbf{x})&=-\frac{\left(\boldsymbol{\beta}^{(1)}+\boldsymbol{\beta}^{(N)}+2\mathbf{I}\right)}{\frac{3}{2}h^2}\boldsymbol{\psi}(\mathbf{x})=-\boldsymbol{\omega}_0\boldsymbol{\psi}(\mathbf{x})\\\boldsymbol{\chi}(\mathbf{x})&=-\frac{1}{2h}\left(\boldsymbol{\beta}^{(N)}-\boldsymbol{\beta}^{(1)}\right)\boldsymbol{\psi}(\mathbf{x})=-\boldsymbol{\chi}_0\boldsymbol{\psi}(\mathbf{x})\end{aligned} \tag{3.18}$$

The relations in Eq. (3.18) reduce the number of unknown kinematic variables from thirteen to nine, linking the new ones introduced for the parabolic and cubic terms in the in-plane displacements to the zigzag rotations.

Substituting Eq. (3.18) into the kinematic field described by Eq. (3.1), the reduced kinematic field can be obtained as shown in Eqs. (3.5) and (3.6), where the higher-order zigzag functions are defined as follows:

$$\boldsymbol{\mu}^{(k)}(x_3) = \left(-x_3^2\boldsymbol{\chi}_0 - x_3^3\boldsymbol{\omega}_0 + \boldsymbol{\varphi}^{(k)}(x_3)\right) \tag{3.19}$$

It can be noted that the new set of higher-order zigzag functions is dependent on the thickness coordinate and on the linear zigzag slopes, i.e. $\boldsymbol{\beta}^{(k)}$. In order to compute the $\boldsymbol{\beta}^{(k)}$ values for each layer, Eq. (3.15) is enforced at each layer interface. The last conditions required to define the zigzag functions completely are the zero values on the top/bottom external surface of the higher-order zigzag functions. Thus,

$$\boldsymbol{\mu}^{(1)}(x_3 = -h/2) = \boldsymbol{\mu}^{(N)}(x_3 = +h/2) = \mathbf{0} \tag{3.20}$$

3.2.4 Assumed transverse normal stress

The assumed transverse normal stress distribution is here considered as a third-order power function of the transverse coordinate [40]:

$$\sigma_{33}^a\left(\mathbf{x}, x_3\right) = \sigma_0^z(\mathbf{x}) + x_3\sigma_1^z(\mathbf{x}) + x_3^2\sigma_2^z(\mathbf{x}) + x_3^3\sigma_3^z(\mathbf{x}) \tag{3.21}$$

As done previously, for the sake of clarity, the time dependence of the assumed stress variable is not reported.

Enforcing at the top and bottom external surfaces the traction boundary conditions, i.e.

$$\begin{aligned} \sigma_{33}^a(\mathbf{x}, x_3 = -h/2) &= -\overline{p}_{3(B)} \\ \sigma_{33}^a(\mathbf{x}, x_3 = h/2) &= \overline{p}_{3(T)} \end{aligned} \tag{3.22}$$

The assumed transverse normal stress is rewritten as follows:

$$\sigma_{33}^a(\mathbf{x}, x_3) = \mathbf{P}_\sigma(x_3)\mathbf{q}_\sigma(\mathbf{x}) + \mathbf{L}(x_3)\overline{\mathbf{q}}_z(\mathbf{x}) \tag{3.23}$$

where

$$\begin{aligned}
&\mathbf{L}(x_3) = \left[\left(\frac{x_3}{h} - \frac{1}{2}\right) \quad \left(\frac{x_3}{h} + \frac{1}{2}\right)\right];\\
&\mathbf{P}_\sigma(x_3) = \left[\left(x_3^2 - \frac{h^2}{4}\right) \quad x_3\left(x_3^2 - \frac{h^2}{4}\right)\right];\\
&\overline{\mathbf{q}}_z(\mathbf{x})^T = \left[\overline{p}_{3(B)} \quad \overline{p}_{3(T)}\right]; \quad \mathbf{q}_\sigma(\mathbf{x})^T = \left[\sigma_2^z \quad \sigma_3^z\right]
\end{aligned} \tag{3.24}$$

3.2.5 Assumed transverse shear stresses

The assumed transverse shear stresses follow the formulation proposed by Auricchio and Sacco [26], where they have been derived by the integration of the local three-dimensional equilibrium equations neglecting the volume body forces, i.e.

$$\begin{aligned}
&\sigma_{11,1}^{(k)}(\mathbf{x}, x_3) + \tau_{12,2}^{(k)}(\mathbf{x}, x_3) + \tau_{13,3}^{(k)}(\mathbf{x}, x_3) = 0\\
&\tau_{12,1}^{(k)}(\mathbf{x}, x_3) + \sigma_{22,2}^{(k)}(\mathbf{x}, x_3) + \tau_{23,3}^{(k)}(\mathbf{x}, x_3) = 0
\end{aligned} \tag{3.25}$$

According to the formulation reported in Ref. [26], the assumed transverse shear stresses are deducted by Eq. (3.25) , in which the in-plane stresses come from the constitutive relations. Whereas the strain quantities are assumed independently with respect to the kinematic field. This assumption can be reported as follows:

$$\begin{aligned}
\boldsymbol{\varepsilon}_p^{(k)}(\mathbf{x}, x_3) = \boldsymbol{\varepsilon}_m(\mathbf{x}) + x_3\boldsymbol{\varepsilon}_\theta(\mathbf{x}) + \mathbf{M}^{(k)}(x_3)\boldsymbol{\varepsilon}_\psi(\mathbf{x}) \rightarrow\\
\rightarrow \mathbf{e}(\mathbf{x}) + x_3\mathbf{k}(\mathbf{x}) + \mathbf{M}^{(k)}(x_3)\mathbf{k}^\psi(\mathbf{x})
\end{aligned} \tag{3.26}$$

where the vectors of the new assumed strain variables are defined as follows: $\mathbf{e}^T = \left[e_{11} \quad e_{22} \quad e_{12}\right]$; $\mathbf{k}^T = \left[k_{11} \quad k_{22} \quad k_{12}\right]$; $\mathbf{k}^{\psi T} = \left[k_{11}^\psi \quad k_{22}^\psi \quad k_{12}^\psi \quad k_{21}^\psi\right]$.

Considering the mixed version of the material constitutive relations, the in-plane stresses have the following expression:

$$\begin{aligned}
\boldsymbol{\sigma}_p^{(k)} &= \breve{\mathbf{C}}_p^{(k)}\boldsymbol{\varepsilon}_p^{(k)}(\mathbf{x}, x_3) + \mathbf{R}^{(k)}\sigma_{33}^a(\mathbf{x}, x_3) =\\
&= \breve{\mathbf{C}}_p^{(k)}\left(\boldsymbol{\varepsilon}_m(\mathbf{x}) + x_3\boldsymbol{\varepsilon}_\theta(\mathbf{x}) + \mathbf{M}^{(k)}(x_3)\boldsymbol{\varepsilon}_\psi(\mathbf{x})\right) + \mathbf{R}^{(k)}\sigma_{33}^a(\mathbf{x}, x_3)
\end{aligned} \tag{3.27}$$

However, the in-plane stresses expressed by Eq. (3.27) could not be yet used to operate the variable substitution of Eq. (3.26) and then the integration part of Eq. (3.25) to obtain the assumed transverse shear stress functions. A further step is

necessary to link the assumed variables of the transverse normal stress distribution $\sigma_{33}^{a}(\mathbf{x}, x_3)$ to the kinematic variables using the weak strain compatibility of the governing functional.

3.3 Variational statement, governing equations and boundary conditions

In this Section, the en-RZT$^{(m)}_{\{3,2\}}$ is formulated by using the variational statement as described by Auricchio and Sacco [26]. The first term ($\delta\Pi_{\text{int}}$) is the work done by the internal stresses. The second term ($\delta\Pi_{HR}$) is the Hellinger-Reissner (HR) functional, in which the compatibility between the transverse shear and normal strains is weakly enforced. Since the assumed transverse shear stresses depend on the new strain quantities, a new penalty functional is added to the variational statement ($\delta\Lambda$). This penalty term guarantees the weak enforcement of the compatibility relations between the strains from the displacement field and the new independent strain variables. According to this assumption, the variational statement can read as follows:

$$\delta\Pi = \delta\Pi_{\text{int}} + \delta\Pi_{HR} + \delta\Lambda - \delta\Pi_{ext} - \delta\Pi_{in} = 0 \tag{3.28}$$

where $\delta\Pi_{\text{int}}$ is the virtual work done by the internal stresses defined as follows:

$$\delta\Pi_{\text{int}} = \int_V \left[\left(\delta\boldsymbol{\varepsilon}_p^{(k)T} \boldsymbol{\sigma}_p^{(k)} + \delta\boldsymbol{\gamma}_t^{(k)T} \boldsymbol{\tau}_t^{a} + \delta\varepsilon_{33}\sigma_{33}^{a} \right) \right] dV \tag{3.29}$$

the $\delta\Pi_{HR}$ is the virtual variation of the Hellinger-Reissner functional for the transverse shear and the transverse normal stress and it reads:

$$\delta\Pi_{HR} = \int_V \left[\delta\boldsymbol{\tau}_t^{aT} \left(\boldsymbol{\gamma}_t^{(k)} - \boldsymbol{\gamma}_t^{(k)a} \right) + \delta\sigma_{33}^{a} \left(\varepsilon_{33} - \varepsilon_{33}^{(k)a} \right) \right] dV \tag{3.30}$$

The virtual variation of the work done by inertial forces $\delta\Pi_{in}$ is expressed as follows;

$$\delta W_{\text{in}} = -\int_{\Omega} \left\langle \rho^{(k)}(x_3)\delta \mathbf{U}^T \ddot{\mathbf{U}} \right\rangle d\Omega \tag{3.31}$$

where $\rho^{(k)}$ is the density of the k^{th} layer. The overdot represents the derivation with respect to the time variable. Remembering $\langle \bullet \rangle = \sum_{k=1}^{N} \int_{x_3^{(k-1)}}^{x_3^{(k)}} (\bullet) dx_3 = \sum_{k=1}^{N} \int_{x_{3(\mathrm{B})}^{(k)}}^{x_{3(\mathrm{T})}^{(k)}} (\bullet) dx_3$.

The $\delta\Lambda$ is the virtual variation of the penalty functional, introduced to ensure the compatibility condition between the assumed strain field and the strains obtained by the assumed displacement field. Thus, it reads:

$$\delta\Lambda = \frac{1}{\eta} \int_V \begin{bmatrix} \left(\delta\boldsymbol{\varepsilon}_m - \delta\mathbf{e}\right)^T \left(\boldsymbol{\varepsilon}_m - \mathbf{e}\right) + \\ + \left(\delta\boldsymbol{\varepsilon}_\theta - \delta\mathbf{k}\right)^T \left(\boldsymbol{\varepsilon}_\theta - \mathbf{k}\right) + \\ + \left(\delta\boldsymbol{\varepsilon}_\psi - \delta\mathbf{k}^\psi\right)^T \left(\boldsymbol{\varepsilon}_\psi - \mathbf{k}^\psi\right) \end{bmatrix} dV \tag{3.32}$$

The penalty parameter η, which needs to be numerically determined, expresses the importance of this term in the governing functional.

Finally, the $\delta\Pi_{ext}$ is the virtual variation of the external applied traction loads (for the sake of clarity, the traction forces $\overline{\mathbf{F}}$ are neglected):

$$\begin{aligned} \delta\Pi_{ext} = & \int_{\Omega} \overline{p}_{1(T)} U_1^{(N)}(x_3 = h/2) d\Omega + \int_{\Omega} \overline{p}_{1(B)} U_1^{(1)}(x_3 = -h/2) d\Omega + \\ & + \int_{\Omega} \overline{p}_{2(T)} U_2^{(N)}(x_3 = h/2) d\Omega + \int_{\Omega} \overline{p}_{2(B)} U_2^{(1)}(x_3 = -h/2) d\Omega + \\ & + \int_{\Omega} \overline{p}_{3(T)} U_3^{(N)}(x_3 = h/2) d\Omega + \int_{\Omega} \overline{p}_{3(B)} U_3^{(1)}(x_3 = -h/2) d\Omega \end{aligned} \tag{3.33}$$

In the previous expressions, superscript a denotes the quantities related to the assumed fields and δ defines the arbitrary virtual variation. It is recalled from Eq. (3.8) that in Eq. (3.29), $\boldsymbol{\varepsilon}_p^{(k)T} = \begin{bmatrix} \varepsilon_{11}^{(k)} & \varepsilon_{22}^{(k)} & \gamma_{12}^{(k)} \end{bmatrix}$ is the vector of in-plane strains obtained by the displacement field; $\boldsymbol{\sigma}_p^{(k)T} = \begin{bmatrix} \sigma_{11}^{(k)} & \sigma_{22}^{(k)} & \tau_{12}^{(k)} \end{bmatrix}$ is the vector of in-plane stresses; $\boldsymbol{\gamma}_t^{(k)T} = \begin{bmatrix} \gamma_{13}^{(k)} & \gamma_{23}^{(k)} \end{bmatrix}$ is the vector of the transverse shear strains computed by the assumed displacement field and ε_{33} is the transverse normal strain according to the strain-displacement relations.

In virtue of the independent assumption of the kinematics, Eq. (3.5), and the transverse normal stress, Eq. (3.23), the variational statement can be split into two contributions:

$$\delta\Pi_{\sigma_{33}} = \int_V \left[\delta\sigma_{33}^a \left(\varepsilon_{33} - \varepsilon_{33}^{(k)a} \right) \right] dV \tag{3.34}$$

and

$$\begin{aligned} &\int_V \left[\left(\delta\boldsymbol{\varepsilon}_p^{(k)T} \boldsymbol{\sigma}_p^{(k)} + \delta\boldsymbol{\gamma}_t^{(k)T} \boldsymbol{\tau}_t^a + \delta\varepsilon_{33}\sigma_{33}^a \right) \right] dV + \int_V \delta\boldsymbol{\tau}_t^{aT} \left(\boldsymbol{\gamma}_t^{(k)} - \boldsymbol{\gamma}_t^{(k)a} \right) dV + \\ &+ \frac{1}{\eta} \int_V \left[\begin{array}{l} \left(\delta\tilde{\partial}\mathbf{u} - \delta\mathbf{e} \right)^T \left(\partial\mathbf{u} - \mathbf{e} \right) + \left(\delta\tilde{\partial}\boldsymbol{\theta} - \delta\mathbf{k} \right)^T \left(\partial\boldsymbol{\theta} - \mathbf{k} \right) \\ + \left(\delta\tilde{\partial}\boldsymbol{\psi} - \delta\mathbf{k}^{\psi} \right)^T \left(\partial\boldsymbol{\psi} - \mathbf{k}^{\psi} \right) \end{array} \right] dV - \delta\Pi_{ext} = 0 \end{aligned} \tag{3.35}$$

that can be solved separately.

Firstly, Eq. (3.34) is solved as a weak form compatibility constraint between the transverse normal strain expressed in terms of the kinematic variables and that coming from the assumed transverse normal stress. Thus, Eq. (3.34) is solved for the assumed stress variables (for the sake of brevity, the final results are reported here, whereas the full expressions are reported Appendix A), and the assumed transverse normal stress has the following expression:

$$\begin{aligned} \sigma_{33}^a(\mathbf{x}, x_3) = &\mathbf{A}_\sigma^u(x_3)\boldsymbol{\varepsilon}_m(\mathbf{x}) + \mathbf{A}_\sigma^\theta(x_3)\boldsymbol{\varepsilon}_\theta(\mathbf{x}) + \\ &+ \mathbf{A}_\sigma^\psi(x_3)\boldsymbol{\varepsilon}_\psi(\mathbf{x}) + \mathbf{A}_\sigma^w(x_3)\mathbf{w}(\mathbf{x}) + \\ &+ \mathbf{A}_\sigma^{q_z}(x_3)\overline{\mathbf{q}}_z(\mathbf{x}) \end{aligned} \tag{3.36}$$

where $\mathbf{A}_\sigma^u(x_3)$, $\mathbf{A}_\sigma^\theta(x_3)$, $\mathbf{A}_\sigma^\psi(x_3)$, $\mathbf{A}_\sigma^w(x_3)$, $\mathbf{A}_\sigma^{q_z}(x_3)$ are the shape functions of the transverse coordinate, and their definition is reported in Appendix A.

Secondly, the expression of the transverse normal stress Eq. (3.36) is introduced in Eq. (3.27) and after introducing the new strain variables, i.e. Eq. (3.26), the integration of Cauchy's equations is performed to obtain the full expression of the assumed transverse shear stresses. After some mathematical passages that, for the sake of clarity, are reported in Appendix B, the final expression of the assumed transverse shear stresses follows:

$$\boldsymbol{\tau}_t^a(\mathbf{x}, x_3) = \mathbf{Z}_p(x_3)\overline{\mathbf{q}}_\mathbf{p}(\mathbf{x}) + \mathbf{Z}_t(x_3)\mathbf{q}_t(\mathbf{x}) + \mathbf{Z}_{qz}(x_3)\partial\overline{\mathbf{q}}_z(\mathbf{x}) \tag{3.37}$$

where $\partial\overline{\mathbf{q}}_z(\mathbf{x})$ represent the derivatives of the transverse distributed load, i.e. $\partial\overline{\mathbf{q}}_z(\mathbf{x})^T = \begin{bmatrix} \overline{p}_{3(B),1} & \overline{p}_{3(T),1} & \overline{p}_{3(B),2} & \overline{p}_{3(T),2} \end{bmatrix}$; $\overline{\mathbf{q}}_\mathbf{p}(\mathbf{x})$ is the vector of the prescribed tractions in the x_1 and x_2 direction at the bottom and top external surfaces, i.e. $\overline{\mathbf{q}}_\mathbf{p}(\mathbf{x})^T = \begin{bmatrix} \overline{p}_{1(B)} & \overline{p}_{2(B)} & \overline{p}_{1(T)} & \overline{p}_{2(T)} \end{bmatrix}$.

Moreover, $\mathbf{q}_t(\mathbf{x})^T = \begin{bmatrix} \partial\mathbf{e}(\mathbf{x})^T & \partial\mathbf{k}(\mathbf{x})^T & \partial\mathbf{k}^\psi(\mathbf{x})^T & \partial\mathbf{w}(\mathbf{x})^T \end{bmatrix}$ is the vector of the derivatives of the strain unknowns and $\mathbf{Z}_p(x_3)$, $\mathbf{Z}_t(x_3)$ and $\mathbf{Z}_{qz}(x_3)$ are the through-the-thickness functions that describe the transverse shear stress distribution and their full expression is reported in Appendix B.

Once the assumed transverse shear stresses are obtained, the Eq. (3.35) can be solved. It represents the variational expression of the work done by strains and stresses and that done by external forces, and it contains a contribution deriving from the weak form compatibility constraint between the transverse shear strains plus the penalty constraint of the strains quantities and performing the integration by parts results in the governing equations with the variationally consistent boundary conditions.

Introducing the assumed transverse normal stress defined by Eq. (3.36) and the assumed transverse shear stresses defined by Eq. (3.37) into the variational statement Eq. (3.35), and performing the conventional integration by parts, the governing equations of the en-RZT$^{(m)}_{\{3,2\}}$ plate can be obtained (the full expression of the various terms are reported in Appendix C) for the static linear bending and the free vibration problems.

3.3.1 Linear bending

Here follows the expressions of the governing equations specified for the linear static bending analysis. Some of the terms inside of the equations are specified in Appendix C.

$$\delta u_1: \quad N_{11,1} + N_{12,2} + \frac{1}{\eta}\left(u_{1,11} - e_{11,1}\right) + \frac{1}{\eta}\left(u_{1,22} + u_{2,12} - e_{12,2}\right) + \overline{p}_1 = 0 \tag{3.38}$$

$$\delta u_2: \quad N_{12,1} + N_{22,2} + \frac{1}{\eta}\left(v_{,yy} - e_{22,y}\right) + \frac{1}{\eta}\left(u_{1,12} + u_{2,11} - e_{12,1}\right) + \overline{p}_2 = 0 \tag{3.39}$$

$$\begin{aligned}\delta w^{(0)}: \quad & Q_{1,1}^{w0}+Q_{2,2}^{w0}-N_1^z-\widehat{Q}^{w0}+\\ & -\begin{pmatrix}\hat{D}_{11}^p\overline{p}_{1(B),1}+\hat{D}_{12}^p\overline{p}_{2(B),1}+\hat{D}_{13}^p\overline{p}_{1(T),1}+\hat{D}_{14}^p\overline{p}_{2(T),1}+\\ +\hat{D}_{41}^p\overline{p}_{1(B),2}+\hat{D}_{42}^p\overline{p}_{2(B),2}+\hat{D}_{43}^p\overline{p}_{1(T),2}+\hat{D}_{44}^p\overline{p}_{2(T),2}\end{pmatrix}+\\ & -\begin{pmatrix}\hat{D}_{41}^q\overline{p}_{3(B),12}+\hat{D}_{42}^q\overline{p}_{3(T),12}+\hat{D}_{43}^q\overline{p}_{3(B),22}+\hat{D}_{44}^q\overline{p}_{3(T),22}+\\ +\hat{D}_{11}^q\overline{p}_{3(B),11}+\hat{D}_{12}^q\overline{p}_{3(T),11}+\hat{D}_{13}^q\overline{p}_{3(B),12}+\hat{D}_{14}^q\overline{p}_{3(T),12}\end{pmatrix}+\overline{q}_3=0\end{aligned} \tag{3.40}$$

$$\begin{aligned}\delta w^{(1)}: \quad & Q_{1,1}^{w1}+Q_{2,2}^{w1}-N_2^z-\widehat{Q}^{w1}+\\ & -\begin{pmatrix}\hat{D}_{21}^p\overline{p}_{1(B),1}+\hat{D}_{22}^p\overline{p}_{2(B),1}+\hat{D}_{23}^p\overline{p}_{1(T),1}+\hat{D}_{24}^p\overline{p}_{2(T),1}+\\ +\hat{D}_{51}^p\overline{p}_{1(B),2}+\hat{D}_{52}^p\overline{p}_{2(B),2}+\hat{D}_{53}^p\overline{p}_{1(T),2}+\hat{D}_{54}^p\overline{p}_{2(T),2}\end{pmatrix}+\\ & -\begin{pmatrix}\hat{D}_{11}^q\overline{p}_{3(B),11}+\hat{D}_{12}^q\overline{p}_{3(T),11}+\hat{D}_{13}^q\overline{p}_{3(B),12}+\hat{D}_{14}^q\overline{p}_{3(T),12}+\\ +\hat{D}_{51}^q\overline{p}_{3(B),12}+\hat{D}_{52}^q\overline{p}_{3(T),12}+\hat{D}_{53}^q\overline{p}_{3(B),22}+\hat{D}_{54}^q\overline{p}_{3(T),22}\end{pmatrix}+\frac{h}{2}\left(\overline{p}_{3(T)}-\overline{p}_{3(B)}\right)=0\end{aligned} \tag{3.41}$$

$$\begin{aligned}\delta w^{(2)}: \quad & Q_{1,1}^{w2}+Q_{2,2}^{w2}-N_3^z-\widehat{Q}^{w2}+\\ & -\begin{pmatrix}\hat{D}_{31}^p\overline{p}_{1(B),1}+\hat{D}_{32}^p\overline{p}_{2(B),1}+\hat{D}_{33}^p\overline{p}_{1(T),1}+\hat{D}_{34}^p\overline{p}_{2(T),1}+\\ +\hat{D}_{61}^p\overline{p}_{1(B),2}+\hat{D}_{62}^p\overline{p}_{2(B),2}+\hat{D}_{63}^p\overline{p}_{1(T),2}+\hat{D}_{64}^p\overline{p}_{2(T),2}\end{pmatrix}+\\ & -\begin{pmatrix}\hat{D}_{31}^q\overline{p}_{3(B),11}+\hat{D}_{32}^q\overline{p}_{3(T),11}+\hat{D}_{33}^q\overline{p}_{3(B),12}+\hat{D}_{34}^q\overline{p}_{3(T),12}+\\ +\hat{D}_{61}^q\overline{p}_{3(B),12}+\hat{D}_{62}^q\overline{p}_{3(T),12}+\hat{D}_{63}^q\overline{p}_{3(B),22}+\hat{D}_{64}^q\overline{p}_{3(T),22}\end{pmatrix}+\frac{h^2}{4}\overline{q}_3=0\end{aligned} \tag{3.42}$$

$$\delta\theta_1: \quad M_{11,1}+M_{12,2}-Q_1+\frac{1}{\eta}\left(\theta_{1,11}-k_{11,1}\right)+\frac{1}{\eta}\left(\theta_{1,22}+\theta_{2,12}-k_{12,2}\right)+\overline{m}_1=0 \tag{3.43}$$

$$\delta\theta_2: \quad M_{12,1}+M_{22,2}-Q_2+\frac{1}{\eta}\left(\theta_{2,22}-k_{22,2}\right)+\frac{1}{\eta}\left(\theta_{1,12}+\theta_{2,11}-k_{12,1}\right)+\overline{m}_2=0 \tag{3.44}$$

$$\delta\psi_1: \quad M_{11,1}^{\phi}+M_{12,2}^{\phi}-Q_1^{\phi}+\frac{1}{\eta}\left(\psi_{1,11}-k_{11,1}^{\psi}\right)+\frac{1}{\eta}\left(\psi_{1,22}-k_{12,2}^{\psi}\right)=0 \tag{3.45}$$

$$\delta\psi_2: \quad M_{21,1}^{\phi}+M_{22,2}^{\phi}-Q_2^{\phi}+\frac{1}{\eta}\left(\psi_{2,22}-k_{22,2}^{\psi}\right)+\frac{1}{\eta}\left(\psi_{2,11}-k_{21,1}^{\psi}\right)=0 \tag{3.46}$$

$$\delta e_{11}: \quad -\frac{1}{\eta}\left(e_{11}-u_{1,1}\right)+E_{11}^{HR}=0 \tag{3.47}$$

$$\delta e_{22}: \quad -\frac{1}{\eta}\left(e_{22}-u_{2,2}\right)+E_{22}^{HR}=0 \tag{3.48}$$

$$\delta e_{12}: \quad -\frac{1}{\eta}\left(e_{12}-u_{1,2}-u_{2,1}\right)+E_{12}^{HR}=0 \tag{3.49}$$

$$\delta k_{11}: \quad -\frac{1}{\eta}\left(k_{11}-\theta_{1,1}\right)+K_{11}^{HR}=0 \tag{3.50}$$

$$\delta k_{22}: \quad -\frac{1}{\eta}\left(k_{22}-\theta_{2,2}\right)+K_{22}^{HR}=0 \tag{3.51}$$

$$\delta k_{12}: \quad -\frac{1}{\eta}\left(k_{12}-\theta_{1,2}-\theta_{2,1}\right)+K_{12}^{HR}=0 \tag{3.52}$$

$$\delta k_{11}^{\psi}: \quad -\frac{1}{\eta}\left(k_{11}^{\psi}-\psi_{1,1}\right)+K_{\psi 11}^{HR}=0 \tag{3.53}$$

$$\delta k_{22}^{\psi}: \quad -\frac{1}{\eta}\left(k_{22}^{\psi}-\psi_{2,2}\right)+K_{\psi 22}^{HR}=0 \tag{3.54}$$

$$\delta k_{12}^{\psi}: \quad -\frac{1}{\eta}\left(k_{12}^{\psi}-\psi_{1,2}\right)+K_{\psi 12}^{HR}=0 \tag{3.55}$$

$$\delta k_{21}^{\psi}: \quad -\frac{1}{\eta}\left(k_{21}^{\psi}-\psi_{2,1}\right)+K_{\psi 21}^{HR}=0 \tag{3.56}$$

3.3.2 Free vibrations

Here follow the expressions of the equations of motions specified for the free vibrations problems. Some of the terms inside of the following governing equations are defined in Appendix C, with the care of neglecting the applied tractions:

$$\begin{aligned}\delta u_1: \quad & N_{11,1}+N_{12,2}+\frac{1}{\eta}\left(u_{1,11}-e_{11,1}\right)+\frac{1}{\eta}\left(u_{1,22}+u_{2,12}-e_{12,2}\right)= \\ & =m^{(0)}\ddot{u}_1+m^{(1)}\ddot{\theta}_1+m_{\mu_{11}}^{(0)}\ddot{\psi}_1+m_{\mu_{12}}^{(0)}\ddot{\psi}_2\end{aligned} \tag{3.57}$$

$$\begin{aligned}\delta u_2: \quad & N_{12,1}+N_{22,2}+\frac{1}{\eta}\left(v_{,yy}-e_{22,y}\right)+\frac{1}{\eta}\left(u_{1,12}+u_{2,11}-e_{12,1}\right)= \\ & =m^{(0)}\ddot{u}_2+m^{(1)}\ddot{\theta}_2+m_{\mu_{21}}^{(0)}\ddot{\psi}_1+m_{\mu_{22}}^{(0)}\ddot{\psi}_2\end{aligned} \tag{3.58}$$

$$\delta w^{(0)}: \quad Q_{1,1}^{w0} + Q_{2,2}^{w0} - N_1^z - \widehat{Q}^{w0} = m^{(0)}\ddot{w}^{(0)} + m^{(1)}\ddot{w}^{(1)} + m^{(2)}\ddot{w}^{(2)} \tag{3.59}$$

$$\delta w^{(1)}: \quad Q_{1,1}^{w1} + Q_{2,2}^{w1} - N_2^z - \widehat{Q}^{w1} = m^{(1)}\ddot{w}^{(0)} + m^{(2)}\ddot{w}^{(1)} + m^{(3)}\ddot{w}^{(2)} \tag{3.60}$$

$$\delta w^{(2)}: \quad Q_{1,1}^{w2} + Q_{2,2}^{w2} - N_3^z - \widehat{Q}^{w2} = m^{(2)}\ddot{w}^{(0)} + m^{(3)}\ddot{w}^{(1)} + m^{(4)}\ddot{w}^{(2)} \tag{3.61}$$

$$\begin{aligned}\delta\theta_1: \quad & M_{11,1} + M_{12,2} - Q_1 + \frac{1}{\eta}\left(\theta_{1,11} - k_{11,1}\right) + \frac{1}{\eta}\left(\theta_{1,22} + \theta_{2,12} - k_{12,2}\right) = \\ & = m^{(1)}\ddot{u}_1 + m^{(2)}\ddot{\theta}_1 + m_{\mu_{11}}^{(1)}\ddot{\psi}_1 + m_{\mu_{12}}^{(1)}\ddot{\psi}_2\end{aligned} \tag{3.62}$$

$$\begin{aligned}\delta\theta_2: \quad & M_{12,1} + M_{22,2} - Q_2 + \frac{1}{\eta}\left(\theta_{2,22} - k_{22,2}\right) + \frac{1}{\eta}\left(\theta_{1,12} + \theta_{2,11} - k_{12,1}\right) = \\ & = m^{(1)}\ddot{u}_1 + m^{(2)}\ddot{\theta}_1 + m_{\mu_{21}}^{(1)}\ddot{\psi}_1 + m_{\mu_{22}}^{(1)}\ddot{\psi}_2\end{aligned} \tag{3.63}$$

$$\begin{aligned}\delta\psi_1: \quad & M_{11,1}^{\phi} + M_{12,2}^{\phi} - Q_1^{\phi} + \frac{1}{\eta}\left(\psi_{1,11} - k_{11,1}^{\psi}\right) + \frac{1}{\eta}\left(\psi_{1,22} - k_{12,2}^{\psi}\right) = \\ & = m_{\mu_{11}}^{(0)}\ddot{u}_1 + m_{\mu_{21}}^{(0)}\ddot{u}_2 + m_{\mu_{11}}^{(1)}\ddot{\theta}_1 + m_{\mu_{21}}^{(1)}\ddot{\theta}_2 + m_{\mu_{11}}^{(2)}\ddot{\psi}_1 + m_{\mu_{12}}^{(2)}\ddot{\psi}_2\end{aligned} \tag{3.64}$$

$$\begin{aligned}\delta\psi_2: \quad & M_{21,1}^{\phi} + M_{22,2}^{\phi} - Q_2^{\phi} + \frac{1}{\eta}\left(\psi_{2,22} - k_{22,2}^{\psi}\right) + \frac{1}{\eta}\left(\psi_{2,11} - k_{21,1}^{\psi}\right) = \\ & = m_{\mu_{12}}^{(0)}\ddot{u}_1 + m_{\mu_{22}}^{(0)}\ddot{u}_2 + m_{\mu_{12}}^{(1)}\ddot{\theta}_1 + m_{\mu_{22}}^{(1)}\ddot{\theta}_2 + m_{\mu_{12}}^{(2)}\ddot{\psi}_1 + m_{\mu_{22}}^{(2)}\ddot{\psi}_2\end{aligned} \tag{3.65}$$

$$\delta e_{11}: \quad -\frac{1}{\eta}\left(e_{11} - u_{1,1}\right) + E_{11}^{HR} = 0 \tag{3.66}$$

$$\delta e_{22}: \quad -\frac{1}{\eta}\left(e_{22} - u_{2,2}\right) + E_{22}^{HR} = 0 \tag{3.67}$$

$$\delta e_{12}: \quad -\frac{1}{\eta}\left(e_{12} - u_{1,2} - u_{2,1}\right) + E_{12}^{HR} = 0 \tag{3.68}$$

$$\delta k_{11}: \quad -\frac{1}{\eta}\left(k_{11} - \theta_{1,1}\right) + K_{11}^{HR} = 0 \tag{3.69}$$

$$\delta k_{22}: \quad -\frac{1}{\eta}\left(k_{22} - \theta_{2,2}\right) + K_{22}^{HR} = 0 \tag{3.70}$$

$$\delta k_{12}: \quad -\frac{1}{\eta}\left(k_{12}-\theta_{1,2}-\theta_{2,1}\right)+K_{12}^{HR}=0 \tag{3.71}$$

$$\delta k_{11}^{\psi}: \quad -\frac{1}{\eta}\left(k_{11}^{\psi}-\psi_{1,1}\right)+K_{\psi 11}^{HR}=0 \tag{3.72}$$

$$\delta k_{22}^{\psi}: \quad -\frac{1}{\eta}\left(k_{22}^{\psi}-\psi_{2,2}\right)+K_{\psi 22}^{HR}=0 \tag{3.73}$$

$$\delta k_{12}^{\psi}: \quad -\frac{1}{\eta}\left(k_{12}^{\psi}-\psi_{1,2}\right)+K_{\psi 12}^{HR}=0 \tag{3.74}$$

$$\delta k_{21}^{\psi}: \quad -\frac{1}{\eta}\left(k_{21}^{\psi}-\psi_{2,1}\right)+K_{\psi 21}^{HR}=0 \tag{3.75}$$

The consistent boundary conditions are (for the sake of brevity, the full expressions of some terms are reported in Appendix C):

$$
\begin{array}{llcll}
u_1=\bar{u}_1 & \text{on } \Gamma_U & \vee & \bar{N}_{11}n_1+\bar{N}_{12}n_2+\dfrac{1}{\eta}\left(u_{1,1}-e_{11}\right)n_1+\dfrac{1}{\eta}\left(u_{1,2}+u_{2,1}-e_{12}\right)n_2 & \text{on } \Gamma_\sigma \\
u_2=\bar{u}_2 & \text{on } \Gamma_U & \vee & \bar{N}_{12}n_1+\bar{N}_{22}n_2+\dfrac{1}{\eta}\left(u_{2,2}-e_{22}\right)n_2+\dfrac{1}{\eta}\left(u_{1,2}+u_{2,1}-e_{12}\right)n_1 & \text{on } \Gamma_\sigma \\
w^{(0)}=\bar{w}^{(0)} & \text{on } \Gamma_U & \vee & \bar{Q}_1^{w0}n_1+\bar{Q}_2^{w0}n_2+{}^{HR}\bar{Q}_1^{w0}n_1+{}^{HR}\bar{Q}_2^{w0}n_2 & \text{on } \Gamma_\sigma \\
w^{(1)}=\bar{w}^{(1)} & \text{on } \Gamma_U & \vee & \bar{Q}_1^{w1}n_1+\bar{Q}_2^{w1}n_2+{}^{HR}\bar{Q}_1^{w1}n_1+{}^{HR}\bar{Q}_2^{w1}n_2 & \text{on } \Gamma_\sigma \\
w^{(2)}=\bar{w}^{(2)} & \text{on } \Gamma_U & \vee & \bar{Q}_1^{w2}n_1+\bar{Q}_2^{w2}n_2+{}^{HR}\bar{Q}_1^{w2}n_1+{}^{HR}\bar{Q}_2^{w2}n_2 & \text{on } \Gamma_\sigma \\
\theta_1=\bar{\theta}_1 & \text{on } \Gamma_U & \vee & \bar{M}_{11}n_1+\bar{M}_{12}n_2+\dfrac{1}{\eta}\left(\theta_{1,1}-k_{11}\right)n_1+\dfrac{1}{\eta}\left(\theta_{1,2}+\theta_{2,1}-k_{12}\right)n_2 & \text{on } \Gamma_\sigma \\
\theta_2=\bar{\theta}_2 & \text{on } \Gamma_U & \vee & \bar{M}_{12}n_1+\bar{M}_{22}n_2+\dfrac{1}{\eta}\left(\theta_{2,2}-k_{22}\right)n_2+\dfrac{1}{\eta}\left(\theta_{1,2}+\theta_{2,1}-k_{12}\right)n_1 & \text{on } \Gamma_\sigma \\
\psi_1=\bar{\psi}_1 & \text{on } \Gamma_U & \vee & \bar{M}_{11}^{\phi}n_1+\bar{M}_{12}^{\phi}n_2+\dfrac{1}{\eta}\left(\psi_{1,1}-k_{11}^{\psi}\right)n_1+\dfrac{1}{\eta}\left(\psi_{1,2}-k_{12}^{\psi}\right)n_2 & \text{on } \Gamma_\sigma \\
\psi_2=\bar{\psi}_2 & \text{on } \Gamma_U & \vee & \bar{M}_{21}^{\phi}n_1+\bar{M}_{22}^{\phi}n_2+\dfrac{1}{\eta}\left(\psi_{2,2}-k_{22}^{\psi}\right)n_2+\dfrac{1}{\eta}\left(\psi_{2,1}-k_{21}^{\psi}\right)n_1 & \text{on } \Gamma_\sigma \\
e_{11}=\bar{e}_{11} & \text{on } \Gamma_U & \vee & {}^{HR}\bar{E}_1^{e11}n_1+{}^{HR}\bar{E}_2^{e11}n_2 & \text{on } \Gamma_\sigma \\
e_{22}=\bar{e}_{22} & \text{on } \Gamma_U & \vee & {}^{HR}\bar{E}_1^{e22}n_1+{}^{HR}\bar{E}_2^{e22}n_2 & \text{on } \Gamma_\sigma \\
e_{12}=\bar{e}_{12} & \text{on } \Gamma_U & \vee & {}^{HR}\bar{E}_1^{e12}n_1+{}^{HR}\bar{E}_2^{e12}n_2 & \text{on } \Gamma_\sigma \\
k_{11}=\bar{k}_{11} & \text{on } \Gamma_U & \vee & {}^{HR}\bar{K}_1^{k11}n_1+{}^{HR}\bar{K}_2^{k11}n_2 & \text{on } \Gamma_\sigma \\
k_{22}=\bar{k}_{22} & \text{on } \Gamma_U & \vee & {}^{HR}\bar{K}_1^{k22}n_1+{}^{HR}\bar{K}_2^{k22}n_2 & \text{on } \Gamma_\sigma \\
k_{12}=\bar{k}_{12} & \text{on } \Gamma_U & \vee & {}^{HR}\bar{K}_1^{k12}n_1+{}^{HR}\bar{K}_2^{k12}n_2 & \text{on } \Gamma_\sigma \\
k_{11}^{\psi}=\bar{k}_{11}^{\psi} & \text{on } \Gamma_U & \vee & {}^{HR}\bar{K}_1^{k11\psi}n_1+{}^{HR}\bar{K}_2^{k11\psi}n_2 & \text{on } \Gamma_\sigma \\
k_{22}^{\psi}=\bar{k}_{22}^{\psi} & \text{on } \Gamma_U & \vee & {}^{HR}\bar{K}_1^{k22\psi}n_1+{}^{HR}\bar{K}_2^{k22\psi}n_2 & \text{on } \Gamma_\sigma \\
k_{12}^{\psi}=\bar{k}_{12}^{\psi} & \text{on } \Gamma_U & \vee & {}^{HR}\bar{K}_1^{k12\psi}n_1+{}^{HR}\bar{K}_2^{k12\psi}n_2 & \text{on } \Gamma_\sigma \\
k_{21}^{\psi}=\bar{k}_{21}^{\psi} & \text{on } \Gamma_U & \vee & {}^{HR}\bar{K}_1^{k21\psi}n_1+{}^{HR}\bar{K}_2^{k21\psi}n_2 & \text{on } \Gamma_\sigma
\end{array}
\tag{3.76}
$$

In Eq. (3.76), $n_1=\cos(x_1,\mathbf{n})$ and $n_2=\cos(x_2,\mathbf{n})$ are the components (direction cosines) of the unit outward normal vector to the cylindrical plate edges.

The resultant forces and moments are defined as:

$$
\begin{aligned}
&\left(\mathbf{N},\mathbf{M},\mathbf{M}^{\phi}\right)=\left\langle\left(1,x_3,\mathbf{M}^{(k)T}\right)\boldsymbol{\sigma}_p^{(k)}\right\rangle \\
&\mathbf{N}^{z}=\left\langle\mathbf{H}_{,3}^{z\,T}\sigma_{33}^{a}\right\rangle \\
&\left(\mathbf{Q}^{w},\mathbf{Q},\mathbf{Q}^{\phi}\right)=\left\langle\left(\mathbf{H}^{zT},\mathbf{I},\partial_3\boldsymbol{\mu}^{T}\right)\boldsymbol{\tau}_t^{a}\right\rangle
\end{aligned}
\tag{3.77}
$$

Moreover, in Eqs. (3.38)-(3.44),

$$\begin{aligned}
&\overline{p}_1 = \overline{p}_{1(B)} + \overline{p}_{1(T)}; \quad \overline{p}_2 = \overline{p}_{2(B)} + \overline{p}_{2(T)};\\
&\overline{m}_1 = \frac{h}{2}\left(\overline{p}_{1(T)} - \overline{p}_{1(B)}\right); \quad \overline{m}_2 = \frac{h}{2}\left(\overline{p}_{2(T)} - \overline{p}_{2(B)}\right);\\
&\overline{q}_3 = \overline{p}_{3(B)} + \overline{p}_{3(T)}
\end{aligned} \tag{3.78}$$

By using the mixed material constitutive relations and the expressions for the assumed transverse normal and shear stresses, i.e. Eqs. (3.36) and (3.37), the following constitutive relations for the en-RZT$^{(m)}_{\{3,2\}}$, are expressed as follows:

$$\begin{aligned}
\mathbf{N} &= \tilde{\mathbf{A}}\boldsymbol{\varepsilon}_m + \tilde{\mathbf{B}}\boldsymbol{\varepsilon}_\theta + \tilde{\mathbf{A}}^{\phi}\boldsymbol{\varepsilon}_\psi + \tilde{\mathbf{A}}^{w}\mathbf{w} + \tilde{\mathbf{A}}^{qz}\overline{\mathbf{q}}_z\\
\mathbf{M} &= \tilde{\mathbf{C}}\boldsymbol{\varepsilon}_m + \tilde{\mathbf{D}}\boldsymbol{\varepsilon}_\theta + \tilde{\mathbf{B}}^{\phi}\boldsymbol{\varepsilon}_\psi + \tilde{\mathbf{B}}^{w}\mathbf{w} + \tilde{\mathbf{B}}^{qz}\overline{\mathbf{q}}_z\\
\mathbf{M}^{\phi} &= \tilde{\mathbf{E}}^{\phi}\boldsymbol{\varepsilon}_m + \tilde{\mathbf{F}}^{\phi}\boldsymbol{\varepsilon}_\theta + \tilde{\mathbf{G}}^{\phi}\boldsymbol{\varepsilon}_\psi + \tilde{\mathbf{C}}^{w}\mathbf{w} + \tilde{\mathbf{C}}^{qz}\overline{\mathbf{q}}_z
\end{aligned} \tag{3.79}$$

$$\mathbf{N}^{z} = \mathbf{A}^{Nz}\boldsymbol{\varepsilon}_m + \mathbf{B}^{Nz}\boldsymbol{\varepsilon}_\theta + \mathbf{C}^{Nz}\boldsymbol{\varepsilon}_\psi + \mathbf{D}^{Nz}\mathbf{w} + \mathbf{E}^{Nz}\overline{\mathbf{q}}_z \tag{3.80}$$

$$\begin{aligned}
\mathbf{Q}^{w} &= \hat{\mathbf{A}}^{wT}\partial\mathbf{e} + \hat{\mathbf{B}}^{wT}\partial\mathbf{k} + \hat{\mathbf{C}}^{wT}\partial\mathbf{k}^{\psi} + \hat{\mathbf{D}}^{wT}\partial\mathbf{w} + \hat{\mathbf{E}}^{w}\partial\overline{\mathbf{q}}_z\\
\mathbf{Q} &= \hat{\mathbf{A}}^{\theta T}\partial\mathbf{e} + \hat{\mathbf{B}}^{\theta T}\partial\mathbf{k} + \hat{\mathbf{C}}^{\theta T}\partial\mathbf{k}^{\psi} + \hat{\mathbf{D}}^{\theta T}\partial\mathbf{w} + \hat{\mathbf{E}}^{\theta}\partial\overline{\mathbf{q}}_z\\
\mathbf{Q}^{\phi} &= \hat{\mathbf{A}}^{\psi T}\partial\mathbf{e} + \hat{\mathbf{B}}^{\psi T}\partial\mathbf{k} + \hat{\mathbf{C}}^{\psi T}\partial\mathbf{k}^{\psi} + \hat{\mathbf{D}}^{\psi T}\partial\mathbf{w} + \hat{\mathbf{E}}^{\psi}\partial\overline{\mathbf{q}}_z
\end{aligned} \tag{3.81}$$

Appendix D reports, for the sake of brevity, the definition of the matrices of the constitutive relations, Eqs. (3.79)-(3.81), and the other matrices in the governing equations, Eqs (3.38)-(3.56), and in the boundary conditions, Eq. (3.76) . Moreover, the inertial quantities that appear in the equations of motions, i.e. Eqs. (3.57) - (3.75) are defined as follows:

$$\begin{aligned}
&\left(m^{(0)}, m^{(1)}, m^{(2)}, m^{(3)}, m^{(4)}\right) = \left\langle \rho^{(k)}\left(1, x_3, x_3^2, x_3^3, x_3^4\right)\right\rangle;\\
&\left(\mathbf{m}_\mu^{(0)}, \mathbf{m}_\mu^{(1)}, \mathbf{m}_\mu^{(2)}\right) = \left\langle \rho^{(k)}\left(\boldsymbol{\mu}^{(k)}, x_3\boldsymbol{\mu}^{(k)}, \boldsymbol{\mu}^{(k)T}\boldsymbol{\mu}^{(k)}\right)\right\rangle
\end{aligned} \tag{3.82}$$

Chapter 4

Beam finite elements based on the mixed {3,2}-enhanced Refined Zigzag Theory

This Chapter proposes a new beam mixed model to investigate the elastodynamic behaviour of multilayered composites and sandwich structures. The model is based on the previously developed en-RZT$^{(m)}_{\{3,2\}}$, simplified to analyse multilayered composite and sandwich beams. However, due to the lamination schemes considered in this Chapter and considering the experimental campaign, the beam formulation neglects the effect of transverse shear coupling in anisotropic multilayered structures.

In the first part of this Chapter, the formulation of the beam problem is presented, and the governing equations and consistent boundary conditions are obtained by using the mixed functional as shown in Chapter 3.

Based on this new higher-order RZT-mixed beam, a finite formulation is also addressed to solve the governing equations in more general cases. Two types of beam elements are formulated considering two interpolation schemes to approximate the kinematic variables and the strain quantities. In order to reduce the total number of variables and to achieve a simple node configuration in which only the nodal degrees of freedom related to kinematic quantities appear, the nodal strains dof's are omitted by implementing the static condensation.

4.1 Introduction

This section presents a brief literature review of the existing RZT-beam-based model and finite element formulation strategies.

The first attempts to formulate a class of simple beam elements based on RZT are given by Gherlone et al. [107] and Oñate et al. [109]. Both groups independently formulated a class of two-node C^0-continuous elements to analyse multilayered composite and sandwich beams. However, like the low-order FSDT-based elements, RZT finite element formulation also suffers from the shear-locking phenomenon. The implemented strategies to overcome this problem are numerous in the literature but are not reviewed here for clarity. However, it is worth citing the *anisoparametric interpolation* strategy adopted by Gherlone et al. [107]. In its methodology, the transverse displacements have been interpolated by polynomial shape functions of one order degree higher than the others. As a result, a locking-free three-node beam element is obtained where the transverse displacement is interpolated using three nodes, whereas the other degrees of freedom are interpolated with only two extreme nodes. The internal node is then condensed out by enforcing a constraint condition on the second derivative of the auxiliary strain measure along the entire element, reobtaining a simple two-node configuration.

In a different way, Oñate et al. [109] implemented in its element formulation the reduced integration technique, a numerical technique able to under-integrate the shear contribution of the stiffness matrix. It has been demonstrated by Tessler [48] that the reduced integration and the *anisoparametric* strategy can give the same results for beam elements. Regardless of the adopted methodology to overcome the shear-locking problem, the proposed RZT elements are demonstrated to be very accurate in global response predictions for deflections, frequencies and in-plane axial stress.

The RZT finite element formulation has been extended by Ejio et al. [160] to the analysis of laminated structures with the inclusion of delamination defects. An iterative process has been implemented by the authors to update the zigzag functions when the material shows degraded properties.

The formulation of higher-order elements to increase the convergence rate has been shown in Di Sciuva et al. [108]. Nallim et al. [161] implemented the hierarchical definition of the shape functions to formulate locking-free beam elements based on the RZT. The kinematic variables are interpolated with two groups of shape functions: Lagrangian polynomials and orthogonal Gram-Schmidt polynomials that vanish at the element's end. This solution guarantees a much more accurate description of displacements, strains, and stresses with low discretization patterns.

In Iurlaro's PhD dissertation [132], a two-node element has been formulated using the exact RZT shape functions to increase the accuracy of the stiffness matrix approximation. As a matter of fact, these elements are able to guarantee no errors in the stiffness matrix evaluation and a superconvergent behaviour.

An alternative method has been proposed by Wimmer and Nachbaguer [162] in which the RZT beam formulation has been used in conjunction with the transfer matrix method to increase the accuracy of the stress predictions without involving any smoothing techniques.

The RZT beam predictive capabilities using the finite element formulation have also been tested for buckling analysis of heterogeneous sandwich beams. Involving a non-linear RZT finite element formulation, Ascione and co-workers [163,164] have investigated numerically and experimentally the buckling analysis of multilayered composite beams. The provided results by the RZT beam model are very close to the experimental ones and with the numerical obtained with computationally expensive high-fidelity FE models.

As highlighted in the previous Chapter, the model accuracy of stress predictions could be increased by adopting appropriate mixed formulations. In the framework of mixed-RZT models, it is worthy of citing the work of Groh and Tessler [123]. Their model considers the delamination effect for the beam's response along with the *anisoparametric interpolation* strategy to formulate locking-free elements. Using the RMVT, Iurlaro et al. [131] developed a third-order RZT model that considers the transverse normal deformability. Using the anisoparametric interpolation strategy and the constraint condition on the auxiliary strain measure, the formulated finite element has demonstrated to be very accurate in global and local response of multilayered beam structures. Similarly, Flores et al. [165], starting from Iurlaro's third-order RZT model, extended the range of model applicability by including discontinuities in the

cross-section for buckling analysis, revealing the greater accuracy of the mixed model for stress description and critical load predictions.

More recently, Kutlu [120] formulated a linear RZT mixed model using the Hellinger-Reissner functional without reducing the variables as done in the RMVT. The provided results in Ref. [120] encourage using the HR formulation to increase the global beam responses prediction of stress quantities.

According to the provided literature framework regarding the RZT-based models, the strength of the mixed formulations in stress predictions and the wide range of applications of RZT model has been shown.

The new mixed higher-order RZT beam model is formulated in the following sections. First, the kinematic assumptions and the constitutive material relations are shown. Then, the transverse normal stress field is assumed as a smoothed function of the transverse coordinate and transverse shear stress distribution is derived from the integration of the local equilibrium equations. Finally, the mixed formulation that involves the penalty term to enforce in a weak manner the strain compatibility has been applied here to obtain the governing equations, along with the consistent boundary conditions, for static and dynamic problems.

Lastly, a finite element formulation is presented based on the newly formulated beam mixed model. Based on two different interpolation schemes, two elements are obtained. The first involves the isoparametric interpolation with the linear shape functions, whereas the second adopts the anisoparametric constrained strategy for the new strain variable. The additional node is then condensed by appropriate strain enforcement to achieve a simple-two node configuration. To further reduce the computational cost of the formulated elements and to take advantage of simplified element formulation for the applied loads, the strain nodal dof's are statically condensed.

4.2 The new-mixed RZT for beams

The basic assumptions of the en-$\text{RZT}^{(m)}_{\{3,2\}}$ model applied to beam structures are recalled here. The governing equations and consistent boundary conditions for bending and free vibration problems are derived using the mixed variational statement, as introduced in Chapter 3.

It is considered a beam of length L and cross-section area $A = b \times h$, where b is the width, and h is the thickness. The beam points are referred to an orthogonal reference system (x_1, x_2, x_3), where x_1 corresponds to the coordinate of the beam longitudinal axis and x_3, the transverse coordinate corresponds to the beam thickness, as shown in Figure 9. Moreover, $x_3 \in \left[-h/2, +h/2\right]$. According to the cylindrical bending assumption, beam deformations are allowed only in the (x_1, x_3) plane, indicating that no out-of-plane displacements are considered. Thus, the transverse shear coupling is neglected here.

As reported in Figure 9, the mechanical loads applied to the beam's external bottom and top surfaces are the distributed transverse loads, $\bar{p}_{3(B)}(x_1)$ and $\bar{p}_{3(T)}(x_1)$, and the distributed axial loads, $\bar{p}_{1(B)}(x_1)$ and $\bar{p}_{1(T)}(x_1)$.

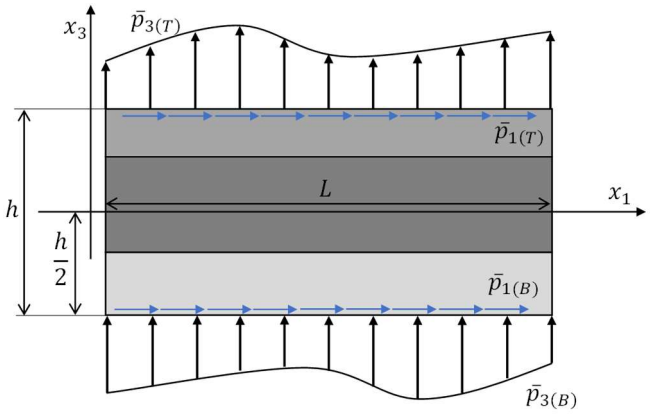

Figure 9: Beam geometry, reference frame and applied loads.

4.2.1 Kinematics, strains and stresses and assumed fields

The displacement components of the orthogonal displacement vector of the en-RZT$^{(m)}_{\{3,2\}}$ beam, read:

$$\begin{aligned} U_1^{(k)}(x_1, x_3; t) &= u(x_1; t) + x_3\theta(x_1; t) + x_3^2\chi(x_1; t) + x_3^3\omega(x_1; t) + \phi^{(k)}(x_3)\psi(x_1; t) \\ U_3(x_1, x_3; t) &= w^{(0)}(x_1; t) + x_3 w^{(1)}(x_1; t) + x_3^2 w^{(2)}(x_1; t) \end{aligned} \tag{4.1}$$

where, $U_1^{(k)}$ and U_3 are the displacements in the x_1 and x_3 directions, respectively. Such as the en-RZT$^{(m)}_{\{3,2\}}$, the transverse displacement is assumed with a smeared parabolic function of the thickness coordinate, independent of the layer. The kinematic variables that appear in Eq. (4.1) are u and $w^{(0)}$ the uniform axial and transverse displacements, θ_1 the average bending rotation, ψ_1 the zigzag rotation, χ, ω, $w^{(1)}$ and $w^{(2)}$ are the kinematic variables related to the higher order terms.

The strain-displacement relations for a beam structure read:

$$\begin{aligned}
&\varepsilon_{11}^{(k)}\left(x_1,x_3;t\right)=U_{1,1}^{(k)}\left(x_1,x_3;t\right)\\
&\varepsilon_{33}\left(x_1,x_3;t\right)=U_{3,3}\left(x_1,x_3;t\right)\\
&\gamma_{13}^{(k)}\left(x_1,x_3;t\right)=U_{3,1}\left(x_1,x_3;t\right)+U_{1,3}^{(k)}\left(x_1,x_3;t\right)
\end{aligned} \tag{4.2}$$

Here follow the beam stress-stress relations written in an appropriate mixed form [166]:

$$\begin{Bmatrix}\sigma_{11}\\ \varepsilon_{33}\\ \tau_{13}\end{Bmatrix}^{(k)}=\begin{bmatrix}E_1 & R_{13} & 0\\ -R_{13} & S_{33} & 0\\ 0 & 0 & G_{13}\end{bmatrix}^{(k)}\begin{Bmatrix}\varepsilon_{11}\\ \sigma_{33}\\ \gamma_{13}\end{Bmatrix}^{(k)} \tag{4.3}$$

where

$$\begin{aligned}
&S_{33}^{(k)}=1/\breve{C}_{33}^{(k)}\\
&R_{13}^{(k)}=\nu_{13}^{(k)}
\end{aligned} \tag{4.4}$$

It can be noted that the displacement field reported by Eq. (4.1) for a beam structure derived from the en-RZT$^{(m)}_{\{3,2\}}$ is formally the same as those introduced by Iurlaro et al. [131]. The only difference relies on the transverse displacement definition. For the sake of conciseness, the passages to reduce and simplify the displacement field are a particular case of the plate problem defined in Chapter 3 and lead to the result provided by Iurlaro et al. [131]. The final expression of the displacement field in which the third-order zigzag function appears is reported as follows:

$$\begin{aligned} U_1^{(k)}(x_1,x_3;t) &= u(x_1;t) + x_3\theta(x_1;t) + \mu^{(k)}(x_3)\psi(x_1;t) \\ U_3(x_1,x_3;t) &= w^{(0)}(x_1;t) + x_3 w^{(1)}(x_1;t) + x_3^2 w^{(2)}(x_1;t) \end{aligned} \tag{4.5}$$

where $\mu^{(k)}$ is the new third-order piecewise continuous zigzag function and its full expression for beam reads:

$$\mu^{(k)}(x_3) = -x_3^2\chi_0 - x_3^3\omega_0 + \phi^{(k)}(x_3) \tag{4.6}$$

The third-order zigzag function is characterized by the partial transverse shear stress continuity at the layer interfaces and the vanishing condition of the zigzag functions at the top and bottom beam surfaces.

The strain components expressed in terms of the kinematic unknowns for the beam model are reported here for clarity:

$$\begin{aligned} \varepsilon_{11}^{(k)}(x_1,x_3) &= u_{,1}(x_1) + x_3\theta_{,1}(x_1) + \mu^{(k)}(x_3)\psi_{,1}(x_1) \\ \varepsilon_{33}(x_1,x_3) &= w^{(1)}(x_1) + 2x_3 w^{(2)}(x_1) \\ \gamma_{13}^{(k)}(x_1,x_3) &= w_{,1}^{(0)}(x_1) + x_3 w_{,1}^{(1)}(x_1) + x_3^2 w_{,1}^{(2)}(x_1) + \theta(x_1) + \partial\mu_{,3}^{(k)}(x_3)\psi(x_1) \end{aligned} \tag{4.7}$$

Since the transverse normal deformability in thick multilayered structures could not be neglected, a smeared cubic function for the transverse normal stress is considered in which the traction conditions at the top and bottom surfaces are enforced. Its expression recalled from the en-RZT$^{(m)}_{\{3,2\}}$ is here reported for clarity:

$$\sigma_{33}^a(x_1,x_3) = \mathbf{P}_\sigma(x_3)\mathbf{q}_\sigma(x_1) + \mathbf{L}(x_3)\overline{\mathbf{q}}_z(x_1) \tag{4.8}$$

where,

$$\begin{aligned} &\mathbf{L}(x_3) = \left[\left(\frac{x_3}{h} - \frac{1}{2}\right) \quad \left(\frac{x_3}{h} + \frac{1}{2}\right)\right]; \quad \mathbf{P}_\sigma(x_3) = \left[\left(x_3^2 - \frac{h^2}{4}\right) \quad x_3\left(x_3^3 - \frac{h^2}{4}\right)\right]; \\ &\overline{\mathbf{q}}_z(x_1)^T = \left[\overline{p}_{3(B)} \quad \overline{p}_{3(T)}\right]; \quad \mathbf{q}_\sigma(x_1)^T = \left[\sigma_2^z \quad \sigma_3^z\right] \end{aligned} \tag{4.9}$$

The assumed transverse shear stress distribution is obtained by integrating Cauchy's equation under the hypothesis of cylindrical bending and in the absence of body forces:

$$\sigma_{11,1}^{(k)} + \tau_{13,3}^{(k)} = 0 \tag{4.10}$$

The in-plane stress comes from the constitutive relation expressed in Eq. (4.3) , with the strains quantities, i.e. the derivatives of the kinematic variables see Eq. (4.7), that are assumed as new independent variables. The in-plane strain, according to this assumption, reads:

$$\begin{aligned} \varepsilon_{11}^{(k)}\left(x_1, x_3\right) = u_{,1}\left(x_1\right) + x_3\theta_{,1}\left(x_1\right) + \mu^{(k)}(x_3)\psi_{,1} \rightarrow \\ \rightarrow e\left(x_1\right) + x_3 k\left(x_1\right) + \mu^{(k)}(x_3)k^{\psi}\left(x_1\right) \end{aligned} \tag{4.11}$$

where the new assumed strain variables are e, k and k^{ψ}. However, the expression for the in-plane stress could not be used yet in Cauchy's equation since it is necessary to enforce prior the compatibility condition between the assumed and derived transverse normal strains given by the Hellinger-Reissner functional described in the following Section.

4.2.2 Mixed variational principle and expressions for the assumed normal and shear transverse stress functions

The mixed variational statement adopted in Chapter 3 for the en-RZT$^{(m)}_{\{3,2\}}$ plate problem is here specified for the beam problem. Its general expression is here recalled:

$$\delta\Pi = \delta\Pi_{\text{int}} + \delta\Pi_{HR} + \delta\Lambda - \delta\Pi_{ext} - \delta\Pi_{in} = 0 \tag{4.12}$$

where $\delta\Pi_{\text{int}}$ is the virtual variation of the internal energy, and it is expressed as:

$$\delta\Pi_{\text{int}} = \int_V \left[\left(\delta\varepsilon_{11}^{(k)}\sigma_{11}^{(k)} + \delta\gamma_{13}^{(k)}\tau_{13}^{a} + \delta\varepsilon_{33}\sigma_{33}^{a} \right) \right] dV \tag{4.13}$$

Moreover, $\delta\Pi_{HR}$ is the Hellinger-Reissner variational contribution that enforces the weak compatibility between the transverse normal and shear strains:

$$\delta\Pi_{HR} = \int_V \left[\delta\tau_{13}^a \left(\gamma_{13}^{(k)} - \gamma_{13}^{(k)a} \right) + \delta\sigma_{33}^a \left(\varepsilon_{33} - \varepsilon_{33}^{(k)a} \right) \right] dV \tag{4.14}$$

The penalty functional expressed by the symbol $\delta\Lambda$ is defined by a penalty parameter η that plays the role of weight function of this term in the governing functional. Its expression according to the new beam B-RZT$^{(m)}_{\{3,2\}}$ is:

$$\delta\Lambda = \frac{1}{\eta}\int_V \begin{bmatrix} \left(\delta u_{,1} - \delta e\right)\left(u_{,1} - e\right) + \\ + \left(\delta\theta_{,1} - \delta k\right)\left(\theta_{,1} - k\right) + \\ + \left(\delta\psi_{,1} - \delta k^{\psi}\right)\left(\psi_{,1} - k^{\psi}\right) \end{bmatrix} dV \tag{4.15}$$

The virtual work done by the inertial forces $\delta\Pi_{in}$ is expressed as follows:

$$\begin{aligned} \delta\Pi_{in} &= \int_V \rho^{(k)} \delta\mathbf{U}^T \ddot{\mathbf{U}} dV = \\ &= \int_V \delta \begin{Bmatrix} u \\ \theta \\ \psi \end{Bmatrix}^T \begin{Bmatrix} 1 \\ x_3 \\ \mu^{(k)} \end{Bmatrix} \rho^{(k)} \begin{bmatrix} 1 & x_3 & \mu^{(k)} \end{bmatrix} \begin{Bmatrix} \ddot{u} \\ \ddot{\theta} \\ \ddot{\psi} \end{Bmatrix} dV + \\ &+ \int_V \delta \begin{Bmatrix} w^{(0)} \\ w^{(1)} \\ w^{(2)} \end{Bmatrix}^T \mathbf{H}^{zT} \rho^{(k)} \mathbf{H}^z \begin{Bmatrix} \ddot{w}^{(0)} \\ \ddot{w}^{(1)} \\ \ddot{w}^{(2)} \end{Bmatrix} dV \end{aligned} \tag{4.16}$$

with $\rho^{(k)}$ the material mass density of the k^{th} layer; the overdot indicates the differentiation with respect to time. Moreover, $\mathbf{H}^z(x_3) = \begin{bmatrix} 1 & x_3 & x_3^2 \end{bmatrix}$ and $\mathbf{d}^T = \begin{bmatrix} u & w^{(0)} & w^{(1)} & w^{(2)} & \theta & \psi \end{bmatrix}$ is the vector of the kinematic unknowns. It is worth noting that the new strain variables do not contribute to the system's inertia.

At last, the virtual work done by the externally applied tractions, $\delta\Pi_{ext}$, reads:

$$\begin{aligned} \delta\Pi_{ext} &= \int_L \overline{p}_{1(T)} U_1^{(N)}(x_3 = h/2) dx_1 + \int_L \overline{p}_{1(B)} U_1^{(1)}(x_3 = -h/2) dx_1 \\ &+ \int_L \overline{p}_{3(T)} U_3^{(N)}(x_3 = h/2) dx_1 + \int_L \overline{p}_{3(B)} U_3^{(1)}(x_3 = -h/2) dx_1 \end{aligned} \tag{4.17}$$

As done in Chapter 3 for plate structures, the first step for the beam model is to enforce the transverse normal strain compatibility in the Hellinger-Reissner functional. The compatibility condition reads:

$$\delta\Pi_{\sigma_{33}} = \int_V \left[\delta\sigma_{33}^a \left(\varepsilon_{33} - \varepsilon_{33}^{(k)a} \right) \right] dV = 0 \tag{4.18}$$

Due to the independent assumption of the stress field, the condition of Eq. (4.18) results in a relation between the stress variables and the kinematic variables. Using the constitutive material equations, i.e. Eq. (4.3), the assumed transverse normal strain reads:

$$\varepsilon_{33}^a(x_1, x_3) = S_{33}^{(k)} \sigma_{33}^a(x_1, x_3) - R_{13}{}^{(k)} \varepsilon_{11}^{(k)}(x_1, x_3) \tag{4.19}$$

After some mathematical passages, here not reported for the sake of clarity, the transverse normal stress is rewritten as a function of the kinematic variables:

$$\begin{aligned} \sigma_{33}^a(x_1, x_3) = {} & A_\sigma^u(x_3) u_{1,1}(x_1) + A_\sigma^\theta(x_3) \theta_{1,1}(x_1) + \\ & + A_\sigma^\psi(x_3) \psi_{1,1}(x_1) + \mathbf{A}_\sigma^w(x_3) \mathbf{w}(x_1) + \mathbf{A}_\sigma^{q_z}(x_3) \overline{\mathbf{q}}_z(x_1) \end{aligned} \tag{4.20}$$

where the functions of the transverse coordinate that appear in Eq. (4.20) have the following expressions:

$$\begin{aligned} A_\sigma^u(x_3) &= \mathbf{P}_\sigma \left\langle S_{33}^{(k)} \mathbf{P}_\sigma{}^T \mathbf{P}_\sigma \right\rangle^{-1} \left\langle \mathbf{P}_\sigma{}^T R_{13}{}^{(k)} \right\rangle; \\ A_\sigma^\theta(x_3) &= \mathbf{P}_\sigma \left\langle S_{33}^{(k)} \mathbf{P}_\sigma{}^T \mathbf{P}_\sigma \right\rangle^{-1} \left\langle \mathbf{P}_\sigma{}^T R_{13}{}^{(k)} x_3 \right\rangle; \\ A_\sigma^\psi(x_3) &= \mathbf{P}_\sigma \left\langle S_{33}^{(k)} \mathbf{P}_\sigma{}^T \mathbf{P}_\sigma \right\rangle^{-1} \left\langle \mathbf{P}_\sigma{}^T R_{13}{}^{(k)} \mu^{(k)} \right\rangle; \\ \mathbf{A}_\sigma^w(x_3) &= \mathbf{P}_\sigma \left\langle S_{33}^{(k)} \mathbf{P}_\sigma{}^T \mathbf{P}_\sigma \right\rangle^{-1} \left\langle \mathbf{P}_\sigma{}^T \mathbf{H}_{,3}^z \right\rangle; \\ \mathbf{A}_\sigma^{q_z}(x_3) &= \left[\mathbf{L} - \mathbf{P}_\sigma \left\langle S_{33}^{(k)} \mathbf{P}_\sigma{}^T \mathbf{P}_\sigma \right\rangle^{-1} \left\langle S_{33}^{(k)} \mathbf{P}_\sigma{}^T \mathbf{L} \right\rangle \right] \end{aligned} \tag{4.21}$$

By taking into account the final expression of the transverse normal stress, i.e. Eq. (4.20) and substituting into the constitutive relations, i.e. Eq. (4.3), and considering the new strain field variables, the complete expression of the in-plane stress reads:

$$\begin{aligned}\sigma_{11}^{(k)} &= \left(E_1^{(k)} + R_{13}{}^{(k)} A_\sigma^u(x_3)\right) e(x_1) + \left(x_3 E_1^{(k)} + R_{13}{}^{(k)} A_\sigma^\theta(x_3)\right) k(x_1) + \\ &+ \left(E_1^{(k)} \mu^{(k)}(x_3) + R_{13}{}^{(k)} A_\sigma^\psi(x_3)\right) k^\psi(x_1) + \\ &+ R_{13}{}^{(k)} \mathbf{A}_\sigma^w(x_3) \mathbf{w}(x_1) + R_{13}{}^{(k)} \mathbf{A}_\sigma^{q_z}(x_3) \overline{\mathbf{q}}_z(x_1)\end{aligned} \tag{4.22}$$

Substituting the expression of the transverse normal stress Eq. (4.20) and integrating by parts Eq. (4.10), yields

$$\begin{aligned}\tau_{13}^a(x_1, x_3) &= -\overline{p}_{1(B)}(x_1) + A^z(x_3) e_{,1}(x_1) + B^z(x_3) k_{,1}(x_1) + \\ &+ D^z(x_3) k_{,1}^\psi(x_1) + \mathbf{E}^\mathbf{z}(x_3) \partial\mathbf{w}(x_1) + \mathbf{F}^\mathbf{z}(x_3) \partial\overline{\mathbf{q}}_z(x_1) + \breve{a}(x_3 + h/2)\end{aligned} \tag{4.23}$$

where $\partial\overline{\mathbf{q}}_z(x_1)$ represent the derivatives of the transverse distributed load, i.e. $\partial\overline{\mathbf{q}}_z(x_1)^T = \lfloor \overline{p}_{3(B),1} \quad \overline{p}_{3(T),1} \rfloor$; $\overline{\mathbf{q}}_\mathbf{p}(x_1)$ is the vector of the prescribed tractions in the x_1 direction at the bottom and top external surfaces, i.e. $\overline{\mathbf{q}}_\mathbf{p}(x_1)^T = \lfloor \overline{p}_{1(B)} \quad \overline{p}_{1(T)} \rfloor$; $\mathbf{q}_t(x_1)^T = \left[e_{,1}(x_1) \quad k_{,1}(x_1) \quad k_{,1}^\psi(x_1) \quad \partial\mathbf{w}(x_1)^T \right]$ is the vector of the derivatives of the strain unknowns and transverse variables. Note that $\partial\mathbf{w}(x_1)^T = \lfloor w_{,1}^{(0)} \quad w_{,1}^{(1)} \quad w_{,1}^{(2)} \rfloor$. Moreover, the through-the-thickness functions are:

$$\begin{aligned}A^z(x_3) &= -\int_{-h/2}^{x_3} \left(E_1^{(k)} + R_{13}^{(k)} A_\sigma^u\right) dx_3 \\ B^z(x_3) &= -\int_{-h/2}^{x_3} \left(x_3 E_1^{(k)} + R_{13}^{(k)} A_\sigma^\theta\right) dx_3 \\ D^z(x_3) &= -\int_{-h/2}^{x_3} \left(E_1^{(k)} \mu^{(k)} + R_{13}^{(k)} A_\sigma^\psi\right) dz \\ \mathbf{E}^\mathbf{z}(x_3) &= \left\lfloor -\left[\int_{-h/2}^{x_3} R_{13}^{(k)} A_{\sigma 11}^w dx_3\right] \quad -\left[\int_{-h/2}^{x_3} R_{13}^{(k)} A_{\sigma 12}^w dx_3\right] \quad -\left[\int_{-h/2}^{x_3} R_{13}^{(k)} A_{\sigma 13}^w dx_3\right] \right\rfloor \\ \mathbf{F}^\mathbf{z}(x_3) &= \left\lfloor -\left[\int_{-h/2}^{x_3} R_{13}^{(k)} A_{\sigma 11}^{q_z} dx_3\right] \quad -\left[\int_{-h/2}^{x_3} R_{13}^{(k)} A_{\sigma 12}^{q_z} dx_3\right] \right\rfloor\end{aligned} \tag{4.24}$$

Enforcing the in-plane traction conditions at the top surface of the beam yields:

$$\begin{aligned}\breve{a} = &-\frac{1}{h}\left(\overline{p}_{1(T)} + \overline{p}_{1(B)}\right) - \frac{1}{h}\left\langle A^z \right\rangle e_{,1} - \frac{1}{h}\left\langle B^z \right\rangle k_{,1} + \\ &-\frac{1}{h}\left\langle D^z \right\rangle k_{,1}^{\psi} + \frac{1}{h}\left\langle \mathbf{E}^{\mathbf{z}} \right\rangle \partial\mathbf{w} + \frac{1}{h}\left\langle \mathbf{F}^{\mathbf{z}} \right\rangle \partial\overline{\mathbf{q}}_z\end{aligned} \tag{4.25}$$

Where $\langle\bullet\rangle = b\sum_{k=1}^{N}\int_{x_3^{(k-1)}}^{x_3^{(k)}}(\bullet)dx_3 = b\sum_{k=1}^{N}\int_{x_{3(B)}^{(k)}}^{x_{3(T)}^{(k)}}(\bullet)dx_3$, indicates the integration performed along the cross-section area.

Substituting Eq. (4.25) into Eq. (4.23) the complete final expression of the assumed transverse shear stress distribution is obtained:

$$\begin{aligned}\tau_{13}^{a}(x_1,x_3) = &\,\overline{p}_{1(B)}(x_1)\left(-1-\frac{1}{h}(x_3+h/2)\right) - \frac{1}{h}(x_3+h/2)\overline{p}_{1(T)}(x_1) + \\ &+\widehat{A}^z(x_3)e_{,1}(x_1) + \widehat{B}^z(x_3)k_{,1}(x_1) + \\ &+\widehat{D}^z(x_3)k_{,1}^{\psi}(x_1) + \widehat{\mathbf{E}}^z(x_3)\partial\mathbf{w}(x_1) + \widehat{\mathbf{F}}^z(x_3)\partial\overline{\mathbf{q}}_z(x_1) = \\ &= \mathbf{Z}_p(x_3)\overline{\mathbf{q}}_{\mathbf{p}}(x_1) + \mathbf{Z}_t(x_3)\mathbf{q}_t(x_1) + \mathbf{Z}_{qz}(x_3)\partial\overline{\mathbf{q}}_z(x_1)\end{aligned} \tag{4.26}$$

where

$$\begin{aligned}\widehat{A}^z(x_3) &= A^z(x_3) - (x_3+h/2)\frac{1}{h}\left\langle A^z \right\rangle \\ \widehat{B}^z(x_3) &= B^z(x_3) - (x_3+h/2)\frac{1}{h}\left\langle B^z \right\rangle \\ \widehat{D}^z(x_3) &= D^z(x_3) - (x_3+h/2)\frac{1}{h}\left\langle D^z \right\rangle \\ \widehat{\mathbf{E}}^z(x_3) &= \mathbf{E}^{\mathbf{z}}(x_3) - (x_3+h/2)\frac{1}{h}\left\langle \mathbf{E}^{\mathbf{z}} \right\rangle \\ \widehat{\mathbf{F}}^z(x_3) &= \mathbf{F}^{\mathbf{z}}(x_3) - (x_3+h/2)\frac{1}{h}\left\langle \mathbf{F}^{\mathbf{z}} \right\rangle \\ \mathbf{Z}_p(x_3) &= \left[\left(-1-\frac{1}{h}(x_3+h/2)\right) \quad -\frac{1}{h}(x_3+h/2)\right] \\ \mathbf{Z}_t(x_3) &= \left[\widehat{A}^z(x_3) \quad \widehat{B}^z(x_3) \quad \widehat{D}^z(x_3) \quad \widehat{\mathbf{E}}^z(x_3)\right] \\ \mathbf{Z}_{qz}(x_3) &= \widehat{\mathbf{F}}^z(x_3)\end{aligned} \tag{4.27}$$

4.3 Governing equations, boundary conditions and new B-RZT$^{(m)}_{\{3,2\}}$ beam constitutive relations

By substituting the displacement field expression, i.e. Eqs. (4.5) into the strain-displacements relations and taking into account the mixed material constitutive equations, i.e. Eq. (4.3), the assumed transverse normal (4.20) and transverse shear (4.26) stresses into the variational statement Eq. (4.12) and integrating by parts, the governing equations of the new B-RZT$^{(m)}_{\{3,2\}}$ are obtained:

$$\delta u: \quad N_{,1}+\frac{1}{\eta}\left(u_{,11}-e_{,1}\right)+\overline{p}_1=m^{(0)}\ddot{u}+m^{(1)}\ddot{\theta}+m_{\mu}^{(0)}\ddot{\psi} \tag{4.28}$$

$$\begin{aligned}\delta w^{(0)}: \quad & Q_{,1}^{w0}-N_1^z-\widehat{Q}^{w0}-\left(\hat{D}_{11}^{p}\overline{p}_{1(B),1}+\hat{D}_{13}^{p}\overline{p}_{1(T),1}\right)+\\ & -\left(\hat{D}_{11}^{q}\overline{p}_{3(B),11}+\hat{D}_{12}^{q}\overline{p}_{3(T),11}\right)+\overline{q}_3=m^{(0)}\ddot{w}^{(0)}+m^{(1)}\ddot{w}^{(1)}+m^{(2)}\ddot{w}^{(2)}\end{aligned} \tag{4.29}$$

$$\begin{aligned}\delta w^{(1)}: \quad & Q_{,1}^{w1}-N_2^z-\widehat{Q}^{w1}-\left(\hat{D}_{21}^{p}\overline{p}_{1(B),1}+\hat{D}_{23}^{p}\overline{p}_{1(T),1}\right)+\\ & -\left(\hat{D}_{11}^{q}\overline{p}_{3(B),11}+\hat{D}_{12}^{q}\overline{p}_{3(T),11}\right)+\frac{h}{2}\left(\overline{p}_{3(T)}-\overline{p}_{3(B)}\right)=\\ & =m^{(1)}\ddot{w}^{(0)}+m^{(2)}\ddot{w}^{(1)}+m^{(3)}\ddot{w}^{(2)}\end{aligned} \tag{4.30}$$

$$\begin{aligned}\delta w^{(2)}: \quad & Q_{,1}^{w2}-N_3^z-\widehat{Q}^{w2}-\left(\hat{D}_{31}^{p}\overline{p}_{1(B),1}+\hat{D}_{33}^{p}\overline{p}_{1(T),1}+\hat{D}_{61}^{p}\overline{p}_{1(B),2}\right)+\\ & -\left(\hat{D}_{31}^{q}\overline{p}_{3(B),11}+\hat{D}_{32}^{q}\overline{p}_{3(T),11}\right)+\frac{h^2}{4}\overline{q}_3=m^{(2)}\ddot{w}^{(0)}+m^{(3)}\ddot{w}^{(1)}+m^{(4)}\ddot{w}^{(2)}\end{aligned} \tag{4.31}$$

$$\delta\theta: \quad M_{,1}-Q+\frac{1}{\eta}\left(\theta_{,11}-k_{,1}\right)+\overline{m}_1=m^{(1)}\ddot{u}+m^{(2)}\ddot{\theta}+m_{\mu}^{(1)}\ddot{\psi} \tag{4.32}$$

$$\delta\psi: \quad M_{,1}^{\phi}-Q^{\phi}+\frac{1}{\eta}\left(\psi_{,11}-k_{,1}^{\psi}\right)=m_{\mu}^{(0)}\ddot{u}+m_{\mu}^{(1)}\ddot{\theta}+m_{\mu}^{(2)}\ddot{\psi} \tag{4.33}$$

$$\delta e: \quad -\frac{1}{\eta}\left(e-u_{,1}\right)+E^{HR}=0 \tag{4.34}$$

$$\delta k: \quad -\frac{1}{\eta}\left(k_{11}-\theta_{1,1}\right)+K^{HR}=0 \tag{4.35}$$

$$\delta k^{\psi}: \quad -\frac{1}{\eta}\left(k^{\psi}-\psi_{,1}\right)+K_{\psi}^{HR}=0 \tag{4.36}$$

Moreover, the consistent boundary conditions follow:

$$\begin{array}{llll}
u=\bar{u} & \text{on } x_1=0,L & \vee & \bar{N}+\frac{1}{\eta}\left(u_{,1}-e\right) \quad \text{on } x_1=0,L \\
w^{(0)}=\bar{w}^{(0)} & \text{on } x_1=0,L & \vee & \bar{Q}^{w0}+{}^{HR}\bar{Q}_1^{w0} \quad \text{on } x_1=0,L \\
w^{(1)}=\bar{w}^{(1)} & \text{on } x_1=0,L & \vee & \bar{Q}^{w1}+{}^{HR}\bar{Q}_1^{w1} \quad \text{on } x_1=0,L \\
w^{(2)}=\bar{w}^{(2)} & \text{on } x_1=0,L & \vee & \bar{Q}^{w2}+{}^{HR}\bar{Q}_1^{w2} \quad \text{on } x_1=0,L \\
\theta=\bar{\theta} & \text{on } x_1=0,L & \vee & \bar{M}+\frac{1}{\eta}\left(\theta_{,1}-k_{11}\right) \quad \text{on } x_1=0,L \\
\psi=\bar{\psi} & \text{on } x_1=0,L & \vee & \bar{M}^{\phi}+\frac{1}{\eta}\left(\psi_{,1}-k^{\psi}\right) \quad \text{on } x_1=0,L \\
e=\bar{e} & \text{on } x_1=0,L & \vee & {}^{HR}\bar{E}_1^{e} \quad \text{on } x_1=0,L \\
k=\bar{k} & \text{on } x_1=0,L & \vee & {}^{HR}\bar{K}_1^{k} \quad \text{on } x_1=0,L \\
k^{\psi}=\bar{k}^{\psi} & \text{on } x_1=0,L & \vee & {}^{HR}\bar{K}_1^{k\psi} \quad \text{on } x_1=0,L
\end{array} \tag{4.37}$$

Moreover, the resultant forces and moments are defined as:

$$\begin{aligned}
&\left(N,M,M^{\phi}\right)=\left\langle\left(1,x_3,\mu^{(k)}(x_3)\right)\sigma_{11}^{(k)}\right\rangle;\\
&\mathbf{N}^{z}=\left\langle\mathbf{H}_{,3}^{zT}\sigma_{33}^{a}\right\rangle;\\
&\left(\mathbf{Q}^{w},Q,Q^{\phi}\right)=\left\langle\left(\mathbf{H}^{zT},1,\partial_3\mu\right)\tau_{13}^{a}\right\rangle
\end{aligned} \tag{4.38}$$

In Eqs. (4.28) - (4.32) the sum of the distributed loads and moments read:

$$\begin{aligned}
&\bar{p}_1=\bar{p}_{1(B)}+\bar{p}_{1(T)};\\
&\bar{m}_1=\frac{h}{2}\left(\bar{p}_{1(T)}-\bar{p}_{1(B)}\right);\\
&\bar{q}_3=\bar{p}_{3(B)}+\bar{p}_{3(T)}
\end{aligned} \tag{4.39}$$

By using the mixed material constitutive relations, i.e. Eq. (4.3), the assumed transverse normal and shear stresses, i.e. Eqs. (4.20) and (4.26), the B-RZT$_{\{3,2\}}^{(m)}$

beam constitutive relations in terms of the kinematic and strains unknowns are expressed as follows:

$$\begin{aligned} N &= \tilde{A}u_{,1} + \tilde{B}\theta_{,1} + \tilde{A}^{\phi}\psi_{,1} + \tilde{\mathbf{A}}^{w}\mathbf{w} + \tilde{\mathbf{A}}^{qz}\overline{\mathbf{q}}_z \\ M &= \tilde{C}u_{,1} + \tilde{D}\theta_{,1} + \tilde{B}^{\phi}\psi_{,1} + \tilde{\mathbf{B}}^{w}\mathbf{w} + \tilde{\mathbf{B}}^{qz}\overline{\mathbf{q}}_z \\ M^{\phi} &= \tilde{E}^{\phi}u_{,1} + \tilde{F}^{\phi}\theta_{,1} + \tilde{G}^{\phi}\psi_{,1} + \tilde{\mathbf{C}}^{w}\mathbf{w} + \tilde{\mathbf{C}}^{qz}\overline{\mathbf{q}}_z \end{aligned} \tag{4.40}$$

$$\mathbf{N}^{z} = \mathbf{A}^{Nz}u_{,1} + \mathbf{B}^{Nz}\theta_{,1} + \mathbf{C}^{Nz}\psi_{,1} + \mathbf{D}^{Nz}\mathbf{w} + \mathbf{E}^{Nz}\overline{\mathbf{q}}_z \tag{4.41}$$

$$\begin{aligned} \mathbf{Q}^{w} &= \hat{\mathbf{A}}^{wT}e_{,1} + \hat{\mathbf{B}}^{wT}k_{,1} + \hat{\mathbf{C}}^{wT}k_{,1}^{\psi} + \hat{\mathbf{D}}^{wT}\partial\mathbf{w} + \hat{\mathbf{E}}^{w}\partial\overline{\mathbf{q}}_z \\ Q &= \hat{A}^{\theta}e_{,1} + \hat{B}^{\theta}k_{,1} + \hat{C}^{\theta}k_{,1}^{\psi} + \hat{\mathbf{D}}^{\theta T}\partial\mathbf{w} + \hat{\mathbf{E}}^{\theta}\partial\overline{\mathbf{q}}_z \\ Q^{\phi} &= \hat{A}^{\psi}e_{,1} + \hat{B}^{\psi}k_{,1} + \hat{C}^{\psi}k_{,1}^{\psi} + \hat{\mathbf{D}}^{\psi T}\partial\mathbf{w} + \hat{\mathbf{E}}^{\psi}\partial\overline{\mathbf{q}}_z \end{aligned} \tag{4.42}$$

where the various stiffness matrices are defined as follows:

$$\begin{aligned} &\tilde{A} = \left\langle E_1^{(k)} + R_{13}{}^{(k)}A_{\sigma}^{u} \right\rangle; \quad \tilde{B} = \left\langle x_3 E_1^{(k)} + R_{13}{}^{(k)}A_{\sigma}^{\theta} \right\rangle; \\ &\tilde{A}^{\phi} = \left\langle E_1^{(k)}\mu^{(k)} + R_{13}{}^{(k)}A_{\sigma}^{\psi} \right\rangle; \\ &\tilde{\mathbf{A}}^{w} = \left\langle R_{13}{}^{(k)}\mathbf{A}_{\sigma}^{w} \right\rangle; \quad \tilde{\mathbf{A}}^{qz} = \left\langle R_{13}{}^{(k)}\mathbf{A}_{\sigma}^{q_z} \right\rangle; \\ &\tilde{C} = \left\langle x_3 E_1^{(k)} + x_3 R_{13}{}^{(k)}A_{\sigma}^{u} \right\rangle; \quad \tilde{D} = \left\langle x_3^2 E_1^{(k)} + x_3 R_{13}{}^{(k)}A_{\sigma}^{\theta} \right\rangle; \\ &\tilde{B}^{\phi} = \left\langle x_3 E_1^{(k)}\mu^{(k)} + zR_{13}{}^{(k)}A_{\sigma}^{\psi} \right\rangle; \\ &\tilde{\mathbf{B}}^{w} = \left\langle x_3 R_{13}{}^{(k)}\mathbf{A}_{\sigma}^{w} \right\rangle; \quad \tilde{\mathbf{B}}^{qz} = \left\langle x_3 R_{13}{}^{(k)}\mathbf{A}_{\sigma}^{q_z} \right\rangle; \\ &\tilde{E}^{\phi} = \left\langle \mu^{(k)}E_1^{(k)} + \mu^{(k)}R_{13}{}^{(k)}A_{\sigma}^{u} \right\rangle; \quad \tilde{F}^{\phi} = \left\langle x_3\mu^{(k)}E_1^{(k)} + \mu^{(k)}R_{13}{}^{(k)}A_{\sigma}^{\theta} \right\rangle; \\ &\tilde{G}^{\phi} = \left\langle \mu^{(k)}E_1^{(k)}\mu^{(k)} + \mu^{(k)}R_{13}{}^{(k)}A_{\sigma}^{\psi} \right\rangle; \\ &\tilde{\mathbf{C}}^{w} = \left\langle \mu^{(k)}R_{13}{}^{(k)}\mathbf{A}_{\sigma}^{w} \right\rangle; \quad \tilde{\mathbf{C}}^{qz} = \left\langle \mu^{(k)}R_{13}{}^{(k)}\mathbf{A}_{\sigma}^{q_z} \right\rangle \\ &\mathbf{A}^{Nz} = \left\langle \mathbf{H}_{,3}^{z\,T}A_{\sigma}^{u} \right\rangle; \quad \mathbf{B}^{Nz} = \left\langle \mathbf{H}_{,3}^{z\,T}A_{\sigma}^{\theta} \right\rangle; \quad \mathbf{C}^{Nz} = \left\langle \mathbf{H}_{,3}^{z\,T}A_{\sigma}^{\psi} \right\rangle; \\ &\mathbf{D}^{Nz} = \left\langle \mathbf{H}_{,3}^{z\,T}\mathbf{A}_{\sigma}^{w} \right\rangle; \quad \mathbf{E}^{Nz} = \left\langle \mathbf{H}_{,3}^{z\,T}\mathbf{A}_{\sigma}^{q_z} \right\rangle \end{aligned} \tag{4.43}$$

Defining $S_t^{(k)} = 1/G_{13}^{(k)}$ the remaining quantities are expressed as follows:

$$
\begin{aligned}
&\hat{\mathbf{A}}^{w} = \left\langle \widehat{A}^{z}\mathbf{H}^{z} \right\rangle; \quad \hat{A}^{\theta} = \left\langle \widehat{A}^{z} \right\rangle; \quad \hat{A}^{\psi} = \left\langle \widehat{A}^{z}\partial_{3}\mu^{(k)} \right\rangle; \\
&\hat{\mathbf{A}}^{p} = \left\langle \widehat{A}^{z}S_{t}^{(k)}\mathbf{Z}_{p} \right\rangle; \quad \hat{A}^{e} = \left\langle \widehat{A}^{z}S_{t}^{(k)}\widehat{A}^{z} \right\rangle; \\
&\hat{A}^{k} = \left\langle \widehat{A}^{z}S_{t}^{(k)}\widehat{B}^{z} \right\rangle; \quad \hat{A}^{k\psi} = \left\langle \widehat{A}^{z}S_{t}^{(k)}\widehat{D}^{z} \right\rangle; \\
&\hat{\mathbf{A}}^{kw} = \left\langle \widehat{A}^{z}S_{t}^{(k)}\widehat{\mathbf{E}}^{z} \right\rangle; \quad \hat{\mathbf{A}}^{q} = \left\langle \widehat{A}^{z}S_{t}^{(k)}\widehat{\mathbf{F}}^{z} \right\rangle; \\
&\hat{\mathbf{B}}^{w} = \left\langle \widehat{B}^{z}\mathbf{H}^{z} \right\rangle; \quad \hat{B}^{\theta} = \left\langle \widehat{B}^{z} \right\rangle; \quad \hat{B}^{\psi} = \left\langle \widehat{B}^{z}\partial_{z}\mu^{(k)} \right\rangle; \\
&\hat{\mathbf{B}}^{p} = \left\langle \widehat{B}^{z}S_{t}^{(k)}\mathbf{Z}_{p} \right\rangle; \quad \hat{B}^{e} = \hat{A}^{k} = \left\langle \widehat{B}^{z}S_{t}^{(k)}\widehat{A}^{z} \right\rangle; \\
&\hat{B}^{k} = \left\langle \widehat{B}^{z}S_{t}^{(k)}\widehat{B}^{z} \right\rangle; \quad \hat{B}^{k\psi} = \left\langle \widehat{B}^{z}S_{t}^{(k)}\widehat{D}^{z} \right\rangle; \\
&\hat{\mathbf{B}}^{kw} = \left\langle \widehat{B}^{z}S_{t}^{(k)}\widehat{\mathbf{E}}^{z} \right\rangle; \quad \hat{\mathbf{B}}^{q} = \left\langle \widehat{B}^{z}S_{t}^{(k)}\widehat{\mathbf{F}}^{z} \right\rangle; \\
&\hat{\mathbf{C}}^{w} = \left\langle \widehat{D}^{z}\mathbf{H}^{z} \right\rangle; \quad \hat{C}^{\theta} = \left\langle \widehat{D}^{z} \right\rangle; \quad \hat{C}^{\psi} = \left\langle \widehat{D}^{z}\partial_{z}\mu^{(k)} \right\rangle; \\
&\hat{\mathbf{C}}^{p} = \left\langle \widehat{D}^{z}S_{t}^{(k)}\mathbf{Z}_{p} \right\rangle; \quad \hat{C}^{e} = \hat{A}^{k\psi} = \left\langle \widehat{D}^{z}S_{t}^{(k)}\widehat{A}^{z} \right\rangle; \\
&\hat{C}^{k} = \hat{B}^{k\psi} = \left\langle \widehat{D}^{z}S_{t}^{(k)}\widehat{B}^{z} \right\rangle; \quad \hat{C}^{k\psi} = \left\langle \widehat{D}^{z}S_{t}^{(k)}\widehat{D}^{z} \right\rangle; \\
&\hat{\mathbf{C}}^{kw} = \left\langle \widehat{D}^{z}S_{t}^{(k)}\widehat{\mathbf{E}}^{z} \right\rangle; \quad \hat{\mathbf{C}}^{q} = \left\langle \widehat{D}^{z}S_{t}^{(k)}\widehat{\mathbf{F}}^{z} \right\rangle; \\
&\hat{\mathbf{D}}^{w} = \left\langle \widehat{\mathbf{E}}^{zT}\mathbf{H}^{z} \right\rangle; \quad \hat{\mathbf{D}}^{\theta} = \left\langle \widehat{\mathbf{E}}^{zT} \right\rangle; \quad \hat{\mathbf{D}}^{\psi} = \left\langle \widehat{\mathbf{E}}^{zT}\partial_{3}\mu^{(k)} \right\rangle; \\
&\hat{\mathbf{D}}^{p} = \left\langle \widehat{\mathbf{E}}^{zT}S_{t}^{(k)}\mathbf{Z}_{p} \right\rangle; \quad \hat{\mathbf{D}}^{e} = \hat{\mathbf{A}}^{kwT} = \left\langle \widehat{\mathbf{E}}^{zT}S_{t}^{(k)}\widehat{A}^{z} \right\rangle; \\
&\hat{\mathbf{D}}^{k} = \hat{\mathbf{B}}^{kwT} = \left\langle \widehat{\mathbf{E}}^{zT}S_{t}^{(k)}\widehat{B}^{z} \right\rangle; \quad \hat{\mathbf{D}}^{k\psi} = \hat{\mathbf{C}}^{kwT} = \left\langle \widehat{\mathbf{E}}^{zT}S_{t}^{(k)}\widehat{D}^{z} \right\rangle; \\
&\hat{\mathbf{D}}^{kw} = \left\langle \widehat{\mathbf{E}}^{zT}S_{t}^{(k)}\widehat{\mathbf{E}}^{z} \right\rangle; \quad \hat{\mathbf{D}}^{q} = \left\langle \widehat{\mathbf{E}}^{zT}S_{t}^{(k)}\widehat{\mathbf{F}}^{z} \right\rangle; \\
&\hat{\mathbf{E}}^{w} = \left\langle \mathbf{H}^{zT}\widehat{\mathbf{F}}^{z} \right\rangle; \quad \hat{\mathbf{E}}^{\theta} = \left\langle \widehat{\mathbf{F}}^{z} \right\rangle; \quad \hat{\mathbf{E}}^{\psi} = \left\langle \partial_{3}\mu^{(k)}\widehat{\mathbf{F}}^{z} \right\rangle
\end{aligned}
\tag{4.44}
$$

Lastly, the inertia quantities that appear in the governing equations read:

$$
\begin{aligned}
&\left(m^{(0)}, m^{(1)}, m^{(2)}, m^{(3)}, m^{(4)}\right) = \left\langle \rho^{(k)}\left(1, x_3, x_3^2, x_3^3, x_3^4\right) \right\rangle; \\
&\left(m_{\mu}^{(0)}, m_{\mu}^{(1)}, m_{\mu}^{(2)}\right) = \left\langle \rho^{(k)}\left(\mu^{(k)}, x_3\mu^{(k)}, \mu^{(k)2}\right) \right\rangle
\end{aligned}
\tag{4.45}
$$

For clarity, the other quantities that appear in the governing equations and consistent boundary conditions not defined here are reported in Appendix E.

4.4 The new-mixed RZT beam elements

The governing equations of the developed B-RZT$^{(m)}_{\{3,2\}}$ model shown in the previous Section can be solved analytically only for particular load cases and boundary conditions, typically sinusoidal pressure and simply-supported edges. Finding a different method to achieve the searched solution is necessary for other cases. Therefore, this Section aims to provide a finite element formulation based on the B-RZT$^{(m)}_{\{3,2\}}$ that can approximate the solution of the governing equations for different lamination schemes, load cases or boundary conditions.

The kinematic and strain variables that appear in the governing functional, i.e. Eq. (4.12), exhibit the highest derivative order with respect to the longitudinal coordinate of the first order. Thus, only the C^0-continuity condition of the shape functions is required to approximate the unknown variables in the finite element formulation.

With the aim of experimental validation, the present finite element formulation is limited only to free vibration problems and bending analysis of thick sandwich structures in which only concentrated loads applied in the node are considered. This simplification clearly restricts the range of applicability of these elements; however, it leads to a simplified expression of E^{HR}, K^{HR} and K^{HR}_{ψ} terms in which the effect of applied distributed loads is not in their expression. Thus, it is possible to achieve a simplified formulation involving the static condensation to reduce the total degrees of freedom by maintaining only the unknown variables of the displacement field.

As stated in the previous literature framework, the shear-locking phenomenon affects the RZT-based elements when applied to investigate the response of thin multilayered structures. However, the range of the span-to-thickness ratios considered in this work is limited to the value for thick multilayered beams; thus, this problem is not addressed here.

According to the C^0-continuity requirement, the simplest formulated element implemented is a two-node with linear Lagrange polynomials as shape functions (*isoparametric interpolation*) for approximating all kinematic and strain variables.

However, a further consideration should be done: the importance of the penalty term in the governing functional. As highlighted in the previous Sections,

the penalty term weakens the compatibility with the new strain variables and the strains computed from the displacement field. In the finite element approximation using the *isoparametric interpolation* with the linear Lagrangian polynomials, the derived quantities of the kinematic unknowns are approximated by constant functions. Conversely, the strain variables that appear in the penalty term are still approximated by the linear shape functions. By starting from the strategy adopted to manage the shear-locking problem in Refs. [48,51,107], and in order to improve the element performances, the *anisoparametric interpolation* strategy is adopted. The variables that appear as the first derivative in the penalty functional are approximated by a polynomial shape function of one-degree order higher than the others. It results that $u(x_1)$, $\theta(x_1)$ and $\psi(x_1)$ are approximated with parabolic shape functions, whereas $e(x_1)$, $k(x_1)$ and $k^{\psi}(x_1)$ are still approximated by the linear Lagrangian functions. As anticipated, the *anisoparametric interpolation* results in a three-node finite element where the internal mid-node approximates only the $u(x_1)$, $\theta(x_1)$ and $\psi(x_1)$ variables.

A final consideration is done due to the complexity introduced by the penalty functional. From a numerical point of view, the penalty parameter value influences the accuracy and convergence of the formulated finite elements. For this reason, an appropriate value should be considered to avoid ill-conditioning of the stiffness matrix.

4.4.1 A new 2-node mixed RZT beam element: the 2B-RZT$^{(m)}_{\{3,2\}}$ element

The first element considered is a two-node element based on the B-RZT$^{(m)}_{\{3,2\}}$ model, hereafter named with the acronym 2B-RZT$^{(m)}_{\{3,2\}}$. For clarity, the kinematic and the strain variables are divided into two groups: the first is represented by the variables of the kinematic field, i.e. $\mathbf{d}_d{}^T = \lfloor u \quad w^{(0)} \quad w^{(1)} \quad w^{(2)} \quad \theta \quad \psi \rfloor$ and the second is represented by the strain variables that come from the expression of the transverse shear stress, i.e. $\mathbf{d}_s{}^T = \lfloor e \quad k \quad k^{\psi} \rfloor$. The topology of the 2B-RZT$^{(m)}_{\{3,2\}}$ element is represented in Figure 10.

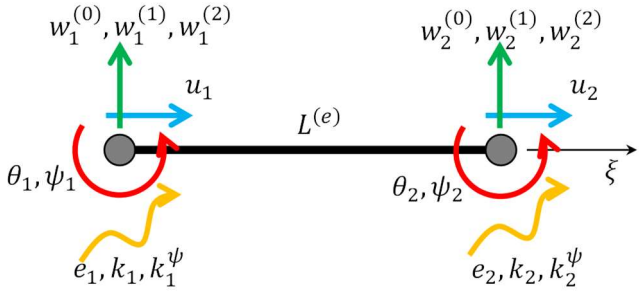

Figure 10: Topology of the 2B-RZT$^{(m)}_{\{3,2\}}$ element.

According to the finite element notation, the unknown quantities interpolated by the nodal values of the 2B-RZT$^{(m)}_{\{3,2\}}$ element are grouped in the two vectors $\mathbf{q}_d^{(e)}$ and $\mathbf{q}_s^{(e)}$ as follows:

$$\begin{Bmatrix} \mathbf{d}_d(x_1;t) \\ \mathbf{d}_s(x_1;t) \end{Bmatrix} = \begin{bmatrix} \mathbf{N}_d(x_1) & \mathbf{0} \\ \mathbf{0} & \mathbf{N}_s(x_1) \end{bmatrix} \begin{Bmatrix} \mathbf{q}_d^{(e)}(t) \\ \mathbf{q}_s^{(e)}(t) \end{Bmatrix} \tag{4.46}$$

where the shape function matrices that interpolate the kinematic and strain quantities, respectively, have the following expressions

$$\mathbf{N}_d = \begin{bmatrix} \mathbf{L} & \mathbf{0} & \mathbf{0} & \mathbf{0} & \mathbf{0} & \mathbf{0} \\ & \mathbf{L} & \mathbf{0} & \mathbf{0} & \mathbf{0} & \mathbf{0} \\ & & \mathbf{L} & \mathbf{0} & \mathbf{0} & \mathbf{0} \\ & & & \mathbf{L} & \mathbf{0} & \mathbf{0} \\ & \textit{sym.} & & & \mathbf{L} & \mathbf{0} \\ & & & & & \mathbf{L} \end{bmatrix} \tag{4.47}$$

$$\mathbf{N}_s = \begin{bmatrix} \mathbf{L} & \mathbf{0} & \mathbf{0} \\ & \mathbf{L} & \mathbf{0} \\ \textit{sym.} & & \mathbf{L} \end{bmatrix} \tag{4.48}$$

In Eqs (4.47) and Eq. (4.48) the elemental shape functions matrices are constituted by the Lagrangian shape functions defined in the natural coordinate

system $\xi = \frac{2x_1}{L^{(e)}} - 1 \in [-1,1]$, where $L^{(e)}$ is the beam element length. Moreover, the vector of the linear shape functions is defined as follows,

$$\begin{aligned} \mathbf{L}(\xi) &= \lfloor L_1(\xi) \quad L_2(\xi) \rfloor = \\ &= \left\lfloor \frac{1}{2}(1-\xi) \quad \frac{1}{2}(1+\xi) \right\rfloor \end{aligned} \tag{4.49}$$

Furthermore, the vectors of the nodal degree of freedoms divided according to the two groups of variables are defined as follows:

$$\begin{aligned} \mathbf{q}_d^{(e)T} &= \lfloor \mathbf{q}^{uT} \quad \mathbf{q}^{w0T} \quad \mathbf{q}^{w1T} \quad \mathbf{q}^{w2T} \quad \mathbf{q}^{\theta T} \quad \mathbf{q}^{\psi T} \rfloor \\ \mathbf{q}_s^{(e)T} &= \lfloor \mathbf{q}^{eT} \quad \mathbf{q}^{kT} \quad \mathbf{q}^{k\psi T} \rfloor \end{aligned} \tag{4.50}$$

with the nodal values vectors:

$$\begin{aligned} &\mathbf{q}^{uT} = \lfloor u_1 \quad u_2 \rfloor; \mathbf{q}^{w0T} = \lfloor w_1^{(0)} \quad w_2^{(0)} \rfloor; \mathbf{q}^{w1T} = \lfloor w_1^{(1)} \quad w_2^{(1)} \rfloor; \\ &\mathbf{q}^{w2T} = \lfloor w_1^{(2)} \quad w_2^{(2)} \rfloor; \mathbf{q}^{\theta T} = \lfloor \theta_1 \quad \theta_2 \rfloor; \mathbf{q}^{\psi T} = \lfloor \psi_1 \quad \psi_2 \rfloor; \end{aligned} \tag{4.51}$$

$$\mathbf{q}^{eT} = \lfloor e_1 \quad e_2 \rfloor; \mathbf{q}^{kT} = \lfloor k_1 \quad k_2 \rfloor; \mathbf{q}^{k\psi T} = \lfloor k_1^{\psi} \quad k_2^{\psi} \rfloor \tag{4.52}$$

The elemental stiffness, mass matrices, and the elemental load vector 2B-RZT$^{(m)}_{\{3,2\}}$ element are derived according to the mixed variational statement, i.e. Eq. (4.12). The variational statement, neglecting the applied distributed loads, reads:

$$\begin{aligned} &\delta\Pi = \int_V \left[\left(\delta\varepsilon_{11}^{(k)} \sigma_{11}^{(k)} + \delta\gamma_{13}^{(k)} \tau_{13}^{a} + \delta\varepsilon_{33} \sigma_{33}^{a} \right) \right] dV + \\ &+ \int_V \left[\delta\tau_{13}^{a} \left(\gamma_{13}^{(k)} - \gamma_{13}^{(k)a} \right) + \delta\sigma_{33}^{a} \left(\varepsilon_{33} - \varepsilon_{33}^{(k)a} \right) \right] dV + \\ &+ \frac{1}{\eta} \int_V \left[\begin{array}{l} \left(\delta u_{,1} - \delta e \right) \left(u_{,1} - e \right) + \\ + \left(\delta\theta_{,1} - \delta k \right) \left(\theta_{,1} - k \right) + \left(\delta\psi_{,1} - \delta k^{\psi} \right) \left(\psi_{,1} - k^{\psi} \right) \end{array} \right] dV + \\ &- \int_V \rho^{(k)} \delta\mathbf{d}_d^T \ddot{\mathbf{d}}_d dV - \sum_{f=1}^{Nf} \overline{F}_f \left(\delta w^{(0)}(x_f) + \frac{h}{2} \delta w^{(1)}(x_f) + \frac{h^2}{4} \delta w^{(2)}(x_f) \right) = 0 \end{aligned} \tag{4.53}$$

where $\bar{F}_f$ is the f^{th} generic transversal concentrated force applied in the x_f point on the top beam surface.

By substituting Eq. (4.46) into Eqs. (4.53) and taking into account the Eqs. (4.3), (4.20) and (4.26) it is possible to obtain the full expression of stiffness and mass matrices and consistent load vector

$$\mathbf{M}^{(e)} = \begin{bmatrix} m^{(0)}\mathbf{L}^T\mathbf{L} & \mathbf{0} & \mathbf{0} & \mathbf{0} & m^{(1)}\mathbf{L}^T\mathbf{L} & m_\mu^{(0)}\mathbf{L}^T\mathbf{L} & \mathbf{0} & \mathbf{0} & \mathbf{0} \\ & m^{(0)}\mathbf{L}^T\mathbf{L} & m^{(1)}\mathbf{L}^T\mathbf{L} & m^{(2)}\mathbf{L}^T\mathbf{L} & \mathbf{0} & \mathbf{0} & \mathbf{0} & \mathbf{0} & \mathbf{0} \\ & & m^{(2)}\mathbf{L}^T\mathbf{L} & m^{(3)}\mathbf{L}^T\mathbf{L} & \mathbf{0} & \mathbf{0} & \mathbf{0} & \mathbf{0} & \mathbf{0} \\ & & & m^{(4)}\mathbf{L}^T\mathbf{L} & \mathbf{0} & \mathbf{0} & \mathbf{0} & \mathbf{0} & \mathbf{0} \\ & & & & m^{(2)}\mathbf{L}^T\mathbf{L} & m_\mu^{(1)}\mathbf{L}^T\mathbf{L} & \mathbf{0} & \mathbf{0} & \mathbf{0} \\ & & & & & m_\mu^{(2)}\mathbf{L}^T\mathbf{L} & \mathbf{0} & \mathbf{0} & \mathbf{0} \\ & & & & & & \mathbf{0} & \mathbf{0} & \mathbf{0} \\ & & sym. & & & & & \mathbf{0} & \mathbf{0} \\ & & & & & & & & \mathbf{0} \end{bmatrix}^{(e)} \tag{4.54}$$

$$\mathbf{K}^{(e)} = \begin{bmatrix} \mathbf{K}_{11} & \mathbf{K}_{12} & \mathbf{K}_{13} & \mathbf{K}_{14} & \mathbf{K}_{15} & \mathbf{K}_{16} & \mathbf{K}_{17} & \mathbf{K}_{18} & \mathbf{K}_{19} \\ & \mathbf{K}_{22} & \mathbf{K}_{23} & \mathbf{K}_{24} & \mathbf{K}_{25} & \mathbf{K}_{26} & \mathbf{K}_{27} & \mathbf{K}_{28} & \mathbf{K}_{29} \\ & & \mathbf{K}_{33} & \mathbf{K}_{34} & \mathbf{K}_{35} & \mathbf{K}_{36} & \mathbf{K}_{37} & \mathbf{K}_{38} & \mathbf{K}_{39} \\ & & & \mathbf{K}_{44} & \mathbf{K}_{45} & \mathbf{K}_{46} & \mathbf{K}_{47} & \mathbf{K}_{48} & \mathbf{K}_{49} \\ & & & & \mathbf{K}_{55} & \mathbf{K}_{56} & \mathbf{K}_{57} & \mathbf{K}_{58} & \mathbf{K}_{59} \\ & & & & & \mathbf{K}_{66} & \mathbf{K}_{67} & \mathbf{K}_{68} & \mathbf{K}_{69} \\ & & & & & & \mathbf{K}_{77} & \mathbf{K}_{78} & \mathbf{K}_{79} \\ & & & & & & & \mathbf{K}_{88} & \mathbf{K}_{89} \\ & & & & & & & & \mathbf{K}_{99} \end{bmatrix}^{(e)} \tag{4.55}$$

with

$$\mathbf{K}_{11}^{(e)} = \mathbf{L}_{,1}{}^{T}\tilde{A}\mathbf{L}_{,1} + \frac{hb}{\eta}\mathbf{L}_{,1}{}^{T}\mathbf{L}_{,1} \qquad \mathbf{K}_{12}^{(e)} = \mathbf{L}_{,1}{}^{T}\tilde{A}_{11}^{w}\mathbf{L} \quad \mathbf{K}_{13}^{(e)} = \mathbf{L}_{,1}{}^{T}\tilde{A}_{12}^{w}\mathbf{L}$$

$$\mathbf{K}_{14}^{(e)} = \mathbf{L}_{,1}{}^{T}\tilde{A}_{13}^{w}\mathbf{L} \quad \mathbf{K}_{15}^{(e)} = \mathbf{L}_{,1}{}^{T}\tilde{B}\mathbf{L}_{,1} \quad \mathbf{K}_{15}^{(e)} = \mathbf{L}_{,1}{}^{T}\tilde{A}^{\phi}\mathbf{L}_{,1} \quad \mathbf{K}_{16}^{(e)} = -\frac{hb}{\eta}\mathbf{L}_{,1}{}^{T}\mathbf{L}$$

$$\mathbf{K}_{17}^{(e)} = \mathbf{K}_{18}^{(e)} = \mathbf{0} \quad \mathbf{K}_{22}^{(e)} = \mathbf{L}^{T}D_{11}^{Nz}\mathbf{L} + \mathbf{L}^{T}\hat{D}_{11}^{w}\mathbf{L}_{,1} + \mathbf{L}_{,1}{}^{T}\hat{D}_{11}^{w}\mathbf{L} - \mathbf{L}_{,1}{}^{T}\hat{D}_{11}^{kw}\mathbf{L}_{,1}$$

$$\mathbf{K}_{23}^{(e)} = \mathbf{L}^{T}D_{12}^{Nz}\mathbf{L} + \mathbf{L}^{T}\hat{D}_{21}^{w}\mathbf{L}_{,1} + \mathbf{L}_{,1}{}^{T}\hat{D}_{12}^{w}\mathbf{L} - \mathbf{L}_{,1}{}^{T}\hat{D}_{12}^{kw}\mathbf{L}_{,1}$$

$$\mathbf{K}_{24}^{(e)} = \mathbf{L}^{T}D_{13}^{Nz}\mathbf{L} + \mathbf{L}^{T}\hat{D}_{31}^{w}\mathbf{L}_{,1} + \mathbf{L}_{,1}{}^{T}\hat{D}_{13}^{w}\mathbf{L} - \mathbf{L}_{,1}{}^{T}\hat{D}_{13}^{kw}\mathbf{L}_{,1}$$

$$\mathbf{K}_{25}^{(e)} = \mathbf{L}^{T}B_{11}^{Nz}\mathbf{L}_{,1} + \mathbf{L}_{,1}{}^{T}\hat{D}_{11}^{\theta}\mathbf{L} \qquad \mathbf{K}_{26}^{(e)} = \mathbf{L}^{T}C_{11}^{Nz}\mathbf{L}_{,1} + \mathbf{L}_{,1}{}^{T}\hat{D}_{11}^{\psi}\mathbf{L}$$

$$\mathbf{K}_{27}^{(e)} = \mathbf{L}^{T}\hat{A}_{11}^{w}\mathbf{L}_{,1} - \mathbf{L}_{,1}{}^{T}\hat{A}_{11}^{kw}\mathbf{L}_{,1} \qquad \mathbf{K}_{28}^{(e)} = \mathbf{L}^{T}\hat{B}_{11}^{w}\mathbf{L}_{,1} - \mathbf{L}_{,1}{}^{T}\hat{B}_{11}^{kw}\mathbf{L}_{,1}$$

$$\mathbf{K}_{29}^{(e)} = \mathbf{L}^{T}\hat{C}_{11}^{w}\mathbf{L}_{,1} - \mathbf{L}_{,1}{}^{T}\hat{C}_{11}^{kw}\mathbf{L}_{,1}$$

$$\mathbf{K}_{33}^{(e)} = \mathbf{L}^{T}D_{22}^{Nz}\mathbf{L} + \mathbf{L}^{T}\hat{D}_{22}^{w}\mathbf{L}_{,1} + \mathbf{L}_{,1}{}^{T}\hat{D}_{22}^{w}\mathbf{L} - \mathbf{L}_{,1}{}^{T}\hat{D}_{22}^{kw}\mathbf{L}_{,1}$$

$$\mathbf{K}_{34}^{(e)} = \mathbf{L}^{T}D_{23}^{Nz}\mathbf{L} + \mathbf{L}^{T}\hat{D}_{32}^{w}\mathbf{L}_{,1} + \mathbf{L}_{,1}{}^{T}\hat{D}_{23}^{w}\mathbf{L} - \mathbf{L}_{,1}{}^{T}\hat{D}_{23}^{kw}\mathbf{L}_{,1}$$

$$\mathbf{K}_{36}^{(e)} = \mathbf{L}^{T}C_{21}^{Nz}\mathbf{L}_{,1} + \mathbf{L}_{,1}{}^{T}\hat{D}_{21}^{\psi}\mathbf{L} \qquad \mathbf{K}_{35}^{(e)} = \mathbf{L}^{T}B_{21}^{Nz}\mathbf{L}_{,1} + \mathbf{L}_{,1}{}^{T}\hat{D}_{21}^{\theta}\mathbf{L}$$

$$\mathbf{K}_{37}^{(e)} = \mathbf{L}^{T}\hat{A}_{12}^{w}\mathbf{L}_{,1} - \mathbf{L}_{,1}{}^{T}\hat{A}_{12}^{kw}\mathbf{L}_{,1} \qquad \mathbf{K}_{38}^{(e)} = \mathbf{L}^{T}\hat{B}_{12}^{w}\mathbf{L}_{,1} - \mathbf{L}_{,x}{}^{T}\hat{B}_{12}^{kw}\mathbf{L}_{,1}$$

$$\mathbf{K}_{39}^{(e)} = \left(\mathbf{L}^{T}\hat{C}_{12}^{w}\mathbf{L}_{,1} - \mathbf{L}_{,1}{}^{T}\hat{C}_{12}^{kw}\mathbf{L}_{,1}\right)$$

$$\mathbf{K}_{44}^{(e)} = \left(\mathbf{L}^{T}D_{33}^{Nz}\mathbf{L} + \mathbf{L}^{T}\hat{D}_{33}^{w}\mathbf{L}_{,1} + \mathbf{L}_{,1}{}^{T}\hat{D}_{33}^{w}\mathbf{L} - \mathbf{L}_{,1}{}^{T}\hat{D}_{33}^{kw}\mathbf{L}_{,1}\right)$$

$$\mathbf{K}_{45}^{(e)} = \left(\mathbf{L}^{T}B_{31}^{Nz}\mathbf{L}_{,1} + \mathbf{L}_{,1}{}^{T}\hat{D}_{31}^{\theta}\mathbf{L}\right) \qquad \mathbf{K}_{46}^{(e)} = \left(\mathbf{L}^{T}C_{31}^{Nz}\mathbf{L}_{,1} + \mathbf{L}_{,1}{}^{T}\hat{D}_{31}^{\psi}\mathbf{L}\right)$$

$$\mathbf{K}_{47}^{(e)} = \left(\mathbf{L}^{T}\hat{A}_{13}^{w}\mathbf{L}_{,1} - \mathbf{L}_{,1}{}^{T}\hat{A}_{13}^{kw}\mathbf{L}_{,1}\right) \qquad \mathbf{K}_{48}^{(e)} = \left(\mathbf{L}^{T}\hat{B}_{13}^{w}\mathbf{L}_{,1} - \mathbf{L}_{,1}{}^{T}\hat{B}_{13}^{kw}\mathbf{L}_{,1}\right)$$

$$\mathbf{K}_{49}^{(e)} = \left(\mathbf{L}^{T}\hat{C}_{13}^{w}\mathbf{L}_{,1} - \mathbf{L}_{,1}{}^{T}\hat{C}_{13}^{kw}\mathbf{L}_{,1}\right) \qquad \mathbf{K}_{55}^{(e)} = \mathbf{L}_{,1}{}^{T}\tilde{D}\mathbf{L}_{,1} + \frac{hb}{\eta}\mathbf{L}_{,1}{}^{T}\mathbf{L}_{,1}$$

$$\mathbf{K}_{56}^{(e)} = \mathbf{L}_{,1}{}^{T}\tilde{B}^{\phi}\mathbf{L}_{,1} \quad \mathbf{K}_{57}^{(e)} = \mathbf{L}^{T}\hat{A}^{\theta}\mathbf{L}_{,1}$$

$$\mathbf{K}_{58}^{(e)} = \mathbf{L}^{T}\hat{B}^{\theta}\mathbf{L}_{,1} - \frac{hb}{\eta}\mathbf{L}_{,1}{}^{T}\mathbf{L} \qquad \mathbf{K}_{59}^{(e)} = \mathbf{L}^{T}\hat{C}^{\theta}\mathbf{L}_{,1}$$

$$\mathbf{K}_{66}^{(e)} = \mathbf{L}_{,1}{}^{T}\tilde{G}^{\phi}\mathbf{L}_{,1} + \frac{hb}{\eta}\mathbf{L}_{,1}{}^{T}\mathbf{L}_{,1} \qquad \mathbf{K}_{67}^{(e)} = \mathbf{L}^{T}\hat{A}^{\psi}\mathbf{L}_{,1} \quad \mathbf{K}_{68}^{(e)} = \mathbf{L}^{T}\hat{B}^{\psi}\mathbf{L}_{,1}$$

$$\mathbf{K}_{69}^{(e)} = \mathbf{L}^{T}\hat{C}^{\psi}\mathbf{L}_{,} - \frac{hb}{\eta}\mathbf{L}_{,1}{}^{T}\mathbf{L} \qquad \mathbf{K}_{77}^{(e)} = \frac{hb}{\eta}\mathbf{L}^{T}\mathbf{L} - \mathbf{L}_{,1}{}^{T}\hat{A}^{e}\mathbf{L}_{,1} \tag{4.56}$$

$$\mathbf{K}_{78}^{(e)} = -\mathbf{L}_{,1}{}^{T}\hat{A}^{k}\mathbf{L}_{,1} \qquad \mathbf{K}_{79}^{(e)} = -\mathbf{L}_{,1}{}^{T}\hat{A}^{k\psi}\mathbf{L}_{,1}$$

$$\mathbf{K}_{88}^{(e)} = \frac{hb}{\eta}\mathbf{L}^{T}\mathbf{L} - \mathbf{L}_{,1}{}^{T}\hat{B}^{k}\mathbf{L}_{,1} \qquad \mathbf{K}_{89}^{(e)} = -\mathbf{L}_{,1}{}^{T}\hat{B}^{k\psi}\mathbf{L}_{,1} \qquad \mathbf{K}_{99}^{(e)} = \frac{hb}{\eta}\mathbf{L}^{T}\mathbf{L} - \mathbf{L}_{,1}{}^{T}\hat{C}^{k\psi}\mathbf{L}_{,1}$$

$$\mathbf{F}^{(e)T} = \left\lfloor \mathbf{0} \quad \bar{\mathbf{F}} \quad \frac{h}{2}\bar{\mathbf{F}} \quad \frac{h^2}{4}\bar{\mathbf{F}} \quad \mathbf{0} \quad \mathbf{0} \quad \mathbf{0} \quad \mathbf{0} \quad \mathbf{0} \right\rfloor^{(e)} \tag{4.57}$$

where $\overline{\mathbf{F}}^{(e)} = \begin{bmatrix} \overline{F}_{n1} & \overline{F}_{n2} \end{bmatrix}^{(e)}$ represents the vector of the forces applied to the e^{th} element left and right node, respectively.

4.4.2 A new 2-node mixed RZT anisoparametric constrained beam element: 2Bc-RZT$^{(m)}_{\{3,2\}}$ element

This paragraph presents the formulation of another new mixed beam element. As shown in the previous Section, the 2B-RZT$^{(m)}_{\{3,2\}}$ element presents all the kinematic and strain variables interpolated by the linear Lagrangian shape functions. In this newly formulated element, the attention is focused on the penalty term. The kinematic variables that appear as derivatives in the penalty term are approximated with a polynomial function of one order degree higher than the strain counterparts. It results in an *anisoparametric interpolation* configuration. This strategy introduces a mid-node for the uniform axial displacement for bending and zigzag rotations. The topology of the three-node B-RZT$^{(m)}_{\{3,2\}}$ element, here named 3B-RZT$^{(m)}_{\{3,2\}}$, is represented in Figure 11.

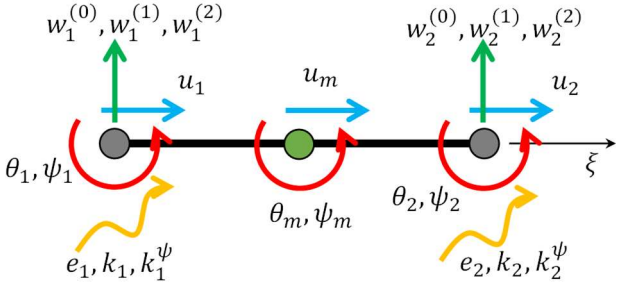

Figure 11: Topology of the new 3B-RZT$^{(m)}_{\{3,2\}}$ element

According to the finite element notation, in a similar way to what has been done for the 2B-RZT$^{(m)}_{\{3,2\}}$ element, the kinematics and strain variables of the 3B-RZT$^{(m)}_{\{3,2\}}$ element are approximated as follows:

$$\begin{Bmatrix} \mathbf{d}_d(x_1;t) \\ \mathbf{d}_s(x_1;t) \end{Bmatrix} = \begin{bmatrix} \mathbf{N}_d^{new}(x_1) & \mathbf{0} \\ \mathbf{0} & \mathbf{N}_s(x_1) \end{bmatrix} \begin{Bmatrix} \mathbf{q}_d^{(e)}(t) \\ \mathbf{q}_s^{(e)}(t) \end{Bmatrix} \tag{4.58}$$

where the new shape function matrix that interpolates the kinematic variables reads:

$$\mathbf{N}_d^{new} = \begin{bmatrix} \mathbf{S} & \mathbf{0} & \mathbf{0} & \mathbf{0} & \mathbf{0} & \mathbf{0} \\ & \mathbf{L} & \mathbf{0} & \mathbf{0} & \mathbf{0} & \mathbf{0} \\ & & \mathbf{L} & \mathbf{0} & \mathbf{0} & \mathbf{0} \\ & & & \mathbf{L} & \mathbf{0} & \mathbf{0} \\ & \textit{sym.} & & & \mathbf{S} & \mathbf{0} \\ & & & & & \mathbf{S} \end{bmatrix} \tag{4.59}$$

Moreover, the shape function matric for the strain variables reads:

$$\mathbf{N}_s = \begin{bmatrix} \mathbf{L} & \mathbf{0} & \mathbf{0} \\ & \mathbf{L} & \mathbf{0} \\ \textit{sym.} & & \mathbf{L} \end{bmatrix} \tag{4.60}$$

In Eq. (4.59), $\mathbf{L}(\xi) = \lfloor L_1(\xi) \quad L_2(\xi) \rfloor$ are the linear Lagrangian shape functions defined for the 2B-RZT$^{(m)}_{\{3,2\}}$ element, and the higher order shape functions are the Serendipity shape functions defined as follows:

$$\begin{aligned} \mathbf{S}(\xi) &= \lfloor S_1(\xi) \quad S_m(\xi) \quad S_2(\xi) \rfloor = \\ &= \left\lfloor \frac{1}{2}\xi(\xi-1) \quad (1-\xi^2) \quad \frac{1}{2}\xi(\xi+1) \right\rfloor \end{aligned} \tag{4.61}$$

According to this interpolation, the nodal dof's vectors are rewritten as follows:

$$\begin{aligned} &\mathbf{q}^{uT} = \lfloor u_1 \quad u_m \quad u_2 \rfloor; \mathbf{q}^{w0T} = \lfloor w_1^{(0)} \quad w_2^{(0)} \rfloor; \\ &\mathbf{q}^{w1T} = \lfloor w_1^{(1)} \quad w_2^{(1)} \rfloor; \mathbf{q}^{w2T} = \lfloor w_1^{(2)} \quad w_2^{(2)} \rfloor; \\ &\mathbf{q}^{\theta T} = \lfloor \theta_1 \quad \theta_m \quad \theta_2 \rfloor; \mathbf{q}^{\psi T} = \lfloor \psi_1 \quad \psi_m \quad \psi_2 \rfloor; \end{aligned} \tag{4.62}$$

$$\mathbf{q}^{eT} = \lfloor e_1 \quad e_2 \rfloor; \mathbf{q}^{kT} = \lfloor k_1 \quad k_2 \rfloor; \mathbf{q}^{k\psi T} = \lfloor k_1^{\psi} \quad k_2^{\psi} \rfloor \tag{4.63}$$

The total number of dof's can be reduced by enforcing a constraint condition on the distribution of the derivative of the strain variables at the element level. The constraint conditions read:

$$\begin{aligned}\frac{d^2u}{dx_1^{(e)2}} &= \frac{de}{dx_1^{(e)}} \\ \frac{d^2\theta}{dx_1^{(e)2}} &= \frac{dk}{dx_1^{(e)}} \\ \frac{d^2\psi}{dx_1^{(e)2}} &= \frac{dk^{\psi}}{dx_1^{(e)}}\end{aligned} \tag{4.64}$$

By adopting Eq.(4.64) it is possible to condense the mid-node nodal dof's, reobtaining a simple two-node configuration. In fact, after some mathematical passages, the internal degrees of freedom are made dependent on the external dof's, it yields,

$$u = L_1(\xi)u_1 + L_2(\xi)u_2 - S_m(\xi)\frac{L^{(e)}}{8}e_1 + S_m(\xi)\frac{L^{(e)}}{8}e_2 \tag{4.65}$$

$$\theta = L_1(\xi)\theta_1 + L_2(\xi)\theta_2 - S_m(\xi)\frac{L^{(e)}}{8}k_1 + S_m(\xi)\frac{L^{(e)}}{8}k_2 \tag{4.66}$$

$$\psi = L_1(\xi)\psi_1 + L_2\psi_2 - S_m(\xi)\frac{L^{(e)}}{8}k_1^{\psi} + S_m(\xi)\frac{L^{(e)}}{8}k_2^{\psi} \tag{4.67}$$

Thus, the shape function matrix is rewritten as follows:

$$\tilde{\mathbf{N}} = \begin{bmatrix} \mathbf{L} & \mathbf{0} & \mathbf{0} & \mathbf{0} & \mathbf{0} & \mathbf{0} & \mathbf{S}_n & \mathbf{0} & \mathbf{0} \\ & \mathbf{L} & \mathbf{0} & \mathbf{0} & \mathbf{0} & \mathbf{0} & \mathbf{0} & \mathbf{0} & \mathbf{0} \\ & & \mathbf{L} & \mathbf{0} & \mathbf{0} & \mathbf{0} & \mathbf{0} & \mathbf{0} & \mathbf{0} \\ & & & \mathbf{L} & \mathbf{0} & \mathbf{0} & \mathbf{0} & \mathbf{0} & \mathbf{0} \\ & & & & \mathbf{L} & \mathbf{0} & \mathbf{0} & \mathbf{S}_n & \mathbf{0} \\ & & & & & \mathbf{L} & \mathbf{0} & \mathbf{0} & \mathbf{S}_n \\ & & \textit{sym.} & & & & \mathbf{L} & \mathbf{0} & \mathbf{0} \\ & & & & & & & \mathbf{L} & \mathbf{0} \\ & & & & & & & & \mathbf{L} \end{bmatrix} \tag{4.68}$$

where $\mathbf{S}_n(\xi)=\frac{L^{(e)}}{8}\begin{bmatrix}-S_m(\xi) & S_m(\xi)\end{bmatrix}$ is the new shape function introduced by the condensation procedure. The resulting element is named after with the acronym 2Bc-RZT$^{(m)}_{\{3,2\}}$.

The 2Bc-RZT$^{(m)}_{\{3,2\}}$ elemental stiffness, mass matrices and load vector are obtained according to the mixed variational statement, i.e. Eq. (4.12). For the sake of clarity, the variational statement, neglecting the applied distributed loads, is here briefly recalled reads:

$$\begin{aligned}
&\delta\Pi=\int_V\left[\left(\delta\varepsilon_{11}^{(k)}\sigma_{11}^{(k)}+\delta\gamma_{13}^{(k)}\tau_{13}^{a}+\delta\varepsilon_{33}\sigma_{33}^{a}\right)\right]dV+\\
&+\int_V\left[\delta\tau_{13}^{a}\left(\gamma_{13}^{(k)}-\gamma_{13}^{(k)a}\right)+\delta\sigma_{33}^{a}\left(\varepsilon_{33}-\varepsilon_{33}^{(k)a}\right)\right]dV+\\
&+\frac{1}{\eta}\int_V\left[\begin{array}{l}\left(\delta u_{,1}-\delta e\right)\left(u_{,1}-e\right)+\\+\left(\delta\theta_{,1}-\delta k\right)\left(\theta_{,1}-k\right)+\left(\delta\psi_{,1}-\delta k^{\psi}\right)\left(\psi_{,1}-k^{\psi}\right)\end{array}\right]dV+\\
&-\int_V\rho^{(k)}\delta\mathbf{d}_d{}^T\ddot{\mathbf{d}}_d dV-\sum_{f=1}^{Nf}\bar{F}_f\left(\delta w^{(0)}(x_f)+\frac{h}{2}\delta w^{(1)}(x_f)+\frac{h^2}{4}\delta w^{(2)}(x_f)\right)=0
\end{aligned}\tag{4.69}$$

where $\bar{F}_f$ is the generic transversal concentrated force applied in the x_f point on the top beam surface.

By substituting Eq. (4.46) into Eqs. (4.53) and considering the Eqs. (4.3), (4.20) and (4.26), the full expression of stiffness and mass matrices and consistent load vector are obtained:

$$\mathbf{M}^{(e)}=\begin{bmatrix}
m^{(0)}\mathbf{L}^T\mathbf{L} & \mathbf{0} & \mathbf{0} & \mathbf{0} & m^{(1)}\mathbf{L}^T\mathbf{L} & m_{\mu}^{(0)}\mathbf{L}^T\mathbf{L} & m^{(0)}\mathbf{L}^T\mathbf{S}_n & \mathbf{0} & \mathbf{0}\\
 & m^{(0)}\mathbf{L}^T\mathbf{L} & m^{(1)}\mathbf{L}^T\mathbf{L} & m^{(2)}\mathbf{L}^T\mathbf{L} & \mathbf{0} & \mathbf{0} & \mathbf{0} & m^{(2)}\mathbf{L}^T\mathbf{S}_n & \mathbf{0}\\
 & & m^{(2)}\mathbf{L}^T\mathbf{L} & m^{(3)}\mathbf{L}^T\mathbf{L} & \mathbf{0} & \mathbf{0} & \mathbf{0} & \mathbf{0} & m_{\mu}^{(2)}\mathbf{L}^T\mathbf{S}_n\\
 & & & m^{(4)}\mathbf{L}^T\mathbf{L} & \mathbf{0} & \mathbf{0} & \mathbf{0} & \mathbf{0} & \mathbf{0}\\
 & & & & m^{(2)}\mathbf{L}^T\mathbf{L} & m_{\mu}^{(1)}\mathbf{L}^T\mathbf{L} & \mathbf{0} & \mathbf{0} & \mathbf{0}\\
 & & & & & m_{\mu}^{(2)}\mathbf{L}^T\mathbf{L} & \mathbf{0} & \mathbf{0} & \mathbf{0}\\
 & & & & & & m^{(0)}\mathbf{S}_n{}^T\mathbf{S}_n & \mathbf{0} & \mathbf{0}\\
 & \textit{sym.} & & & & & & m^{(2)}\mathbf{S}_n{}^T\mathbf{S}_n & \mathbf{0}\\
 & & & & & & & & m_{\mu}^{(2)}\mathbf{S}_n{}^T\mathbf{S}_n
\end{bmatrix}^{(e)}\tag{4.70}$$

$$\mathbf{K}^{(e)} = \begin{bmatrix} \mathbf{K}_{11} & \mathbf{K}_{12} & \mathbf{K}_{13} & \mathbf{K}_{14} & \mathbf{K}_{15} & \mathbf{K}_{16} & \mathbf{K}_{17} & \mathbf{K}_{18} & \mathbf{K}_{19} \\ & \mathbf{K}_{22} & \mathbf{K}_{23} & \mathbf{K}_{24} & \mathbf{K}_{25} & \mathbf{K}_{26} & \mathbf{K}_{27} & \mathbf{K}_{28} & \mathbf{K}_{29} \\ & & \mathbf{K}_{33} & \mathbf{K}_{34} & \mathbf{K}_{35} & \mathbf{K}_{36} & \mathbf{K}_{37} & \mathbf{K}_{38} & \mathbf{K}_{39} \\ & & & \mathbf{K}_{44} & \mathbf{K}_{45} & \mathbf{K}_{46} & \mathbf{K}_{47} & \mathbf{K}_{48} & \mathbf{K}_{49} \\ & & & & \mathbf{K}_{55} & \mathbf{K}_{56} & \mathbf{K}_{57} & \mathbf{K}_{58} & \mathbf{K}_{59} \\ & & & & & \mathbf{K}_{66} & \mathbf{K}_{67} & \mathbf{K}_{68} & \mathbf{K}_{69} \\ & & & & & & \mathbf{K}_{77} & \mathbf{K}_{78} & \mathbf{K}_{79} \\ & & & & & & & \mathbf{K}_{88} & \mathbf{K}_{89} \\ & & & & & & & & \mathbf{K}_{99} \end{bmatrix}^{(e)} \tag{4.71}$$

with

$$
\begin{aligned}
&\mathbf{K}_{11}^{(e)} = \mathbf{L}_{,1}{}^{T}\tilde{A}\mathbf{L}_{,1} + \frac{hb}{\eta}\mathbf{L}_{,1}{}^{T}\mathbf{L}_{,1} \qquad \mathbf{K}_{12}^{(e)} = \mathbf{L}_{,1}{}^{T}\tilde{A}_{11}^{w}\mathbf{L} \qquad \mathbf{K}_{13}^{(e)} = \mathbf{L}_{,1}{}^{T}\tilde{A}_{12}^{w}\mathbf{L} \qquad \mathbf{K}_{14}^{(e)} = \mathbf{L}_{,1}{}^{T}\tilde{A}_{13}^{w}\mathbf{L}\\
&\mathbf{K}_{15}^{(e)} = \mathbf{L}_{,1}{}^{T}\tilde{B}\mathbf{L}_{,1} \qquad \mathbf{K}_{16}^{(e)} = \mathbf{L}_{,1}{}^{T}\tilde{A}^{\phi}\mathbf{L}_{,1} \qquad \mathbf{K}_{17}^{(e)} = \mathbf{L}_{,1}{}^{T}\tilde{A}\mathbf{S}_{n,1} - \frac{hb}{\eta}\mathbf{L}_{,1}{}^{T}\mathbf{L} + \frac{hb}{\eta}\mathbf{L}_{,1}{}^{T}\mathbf{S}_{n,x}\\
&\mathbf{K}_{18}^{(e)} = \mathbf{L}_{,1}{}^{T}\tilde{B}\mathbf{S}_{n,1} \qquad \mathbf{K}_{19}^{(e)} = \mathbf{L}_{,1}{}^{T}\tilde{A}^{\phi}\mathbf{S}_{n,1} \qquad \mathbf{K}_{22}^{(e)} = \mathbf{L}^{T}D_{11}^{Nz}\mathbf{L} + \mathbf{L}_{,1}{}^{T}\hat{D}_{11}^{w}\mathbf{L}_{,1} + \mathbf{L}_{,1}{}^{T}\hat{D}_{11}^{w}\mathbf{L}_{,1} - \mathbf{L}_{,1}{}^{T}\hat{D}_{11}^{kw}\mathbf{L}_{,1}\\
&\mathbf{K}_{23}^{(e)} = \mathbf{L}^{T}D_{12}^{Nz}\mathbf{L} + \mathbf{L}_{,1}{}^{T}\hat{D}_{21}^{w}\mathbf{L}_{,1} + \mathbf{L}_{,1}{}^{T}\hat{D}_{12}^{w}\mathbf{L}_{,1} - \mathbf{L}_{,1}{}^{T}\hat{D}_{12}^{kw}\mathbf{L}_{,1} \qquad \mathbf{K}_{24}^{(e)} = \mathbf{L}^{T}D_{13}^{Nz}\mathbf{L} + \mathbf{L}_{,1}{}^{T}\hat{D}_{31}^{w}\mathbf{L}_{,1} + \mathbf{L}_{,1}{}^{T}\hat{D}_{13}^{w}\mathbf{L}_{,1} - \mathbf{L}_{,1}{}^{T}\hat{D}_{13}^{kw}\mathbf{L}_{,1}\\
&\mathbf{K}_{25}^{(e)} = \mathbf{L}^{T}B_{11}^{Nz}\mathbf{L}_{,1} + \mathbf{L}_{,1}{}^{T}\hat{D}_{11}^{\theta}\mathbf{L} \qquad \mathbf{K}_{26}^{(e)} = \mathbf{L}^{T}C_{11}^{Nz}\mathbf{L}_{,1} + \mathbf{L}_{,1}{}^{T}\hat{D}_{11}^{\psi}\mathbf{L} \qquad \mathbf{K}_{27}^{(e)} = \mathbf{L}_{,1}{}^{T}\hat{A}_{11}^{w}\mathbf{L}_{,1} - \mathbf{L}_{,1}{}^{T}\hat{A}_{11}^{kw}\mathbf{L}_{,1} + \mathbf{L}^{T}A_{11}^{Nz}\mathbf{S}_{n,1}\\
&\mathbf{K}_{28}^{(e)} = \mathbf{L}_{,1}{}^{T}\hat{B}_{11}^{w}\mathbf{L}_{,1} - \mathbf{L}_{,x}{}^{T}\hat{B}_{11}^{kw}\mathbf{L}_{,1} + \mathbf{L}^{T}B_{11}^{Nz}\mathbf{S}_{n,1} + \mathbf{L}_{,x}{}^{T}\hat{D}_{11}^{\theta}\mathbf{S}_{n} \qquad \mathbf{K}_{29}^{(e)} = \mathbf{L}_{,1}{}^{T}\hat{C}_{11}^{w}\mathbf{L}_{,1} - \mathbf{L}_{,1}{}^{T}\hat{C}_{11}^{kw}\mathbf{L}_{,1} + \mathbf{L}^{T}C_{11}^{Nz}\mathbf{S}_{n,1} + \mathbf{L}_{,1}{}^{T}\hat{D}_{11}^{\psi}\mathbf{S}_{n}\\
&\mathbf{K}_{33}^{(e)} = \mathbf{L}^{T}D_{22}^{Nz}\mathbf{L} + \mathbf{L}_{,1}{}^{T}\hat{D}_{22}^{w}\mathbf{L}_{,1} + \mathbf{L}_{,1}{}^{T}\hat{D}_{22}^{w}\mathbf{L}_{,1} - \mathbf{L}_{,1}{}^{T}\hat{D}_{22}^{kw}\mathbf{L}_{,1} \qquad \mathbf{K}_{34}^{(e)} = \mathbf{L}^{T}D_{23}^{Nz}\mathbf{L} + \mathbf{L}_{,1}{}^{T}\hat{D}_{32}^{w}\mathbf{L}_{,1} + \mathbf{L}_{,1}{}^{T}\hat{D}_{23}^{w}\mathbf{L}_{,1} - \mathbf{L}_{,1}{}^{T}\hat{D}_{23}^{kw}\mathbf{L}_{,1}\\
&\mathbf{K}_{35}^{(e)} = \mathbf{L}^{T}B_{21}^{Nz}\mathbf{L}_{,1} + \mathbf{L}_{,1}{}^{T}\hat{D}_{21}^{\theta}\mathbf{L} \qquad \mathbf{K}_{36}^{(e)} = \mathbf{L}^{T}C_{21}^{Nz}\mathbf{L}_{,1} + \mathbf{L}_{,1}{}^{T}\hat{D}_{21}^{\psi}\mathbf{L}\\
&\mathbf{K}_{37}^{(e)} = \mathbf{L}_{,1}{}^{T}\hat{A}_{12}^{w}\mathbf{L}_{,1} - \mathbf{L}_{,1}{}^{T}\hat{A}_{12}^{kw}\mathbf{L}_{,1} + \mathbf{L}^{T}A_{21}^{Nz}\mathbf{S}_{n,1} \qquad \mathbf{K}_{38}^{(e)} = \mathbf{L}_{,1}{}^{T}\hat{B}_{12}^{w}\mathbf{L}_{,1} - \mathbf{L}_{,1}{}^{T}\hat{B}_{12}^{kw}\mathbf{L}_{,1} + \mathbf{L}^{T}B_{21}^{Nz}\mathbf{S}_{n,1} + \mathbf{L}_{,1}{}^{T}\hat{D}^{\theta}\mathbf{S}_{n}\\
&\mathbf{K}_{39}^{(e)} = \mathbf{L}_{,1}{}^{T}\hat{C}_{12}^{w}\mathbf{L}_{,1} - \mathbf{L}_{,1}{}^{T}\hat{C}_{12}^{kw}\mathbf{L}_{,1} + \mathbf{L}^{T}C_{21}^{Nz}\mathbf{S}_{n,1} + \mathbf{L}_{,1}{}^{T}\hat{D}_{21}^{\psi}\mathbf{S}_{n} \qquad \mathbf{K}_{44}^{(e)} = \mathbf{L}^{T}D_{33}^{Nz}\mathbf{L} + \mathbf{L}_{,1}{}^{T}\hat{D}_{33}^{w}\mathbf{L}_{,1} + \mathbf{L}_{,x}{}^{T}\hat{D}_{33}^{w}\mathbf{L}_{,1} - \mathbf{L}_{,x}{}^{T}\hat{D}_{33}^{kw}\mathbf{L}_{,1}\\
&\mathbf{K}_{45}^{(e)} = \mathbf{L}^{T}B_{31}^{Nz}\mathbf{L}_{,1} + \mathbf{L}_{,x}{}^{T}\hat{D}_{31}^{\theta}\mathbf{L} \qquad \mathbf{K}_{46}^{(e)} = \mathbf{L}^{T}C_{31}^{Nz}\mathbf{L}_{,1} + \mathbf{L}_{,1}{}^{T}\hat{D}_{31}^{\psi}\mathbf{L} \qquad \mathbf{K}_{47}^{(e)} = \mathbf{L}_{,1}{}^{T}\hat{A}_{13}^{w}\mathbf{L}_{,1} - \mathbf{L}_{,1}{}^{T}\hat{A}_{13}^{kw}\mathbf{L}_{,1} + \mathbf{L}^{T}A_{31}^{Nz}\mathbf{S}_{n,1}\\
&\mathbf{K}_{48}^{(e)} = \mathbf{L}_{,1}{}^{T}\hat{B}_{13}^{w}\mathbf{L}_{,1} - \mathbf{L}_{,1}{}^{T}\hat{B}_{13}^{kw}\mathbf{L}_{,1} + \mathbf{L}^{T}B_{31}^{Nz}\mathbf{S}_{n,1} + \mathbf{L}_{,1}{}^{T}\hat{D}_{31}^{\theta}\mathbf{S}_{n}\\
&\mathbf{K}_{49}^{(e)} = \mathbf{L}_{,1}{}^{T}\hat{C}_{13}^{w}\mathbf{L}_{,1} - \mathbf{L}_{,x}{}^{T}\hat{C}_{13}^{kw}\mathbf{L}_{,1} + \mathbf{L}^{T}C_{31}^{Nz}\mathbf{S}_{n,x} + \mathbf{L}_{,1}{}^{T}\hat{D}_{31}^{\psi}\mathbf{S}_{n}\\
&\mathbf{K}_{55}^{(e)} = \mathbf{L}_{,1}{}^{T}\tilde{D}\mathbf{L}_{,1} + \frac{hb}{\eta}\mathbf{L}_{,1}{}^{T}\mathbf{L}_{,1} \qquad \mathbf{K}_{56}^{(e)} = \mathbf{L}_{,1}{}^{T}\tilde{B}^{\phi}\mathbf{L}_{,1} \qquad \mathbf{K}_{57}^{(e)} = \mathbf{L}^{T}\hat{A}^{\theta}\mathbf{L}_{,1} + \mathbf{L}_{,1}{}^{T}\tilde{B}\mathbf{S}_{n,1}\\
&\mathbf{K}_{58}^{(e)} = \mathbf{L}^{T}\hat{B}^{\theta}\mathbf{L}_{,1} - \frac{hb}{\eta}\mathbf{L}_{,1}{}^{T}\mathbf{L} + \mathbf{L}_{,1}{}^{T}\tilde{D}\mathbf{S}_{n,1} + \frac{hb}{\eta}\mathbf{L}_{,1}{}^{T}\mathbf{S}_{n,1} \qquad \mathbf{K}_{59}^{(e)} = \mathbf{L}^{T}\hat{C}^{\theta}\mathbf{L}_{,1} + \mathbf{L}_{,1}{}^{T}\tilde{B}^{\phi}\mathbf{S}_{n,1}\\
&\mathbf{K}_{66}^{(e)} = \mathbf{L}_{,1}{}^{T}\tilde{G}^{\phi}\mathbf{L}_{,1} + \frac{hb}{\eta}\mathbf{L}_{,1}{}^{T}\mathbf{L}_{,1} \qquad \mathbf{K}_{67}^{(e)} = \left(\mathbf{L}^{T}\hat{A}^{\psi}\mathbf{L}_{,1} + \mathbf{L}_{,1}{}^{T}\tilde{A}^{\phi}\mathbf{S}_{n,1}\right) \qquad \mathbf{K}_{68}^{(e)} = \left(\mathbf{L}^{T}\hat{B}^{\psi}\mathbf{L}_{,1} + \mathbf{L}_{,1}{}^{T}\tilde{B}^{\phi}\mathbf{S}_{n,1}\right)\\
&\mathbf{K}_{69}^{(e)} = \mathbf{L}^{T}\hat{C}^{\psi}\mathbf{L}_{,1} - \frac{hb}{\eta}\mathbf{L}_{,1}{}^{T}\mathbf{L} + \mathbf{L}_{,1}{}^{T}\tilde{G}^{\phi}\mathbf{S}_{n,1} + \frac{hb}{\eta}\mathbf{L}_{,1}{}^{T}\mathbf{S}_{n,1}\\
&\mathbf{K}_{77}^{(e)} = \frac{hb}{\eta}\mathbf{L}^{T}\mathbf{L} - \mathbf{L}_{,1}{}^{T}\hat{A}^{e}\mathbf{L}_{,1} + \mathbf{S}_{n,1}{}^{T}\tilde{A}\mathbf{S}_{n,1} + \frac{hb}{\eta}\mathbf{S}_{n,1}{}^{T}\mathbf{S}_{n,1} - \frac{hb}{\eta}\mathbf{S}_{n,1}{}^{T}\mathbf{L} - \frac{hb}{\eta}\mathbf{L}^{T}\mathbf{S}_{n,1}\\
&\mathbf{K}_{78}^{(e)} = -\mathbf{L}_{,1}{}^{T}\hat{A}^{k}\mathbf{L}_{,1} + \mathbf{S}_{n,1}{}^{T}\tilde{B}\mathbf{S}_{n,1} + \mathbf{L}_{,1}{}^{T}\hat{A}^{\theta}\mathbf{S}_{n} \qquad \mathbf{K}_{79}^{(e)} = -\mathbf{L}_{,1}{}^{T}\hat{A}^{k\psi}\mathbf{L}_{,1} + \mathbf{S}_{n,1}{}^{T}\tilde{A}^{\phi}\mathbf{S}_{n,1} + \mathbf{L}_{,1}{}^{T}\hat{A}^{\psi}\mathbf{S}_{n}\\
&\mathbf{K}_{88}^{(e)} = \frac{hb}{\eta}\mathbf{L}^{T}\mathbf{L} - \mathbf{L}_{,1}{}^{T}\hat{B}^{k}\mathbf{L}_{,1} + \mathbf{S}_{n,1}{}^{T}\tilde{D}\mathbf{S}_{n,1} + \mathbf{S}_{n}{}^{T}\hat{B}^{\theta}\mathbf{L}_{,1} + \mathbf{L}_{,x}{}^{T}\hat{B}^{\theta}\mathbf{S}_{n} + \frac{hb}{\eta}\mathbf{S}_{n,1}{}^{T}\mathbf{S}_{n,1} - \frac{hb}{\eta}\mathbf{S}_{n,1}{}^{T}\mathbf{L} - \frac{hb}{\eta}\mathbf{L}^{T}\mathbf{S}_{n,1}\\
&\mathbf{K}_{89}^{(e)} = -\mathbf{L}_{,1}{}^{T}\hat{B}^{k\psi}\mathbf{L}_{,1} + \mathbf{S}_{n,1}{}^{T}\tilde{B}^{\phi}\mathbf{S}_{n,1} + \mathbf{S}_{n}{}^{T}\hat{C}^{\theta}\mathbf{L}_{,1} + \mathbf{L}_{,1}{}^{T}\hat{B}^{\psi}\mathbf{S}_{n}\\
&\mathbf{K}_{99}^{(e)} = \frac{hb}{\eta}\mathbf{L}^{T}\mathbf{L} - \mathbf{L}_{,1}{}^{T}\hat{C}^{k\psi}\mathbf{L}_{,1} + \mathbf{S}_{n,1}{}^{T}\tilde{G}^{\phi}\mathbf{S}_{n,1} + \mathbf{S}_{n}{}^{T}\hat{C}^{\psi}\mathbf{L}_{,1} + \mathbf{L}_{,1}{}^{T}\hat{C}^{\psi}\mathbf{S}_{n} + \frac{hb}{\eta}\mathbf{S}_{n,1}{}^{T}\mathbf{S}_{n,1} - \frac{hb}{\eta}\mathbf{S}_{n,1}{}^{T}\mathbf{L} - \frac{hb}{\eta}\mathbf{L}^{T}\mathbf{S}_{n,1}
\end{aligned}
\tag{4.72}
$$

$$
\mathbf{F}^{(e)T} = \left\lfloor \mathbf{0} \quad \overline{\mathbf{F}} \quad \frac{h}{2}\overline{\mathbf{F}} \quad \frac{h^2}{4}\overline{\mathbf{F}} \quad \mathbf{0} \quad \mathbf{0} \quad \mathbf{0} \quad \mathbf{0} \quad \mathbf{0} \right\rfloor^{(e)} \tag{4.73}
$$

with $\overline{\mathbf{F}}^{(e)} = \left\lfloor \overline{F}_{n1} \quad \overline{F}_{n2} \right\rfloor^{(e)}$ represents the vector of the forces of the e^{th} element applied to the left and right node, respectively. It is worth noting that the elemental nodal force vector has the same expression for both elements. Moreover, for 2Bc-RZT$_{\{3,2\}}^{(m)}$ element, due to the constraint condition to condense the mid-node dof's, the elemental mass matrix have not null values on the diagonal for the strain degrees of freedom and presents coupling terms with the corresponding in-plane displacement and rotations.

4.5 The static condensation procedure

As a result of the previous element formulations, both elements involve eighteen dof's (nine dof's for each node), which could be computationally expensive. Therefore, it is possible to adopt the static condensation technique to reduce the computational cost but maintain the same accuracy. At the element level, the governing equations are expressed as follows

$$\mathbf{M}^{(e)}\ddot{\mathbf{q}}^{(e)} + \mathbf{K}^{(e)}\mathbf{q}^{(e)} = \mathbf{F}^{(e)} \tag{4.74}$$

Explicitating in Eq. (4.74) the two groups of variables:

$$\begin{bmatrix} \mathbf{M}_{dd}^{(e)} & \mathbf{M}_{ds}^{(e)} \\ \mathbf{M}_{ds}^{(e)T} & \mathbf{M}_{ss}^{(e)} \end{bmatrix} \begin{Bmatrix} \ddot{\mathbf{q}}_d^{(e)} \\ \ddot{\mathbf{q}}_s^{(e)} \end{Bmatrix} + \begin{bmatrix} \mathbf{K}_{dd}^{(e)} & \mathbf{K}_{ds}^{(e)} \\ \mathbf{K}_{ds}^{(e)T} & \mathbf{K}_{ss}^{(e)} \end{bmatrix} \begin{Bmatrix} \mathbf{q}_d^{(e)} \\ \mathbf{q}_s^{(e)} \end{Bmatrix} = \begin{Bmatrix} \mathbf{F}_d^{(e)} \\ \mathbf{0} \end{Bmatrix} \tag{4.75}$$

The second line of Eq. (4.75) could be solved statically by making $\mathbf{q}_s^{(e)}$ depending on the $\mathbf{q}_d^{(e)}$ variables. It reads:

$$\mathbf{K}_{ds}^{(e)T}\mathbf{q}_d^{(e)} + \mathbf{K}_{ss}^{(e)}\mathbf{q}_s^{(e)} = \mathbf{0} \rightarrow \mathbf{q}_s^{(e)} = -\mathbf{K}_{ss}^{(e)-1}\mathbf{K}_{ds}^{(e)T}\mathbf{q}_d^{(e)} \tag{4.76}$$

Substituting Eq. (4.76) into Eq. (4.75), it yields a new expression of the equations of motions:

$$\mathbf{M}_{dd}^{(e)}\ddot{\mathbf{q}}_d^{(e)} + \left(\mathbf{K}_{dd}^{(e)} - \mathbf{K}_{ss}^{(e)-1}\mathbf{K}_{ds}^{(e)T}\right)\mathbf{q}_d^{(e)} = \mathbf{F}_d^{(e)} \tag{4.77}$$

Moreover,

$$\mathbf{M}_{dd}^{(e)}\ddot{\mathbf{q}}_d^{(e)} + \hat{\mathbf{K}}_{dd}^{(e)}\mathbf{q}_d^{(e)} = \mathbf{F}_d^{(e)} \tag{4.78}$$

with $\hat{\mathbf{K}}_{dd}^{(e)} = \left(\mathbf{K}_{dd}^{(e)} - \mathbf{K}_{ss}^{(e)-1}\mathbf{K}_{ds}^{(e)T}\right)$.

It is important to note that for 2Bc-RZT$_{\{3,2\}}^{(m)}$, $\mathbf{M}_{ds}^{(e)} \neq \mathbf{0}$ and $\mathbf{M}_{ss}^{(e)} \neq \mathbf{0}$. This effect introduces an approximation on the mass matrix that neglects the inertia effect of the strain quantities introduced by the constraint element conditions. However, the condensation of the strain dof's is able to provide the exact stiffness

matrix for both reduced elements when the static analysis with only concentrated nodal forces is considered.

The total number of dof's of both elements is reduced from eighteen to twelve. For clarity, the full expressions of the reduced mass and stiffness matrices of 2B-RZT$^{(m)}_{\{3,2\}}$ and 2Bc-RZT$^{(m)}_{\{3,2\}}$ elements are not reported here; however, they could be easily obtained by substituting the expression of elemental stiffness and mass matrices in Eq. (4.77).

Chapter 5

Numerical assessments

In this Chapter, the previously developed plates and beams models are numerically assessed to evaluate the global and local response of multilayered composites and sandwich structures. The numerical results are compared with those coming from the three-dimensional solutions available in the current literature. Whenever the exact elasticity solutions are unavailable, the reference results are obtained through appropriate high-fidelity FE models using MSC - PATRAN®/NASTRAN® commercial codes.

In this numerical assessment, particular attention is paid to lamination schemes in which the effect of transverse shear coupling is not negligible. The angle-ply multilayered structures represent a class of laminated plates studied in this chapter. In the following sections, the novelties and limitations of the enhanced models (en-RZT and en-RZT$^{(m)}_{\{3,2\}}$) in predicting the global and local responses of multilayered angle-ply structures are presented. Moreover, multilayered cross-ply and sandwich plates are also assessed to highlight the computational advantages introduced by the newly developed mixed model the en-RZT$^{(m)}_{\{3,2\}}$. In particular, the latter model is applied to the analysis of thick multilayered structures for bending and free vibration analysis since the transverse normal deformability has been considered in the formulation.

The newly mixed beam model has been used to evaluate the global and local responses of displacement, strain and stress distributions, and natural frequencies of thick multilayered composite and sandwich beams. In addition, analytical and

finite element solutions have been assessed with the high-fidelity FE models with NASTRAN® finite elements, better representing those created for the experimental campaign.

Some of this Chapter's contents have been subjected to publications in International Journals [136,137,150] or presented at International Conferences [149,167,168]. However, in this thesis's work, some of the already presented results are further commented on and better explained to highlight the significant novelties and the limitations of the presented approaches.

5.1 En-RZT assessment

In this Section, the linear en-RZT plate model is assessed for static, dynamic and stability analysis. For simplicity, numerical examples are related to rectangular flat plates with the edges parallel to the axis (x_1,x_2), as shown in Figure 12. The length of the plate (in the x_1 direction) is denoted with a, and the width (in the x_2 direction) is denoted with b. The origin of the axes corresponds to the lower-left corner of the plate.

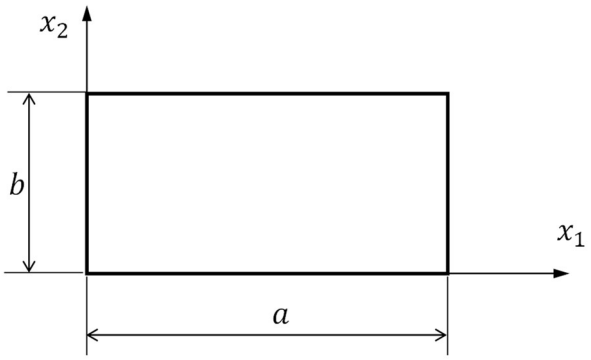

Figure 12: Rectangular plate dimensions and coordinate system.

Table 1 and Table 2 report the materials properties and laminate stacking sequences, respectively, of the investigated multilayered composite and sandwich plates for the en-RZT assessment.

Table 1:Material nomenclature and properties. The elastic moduli are given in GPa, and the mass density in kg/m^3.

Material Name	E_1	E_2	E_3	ν_{12}	ν_{13}	ν_{23}	G_{12}	G_{13}	G_{23}	ρ
A	175	7	7	0.25	0.25	0.25	3.5	3.5	1.4	-
B	157.4	9.584	9.584	0.32	0.32	0.49	5.93	5.93	3.227	-
C	0.104	0.104	0.104	0.3	0.3	0.49	0.5	0.5	0.35	-
D	40	1	1	0.25	0.25	0.25	0.6	0.6	0.5	1
E	15	1	1	0.3	0.3	0.35	0.5	0.5	0.35	1
F	1	1	1	0.3	0.3	0.3	0.39	0.39	0.39	-
G	14	1	1	0.3	0.3	0.49	0.533	0.533	0.323	1

Table 2: Laminate stacking sequences (starting from the bottom layer) and nomenclatures. The orientations are given in degrees.

Laminate ID	Normalized thickness $h^{(k)}/h$	Lamina materials	Lamina orientations [°]
L1	(0.5/0.5)	(A/A)	(0/90)
L2	(0.25/0.5/0.25)	(A/A/A)	(0/90/0)
L3	(0.5/0.5)	(A/A)	$(-Y/+Y)$
L4	(0.05/0.05/0.8/0.05/0.05)	(B/B/C/B/B)	(30/-45/0/45/-30)
L5	(0.25/0.5/0.25)	(A/A/A)	(30/-30/30)
L6	(0.25/0.25/0.25/0.25)	(D/D/D/D)	$(-Y/+Y/-Y/+Y)$
L7	$\left(\frac{1}{n}/\frac{1}{n}\right)_n$	$(E/E)_n$	$(-Y/+Y)_n$
L8	(0.25/0.5/0.25)	(E/E/E)	(+45/-45/+45)
L9	$(0.1/0.1)_5$	$(E/E)_5$	$(-Y/+Y)_5$
L10	(0.3333/0.3333/0.3333)	(A/A/A)	(45/-45/45)
L11	(0.25/0.25/0.25/0.25)	(G/G/G/G)	(45/-45/45/-45)
L12	$\left(\frac{1}{n}/\frac{1}{n}\right)_n$	$(D/D)_n$	$(45/-45)_n$
S1	0.05/0.05/0.8/0.05/0.05	(D/D/F/D/D)	(+45/-45/0/-45/+45)
S2	0.05/0.05/0.8/0.05/0.05	(D/D/F/D/D)	(+45/-45/0/+45-45)

5.1.1 Enhanced zigzag functions

As shown in Chapter 2, one of the major novelties of the en-RZT is its generalized formulation for the analysis of multilayered plates. The enhanced zigzag functions are characterized for general laminated structures in which the effect of transverse shear coupling is assumed to be present. However, if the lamination scheme does not exhibit this behaviour, the zigzag functions

formulated according to the standard RZT are easily recovered. In order to highlight this important aspect of generalization, in the following examples, the enhanced zigzag functions and the standard ones are computed and compared for several lamination schemes that include/neglect the effect of transverse shear coupling. In the following figures, the label "standard" means the zigzag functions computed according to the formulation of the standard RZT. Whereas the label "enhanced" refers to the zigzag functions computed according to the enhanced linear RZT model.

The first laminate considered is a two-layered anti-symmetric cross-ply named L1. A second laminate type that does not include the transverse shear coupling effect, named L2, is a three-layered symmetric cross-ply.

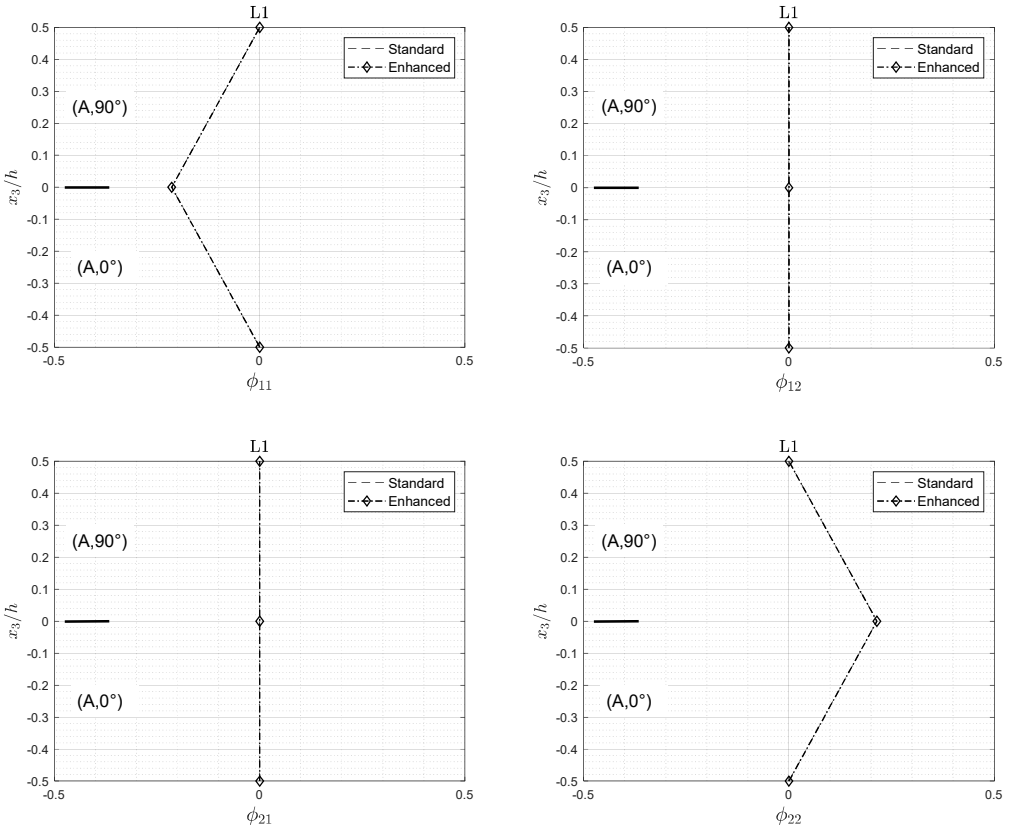

Figure 13: Standard and enhanced zigzag functions for anti-symmetric cross-ply (L1).

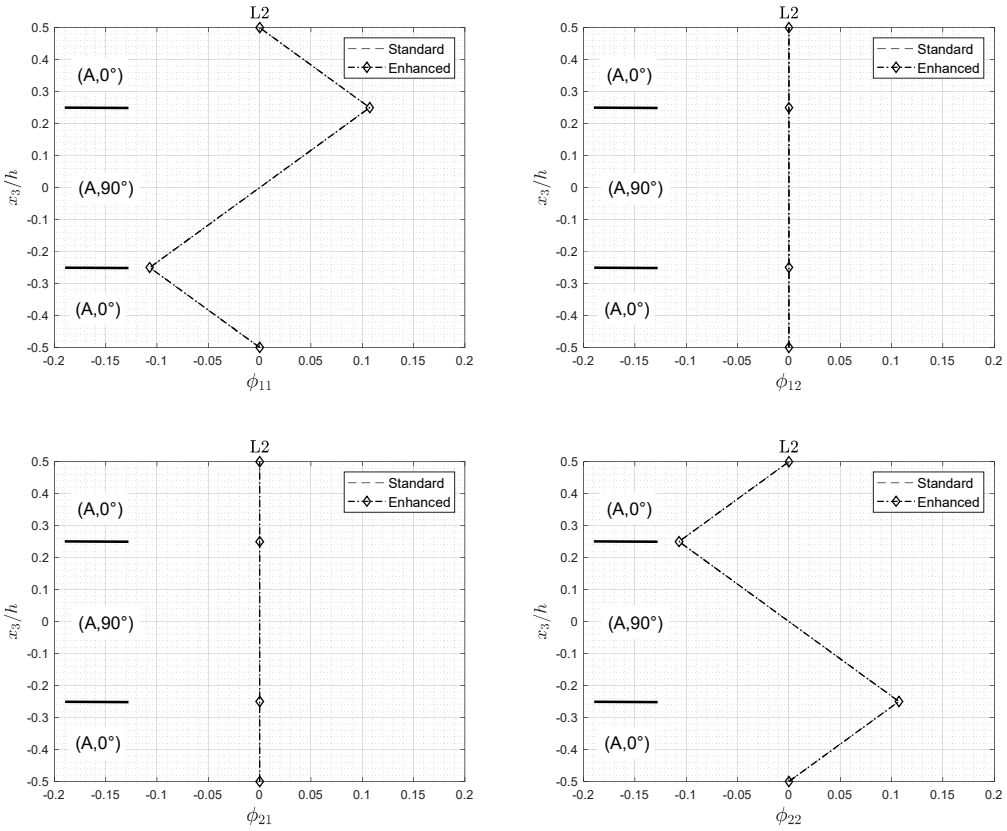

Figure 14: Standard and enhanced zigzag functions for symmetric cross-ply (L2).

It is clear from Figure 13 and Figure 14 that the zigzag functions ϕ_{12} and ϕ_{21} are not evaluated in the standard zigzag formulation. However, as expected in the enhanced formulation, they remain null across the entire thickness because the effect of transverse shear coupling is not present in these laminate configurations. Moreover, the through-the-thickness distributions of the two zigzag functions reported in Figure 13 and Figure 14 are the same and no differences in their values are obtained.

The novelty introduced by the enhanced model is shown in Figure 15. A two-layered anti-symmetric angle ply (L3) is considered with 15° as absolute value of the lamination angle. The standard zigzag functions are null due to the anti-symmetric lamination scheme in which the transformed transverse shear stiffness coefficients, i.e. $\breve{C}_{44}^{(k)}$ and $\breve{C}_{55}^{(k)}$, are constant along the whole thickness. In addition, the standard RZT cannot describe the expected transverse shear coupling, whereas the en-RZT is able to include it. Moreover, it is worth noting that in the enhanced model, zigzag functions, ϕ_{11} and ϕ_{22}, are still null. Furthermore, considering the

three-dimensional elasticity solution provided by Savoia and Reddy [13], the transverse shear coupling effect produces layer-wise distributions very similar in their shapes to those represented by ϕ_{12} and ϕ_{21} functions. Moreover, the two enhanced zigzag functions allow using the RZT kinematics to investigate these structures.

Thus, the standard RZT is not able to investigate this typology of multilayered structures, in which the lamination scheme is characterized by periodic laminates with the same absolute value for the lamination angle. As a result, the zigzag functions are null in such cases, and the RZT model degenerates into the FSDT.

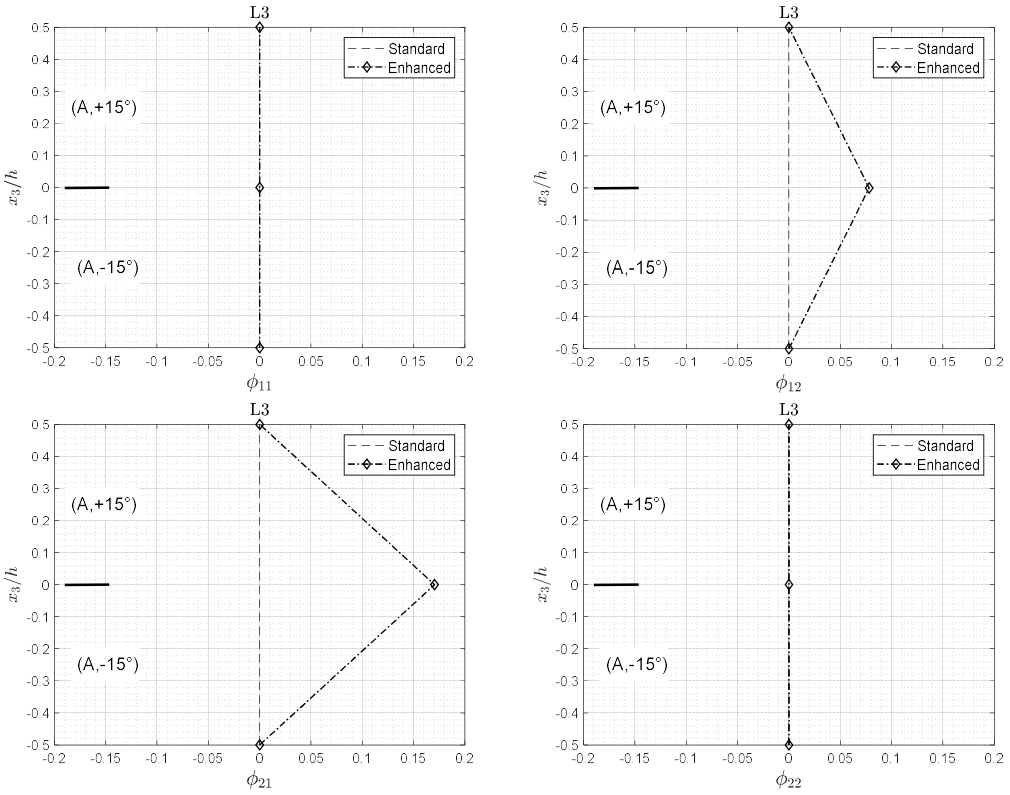

Figure 15: Standard and enhanced zigzag functions for anti-symmetric angle-ply (L3).

Figure 16 reports the computed standard and zigzag functions related to an anti-symmetric multilayered sandwich plate. The same plate has been studied statically in the original standard RZT formulation, see Ref. [103]. The presence of the isotropic core layer in the laminate stacking sequence allows the standard formulation to compute the zigzag functions. However, it is important to note that

the enhanced formulation can also compute the coupling functions. Particular attention should be paid to the order of magnitude of the coupling function: its value is almost negligible with respect to the values of the other two functions. Although the ϕ_{11} and ϕ_{22} seems to be the same for the two formulations, very few differences are present. However, the coupling effect neglected in the original formulation has been a valid approximation explained a-posteriori, thanks to the enhanced zigzag functions.

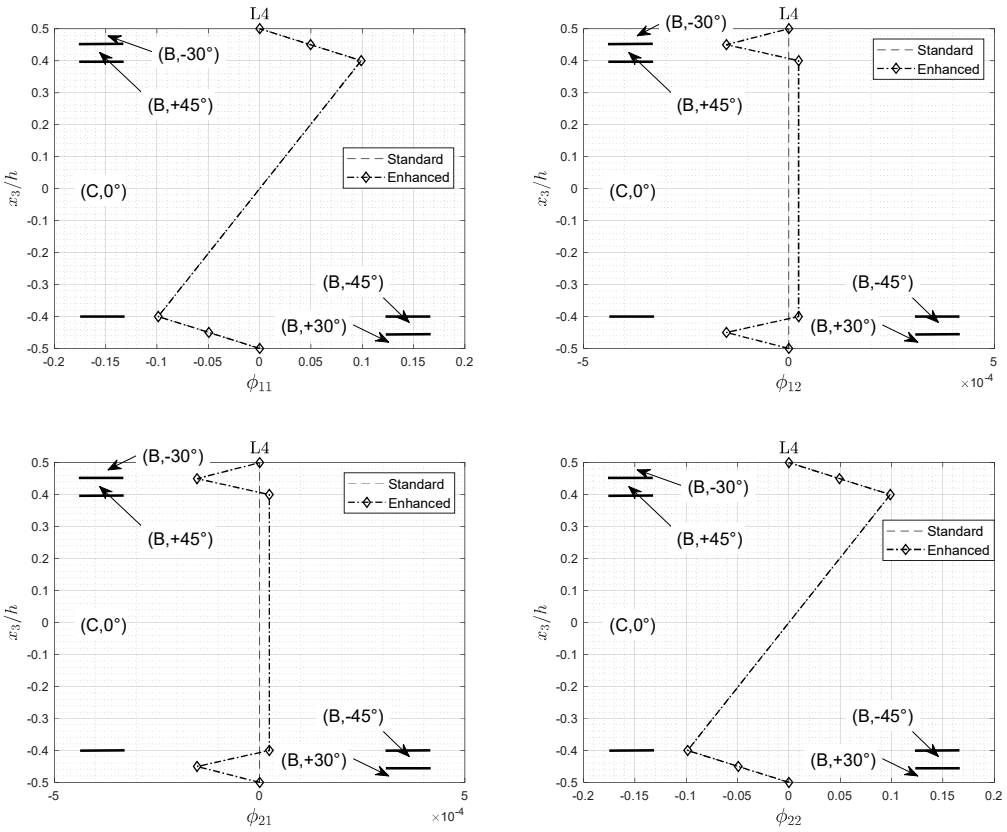

Figure 16: Standard and enhanced zigzag functions for an anti-symmetric angle-ply sandwich (L4).

Even if the standard RZT model works well, i.e. angle-ply sandwich plates, the enhancement must be considered in a general way to achieve more reliable results without any approximations.

5.1.2 Static, free vibration and stability problems

In the following examples, the static, stability and free vibration problems are assessed. Specifying the boundary conditions and loads applied to the plate is necessary to compute the structure's response. The boundary conditions provided in Chapter 2 for the en-RZT plate are expressed in terms of the plate dimensions and lamination schemes.

For cross-ply multilayered composite and sandwich plates simply-supported on all edges, the set of boundary conditions, here named SS-1, reads

- Along the edges $x_1 = 0, a$: $u_2 = w = N_{11} = M_{11} = M_{11}^{\phi} = 0$
- Along the edges $x_2 = 0, b$: $u_1 = w = N_{22} = M_{22} = M_{22}^{\phi} = 0$

For anti-symmetric angle-ply simply-supported on all edges, the boundary conditions, here named with SS-2, read

- Along the edges $x_1 = 0, a$: $u_1 = w = N_{12} = M_{11} = M_{11}^{\phi} = 0$
- Along the edges $x_2 = 0, b$: $u_2 = w = N_{12} = M_{22} = M_{22}^{\phi} = 0$

The traction-free boundary conditions read,

- Along the edges $x_1 = 0, a$:
$$N_{11} = N_{12} = M_{11} = M_{12} = M_{11}^{\phi} = M_{12}^{\phi} = Q_1 = 0$$
- Along the edges $x_2 = 0, b$:
$$N_{12} = N_{22} = M_{12} = M_{22} = M_{12}^{\phi} = M_{22}^{\phi} = Q_2 = 0$$

At last, the clamped boundary conditions read

- Along the edges $x_1 = 0, a: u_1 = u_2 = w = \theta_1 = \theta_2 = \psi_1 = \psi_2 = 0$
- Along the edges $x_2 = 0, b: u_1 = u_2 = w = \theta_1 = \theta_2 = \psi_1 = \psi_2 = 0$

Due to the mathematical difficulty in obtaining an exact analytical solution of the governing equations for any boundary conditions and load cases, the en-RZT

analytical solutions using Navier's method are obtained only for plates with simply-supported edges under bi-sinusoidal load pressure.

For cross-ply plates (SS-1) under bi-sinusoidal transverse pressure and free vibration problems, the assumed solution involves the following trigonometric expansions [135]:

$$\begin{aligned} w &= W \sin\left(\pi x_1 / a\right) \sin\left(\pi x_2 / b\right) \\ \begin{Bmatrix} u_1 \\ \theta_1 \\ \psi_1 \end{Bmatrix} &= \begin{Bmatrix} U \\ \Theta_1 \\ \Psi_1 \end{Bmatrix} \cos\left(\pi x_1 / a\right) \sin\left(\pi x_2 / b\right) \\ \begin{Bmatrix} u_2 \\ \theta_2 \\ \psi_2 \end{Bmatrix} &= \begin{Bmatrix} V \\ \Theta_2 \\ \Psi_2 \end{Bmatrix} \sin\left(\pi x_1 / a\right) \cos\left(\pi x_2 / b\right) \end{aligned} \tag{5.1}$$

where $\{U, V, W, \Theta_1, \Theta_2, \Psi_1, \Psi_2\}$ are the unknown amplitudes of the kinematic variables.

For simply-supported (SS-2) anti-symmetric angle-ply laminates, the trigonometric expansion that satisfies the equations of motion and BCs differs from Eq. (5.1) only for the u_1 and u_2 variables. They are given by

$$\begin{aligned} u_1 &= U \sin\left(\pi x_1 / a\right) \cos\left(\pi x_2 / b\right) \\ u_2 &= V \cos\left(\pi x_1 / a\right) \sin\left(\pi x_2 / b\right) \end{aligned} \tag{5.2}$$

For any other boundary conditions cases or more general lamination scheme, the en-RZT exact analytical solution does not exist, and an approximated method should be used. An approximated solution has been developed using the Ritz method and has been implemented in Ref. [169], where it has been assessed that 11 orthogonal polynomials in each direction are enough to obtain the converged approximate solutions.

The non-dimensional quantities, if not otherwise specified, are defined as follows:

$$\left\{\bar{U}_1,\bar{U}_2\right\}=100\frac{E_2^{(1)}h^2}{\bar{p}_0a^3}\left\{U_1,U_2\right\};\qquad \bar{U}_3=100\frac{E_2^{(1)}h^3}{\bar{p}_0a^4}U_3;$$
$$\left\{\bar{\sigma}_{11},\bar{\sigma}_{22},\bar{\tau}_{12}\right\}=\frac{h^2\left\{\sigma_{11},\sigma_{22},\tau_{12}\right\}}{\bar{p}_0a^2};\qquad \left\{\bar{\tau}_{13},\bar{\tau}_{23}\right\}=\frac{h\left\{\tau_{13},\tau_{23}\right\}}{\bar{p}_0a};\qquad (5.3)$$
$$\bar{\omega}=\omega\frac{a^2}{h}\sqrt{\frac{\rho^{(1)}}{E_2^{(1)}}}$$

where $E_2^{(1)}$ and $\rho^{(1)}$ are the Young modulus in the in-plane transverse direction and the mass density of the first layer, respectively. Moreover, in Eq. (5.3), $\bar{p}_0$ is the maximum intensity of applied transverse pressure.

5.1.2 Linear bending

In this section, the linear bending analysis of general simply-supported multilayered composite and sandwich plates is assessed. Since the enhanced zigzag functions are able to give the same results as the standard ones for cross-ply lamination schemes, only angle-ply stacking sequences are considered in this study. The three-dimensional solution for the investigated angle-ply plates has been obtained by Savoia and Reddy [13].

Problem 1

This first numerical assessment considers a simply-supported (SS-2) two-layered angle-ply plate (L3) subjected to a bi-sinusoidal transverse pressure $\bar{p}_3(x_1,x_2)=\bar{p}_0\sin\left(\pi x_1/a\right)\sin\left(\pi x_2/b\right)$. Table 3, Table 4 and Table 5 report the normalized central maximum deflections computed using the en-RZT compared with the 3D solution of Savoia and Reddy [13] for various span-to-thickness ratios and plate geometry. For comparison purposes, other models are also considered, the CLT [170], FSDT [29] with Raman and Davalos shear correction factor [33], Reddy's TSDT [54] and the linear Di Sciuva's ZZT [89]. The shear correction factor for the investigated laminates has been reported at the bottom of each plate. As remarked previously, the RZT has not been considered in this assessment since the null zigzag functions lead to degenerating into the FSDT.

Table 3: Normalized maximum deflections for simply-supported (SS-2) thick (*a/h=4*) square (*a/b=1*) angle-ply plates (L3) under bi-sinusoidal transverse pressure.

Y = [°]	**3D** [13]	**En-RZT**	**ZZT**	**TSDT**	**FSDT** $\left(k_1^2 = k_2^2 = ad\ hoc\right)$	**CLT**
15	1.7059	1.6054	1.5111	1.6594	1.7571[(a)]	0.6205
30	1.7297	1.6358	1.3250	1.6005	1.8765[(b)]	0.6842
45	1.6887	1.5926	1.2106	1.5497	1.9154[(c)]	0.6547

[(a)] $k_1^2 = k_2^2 = 0.8384$; [(b)] $k_1^2 = k_2^2 = 0.7605$; [(c)] $k_1^2 = k_2^2 = 0.7176$.

Table 4: Normalized maximum deflections for simply-supported (SS-2) moderately thick (*a/h=10*) square (*a/b=1*) angle-ply plates (L3) under bi-sinusoidal transverse pressure.

Y = [°]	**3D** [13]	**En-RZT**	**ZZT**	**TSDT**	**FSDT** $\left(k_1^2 = k_2^2 = ad\ hoc\right)$	**CLT**
15	0.8027	0.7821	0.7724	0.7952	0.8062[(a)]	0.6205
30	0.8568	0.8388	0.8085	0.8355	0.8751[(b)]	0.6842
45	0.8250	0.8068	0.7774	0.8028	0.8564[(c)]	0.6547

[(a)] $k_1^2 = k_2^2 = 0.8384$; [(b)] $k_1^2 = k_2^2 = 0.7605$; [(c)] $k_1^2 = k_2^2 = 0.7176$.

Table 5: Normalized maximum deflections for simply-supported (SS-2) thick (*a/h=4*) rectangular (*a/b=1/3*) angle-ply plates (L3) under bi-sinusoidal transverse pressure.

Y = [°]	**3D** [13]	**En-RZT**	**ZZT**	**TSDT**	**FSDT** $\left(k_1^2 = k_2^2 = ad\ hoc\right)$	**CLT**
15	2.4903	2.3578	2.2711	2.4302	2.5883[(a)]	1.0778
30	3.4118	3.2606	2.8696	3.2462	3.6599[(b)]	1.8257
45	4.7596	4.5650	3.9749	4.5582	5.1791[(c)]	2.8142

[(a)] $k_1^2 = k_2^2 = 0.8384$; [(b)] $k_1^2 = k_2^2 = 0.7605$; [(c)] $k_1^2 = k_2^2 = 0.7176$.

As shown in Table 3, Table 4 and Table 5, the en-RZT is able to provide enough accurate results for maximum deflection of thick and moderately thick square and rectangular angle-ply plates. Although the FSDT seems to give more accurate results, the en-RZT does not require any shear corrector factor to achieve the same level of accuracy. Therefore, the TSDT can give accurate results in this case, but it is known that from a computational point of view, this theory requires C^1-continuity of the shape functions. Moreover, it cannot predict the correct transverse shear stress distributions at clamped edges and satisfy the transverse shear stress continuity at the layer interfaces. In addition, the TSDT, when used for thick angle-ply laminate, cannot predict the correct variation of stiffness with the lamination angle. As a further comparison with other existing zigzag models, the linear ZZT is accurate enough for moderately thick plates to predict the maximum transverse displacements. However, it leads to higher errors for thick cases, in which the non-linear effect on the through-the-thickness distributions and the transverse normal deformability are predominant.

Problem 2

In this second problem, an anti-symmetric angle-ply sandwich plate (L4) under bi-sinusoidal transverse pressure and simply-supported on all edges (SS-2) is here considered. This kind of laminate could be investigated using the standard RZT since the presence of the core layer in the lamination scheme guarantees the model's ability to compute the zigzag functions.

In Table 6, the results of maximum central displacements are reported and computed using different methods in defining the zigzag functions. It is important to remark that the standard RZT is able to investigate this multilayered angle-ply structure only because it is a sandwich structure. Moreover, the reported results indicated with the label RZT($C_{I\alpha}$) are obtained through the standard formulation of RZT but compute the zigzag slope differently. Its expression is here reported from Ref. [134], and it reads:

$$C_{I\alpha} = \frac{1}{h}\sum_{k=1}^{N} h^{(k)} S_{t_{\alpha\alpha}}^{(k)}; \qquad \beta_{\alpha}^{(k)} = \frac{S_{t_{\alpha\alpha}}^{(k)}}{C_{I\alpha}} - 1 \qquad (\alpha = 1,2) \tag{5.4}$$

where $S_{t_{11}}^{(k)} = 1/G_{13}^{(k)}$ and $S_{t_{22}}^{(k)} = 1/G_{23}^{(k)}$.

It should be noted that this particular expression is able to give the same zigzag slope of en-RZT only for $\beta_{11}^{(k)}, \beta_{22}^{(k)}$, but it cannot compute the transverse shear coupling contributions necessary for the most general angle-ply laminates.

Table 6: Normalized maximum deflections for simply-supported (SS-2) thick (*a/h=5*, *a/b=1*) angle-ply sandwich plate (L4) under bi-sinusoidal transverse pressure.

3D [134]	**En-RZT**	**RZT** [134]	**RZT ($C_{I\alpha}$)** [134]	**ZZT** [134]
44.2299	44.1582	44.1629	44.1663	36.7866

As shown in Table 6, the en-RZT and RZT with the ($C_{I\alpha}$) method for the zigzag functions are more accurate than the other models if compared with the three-dimensional result. As anticipated in the previous section in the enhanced zigzag function assessment, a transverse shear coupling is expected to be negligible for this laminate configuration due to the presence of the isotropic core layer. In fact, as reported in Table 6, the values for the normalized maximum deflection given by these models are almost the same. Furthermore, despite its ability to include the transverse shear coupling effect and enforce the complete transverse shear continuity across the entire laminate, the Di Sciuva's zigzag model overestimates the core layer's stiffness resulting in lower values for the displacements with respect to the exact 3D solution.

Problem 3

To further assess the accuracy of en-RZT, especially in through-the-thickness distributions of local quantities, the case of a three-layered symmetric angle-ply laminate (L5) is studied. The problem considered here is the case of cylindrical bending under transverse pressure. For this problem, the three-dimensional elasticity solution has been obtained by Pagano [5]. In order to study this configuration according to the provided Navier's solution, it should be replicated, as highlighted by Pagano [5], the plane strain condition in which the kinematic variables do not have any variation along the x_2 axis. This condition could be reached using the proposed Navier's method with the trigonometric functions indicated previously by considering the plate along the x_2 axis of infinite width or

a value sensibly higher (such as $b/a=1000$) than the length in x_1 direction. This particular configuration guarantees that the simply-supported edges at $x_2=0,b$ do not influence the plate behaviour under cylindrical bending assumptions, and the applied load tends to assume the form of a single sine along the x_1 direction, i.e. $\bar{p}_3(x_1)=\bar{p}_0\sin(\pi x_1/a)$.

The three-dimensional elasticity solution for anisotropic laminated structures in cylindrical bending has been provided by Pagano [5], and it has been used as reference solution. The FSDT has also been used for comparison purposes, and the provided results consider a shear correction factor $k_1^2=k_2^2=5/6$.

The transverse shear stress distributions obtained using the FSDT, Di Sciuva's ZZT and en-RZT are compared with the exact three-dimensional solution. The transverse shear stresses are evaluated by integrating the 3D local equilibrium equations to evaluate the prediction capabilities of through-the-thickness behaviour better. Even if the transverse shear stresses computed using the constitutive material relation are correct in an average sense, the integrated ones are considered only in evaluating the maximum values and the distribution at the layer interfaces.

Figure 17 shows the through-the-thickness distributions of in-plane and transverse displacement and stresses of thick (*a/h*=4) angle-ply laminate (L5). The effect of transverse normal deformability has made less influence in the three-dimensional solution by dividing equally the transverse normal load into two pressures applied on top and bottom external surfaces.

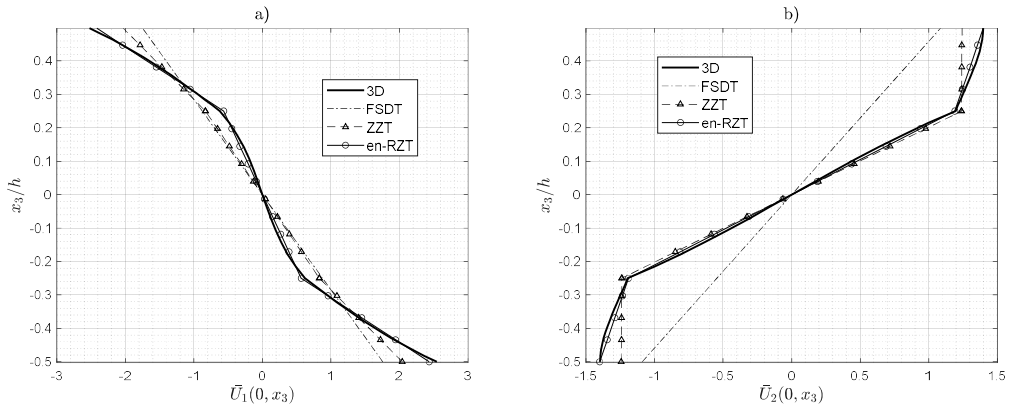

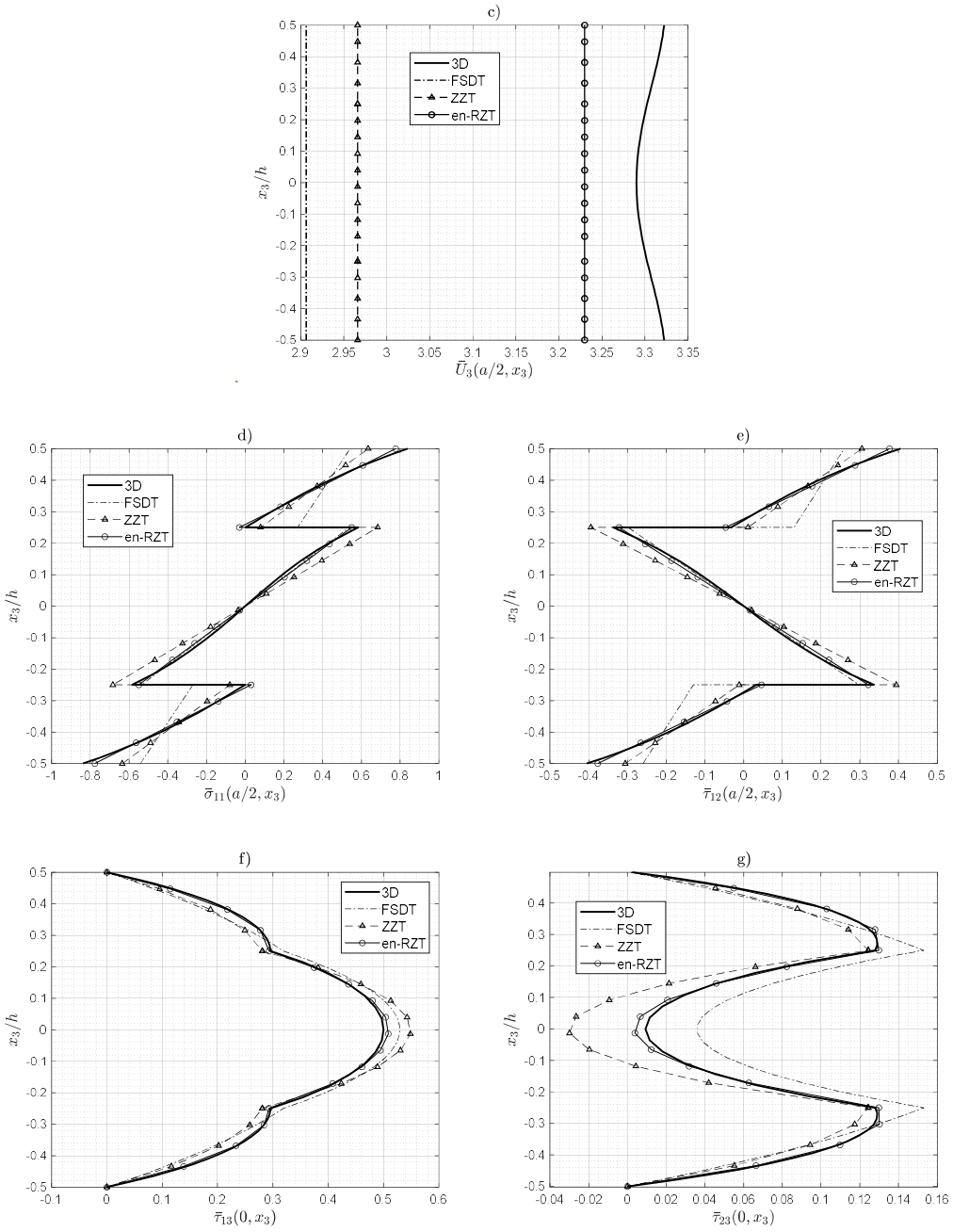

Figure 17: Cylindrical bending of symmetric angle-ply laminate (L5), simply-supported under sinusoidal transverse pressure (*a/h=4*). In f) and g), the values are computed using the integration of local equilibrium equations.

As shown in Figure 17-a) and b), the en-RZT through-the-thickness in-plane distributions are very close to the three-dimensional ones. In Figure 17-c), the en-

RZT is the constant value closer to the transverse displacement pattern. Although, as expected, the three-dimensional behaviour demonstrates a through-the-thickness non-linear pattern of the displacements and stresses, see from Figure 17-a) to Figure 17-e), the linear en-RZT distributions agree with the 3D Pagano's solution, whereas the other theories are less accurate.

The transverse shear stress distributions, computed a-posteriori through the integration of local equilibrium equations, are very close to the exact 3D results, especially at the layer interfaces. Furthermore, the en-RZT with respect to Di Sciuva's zigzag model gives a through-the-thickness distribution closer to the exact one in the internal layer. One of the advantages of the en-RZT and the standard RZT is the partial transverse shear stress continuity for the definition of the zigzag functions that are able to predict the transverse shear deformability more precisely.

5.1.3 Linear buckling

This section evaluates the critical buckling loads of multilayered angle-ply laminated plates computed using the en-RZT. Based on the static results' accuracy, this numerical investigation aims to provide some benchmark results for future comparisons. In addition, the effects of in-plane load combination, boundary conditions, geometries and lamination stacking sequences are addressed to investigate the critical behaviour of laminated angle-ply plates. Due to the lack of three-dimensional results in the literature framework related to the buckling of angle-ply structures, the numerical comparisons shown in this Section are made with other existing refined higher-order models. The results reported in this section have been presented in Ref. [137] and are further explained. If not otherwise specified, the normalized critical buckling load (λ_{cr}) is computed as follows:

$$\lambda_{cr} = \frac{\lambda a^2}{E_2^{(1)} h^3} \tag{5.5}$$

where $E_2^{(1)}$ is the Young's modulus in the in-plane transverse direction of the first layer. Note that $\lambda = \overline{P}_{11}$ and $r_{11} = \overline{P}_{22} \big/ \overline{P}_{11}$.

As highlighted in Chapter 2, for anti-symmetric angle-ply lamination schemes, the pre-buckling state where the plate remains flat is possible only when

only in-plane normal loads are applied and for simply-supported and clamped boundary conditions. Thus, no in-plane shear loads are applied in the investigated examples for these multilayered plates. Clearly, this condition does not apply to the symmetric angle-ply structures since the plate remains flat till the buckling load is reached when in-plane compressive and shear loads are applied

Problem 1

This first numerical example for buckling analysis considers a simply-supported (SS-2) four-layered (L6) antisymmetric angle-ply plate subjected to a uniaxial compressive load $\left(\bar{P}_{11}\right)$ acting in the x_1 direction. The solution has been obtained using the Ritz method, where eleven orthogonal Gram-Schmidt functions have been used. The results taken as reference solution for this problem have been provided by Matsunaga [171]. However, as stated by Matsunaga in Ref. [171], his developed two-dimensional higher-order theory underestimates the stiffness of laminated structures when applied to the bending problems with respect to the three-dimensional solution. Thus, this similar behaviour is expected for critical buckling loads and needs to be addressed in the comparison.

Table 7: Critical buckling loads (in N/mm) for uniaxial compressive loads of laminate L6, simply-supported on all edges (SS-2).

		a/b					
a/h	**Y = [°]**	**0.5**		**1**		**2**	
		Ref. [171]	**En-RZT**	**Ref.** [171]	**En-RZT**	**Ref.** [171]	**En-RZT**
	30	0.1592	0.1786	0.2889	0.3381	0.7939	0.9833
10	**45**	0.1269	0.1425	0.3134	0.3714	1.0806	1.3760
	60	0.08547	0.09378	0.2889	0.3381	1.2924	1.6228
	30	0.5307	0.5512	0.1054	0.1115	0.3417	0.3751
20	**45**	0.04114	0.04269	0.1169	0.1244	0.5078	0.5699
	60	0.02630	0.02706	0.1054	0.1115	0.6369	0.7142
	30	0.009377	0.009440	0.01939	0.01959	0.06927	0.07057
50	**45**	0.007188	0.007234	0.02174	0.02199	0.1093	0.1120
	60	0.004503	0.004525	0.01939	0.01959	0.1416	0.1452

The comparison provided by Table 7 shows the combined effect of lamination schemes, plate geometry and span-to-thickness ratio. As expected, the en-RZT critical values are slightly higher than the reference ones. Furthermore, with the increasing of the span-to-thickness ratio, the en-RZT results are closer to those of Matsunaga's model. In fact, the effect of shear deformability decreases when the span-to-thickness ratio reaches the values of thin plates. As expected, the critical buckling loads are very sensible to the lamination angles and geometry for thicker plates. Therefore, the combination of them could increase/decrease its value, confirming the tailoring properties of composite material to optimize the structural response.

Problem 2

In this second example, the effect of various design parameters, such as the number of layers, ply orientations, aspect ratio, boundary conditions, and lamination symmetry/asymmetry, has been addressed in the computation of the critical buckling loads.

Due to the impossibility of obtaining the analytical solution for the various cases, the provided results are computed through the approximated Ritz method. The minimum number of orthogonal Gram-Schmidt polynomials used to reach the converged solutions is eight. In the following, S stands for the edge simply-supported and C for clamped edge. In the next examples, the simply-supported condition is referred to the SS-2 case since antisymmetric angle-ply lamination schemes are considered.

In Figure 18 and Figure 19, the normalized buckling loads are reported for different boundary conditions, number of layers and lamination angles. Figure 18 and Figure 19, respectively, address the effect of uniaxial or biaxial ($r_{11}=1$) compressive loads. All the plates have a span-to-thickness ratio equal to eight ($a/h=8$). Three different sets of boundary conditions are considered: simply-supported on all edges (SSSS); simply-supported (SS-2) on two edges perpendicular to x_1 axis, the other two edges are clamped (SCSC); fully clamped plate (CCCC).

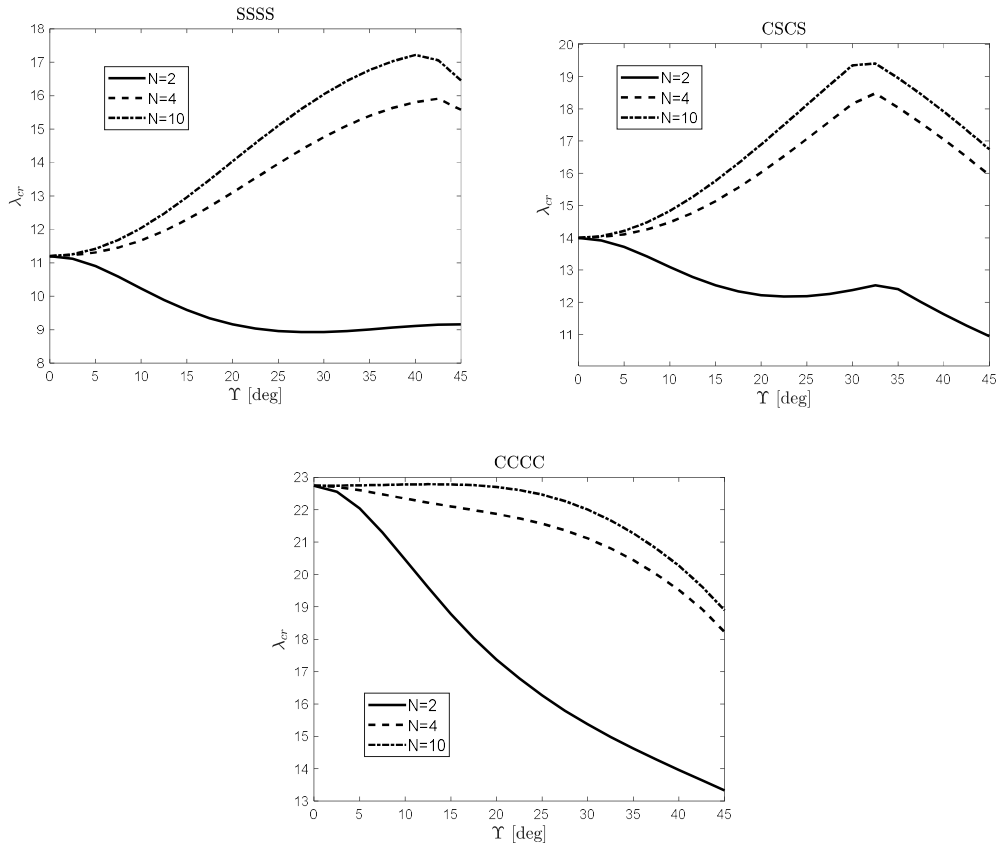

Figure 18: Uniaxial buckling parameters for L7 square plates.

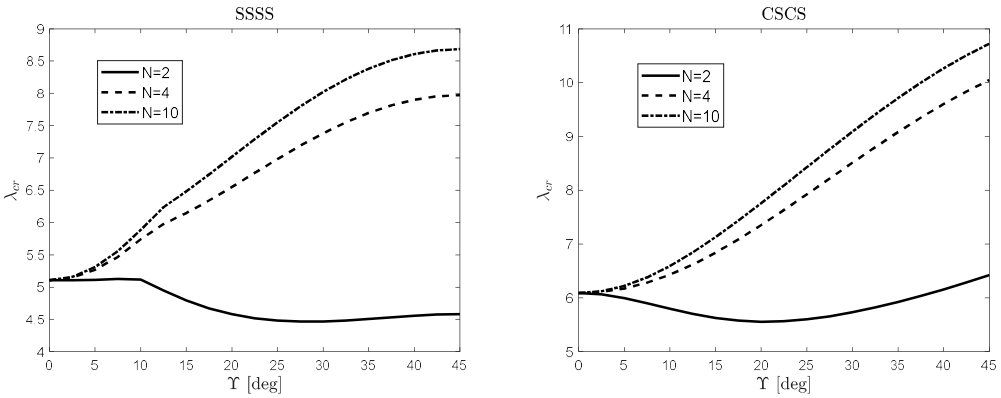

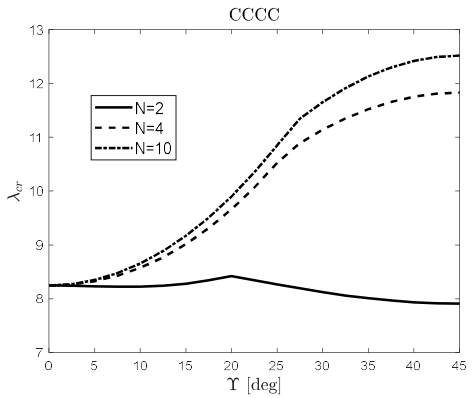

Figure 19: Biaxial buckling parameters for L7 square plate.

The effect of the number of layers on the critical buckling loads is represented in Figure 18 and Figure 19. As expected, the critical load parameter is higher for plates with more layers at the same geometric configuration (aspect ratio and span-to-thickness ratio). In fact, this typical behaviour could be commonly found in the literature framework, and its trend is to approximate the isotropic behaviour of metal panels. It is interesting to note the effect on the buckling load parameter given by the material anisotropy as a consequence of the lamination angle. In the SSSS case for the uniaxial compressive load, the maximum values of the critical buckling load do not correspond to the 45° case, as Jones [2] reported for the Classical Laminate Theory. In fact, the en-RZT is able to predict more precisely the effect of transverse shear coupling due to the more pronounced laminate anisotropy. Differently, when the plates are under biaxial compressive loads, the effect of anisotropy of the lamination angle in two-layered structures is almost irrelevant at the various boundary conditions. In addition, in biaxial compressive cases and multilayered plates with more than two layers, the highest value for the critical buckling load is reached at 45°.

Figure 20 shows for a four-layered antisymmetric angle-ply (a/b=1) plate (L6) the effect of boundary conditions on the buckling loads for uniaxial and biaxial cases. As expected, the boundary condition strongly influences the buckling load parameter, and the fully clamped case can give the highest critical values for any orientation angle.

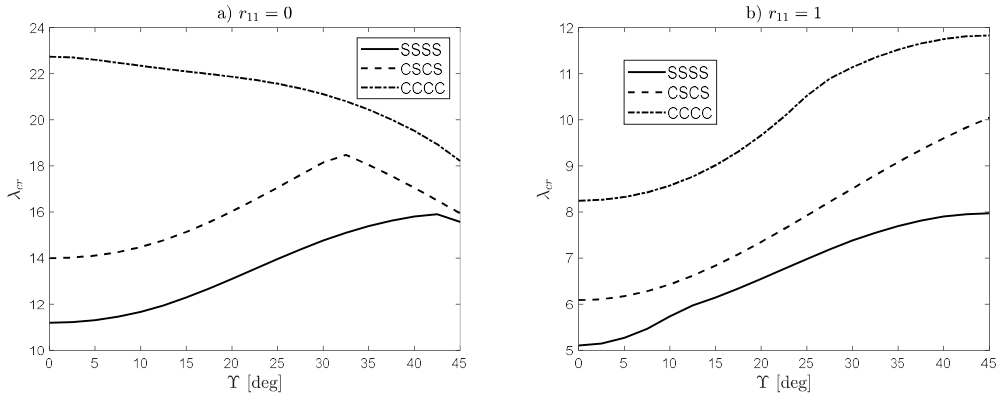

Figure 20: Effect of BCs on buckling parameter for a) uniaxial (r_{11}=0) and b) biaxial (r_{11}=1) compressive load on L6 plate.

In the following examples, symmetric square and rectangular angle-ply plates are investigated. Due to the symmetric lamination scheme, the simply-supported SS-1 conditions are considered here. Moreover, different combinations of boundary conditions and load combinations are addressed.

The laminate (L8) is manufactured with three layers oriented with an absolute value of the lamination angle of 45°. Table 8 reports the buckling load parameters computed for a span-to-thickness ratio of eight, varying the boundary conditions and the aspect ratio.

Table 8: Buckling load parameters for symmetric angle-ply rectangular plate (L8).

	r_{11}=0			r_{11}=1		
a/b	**0.5**	**1**	**2**	**0.5**	**1**	**2**
SFSF (SS-1)	2.444	2.044	1.369	2.118	1.774	1.254
SSSS (SS-1)	5.384	12.942	21.783	4.299	6.569	10.618
SCSC (SS-1)	9.659	14.369	21.773	8.081	8.524	11.030
CCCC	9.931	15.288	21.898	8.145	9.743	14.606

As expected, Table 8 shows a significant reduction in critical values for biaxial load compression cases. On the contrary, the geometry effect could increase or decrease these values, depending on the boundary conditions.

As a final comparison, the effect of boundary conditions and lamination scheme is investigated for sandwich plates with symmetric and antisymmetric face-sheets. For this numerical example, two cases are considered: simply-supported on all edges (SS-1) and fully clamped on all edges (CCCC). In Figure 21 are displayed the corresponding buckling mode shapes and normalized buckling loads for uniaxial compression.

It is interesting to note, from Figure 21, that for the lowest buckling load value, the corresponding buckling mode shape is not typical, with one half-wave in each direction.

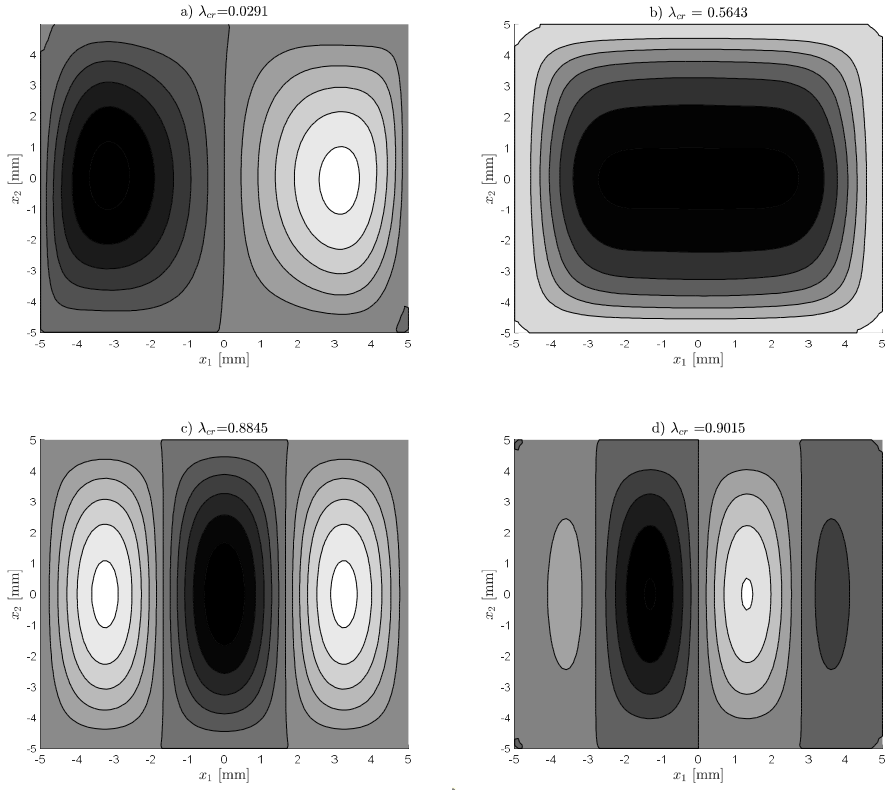

Figure 21: Buckling mode shape for sandwich S1 (a-b) and S2 (c-d) under uniaxial compressive load. Simply-supported on all edges (SSSS) for cases a) and c), fully clamped (CCCC) for c) and d).

5.1.4 Free vibrations

In this Section, the free vibration problem for general multilayered composite plates is numerically assessed using the en-RZT. More specifically, the en-RZT results for the fundamental frequencies have been compared with those available

in the current literature, coming from the three-dimensional elasticity or other higher-order models. According to Navier's method, the analytical solution can be obtained for the simply-supported condition on all plate edges. The trigonometric functions that satisfy the boundary conditions of simply-supported (SS-2) angle-ply multilayered plates read:

$$
\begin{aligned}
&w(\mathbf{x};t) = W\sin(\pi x_1/a)\sin(\pi x_2/b)\sin(\omega_0 t)\\
&\begin{Bmatrix} u_2(\mathbf{x};t)\\ \theta_1(\mathbf{x};t)\\ \psi_1(\mathbf{x};t)\end{Bmatrix} = \begin{Bmatrix} V\\ \Theta_1\\ \Psi_1\end{Bmatrix}\cos(\pi x_1/a)\sin(\pi x_2/b)\sin(\omega_0 t)\\
&\begin{Bmatrix} u_1(\mathbf{x};t)\\ \theta_2(\mathbf{x};t)\\ \psi_2(\mathbf{x};t)\end{Bmatrix} = \begin{Bmatrix} U\\ \Theta_2\\ \Psi_2\end{Bmatrix}\sin(\pi x_1/a)\cos(\pi x_2/b)\sin(\omega_0 t)
\end{aligned}
\tag{5.6}
$$

where $\{U,V,W,\Theta_1,\Theta_2,\Psi_1,\Psi_2\}$ are the unknown amplitudes of the kinematic variables and ω_0 is the fundamental circular frequency.

An approximate solution is available using the Ritz method for the other boundary conditions or different lamination schemes. The converged solution for the fundamental frequency is ensured by using eleven orthogonal Gram-Schmidt polynomials.

Problem 1

In this first example, the fundamental frequencies of a squared ten-layered anti-symmetric angle-ply (L9) plate are evaluated using the en-RZT. The square plate (*a/b=1*) is simply-supported (SS-2) on all edges, and for this laminate, various span-to-thickness ratios (*a/h*) are considered. The exact three-dimensional solution of the fundamental frequencies varying the lamination angle has been obtained by Noor and Burton [12], and it has been considered here as the reference solution.

In Table 9 are listed the fundamental non-dimensional frequencies computed using various models. In the FSDT, it has been considered a shear correction factor $k_1^2 = k_2^2 = 1$ to compute the fundamental frequency. The CLT results include the contribution of rotary inertia. From Table 9, the fundamental frequencies are predicted using the en-RZT with errors that do not exceed 7% for very thick plates (span-to-thickness ratio of 4). Although the en-RZT includes the effect of transverse shear coupling in its formulation, the transverse normal

deformability is still neglected, and this assumption limits the range of applicability. Similar results have also been obtained using the linear Di Sciuva ZZT. Reddy's TSDT seems to predict the fundamental frequencies of angle-ply structures quite accurately, but it should be noted (from the static analysis) that the transverse shear description is not always correct. As expected, the FSDT results are sensitive to the shear correction factor and when it is not considered, the predicted frequencies differ from the exact solution. As expected, CLT overestimates the non-dimensional fundamental frequencies but is considered a benchmark test when the en-RZT is applied for thin plates. As shown in Table 9, the en-RZT non-dimensional frequencies are coherent with those computed with other theories, especially with the linear ZZT in which the local kinematic field is formally consistent. The differences in the zigzag function formulation are the key to the predictivity capabilities of the two zigzag models.

Table 9: Non-dimensional fundamental frequencies $\bar{\omega}_0 = \omega_0 \sqrt{\rho^{(1)} h^2 / E_2^{(1)}}$ of simply-supported (SS-2) ten-layered anti-symmetric angle-ply square plate (L9).

	Y = 15°					
a/h	**3D** [12]	**en-RZT**	**ZZT** [89]	**TSDT** [54]	**FSDT** [29]	**CLT** [170]
4	0.4934	0.5192	0.5157	0.4958	0.5202	0.7898
5	0.3588	0.3748	0.3729	0.3601	0.3755	0.5147
10	0.1162	0.1184	0.1182	0.1163	0.1185	0.1319
100	0.001328	0.001328	0.001328	0.001328	0.001328	0.001330
	Y = 30°					
4	0.5286	0.5629	0.5456	0.5374	0.5666	0.8992
5	0.3889	0.4105	0.3983	0.3940	0.4127	0.5858
10	0.1296	0.1328	0.1305	0.1303	0.1331	0.1500
100	0.001510	0.001511	0.001510	0.001510	0.001511	0.001513
	Y = 45°					
4	0.5400	0.5773	0.5547	0.5517	0.5825	0.7854
5	0.3993	0.4231	0.4056	0.4061	0.4263	0.6186
10	0.1351	0.1388	0.1349	0.1361	0.1392	0.1585
100	0.001595	0.001595	0.001594	0.001595	0.001595	0.001598

Problem 2

Another example shows the analysis of the fundamental frequencies of a square symmetric angle-ply plate (L10) under different boundary conditions. Due

to the lamination scheme and the considered boundary conditions, an approximated solution using the Ritz method has been used to compute the fundamental undamped frequencies. Since the three-dimensional solution is not available, the results of the higher-order zigzag model of Di Sciuva and Icardi [172] have been compared. The author combined Reddy's TSDT and the linear zigzag model in their model, obtaining the Refined Higher-order Shear Deformation Theory (RHSDT). In Table 10 are quoted the non-dimensional fundamental frequencies obtained by Di Sciuva and Icardi [172] using finite elements formulated with RHSDT. Further comparisons are made with finite elements formulated using the FSDT with shear correction factor $k_1^2 = k_2^2 = 5/6$, the TSDT and the linear Di Sciuva's ZZT (RFQ40). The fundamental frequencies are evaluated for three sets of boundary conditions: the first is the simply-supported (SS-1) on all edges, here named SSSS; the second considers two opposite edges simply-supported clamped the others (SCSC); the third assumes a fully clamped plate (CCCC). The fundamental frequencies computed using the en-RZT, as shown in Table 10, agree with those predicted by other models. As expected, the frequency estimation differences using various models decrease with the increase of the span-to-thickness ratio.

Table 10: Non-dimensional fundamental frequencies for symmetric angle-ply square plate (L10) for various boundary conditions.

	FSDT [172]	**TSDT** [172]	**ZZT** [172]	**RHSDT** [172]	**en-RZT**
a/h			**SSSS**		
10	13.766	13.163	12.692	12.909	12.604
50	16.606	16.545	16.505	16.467	16.594
			CCCC		
10	18.969	17.586	17.606	17.242	15.934
50	27.207	26.936	26.917	26.794	26.417
			SCSC		
10	15.571	15.519	15.487	15.177	14.084
50	22.253	22.088	22.061	21.981	21.633

A second plate case with a different lamination scheme is also considered. The fundamental frequencies of an anti-symmetric four-layered angle-ply (L11) under various boundary conditions have been computed using the en-RZT and compared with the reference results provided by Di Sciuva and Icardi [172] using

finite elements for FSDT, TSDT and RHSDT models. In Table 11 are reported the results for the non-dimensional fundamental frequencies considering a span-to-thickness ratio of 20.

Table 11: Non-dimensional fundamental frequencies for relatively thick (*a/h=20*) anti-symmetric angle-ply square plate (L11) under various boundary conditions.

	FSDT [172]	**TSDT** [172]	**RHSDT** [172]	**en-RZT**
SSSS	13.769	13.645	13.576	13.364
SCSC	18.117	17.814	17.783	17.298
CCCC	21.710	21.255	21.242	20.650

Results of Table 10 and Table 11 prove that en-RZT is able to guarantee the same accuracy as the higher order zigzag theory (RHSDT) to predict the fundamental frequency for relatively thick angle-ply plates.

Problem 3

As a final comparison, the non-dimensional frequencies of various simply-supported (SS-2) anti-symmetric angle-ply square plate is done. The laminate named (L12) presents three different lamination schemes (reported in Table 12). For each lamination scheme and various aspect ratios, the fundamental frequency of the en-RZT is compared with the reference results computed using a twelve-variable refined theory developed by Swaminathan and Patil [173]. It is revealed that the en-RZT results are coherent with those provided by other refined models for a wide range of lamination schemes and span-to-thickness ratios.

Table 12: Non-dimensional fundamental frequencies for simply-supported angle-ply (L12) square plate.

	a/h	**4**	**5**	**10**	**25**	**50**	**100**
(45/-45)	**Ref.** [173]	8.8426	10.0350	12.9115	14.3500	14.6012	14.6668
	en-RZT	8.7596	9.9353	12.8211	14.2899	14.5481	14.6150
$(45/-45)_2$	**Ref.** [173]	10.0731	11.9465	17.8773	22.2554	23.1949	23.4499
	en-RZT	11.4573	13.4370	19.0657	22.5932	23.2830	23.4660
$(45/-45)_4$	**Ref.** [173]	10.7473	12.7523	19.1258	23.8713	24.8959	25.1741
	en-RZT	11.6321	13.7316	19.9614	24.1221	24.9647	25.1900

5.2 Assessment of the en-RZT$^{(m)}_{\{3,2\}}$

In this section, the en-RZT$^{(m)}_{\{3,2\}}$ is numerically assessed for static bending and free vibration problems. As anticipated, some of the contents of this assessment have been published in Ref. [150]. However, the published results are here further commented on and assessed. By considering a rectangular plate, the boundary conditions expressed in Chapter 3 can be specified as follows:

- SS-1 → Simply-supported cross-ply and sandwich plates

$$
\begin{aligned}
&@\, x_1 = 0, a \\
&\quad u_2 = w^{(0)} = w^{(1)} = w^{(2)} = \theta_2 = \psi_2 = e_{11} = k_{11} = k_{11}^{\psi} = 0 \\
&\quad N_{11} + \frac{1}{\eta}\left(u_{1,1} - e_{11}\right) = M_{11} + \frac{1}{\eta}\left(\theta_{1,1} - k_{11}\right) = M_{11}^{\phi} + \frac{1}{\eta}\left(\psi_{1,1} - k_{11}^{\psi}\right) = \\
&\quad = {}^{HR}E_1^{e22} = {}^{HR}E_1^{e12} = {}^{HR}K_1^{k22} = {}^{HR}K_1^{k12} = {}^{HR}K_1^{k22\psi} = {}^{HR}K_1^{k12\psi} = {}^{HR}K_1^{k21\psi} = 0 \\
&@\, x_2 = 0, b \\
&\quad u_1 = w^{(0)} = w^{(1)} = w^{(2)} = \theta_1 = \psi_1 = e_{22} = k_{22} = k_{22}^{\psi} = 0 \\
&\quad N_{22} + \frac{1}{\eta}\left(u_{2,2} - e_{22}\right) = M_{22} + \frac{1}{\eta}\left(\theta_{2,2} - k_{22}\right) = M_{22}^{\phi} + \frac{1}{\eta}\left(\psi_{2,2} - k_{22}^{\psi}\right) = \\
&\quad = {}^{HR}E_2^{e11} = {}^{HR}E_2^{e12} = {}^{HR}K_2^{k11} = {}^{HR}K_2^{k12} = {}^{HR}K_2^{k11\psi} = {}^{HR}K_2^{k12\psi} = {}^{HR}K_2^{k21\psi} = 0
\end{aligned}
\tag{5.7}
$$

- SS-2 → Simply-supported antisymmetric angle-ply

$$
\begin{aligned}
&@\, x_1 = 0, a \\
&\quad u_1 = w^{(0)} = w^{(1)} = w^{(2)} = \theta_2 = \psi_2 = e_{12} = k_{11} = k_{11}^{\psi} = 0 \\
&\quad N_{12} + \frac{1}{\eta}\left(u_{1,2} + u_{2,1} - e_{12}\right) = M_{11} + \frac{1}{\eta}\left(\theta_{1,1} - k_{11}\right) = M_{11}^{\phi} + \frac{1}{\eta}\left(\psi_{1,1} - k_{11}^{\psi}\right) = \\
&\quad = {}^{HR}E_1^{e11} = {}^{HR}E_1^{e22} = {}^{HR}K_1^{k22} = {}^{HR}K_1^{k12} = {}^{HR}K_1^{k22\psi} = {}^{HR}K_1^{k12\psi} = {}^{HR}K_1^{k21\psi} = 0 \\
&@\, x_2 = 0, b \\
&\quad u_2 = w^{(0)} = w^{(1)} = w^{(2)} = \theta_1 = \psi_1 = e_{12} = k_{22} = k_{22}^{\psi} = 0 \\
&\quad N_{12} + \frac{1}{\eta}\left(u_{1,2} + u_{2,1} - e_{12}\right) = M_{22} + \frac{1}{\eta}\left(\theta_{2,2} - k_{22}\right) = M_{22}^{\phi} + \frac{1}{\eta}\left(\psi_{2,2} - k_{22}^{\psi}\right) = \\
&\quad = {}^{HR}E_2^{e11} = {}^{HR}E_2^{e22} = {}^{HR}K_2^{k11} = {}^{HR}K_2^{k12} = {}^{HR}K_2^{k11\psi} = {}^{HR}K_2^{k12\psi} = {}^{HR}K_2^{k21\psi} = 0
\end{aligned}
\tag{5.8}
$$

Due to the lack of numerical results available in the literature that consider the effect of the in-plane tractions and in order to use the analytical solution provided

by Navier's method, the in-plane prescribed tractions on top and bottom surfaces are neglected, thus:

$$\overline{p}_{1(B)} = 0;\ \ \overline{p}_{1(T)} = 0;\quad \overline{p}_{2(B)} = 0;\quad \overline{p}_{2(T)} = 0 \tag{5.9}$$

If not otherwise specified, the transverse pressures (assumed as sinusoidal functions) applied to the bottom and top surfaces have the following expressions:

$$\begin{aligned} \overline{p}_{3(B)} &= \overline{q}_{3(B)} \sin\left(\pi / a x_1\right) \sin\left(\pi / b x_2\right) \\ \overline{p}_{3(T)} &= \overline{q}_{3(T)} \sin\left(\pi / a x_1\right) \sin\left(\pi / b x_2\right) \end{aligned} \tag{5.10}$$

where $\overline{q}_{3(B)}$ and $\overline{q}_{3(T)}$ are the maximum values.

The exact analytical solution is available through Navier's method for this boundary value problem. For cross-ply rectangular multilayered plates with simply-supported boundary conditions (SS-1) under bi-sinusoidal transverse pressure, the equilibrium equations and the boundary conditions can be satisfied by the following set of trigonometric functions:

$$\begin{aligned}
&u_1(\mathbf{x}) = U\cos(\lambda_m x_1)\sin(\lambda_n x_2);\quad u_2(\mathbf{x}) = V\sin(\lambda_m x_1)\cos(\lambda_n x_2);\\
&w^{(0)}(\mathbf{x}) = W^{(0)}\sin(\lambda_m x_1)\sin(\lambda_n x_2);\quad w^{(1)}(\mathbf{x}) = W^{(1)}\sin(\lambda_m x_1)\sin(\lambda_n x_2);\\
&w^{(2)}(\mathbf{x}) = W^{(2)}\sin(\lambda_m x_1)\sin(\lambda_n x_2);\\
&\theta_1(\mathbf{x}) = \Theta_1\cos(\lambda_m x_1)\sin(\lambda_n x_2);\quad \theta_2(\mathbf{x}) = \Theta_2\sin(\lambda_m x_1)\cos(\lambda_n x_2);\\
&\psi_1(\mathbf{x}) = \Psi_1\cos(\lambda_m x_1)\sin(\lambda_n x_2);\quad \psi_2(\mathbf{x}) = \Psi_2\sin(\lambda_m x_1)\cos(\lambda_n x_2);\\
&e_{11}(\mathbf{x}) = E_{11}\sin(\lambda_m x_1)\sin(\lambda_n x_2);\quad e_{22}(\mathbf{x}) = E_{22}\sin(\lambda_m x_1)\sin(\lambda_n x_2);\\
&e_{12}(\mathbf{x}) = E_{12}\cos(\lambda_m x_1)\cos(\lambda_n x_2);\\
&k_{11}(\mathbf{x}) = K_{11}\sin(\lambda_m x_1)\sin(\lambda_n x_2);\quad k_{22}(\mathbf{x}) = K_{22}\sin(\lambda_m x_1)\sin(\lambda_n x_2);\\
&k_{12}(\mathbf{x}) = K_{12}\cos(\lambda_m x_1)\cos(\lambda_n x_2);\\
&k_{11}^{\psi}(\mathbf{x}) = K_{11}^{\psi}\sin(\lambda_m x_1)\sin(\lambda_n x_2);\quad k_{22}^{\psi}(\mathbf{x}) = K_{22}^{\psi}\sin(\lambda_m x_1)\sin(\lambda_n x_2);\\
&k_{12}^{\psi}(\mathbf{x}) = K_{12}^{\psi}\cos(\lambda_m x_1)\cos(\lambda_n x_2);\quad k_{21}^{\psi}(\mathbf{x}) = K_{21}^{\psi}\cos(\lambda_m x_1)\cos(\lambda_n x_2)
\end{aligned} \tag{5.11}$$

where $\lambda_m = m\pi/a$; $\lambda_n = n\pi/b$ (m, n are half-wave numbers in x_1 and x_2 directions, respectively).

Furthermore, for antisymmetric angle-ply laminated plates, simply-supported (SS-2) on all edges is possible to use Navier's method to obtain the exact analytical solution. In this case, the trigonometric functions that satisfy the

governing equations and the consistent boundary conditions are the following ones:

$$
\begin{aligned}
&u_1(\mathbf{x}) = U\sin(\lambda_m x_1)\cos(\lambda_n x_2); \quad u_2(\mathbf{x}) = V\cos(\lambda_m x_1)\sin(\lambda_n x_2);\\
&w^{(0)}(\mathbf{x}) = W^{(0)}\sin(\lambda_m x_1)\sin(\lambda_n x_2); \quad w^{(1)}(\mathbf{x}) = W^{(1)}\sin(\lambda_m x_1)\sin(\lambda_n x_2);\\
&w^{(2)}(\mathbf{x}) = W^{(2)}\sin(\lambda_m x_1)\sin(\lambda_n x_2);\\
&\theta_1(\mathbf{x}) = \Theta_1\cos(\lambda_m x_1)\sin(\lambda_n x_2); \quad \theta_2(\mathbf{x}) = \Theta_2\sin(\lambda_m x_1)\cos(\lambda_n x_2);\\
&\psi_1(\mathbf{x}) = \Psi_1\cos(\lambda_m x_1)\sin(\lambda_n x_2); \quad \psi_2(\mathbf{x}) = \Psi_2\sin(\lambda_m x_1)\cos(\lambda_n x_2);\\
&e_{11}(\mathbf{x}) = E_{11}\cos(\lambda_m x_1)\cos(\lambda_n x_2); \quad e_{22}(\mathbf{x}) = E_{22}\cos(\lambda_m x_1)\cos(\lambda_n x_2);\\
&e_{12}(\mathbf{x}) = E_{12}\sin(\lambda_m x_1)\sin(\lambda_n x_2);\\
&k_{11}(\mathbf{x}) = K_{11}\sin(\lambda_m x_1)\sin(\lambda_n x_2); \quad k_{22}(\mathbf{x}) = K_{22}\sin(\lambda_m x_1)\sin(\lambda_n x_2);\\
&k_{12}(\mathbf{x}) = K_{12}\cos(\lambda_m x_1)\cos(\lambda_n x_2);\\
&k^{\psi}_{11}(\mathbf{x}) = K^{\psi}_{11}\sin(\lambda_m x_1)\sin(\lambda_n x_2); \quad k^{\psi}_{22}(\mathbf{x}) = K^{\psi}_{22}\sin(\lambda_m x_1)\sin(\lambda_n x_2);\\
&k^{\psi}_{12}(\mathbf{x}) = K^{\psi}_{12}\cos(\lambda_m x_1)\cos(\lambda_n x_2); \quad k^{\psi}_{21}(\mathbf{x}) = K^{\psi}_{21}\cos(\lambda_m x_1)\cos(\lambda_n x_2)
\end{aligned}
\tag{5.12}
$$

When the applied load corresponds to the bi-sinusoidal pressure, as those described by Eq. (5.10), in the trigonometric expansions, it is posed: $m = n = 1$.

The non-dimensional quantities, if not otherwise specified, are defined as follows:

$$
\begin{aligned}
&\left\{\bar{U}_1, \bar{U}_2\right\} = 1000\frac{E_2^{(1)}h^2}{\bar{p}_3 a^3}\left\{U_1, U_2\right\}; \qquad \bar{U}_3 = 100\frac{E_2^{(1)}h^3}{\bar{p}_3 a^4}U_3;\\
&\left\{\bar{\sigma}_{11}, \bar{\sigma}_{22}, \bar{\sigma}_{33}, \bar{\tau}_{12}\right\} = \frac{h^2\left\{\sigma_{11}, \sigma_{22}, \sigma_{33}, \tau_{12}\right\}}{\bar{p}_3 a^2}; \qquad \left\{\bar{\tau}_{13}, \bar{\tau}_{23}\right\} = \frac{10h\left\{\tau_{13}, \tau_{23}\right\}}{\bar{p}_3 a};
\end{aligned}
\tag{5.13}
$$

Note that $\bar{p}_3 = \bar{q}_{3(B)} + \bar{q}_{3(T)}$, and $E_2^{(1)}$ is the Young's modulus in the in-plane transverse direction of the first layer.

Table 13 and Table 14, respectively, report the materials and laminate stacking sequences of the investigated multilayered composite and sandwich plates for the RZT mixed assessments.

Table 13: Material nomenclature and properties. The elastic moduli are in MPa, and the mass density is in kg/m^3.

Material Name	E_1	E_2	E_3	ν_{12}	ν_{13}	ν_{23}	G_{12}	G_{13}	G_{23}	ρ
A	25	1	1	0.25	0.25	0.25	0.5	0.5	0.2	1000
B	110000	7857	7857	0.33	0.33	0.49	3292	3292	1292	1600
C	40.3	40.3	40.3	0.3	0.3	0.3	12	12	12	112
D	15	1	1	0.3	0.3	0.35	0.5	0.5	0.35	1

Table 14: Laminate stacking sequences and nomenclature. The orientations are in degree.

Laminate ID	Normalized thickness $h^{(k)}/h$	Lamina materials	Lamina orientations [°]
L1	A/A/A	0.25/0.5/0.25	0/90/0
L2	A/A	0.5/0.5	-15/15
L3	A/A/A/A	0.25/0.25/0.25/0.25	-30/30/-30/30
L4	A/A/A	0.3333/0.3333/0.3333	0/90/0
L5	$(D/D)_5$	$(0.1/0.1)_5$	$(-\theta/+\theta)_5$
S1	B/B/C/B/B	0.05/0.05/0.8/0.05/0.05	0/90/Core/90/0

5.2.1 Penalty parameter estimation

As highlighted in Chapter 3, the accuracy of the en-RZT$^{(m)}_{\{3,2\}}$ results strictly depends on the value considered for the penalty parameter η. This quantity is related to the penalty functional for the weak enforcement of the strain quantities compatibility.

For lower values of η, the compatibility between the assumed strain variables and the strains derived from the kinematic field is significantly important in the governing functional. Vice versa, for increasing η the compatibility is less important in the global functional, and discrepancies could arise.

In order to evaluate the best range of η values that can guarantee good accuracy of the results, firstly, a parametric investigation has been performed. Both simply-supported (SS-1) cross-ply laminate L1, and the simply-supported (SS-2) anti-symmetric angle-ply L2 have been considered under a bi-sinusoidal transverse pressure. The central deflection has been computed for both cases and compared with the three-dimensional analytical solution of Pagano [4,5]. Since the en-RZT$^{(m)}_{\{3,2\}}$ and Pagano's model are able to describe through the thickness variation of the transverse displacements, to compare the percent errors, an average value integrated along the thickness direction is computed. The results varying the value for η parameter are reported in Table 15. At the same time, the sum of absolute errors is evaluated between all the new strain variables and the components of the corresponding strains derived from the displacement field in $x_1 = a/2, x_2 = b/2$ for both plates.

Table 15: Percent errors for averaged central deflections and sum of absolute strain errors in the central point.

	η	**1.00E-04**	**1.00E-05**	**1.00E-06**	**1.00E-07**	**1.00E-08**	**1.00E-09**	**1.00E-10**
deflection	**L1**	0.00	0.00	0.00	0.00	0.00	0.00	0.00
	L2	0.21	0.21	0.21	0.21	0.21	0.21	0.21
strains	**L1**	1833.03	209.02	21.20	2.12	0.21	0.02	0.00
	L2	0.47	0.05	0.00	0.00	0.00	0.00	0.00

The percent errors on the displacements decrease with the decreasing of the penalty parameter value and after the valued $\eta = 10^{-5}$ the deflection is almost insensible to any variation. Similarly, the lower the penalty parameter's value, the better the strain compatibility is enforced between the new strain variables and the strains obtained by the displacement field.

Thus, the selected penalty parameter value for this numerical analysis is $\eta = 10^{-10}$, that can guarantee good accuracy on the maximum displacement and, at the same time, good compatibility between the strain quantities.

5.2.2 Linear bending

This Section assesses the linear bending problem behaviour of general multilayered structures. Firstly, multilayered cross-ply and sandwich plates are studied to highlight the novelties introduced by the new mixed formulation. Secondly, angle-ply antisymmetric multilayered plates are statically assessed. Finally, the exact three-dimensional solution for cross-ply and angle-ply plates has been obtained by Pagano [4,5] and are used to obtain the reference results.

Problem 1 – Cross-ply laminated plate

This first numerical example considers a three-layered square (*a/b=1*) cross-ply plate (L1). The plate is simply-supported (SS-1) on all edges, and the span-to-thickness ratio is *a/h=4*, corresponding to the case of a thick plate. The distributed load is applied on the top surface only, i.e. $\overline{q}_{3(B)} = 0$, to assess the plate behaviour when the transverse normal deformability is not negligible. This load condition is able to exacerbate the transverse normal deformability of the structure. In Figure 22 (a-i), the through-the-thickness distributions of the normalized quantities are shown for the simply-supported three-layered symmetric cross-ply.

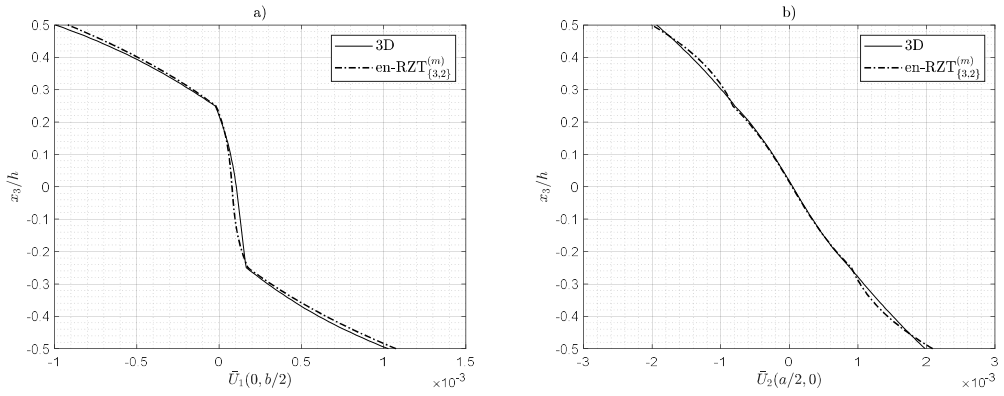

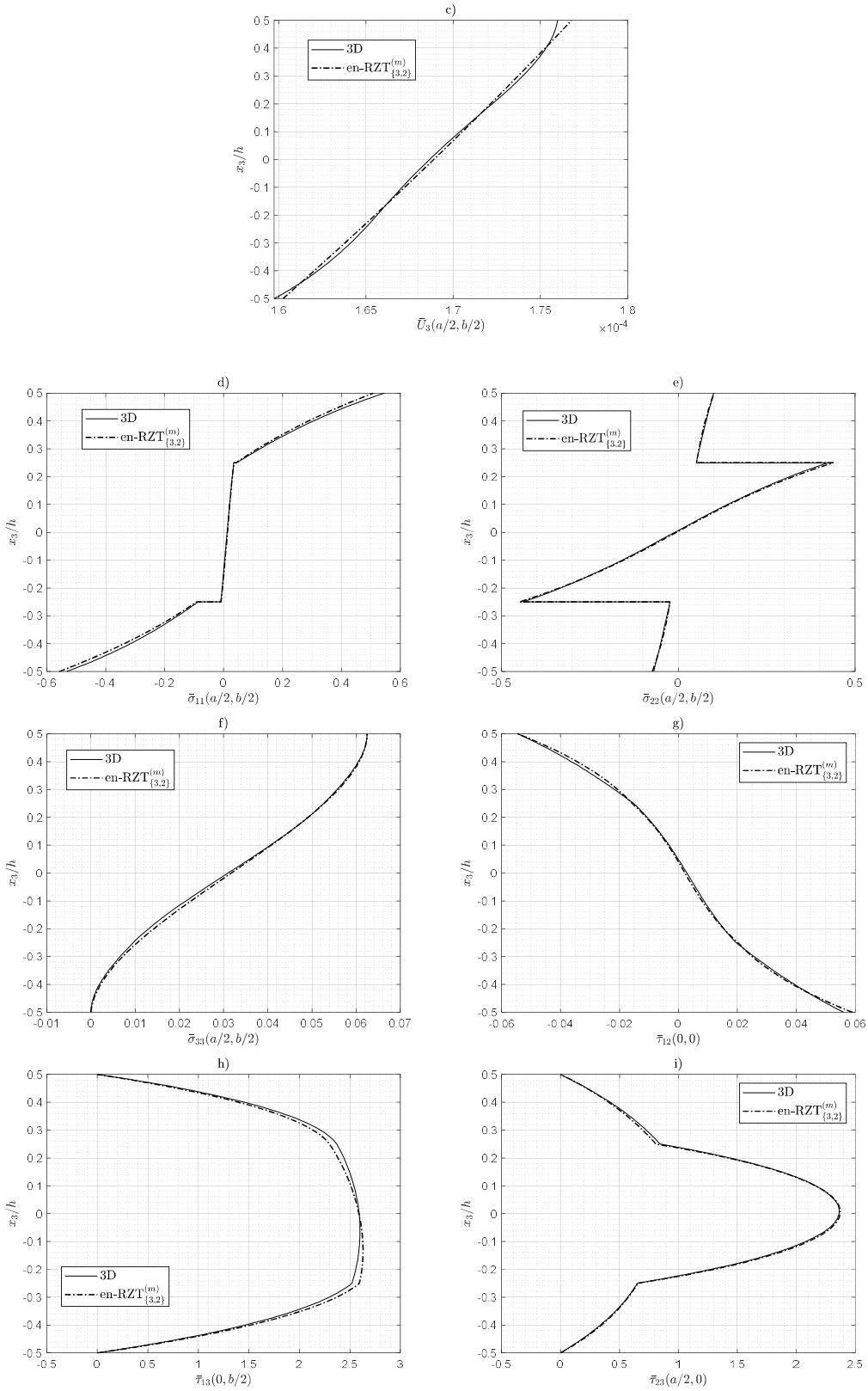
c)
3D
en-RZT$^{(m)}_{\{3,2\}}$
x_3/h
$\bar{U}_3(a/2,b/2)$
$\times 10^{-4}$
d)
$\bar{\sigma}_{11}(a/2,b/2)$
e)
$\bar{\sigma}_{22}(a/2,b/2)$
f)
$\bar{\sigma}_{33}(a/2,b/2)$
g)
$\bar{\tau}_{12}(0,0)$
h)
$\bar{\tau}_{13}(0,b/2)$
i)
$\bar{\tau}_{23}(a/2,0)$

Figure 22: Normalized through-the-thickness distributions for displacements and stresses in a simply-supported (SS-1) square (*a/b=1*) thick (*a/h=4*) three-layered cross-ply under bi-sinusoidal pressure on the top surface.

Figure 22 a) and b) show how the en-RZT$^{(m)}_{\{3,2\}}$ is able to match the exact three-dimensional distributions for in-plane displacements. Moreover, the assumed parabolic expansion for the transverse displacement can predict the exact 3D transverse displacement distribution with good agreement. As expected, the non-linear distributions for in-plane stresses obtained using the constitutive relation of the en-RZT$^{(m)}_{\{3,2\}}$ are very close to the exact three-dimensional ones. Also, the transverse normal stress agrees with great precision with the exact three-dimensional result. Finally, the transverse shear stress distributions given by the assumed functions precisely match the three-dimensional through-the-thickness distributions.

Problem 2 – Cross-ply sandwich plate

In the next example, a multilayered thick sandwich plate with cross-ply face-sheets (S1) and simply-supported (SS-1) edges is considered. Again, the length-to-thickness ratio is *a/h=4* and *a/b=1*, with the ratio between the core's thickness and each face's thickness equal to $h_c/h_f=8$. Like in the previous example, the bi-sinusoidal transverse load is applied only to the top surface of the sandwich plate.

Figure 23 (a-i) shows the normalized through-the-thickness distributions of non-dimensional displacements and stresses for the simply-supported square multilayered sandwich plate.

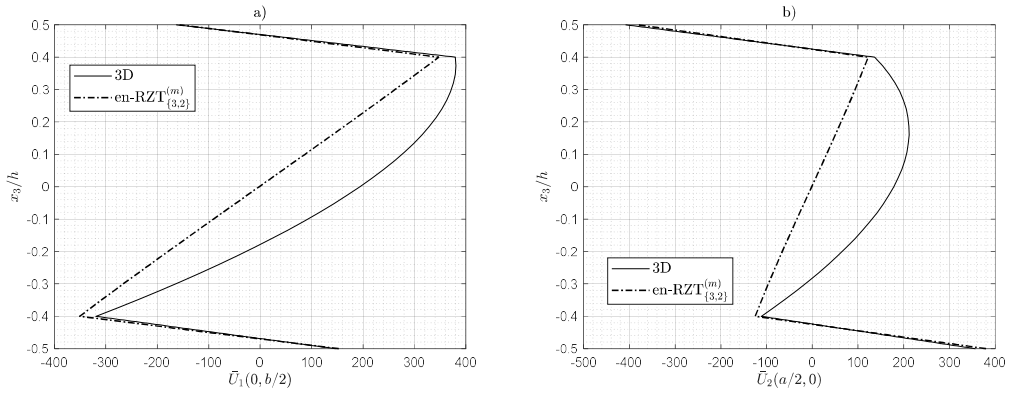

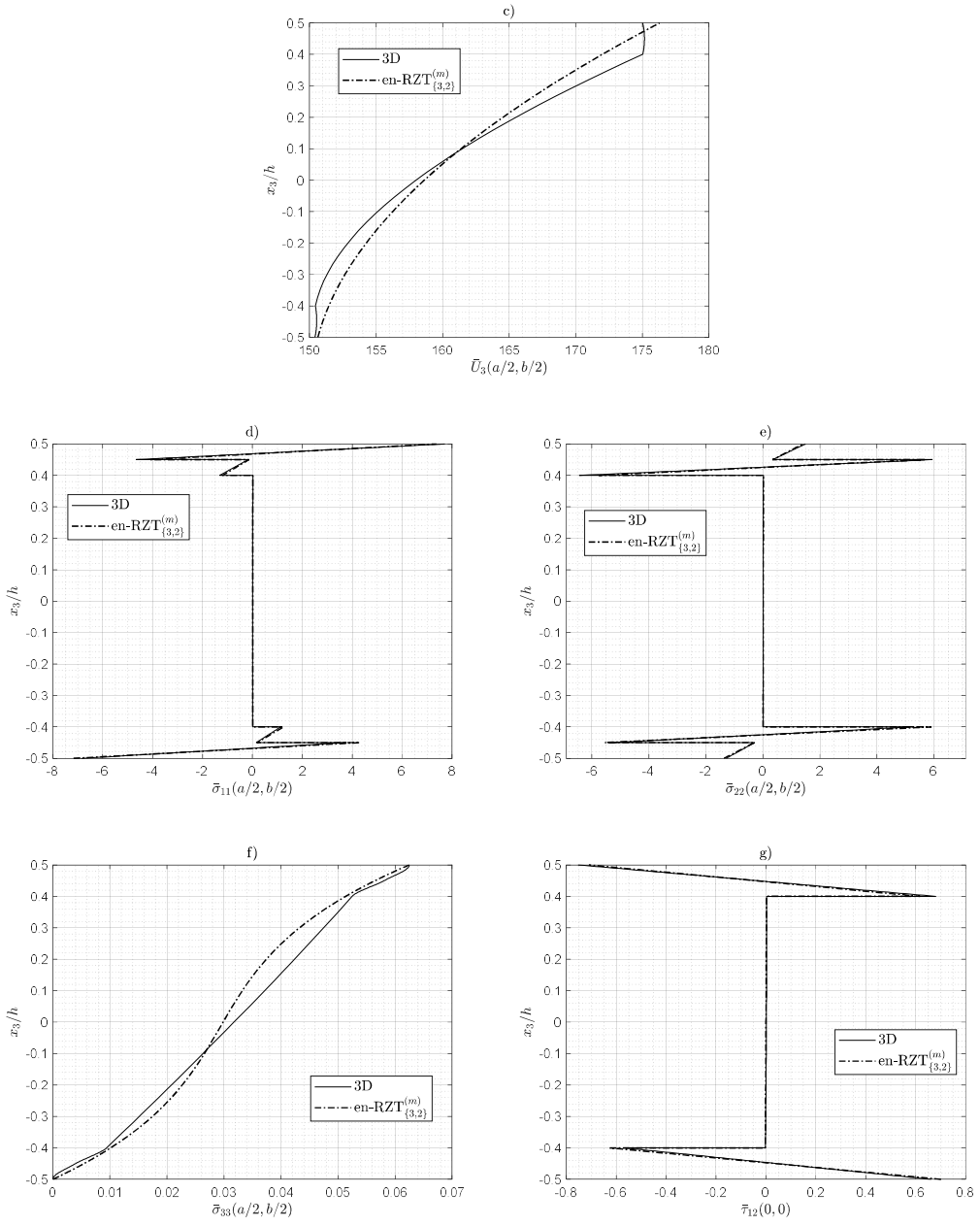
c)
3D
en-RZT$^{(m)}_{\{3,2\}}$
x_3/h
$\bar{U}_3(a/2,b/2)$
d)
$\bar{\sigma}_{11}(a/2,b/2)$
e)
$\bar{\sigma}_{22}(a/2,b/2)$
f)
$\bar{\sigma}_{33}(a/2,b/2)$
g)
$\bar{\tau}_{12}(0,0)$

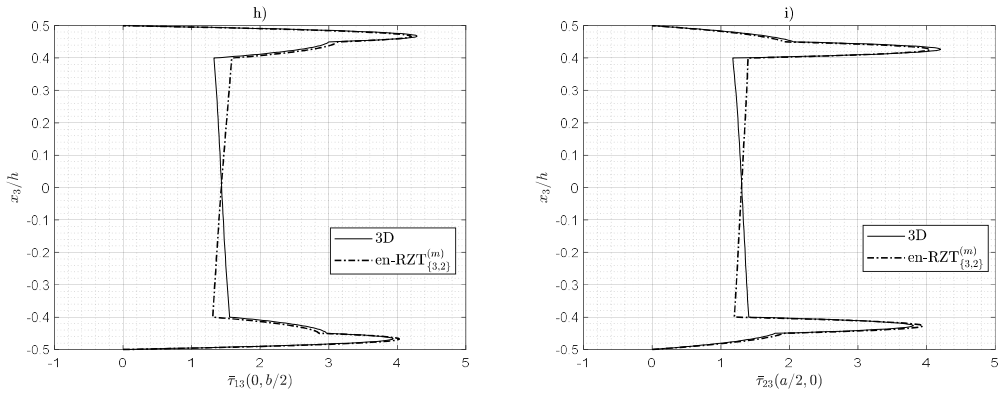

Figure 23: Normalized through-the-thickness distributions for displacements and stresses in a simply-supported (SS-1) square (*a/b=1*) thick (*a/h=4*) sandwich with cross-ply face-sheets and soft core, under bi-sinusoidal pressure on the top surface.

As expected, in sandwich structures with a soft core, the effect of transverse normal deformability is more pronounced, affecting the through-the-thickness distribution of the transverse displacement and leading to more complex distributions of in-plane displacements and stresses. However, the assumed transverse normal stress can still follow the three-dimensional distribution, although some discrepancies exist in the core layer. Also, the parabolic transverse displacement provided by the present model is very close to the exact one, but the in-plane displacements approximation is accurate only in the face-sheets. The main reason is that the higher-order zigzag functions cannot represent the non-symmetric distributions of displacements in the core. On the other hand, the in-plane stresses are very close to the exact ones, especially at the layer interfaces. Also, the prediction of the transverse shear stresses computed according to the assumed functions is very accurate compared to the three-dimensional solution. The differences in the transverse shear distributions detectable in the core layer are due to the simplified description of the transverse displacement and transverse normal stress.

Problem 3 – Angle-ply multilayered plates

In this Section, the family of angle-ply multilayered structures is investigated. In this first example, a two-layered antisymmetric angle-ply plate (L2) is considered. The simply-supported conditions (SS-2) are considered here, and to use Navier's solution and to compare the results with the exact analytical solution provided by Pagano [5] under cylindrical bending assumptions specialized for the

anisotropic structures, the length *b* (along the x_2 direction) is assumed to be much higher than the size along the x_1 direction (*b/a=1000*). This particular configuration guarantees that the simply-supported edges at $x_2 = 0, b$ do not influence the plate behaviour under cylindrical bending assumptions, and the applied load tends to assume the form of a single sine along the x_1 direction, i.e. $\overline{p}_3(x_1) = \overline{p}_0 \sin(\pi x_1 / a)$. In addition, the length-to-thickness ratio here is *a/h=4*, typical for a thick plate. As observed in the previous numerical examples, the transverse normal stretching effect is typical of sandwich structures, where the core has a very low stiffness with respect to the face-sheets. In fact, in monolithic multilayered structures, the transverse normal deformability has an almost negligible effect on the laminate behaviour. For this reason, in the next examples, the bi-sinusoidal transverse pressure has been equally divided between the top and the bottom surfaces.

Figure 24 (a-i) show the through-the-thickness normalized quantities for the antisymmetric two-layered angle-ply plate.

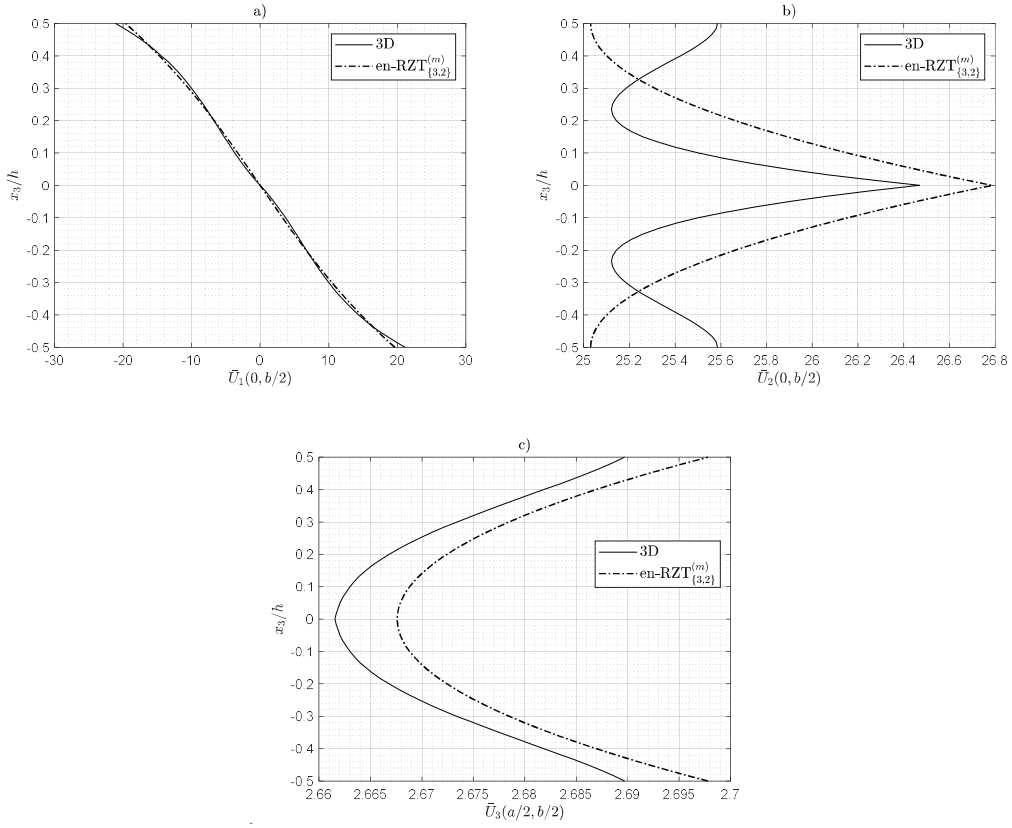

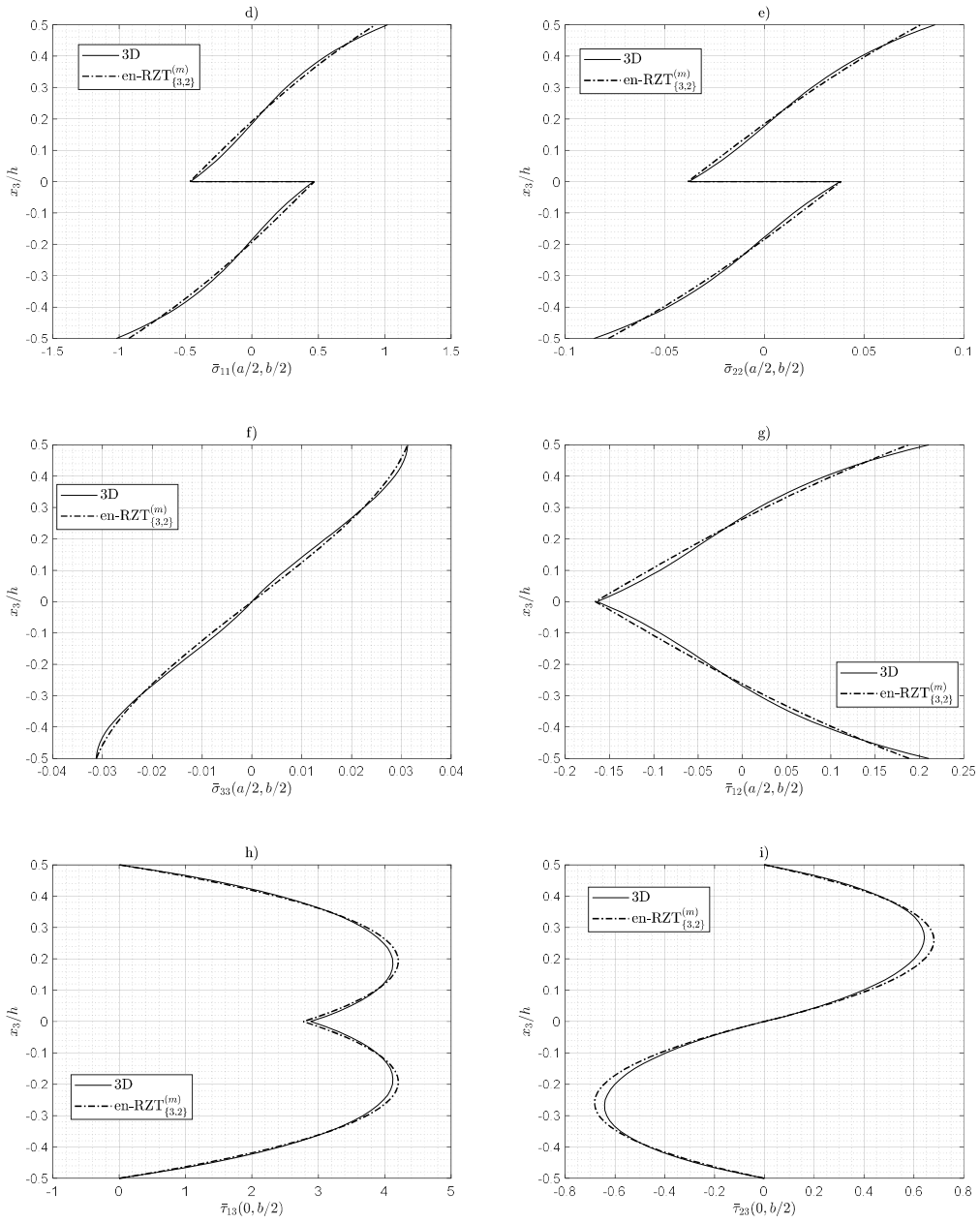

Figure 24: Normalized through-the-thickness distributions for displacements and stresses in a simply-supported (SS-2) thick (*a/h=4*) antisymmetric two-layered angle-ply [-15/15] under bi-sinusoidal pressure acting on top and bottom surfaces.

From Figure 24, for through-the-thickness in-plane displacements and stresses coming from the en-RZT$^{(m)}_{\{3,2\}}$, the same accuracy with respect to the three-dimensional solution is observed. The novelty of this mixed model in the transverse shear stresses assumption can provide remarkable accuracy in

predicting these quantities. As shown in Figure 24 h) and i), the percent errors between the en-RZT$^{(m)}_{\{3,2\}}$ and the exact results for the peak values are 1.93% and 6.54% for τ_{13} and τ_{23}, respectively.

In order to assess the ability of the present mixed model to predict more complex transverse shear stress distributions for angle-ply multilayered structures, an anti-symmetric angle-ply laminate with more layers is considered (L3). Also, for this case, the simply-supported condition (SS-2) and cylindrical bending assumption for the exact three-dimensional solution are considered to compare the numerical results with Pagano's solution [3]. Figure 25 shows the results for normalized through-the-thickness quantities.

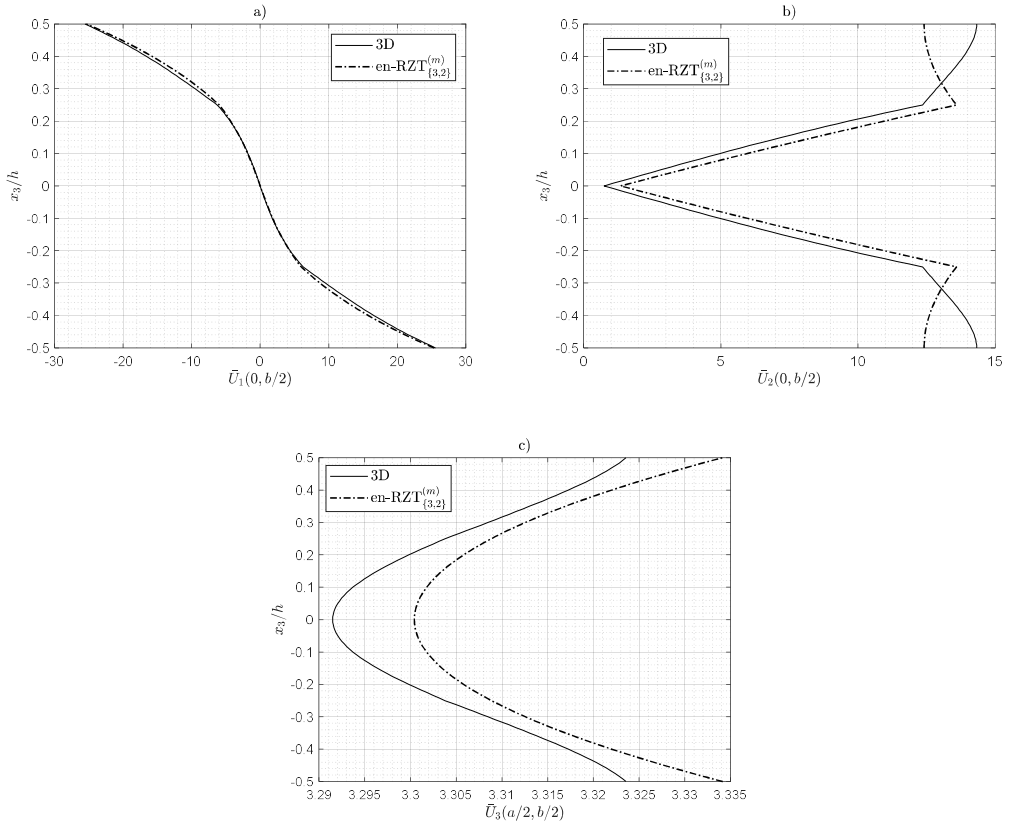

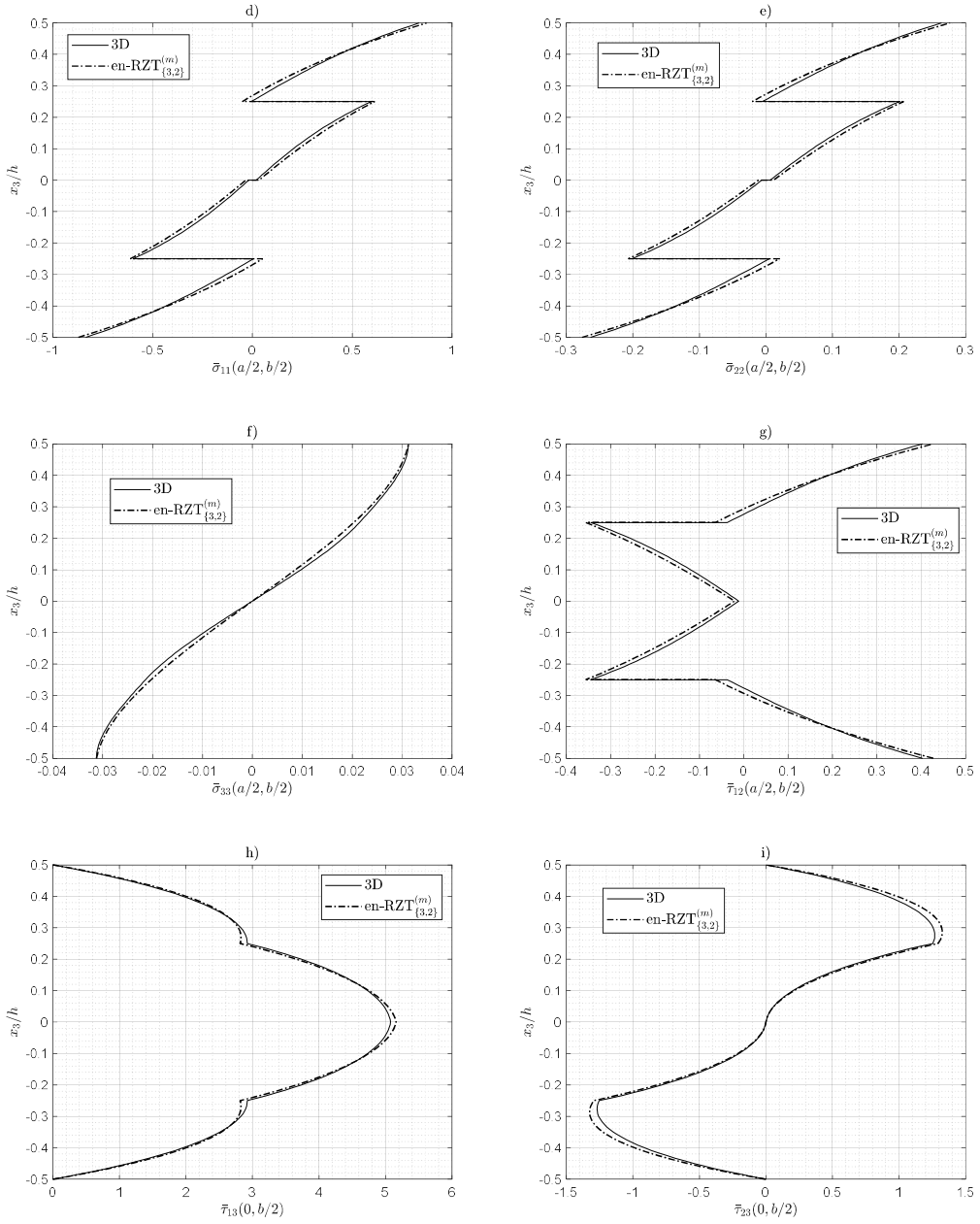

Figure 25: Normalized through-the-thickness distributions for displacements and stresses in a simply-supported (SS-2) thick (*a/h=4*) antisymmetric four-layered angle-ply [-30/30/-30/30] under bi-sinusoidal pressure acting on top and bottom surfaces.

As expected, thanks to the mixed formulation, the en-RZT$^{(m)}_{\{3,2\}}$ is able to provide very accurate results for transverse shear stress distributions also with more complex lamination schemes. Furthermore, the third-order zigzag functions

are able to provide the non-linear through-the-thickness distribution for in-plane displacements and in-plane stresses. As a result, the parabolic transverse displacement and all the transverse stress distributions are in very good agreement with the exact three-dimensional solution.

5.2.3 Free vibrations

In this Section, the natural frequencies of simply-supported multilayered composite and sandwich plates are evaluated using the en-RZT$^{(m)}_{\{3,2\}}$.

For cross-ply and sandwich plates with simply-supported edges, the boundary conditions correspond SS-1 case, see Eq. (5.7). Whereas for anti-symmetric angle-ply multilayered plates with simply-supported edges, boundaries correspond to the SS-2 case, see Eq. (5.8).

According to Navier's method, the exact analytical solution can be obtained for cross-ply rectangular multilayered plates with simply-supported boundary conditions (SS-1) using the following approximation:

$$
\begin{aligned}
u_1(\mathbf{x};t) &= \sum_{m=1}^{M}\sum_{n=1}^{N} U_{mn}\cos(\lambda_m x_1)\sin(\lambda_n x_2)\sin\left(\omega_{mn}t\right);\\
u_2(\mathbf{x};t) &= \sum_{m=1}^{M}\sum_{n=1}^{N} V_{mn}\sin(\lambda_m x_1)\cos(\lambda_n x_2)\sin\left(\omega_{mn}t\right);\\
w^{(0)}(\mathbf{x};t) &= \sum_{m}^{M}\sum_{n}^{N} W^{(0)}_{mn}\sin(\lambda_m x_1)\sin(\lambda_n x_2)\sin\left(\omega_{mn}t\right);\\
w^{(1)}(\mathbf{x};t) &= \sum_{m}^{M}\sum_{n}^{N} W^{(1)}_{mn}\sin(\lambda_m x_1)\sin(\lambda_n x_2)\sin\left(\omega_{mn}t\right);\\
w^{(2)}(\mathbf{x};t) &= \sum_{m}^{M}\sum_{n}^{N} W^{(2)}_{mn}\sin(\lambda_m x_1)\sin(\lambda_n x_2)\sin\left(\omega_{mn}t\right);\\
\theta_1(\mathbf{x};t) &= \sum_{m}^{M}\sum_{n}^{N} \Theta_{1_{mn}}\cos(\lambda_m x_1)\sin(\lambda_n x_2)\sin\left(\omega_{mn}t\right);\\
\theta_2(\mathbf{x};t) &= \sum_{m}^{M}\sum_{n}^{N} \Theta_{2_{mn}}\sin(\lambda_m x_1)\cos(\lambda_n x_2)\sin\left(\omega_{mn}t\right);\\
\psi_1(\mathbf{x};t) &= \sum_{m}^{M}\sum_{n}^{N} \Psi_{1_{mn}}\cos(\lambda_m x_1)\sin(\lambda_n x_2)\sin\left(\omega_{mn}t\right);\\
\psi_2(\mathbf{x};t) &= \sum_{m}^{M}\sum_{n}^{N} \Psi_{2_{mn}}\sin(\lambda_m x_1)\cos(\lambda_n x_2)\sin\left(\omega_{mn}t\right);
\end{aligned}
\tag{5.14}
$$

and for the strains variables:

$$
\begin{aligned}
e_{11}(\mathbf{x};t) &= \sum_{m}^{M}\sum_{n}^{N} E_{11_{mn}} \sin(\lambda_m x_1)\sin(\lambda_n x_2)\sin\left(\omega_{mn} t\right);\\
e_{22}(\mathbf{x};t) &= \sum_{m}^{M}\sum_{n}^{N} E_{22_{mn}} \sin(\lambda_m x_1)\sin(\lambda_n x_2)\sin\left(\omega_{mn} t\right);\\
e_{12}(\mathbf{x};t) &= \sum_{m}^{M}\sum_{n}^{N} E_{12_{mn}} \cos(\lambda_m x_1)\cos(\lambda_n x_2)\sin\left(\omega_{mn} t\right);\\
k_{11}(\mathbf{x};t) &= \sum_{m}^{M}\sum_{n}^{N} K_{11_{mn}} \sin(\lambda_m x_1)\sin(\lambda_n x_2)\sin\left(\omega_{mn} t\right);\\
k_{22}(\mathbf{x};t) &= \sum_{m}^{M}\sum_{n}^{N} K_{22_{mn}} \sin(\lambda_m x_1)\sin(\lambda_n x_2)\sin\left(\omega_{mn} t\right);\\
k_{12}(\mathbf{x};t) &= \sum_{m}^{M}\sum_{n}^{N} K_{12_{mn}} \cos(\lambda_m x_1)\cos(\lambda_n x_2)\sin\left(\omega_{mn} t\right);\\
k^{\psi}_{11}(\mathbf{x};t) &= \sum_{m}^{M}\sum_{n}^{N} K^{\psi}_{11_{mn}} \sin(\lambda_m x_1)\sin(\lambda_n x_2)\sin\left(\omega_{mn} t\right);\\
k^{\psi}_{22}(\mathbf{x};t) &= \sum_{m}^{M}\sum_{n}^{N} K^{\psi}_{22_{mn}} \sin(\lambda_m x_1)\sin(\lambda_n x_2)\sin\left(\omega_{mn} t\right);\\
k^{\psi}_{12}(\mathbf{x};t) &= \sum_{m}^{M}\sum_{n}^{N} K^{\psi}_{12_{mn}} \cos(\lambda_m x_1)\cos(\lambda_n x_2)\sin\left(\omega_{mn} t\right);\\
k^{\psi}_{21}(\mathbf{x};t) &= \sum_{m}^{M}\sum_{n}^{N} K^{\psi}_{21_{mn}} \cos(\lambda_m x_1)\cos(\lambda_n x_2)\sin\left(\omega_{mn} t\right)
\end{aligned}
\tag{5.15}
$$

Moreover, it is possible to obtain an exact analytical solution by Navier's method for antisymmetric angle-ply laminated plates simply-supported (SS-2) boundary conditions. In this case, the trigonometric functions that satisfy the governing equations and the consistent boundary conditions differ from the previous only for the following variables:

$$
\begin{aligned}
u_1(\mathbf{x};t) &= \sum_{m=1}^{M}\sum_{n=1}^{N} U_{mn} \sin(\lambda_m x_1)\cos(\lambda_n x_2)\sin\left(\omega_{mn} t\right);\\
u_2(\mathbf{x};t) &= \sum_{m=1}^{M}\sum_{n=1}^{N} V_{mn} \cos(\lambda_m x_1)\sin(\lambda_n x_2)\sin\left(\omega_{mn} t\right);\\
e_{11}(\mathbf{x};t) &= \sum_{m}^{M}\sum_{n}^{N} E_{11_{mn}} \cos(\lambda_m x_1)\cos(\lambda_n x_2)\sin\left(\omega_{mn} t\right);\\
e_{22}(\mathbf{x};t) &= \sum_{m}^{M}\sum_{n}^{N} E_{22_{mn}} \cos(\lambda_m x_1)\cos(\lambda_n x_2)\sin\left(\omega_{mn} t\right);\\
e_{12}(\mathbf{x};t) &= \sum_{m}^{M}\sum_{n}^{N} E_{12_{mn}} \sin(\lambda_m x_1)\sin(\lambda_n x_2)\sin\left(\omega_{mn} t\right);
\end{aligned}
\tag{5.16}
$$

where $\lambda_m = m\pi/a$; $\lambda_n = n\pi/b$ (m, n are half-wave numbers in x_1 and x_2 directions, respectively). In the previous expressions, ω_{mn} is the mn^{th} circular frequency.

If not otherwise specified, the circular frequencies are normalized as follows:

$$\bar{\omega}_{mn} = \omega_{mn} a^2 \sqrt{\rho^{(1)}/E_2^{(1)}} \tag{5.17}$$

where $\rho^{(1)}, E_2^{(1)}$ are the mass density and the in-plane transverse Young's modulus of the first layer.

Problem 1 – Cross-ply three-layered plate

A simply-supported (SS-1) three-layered cross-ply square ($a/b=1$) plate is considered. The span-to-thickness ratio considered is a/h=4. The reference solution for the first seventeen flexural frequencies has been obtained using a high-fidelity 3D FE NASTRAN model, which used 134400 solid HEXA8 elements, as shown in Figure 26. In the three-dimensional NASTRAN® model, the boundary conditions corresponding to the simply-supported case consider the constraints given by Eq. (5.7). In Table 16, the non-dimensional circular frequencies of the en-RZT$^{(m)}_{\{3,2\}}$ and the relative errors are presented. As anticipated, the circular frequencies for the computed modal shapes are given in terms of m and n, which are half-wave numbers in the x_1 and x_2 directions, respectively. As observed, it is clear the exceptional accuracy of en-RZT$^{(m)}_{\{3,2\}}$ to predict the first natural frequencies with a maximum value below 1.5%. As expected, the effect of transverse normal deformation is more pronounced for more complex modal shapes, and the simplified assumption on the assumed transverse normal stress and transverse displacement is no longer valid.

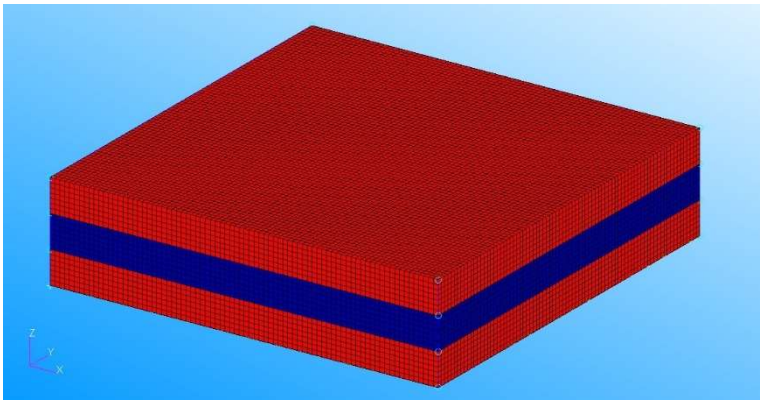

Figure 26: Three-layered cross-ply (L1) square plate using solid HEXA8 NASTRAN® elements (in red, the layers oriented at 0°, in blue, the layer oriented at 90°).

Table 16: First seventeen non-dimensional circular frequencies and percent errors of laminate L1 (*a/b=1, a/h=4*), simply-supported on all edges.

m	***n***	**3D – NASTRAN®**	**en-RZT$^{(m)}_{\{3,2\}}$**	**%err**
1	**1**	6.9220	6.9300	0.11
1	**2**	11.5628	11.5538	-0.08
1	**3**	17.8022	17.6968	-0.59
1	**4**	24.4050	24.1394	-1.09
1	**5**	31.0484	30.5973	-1.45
2	**1**	14.0877	14.0804	-0.05
2	**2**	16.9297	16.9312	0.01
2	**3**	21.7052	21.6240	-0.37
2	**4**	27.3999	27.1672	-0.85
2	**5**	33.4689	33.0604	-1.22
3	**1**	21.8757	21.7745	-0.46
3	**2**	23.8554	23.7895	-0.28
3	**3**	27.4805	27.3489	-0.48
3	**4**	32.1934	31.9200	-0.85
4	**1**	29.7903	29.5193	-0.91
4	**2**	31.3149	31.0986	-0.69
4	**4**	34.1902	33.9223	-0.78

Problem 2 – Cross-ply sandwich plate

In this second example, a simply-supported (SS-1) multilayered cross-ply thick sandwich plate (S1) is considered. The square sandwich plate (*a/b=1*) has a core-to-face thickness ratio of 8, representing a typical value for sandwich applications. The span-to-thickness ratio is *a/h*=4, a value to assess the en-RZT$^{(m)}_{\{3,2\}}$ also for thick sandwich case. The first thirteen nondimensional circular frequencies are compared with the reference solution obtained using a high-fidelity FE model with NASTRAN® 153600 solid HEXA8 element to ensure an accurate 3D solution. In Figure 27, the discretized solid model is shown.

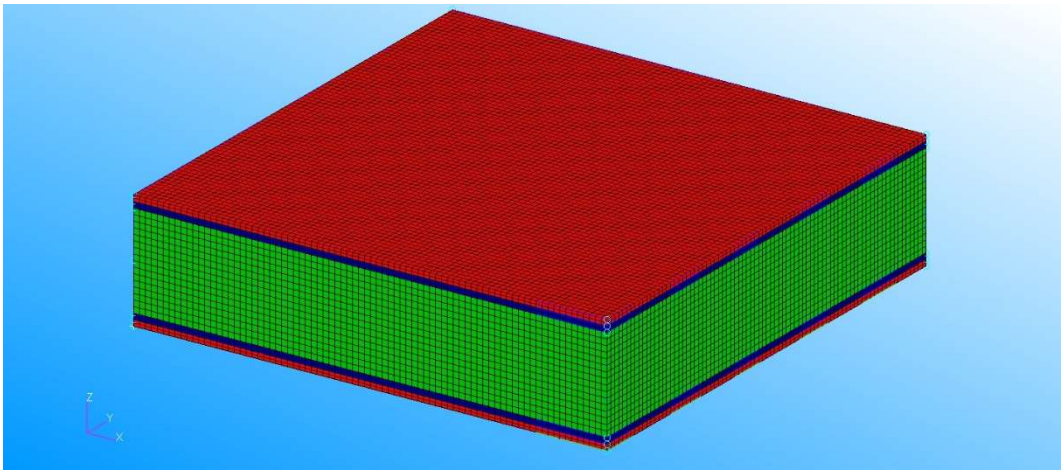

Figure 27: Cross-ply sandwich (S1) square plate discretization using solid HEXA8 NASTRAN® elements (in red, the layers oriented at 0°, in blue, the layer oriented at 90° and in green, the core layer).

In the three-dimensional NASTRAN® model, as done for the previous model, the boundary conditions corresponding to the simply-supported case consider the constraints given by Eq. (5.7).

In Table 17, the first thirteen transverse flexural non-dimensional circular frequencies and the corresponding relative percent errors are reported. The 3D frequencies are given in terms of *m* and *n,* which are half-wave numbers in the x_1 and x_2 directions of the corresponding modal shape, respectively.

Table 17: First thirteen non-dimensional circular frequencies and percent errors of sandwich S1 (*a/b=1, a/h=4*), simply-supported on all edges.

m	*n*	3D – NASTRAN®	en-RZT$^{(m)}_{\{3,2\}}$	%err
1	**1**	1553.44	1552.88	-0.04
1	**2**	2890.63	2887.52	-0.11
1	**3**	5093.03	5073.77	-0.38
1	**4**	8085.80	8025.21	-0.75
2	**1**	2977.16	2980.10	0.10
2	**2**	3974.27	3977.32	0.08
2	**3**	5914.13	5899.67	-0.24
2	**4**	8745.63	8684.72	-0.70
3	**1**	5224.87	5221.16	-0.07
3	**2**	5984.38	5899.67	-1.42
3	**3**	7583.41	7560.59	-0.30
4	**1**	8251.34	8188.65	-0.76
4	**2**	8866.66	8802.04	-0.73

The results of Table 17 confirm the accuracy in frequency prediction with errors below the 1.5%. In sandwich structures, the effect of transverse shear and normal deformability is more pronounced than the cross-ply multilayered plates; however, the en-RZT$^{(m)}_{\{3,2\}}$ is sufficiently accurate to predict even the frequencies of more complex modal shapes.

Problem 3 – Multilayered angle-ply plate

In this example, a square anti-symmetric ten-layered angle-ply plate (L5) is considered. The plate is simply-supported on all edges, according to the SS-2 conditions, since the plate belongs to the class of anti-symmetric angle-ply structures. The exact three-dimensional solution for the fundamental frequency is provided by Noor and Burton [12] and is considered as the reference result. The fundamental frequencies are evaluated using the en-RZT$^{(m)}_{\{3,2\}}$ for different values of span-to-thickness ratio and different lamination angles. In order to avoid ill-conditioned stiffness matrix due to some combinations of the values for the span-

to-thickness ratio and the penalty term, the penalty parameter has a value of 1e-5, still valid to accurately enforce the strain compatibility as reported in the previous section.

Table 18 shows the non-dimensional fundamental frequencies and the percent errors with respect to the frequencies computed by the exact three-dimensional solution of Noor and Burton [12]

Table 18: Non-dimensional fundamental frequencies $\bar{\omega}_{11} = \omega_{11}\sqrt{\rho^{(1)}h^2 / E_2^{(1)}}$ and percent errors (in brackets) of simply-supported (SS-2) ten-layered anti-symmetric angle-ply square plate (L9).

	Y[º]		
a/h	**15**	**30**	**45**
100	0.001328 (0.02)	0.001511 (0.05)	0.001595 (0.01)
10	0.1163 (0.07)	0.1296 (0.03)	0.1352 (0.06)
6.667	0.2307 (0.14)	0.2533 (0.03)	0.2618 (0.04)
5	0.3594 (0.17)	0.3890 (0.03)	0.3993 (0.00)
4	0.4944 (0.20)	0.5286 (-0.01)	0.5397 (-0.06)
3.333	0.6321 (0.22)	0.6687 (-0.07)	0.6801 (-0.13)

Table 18 confirms the accuracy of the en-RZT$^{(m)}_{\{3,2\}}$ to compute the frequencies for angle-ply multilayered plates accurately. It should be noted that remarkably low errors are obtained for the highly thick case.

5.3 Assessment of the new B-RZT$^{(m)}_{\{3,2\}}$ beam model

In this section, it is assessed the new beam B-RZT$^{(m)}_{\{3,2\}}$ model for the analysis of thick multilayered composite and sandwich beams. The boundary conditions expressed in Chapter 4 are here specified for a beam of length L and simply-supported on both edges:

$$
\begin{aligned}
&@\, x_1 = 0, L \\
&\quad w^{(0)} = w^{(1)} = w^{(2)} = e_{11} = k_{11} = k_{11}^{\psi} = 0 \\
&\quad N_{11} + \frac{1}{\eta}\left(u_{1,1} - e_{11}\right) = M_{11} + \frac{1}{\eta}\left(\theta_{1,1} - k_{11}\right) = M_{11}^{\phi} + \frac{1}{\eta}\left(\psi_{1,1} - k_{11}^{\psi}\right) = 0
\end{aligned}
\tag{5.18}
$$

The constraints on $w^{(0)}, w^{(1)}$ and $w^{(2)}$ variables in Eq. (5.18) assume in an ideal way the supported condition, i.e. the transverse displacement is enforced to be null along the whole beam thickness.

The numerical results provided for this model assume only a transverse pressure applied on the beam structures, i.e. the in-plane tractions acting on the bottom and top surfaces are neglected

$$
\overline{p}_{1(B)} = 0; \;\; \overline{p}_{1(T)} = 0; \tag{5.19}
$$

If not otherwise specified, the transverse pressures applied to the bottom and top surfaces have the following expressions:

$$
\begin{aligned}
\overline{p}_{3(B)} &= \overline{q}_{3(B)} \sin\left(\pi / L x_1\right) \\
\overline{p}_{3(T)} &= \overline{q}_{3(T)} \sin\left(\pi / L x_1\right)
\end{aligned}
\tag{5.20}
$$

where $\overline{q}_{3(B)}$ and $\overline{q}_{3(T)}$ are the maximum values.

Using Navier's method, the exact analytical solution able to satisfy both governing equations and boundary conditions involves the following trigonometric expansions:

$$
\begin{aligned}
u_1(x_1;t) &= \sum_{m=1}^{M} U_m \cos(\lambda_m x_1)\sin(\omega_m t);\\
w^{(0)}(x_1;t) &= \sum_{m=1}^{M} W_m^{(0)} \sin(\lambda_m x_1)\sin(\omega_m t);\\
w^{(1)}(x_1;t) &= \sum_{m=1}^{M} W_m^{(1)} \sin(\lambda_m x_1)\sin(\omega_m t);\\
w^{(2)}(x_1;t) &= \sum_{m=1}^{M} W_m^{(2)} \sin(\lambda_m x_1)\sin(\omega_m t);\\
\theta_1(x_1;t) &= \sum_{m=1}^{M} \Theta_{1_m} \cos(\lambda_m x_1)\sin(\omega_m t);\\
\psi_1(x_1;t) &= \sum_{m=1}^{M} \Psi_{1_m} \cos(\lambda_m x_1)\sin(\omega_m t);\\
e_{11}(x_1;t) &= \sum_{m=1}^{M} E_{11_m} \sin(\lambda_m x_1)\sin(\omega_m t);\\
k_{11}(x_1;t) &= \sum_{m=1}^{M} K_{11_m} \sin(\lambda_m x_1)\sin(\omega_m t);\\
k_{11}^{\psi}(x_1;t) &= \sum_{m=1}^{M} K_{11_m}^{\psi} \sin(\lambda_m x_1)\sin(\omega_m t);
\end{aligned}
\tag{5.21}
$$

where $\lambda_m = m\pi/L$ and m is the half-wave number in x_1 direction. For the bending problem of the simply-supported beam under sinusoidal transverse pressure, M is equal to 1.

The non-dimensional quantities, if not otherwise specified, are defined as follows:

$$
\begin{gathered}
\bar{U}_1 = 1000\frac{E_2^{(1)}h^2}{\bar{p}_3 L^3}U_1; \qquad \bar{U}_3 = 100\frac{E_2^{(1)}h^3}{\bar{p}_3 L^4}U_3;\\
\{\bar{\sigma}_{11},\bar{\sigma}_{33}\} = \frac{h^2\{\sigma_{11},\sigma_{33}\}}{\bar{p}_3 L^2}; \qquad \bar{\tau}_{13} = \frac{10h\tau_{13}}{\bar{p}_3 L};\\
\bar{\omega}_m = \omega_m L^2\sqrt{\rho^{(1)}/E_2^{(1)}}
\end{gathered}
\tag{5.22}
$$

Note that $\bar{p}_3 = \bar{q}_{3(B)} + \bar{q}_{3(T)}$ and $E_2^{(1)}$ is the Young's modulus in the in-plane transverse direction of the first layer.

5.3.1 Linear bending

In this Section, the linear bending analysis is performed to assess the response of two types of beam structures. The first problem considers a simply-supported cross-ply (L1) thick beams. The second problem assesses the behaviour of a simply-supported cross-ply sandwich (S1) thick beam. Both beams have a length-to-thickness ratio equal to four ($L/h=4$). The transverse sinusoidal distributed load is applied only on the top external surface to observe the effect of transverse normal deformability. The reference solution has been obtained by a high-fidelity FE model using 40000 membrane QUAD8 NASTRAN® elements. In Figure 28 and Figure 29, the high-fidelity FE parabolic QUAD8 elements are shown, respectively, for L1 and S1 beams.

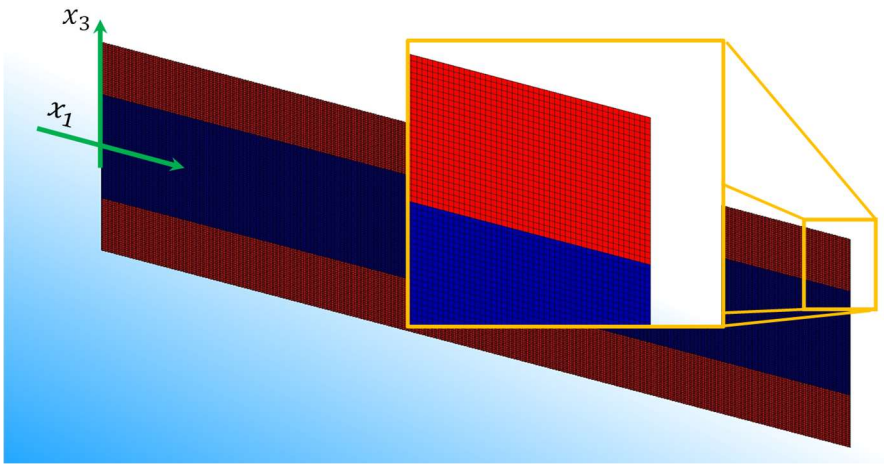

Figure 28: High-fidelity FE model: beam L1, 40000 parabolic quadrangular QUAD8 NASTRAN® elements (in red, the layers oriented at 0°, in blue, the layer oriented at 90).

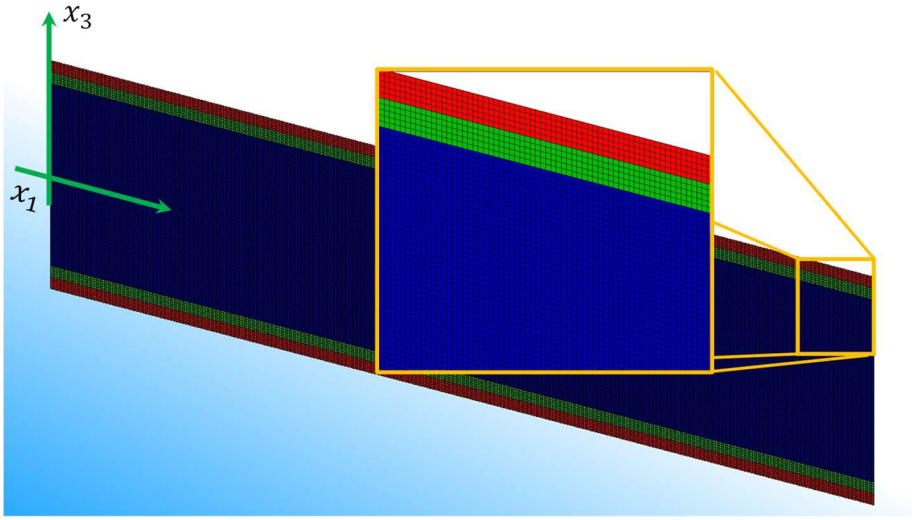

Figure 29: High-fidelity FE model: beam S1, 40000 parabolic quadrangular QUAD8 NASTRAN® elements (in red, the layers oriented at 0°, in light blue the layer oriented at 90° and in blue, the core layer).

The normalized through-the-thickness distributions of the displacements, stresses and strains for cross-ply L1 and sandwich S1 beams are reported in Figure 30 and Figure 31, respectively.

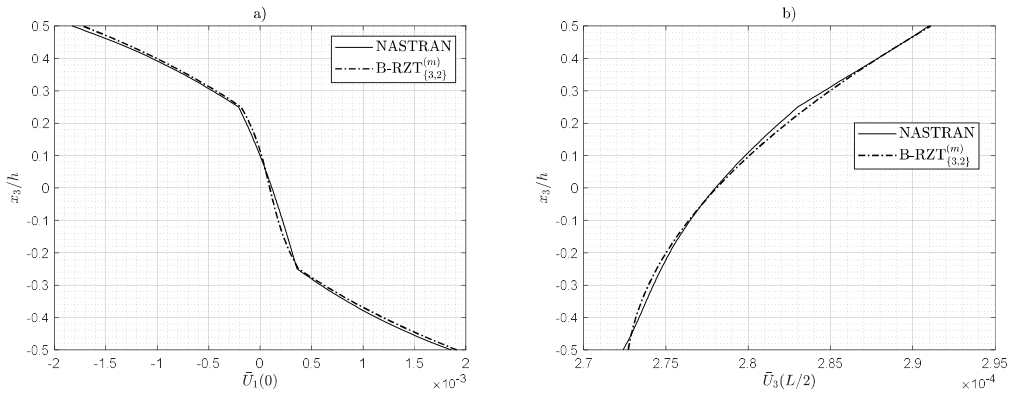

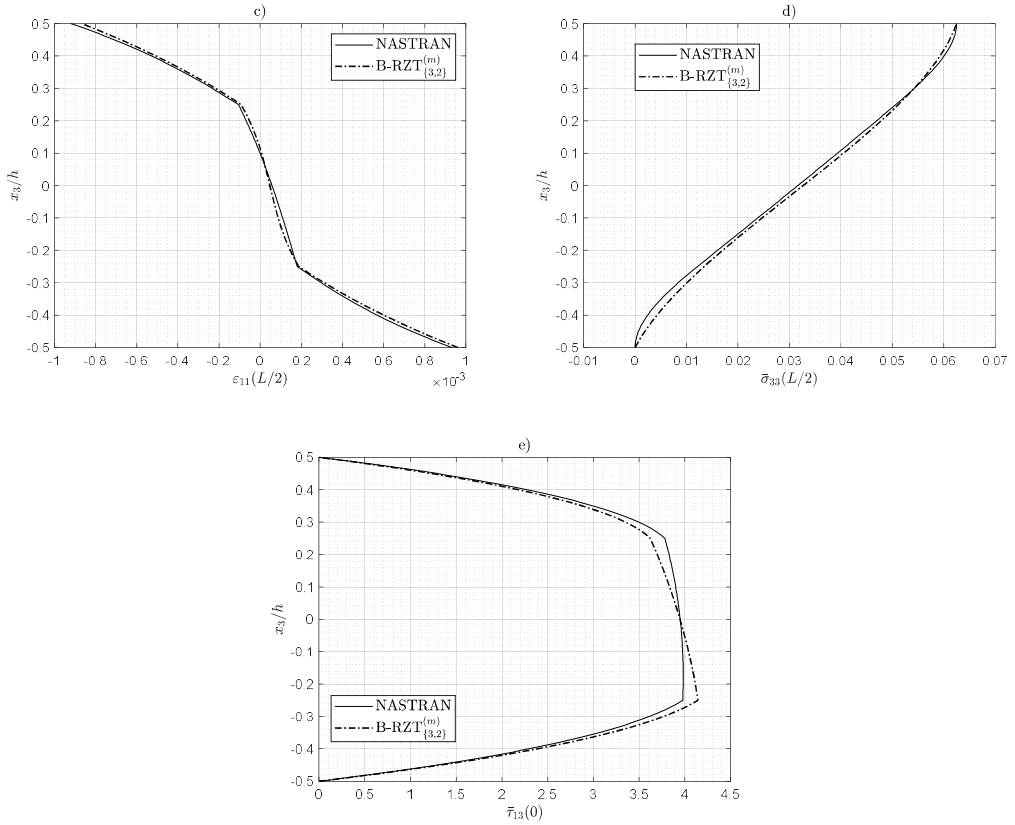

Figure 30: Through-the-thickness distributions of normalized displacements, strains and stresses of cross-ply (L1) simply-supported thick beam (*L/h=4*)

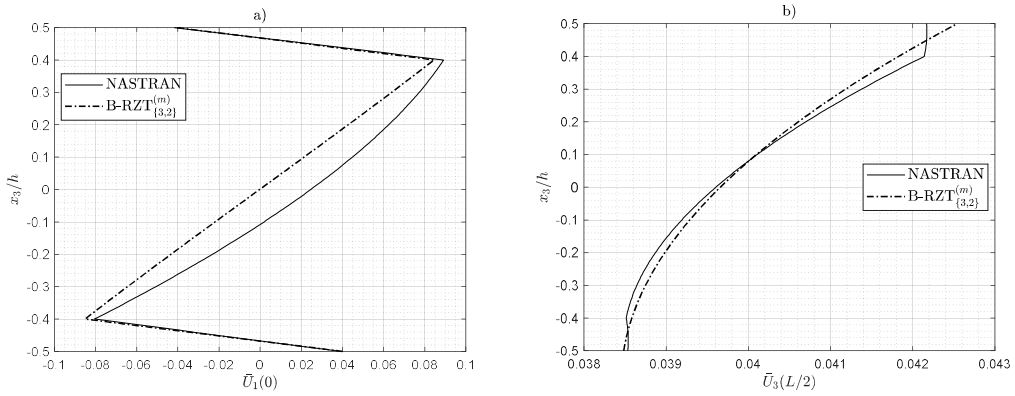

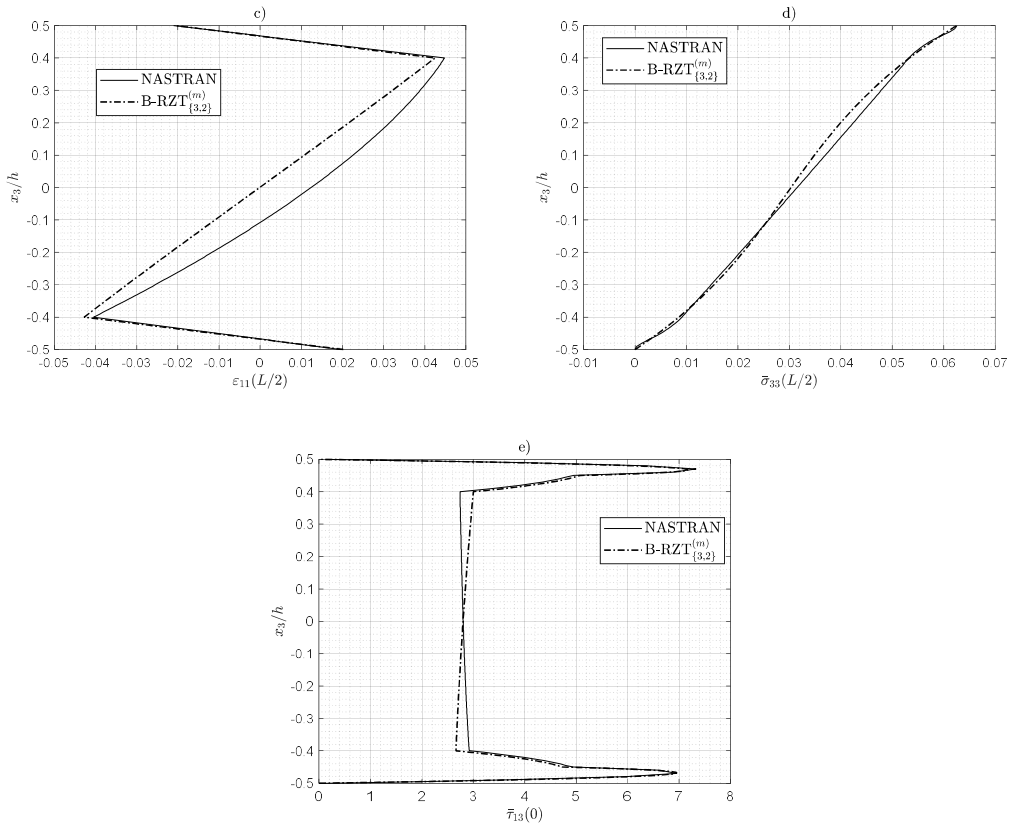

Figure 31: Through-the-thickness distributions of normalized displacements, strains and stresses of cross-ply sandwich (S1) simply-supported thick beam (*L/h=4*)

The through-the-thickness distributions of the local quantities provided by the B-RZT$^{(m)}_{\{3,2\}}$ model are in good agreement with the high-fidelity FE solution using Nastran. The in-plane and transverse displacement patterns shown in Figure 30 for the cross-ply beam correctly represent the three-dimensional behaviour. Moreover, the effect of transverse normal deformability identified by the transverse normal stress distribution is well described. Only a few discrepancies are detectable in the transverse normal stress slope next to the external surface, but they do not affect the transverse shear distribution in that area. As highlighted in the plate model, some differences in shear stress evaluation are noticeable only in the middle layer. This effect could be explained by considering the third Cauchy's equation relating the transverse shear stress with the transverse normal stress, that in this model is not enforced.

Concerning the behaviour of the cross-ply sandwich beam shown in Figure 31, the same considerations done for the plate case are valid here. More specifically, the effect of transverse deformability in the core layer is higher than in the other layers. Therefore, it results in a less accurate representation of the transverse normal stress distribution and a less accurate prediction of the core layer's displacements, strain and stresses. However, the values of strains and stresses reached at the layer interfaces are very close to the exact ones.

5.3.2 Free vibrations

In this section, the dynamic behaviour of B-RZT$^{(m)}_{\{3,2\}}$ model is assessed by evaluating the natural circular frequencies of multilayered composite and sandwich thick beams. Two beam structures are considered: a three-layered cross-ply beam (L1) and a cross-ply sandwich beam (S1). The simply-supported condition has been considered in both examples, and the length-to-thickness ratio is equal to 4. The reference results for the flexural modal shapes and corresponding circular frequencies are obtained using a high-fidelity FE model with Nastran 40000 QUAD8 membrane elements, as reported in the static analysis, see Figure 28 and Figure 29.

Table 19: First ten flexural normalized circular frequencies and percent errors of simply-supported cross-ply L1 beam (*L/h=4*).

Mode	**NASTRAN®**	**B-RZT$^{(m)}_{\{3,2\}}$**	**err%**
1	968.8	968.8	-0.04
2	2278.7	2277.8	-0.08
3	3622.7	3618.9	-0.13
4	4991.6	4981.5	-0.22
5	6369.6	6350.5	-0.30

6	7746.6	7718.0	-0.37
7	9116.0	9081.6	-0.38
8	10473.0	10440.9	-0.32
9	11813.0	11796.3	-0.17
10	13131.7	13148.6	0.08

Table 20: First six flexural normalized circular frequencies and percent errors of simply-supported sandwich S1 beam (*L/h=4*).

Mode	**NASTRAN®**	**B-RZT$^{(m)}_{\{3,2\}}$**	**err%**
1	177.0	177.0	-0.07
2	430.9	431.1	0.02
3	796.2	797.2	0.12
4	1276.2	1273.3	-0.23
5	1853.0	1835.6	-0.98
6	2474.7	2450.4	-1.11

Table 19 and Table 20 report the first ten and six flexural normalized circular frequencies of L1 and S1 beams, respectively. The B-RZT$^{(m)}_{\{3,2\}}$ model predicts the first frequencies of both beams with less than 1.2% error. The percent errors for the cross-ply L1 beam are generally lower than the sandwich one due to the more accurate representation of the transverse normal deformability. In sandwich structures, both frequencies and through-the-thickness quantities are very sensible for correctly modelling the transverse normal deformability.

5.4 The new RZT$^{(m)}$ finite elements assessment

This section is dedicated to the numerical assessment of the proposed finite beam elements based on the B-RZT$^{(m)}_{\{3,2\}}$ model described in Chapter 4. The implemented elements are employed to solve static and free vibration problems of

cross-ply and sandwich thick beams. The aim is to assess the elements' improvements in predicting global and local quantities and their limitations.

The first part is dedicated to the convergence analysis of the 2B-RZT$^{(m)}_{\{3,2\}}$ and 2Bc-RZT$^{(m)}_{\{3,2\}}$ elements. Then, based on the convergence analysis results performed on different simply-supported thick beams, the element response capabilities are assessed for the three-point bending problem and for the free vibration of simply-supported beams.

5.4.1 Convergence analysis

In this Section, the convergent behaviour of the 2B-RZT$^{(m)}_{\{3,2\}}$ and 2Bc-RZT$^{(m)}_{\{3,2\}}$ elements is performed. The problem of simply-supported multilayered cross-ply (L1) and sandwich (S1) beams under a concentrated force is considered to evaluate the convergence behaviour. The reference solution is based on the same high-fidelity FE model with NASTRAN® using 40000 QUAD8 membrane elements, as considered in the previous Section. Since all the elements assume a transverse displacement varying along the thickness coordinate, an averaged value has been considered for the convergence analysis evaluated at the beam mid-span. It reads:

$$w_{fem/ref} = \frac{1}{h}\int_{h} U_3(x_3)dx_3 \tag{5.23}$$

Due to the numerical approximation introduced by the finite element method, the η value is settled to be 1e-5 to avoid ill-conditioning problems of the stiffness matrix. This assumption for the η value makes the strain compatibility given by the penalty functional term less important. However, this problem could be easily overcome by increasing the number of elements that discretize the beam structure.

For the convergence study, the beams are simply-supported on both edges according to constraint conditions adopted for the analytical model, see Eq. (5.18) , in which the whole through-the-thickness transverse displacement is enforced to be null on the supported edges. It should be noted from Eq. (5.18) that also the strain nodal dof's need to be constrained at the edges. However, they do not appear in the element formulation, and only the kinematic variables are constrained as follows:

$$\begin{aligned} &@x_1 = 0, L \qquad w^{(0)} = w^{(1)} = w^{(2)} = 0 \\ &@x_1 = L/2 \qquad u = 0 \end{aligned} \tag{5.24}$$

The concentrated force is applied at the mid-span point on the top surface. For the sake of clarity, the nodal force vector of the structure limited to the central node, where the force is applied, has the following expression:

$$\mathbf{F}(x_1 = L/2) = \begin{bmatrix} 0 & \bar{F} & \frac{h}{2}\bar{F} & \frac{h^2}{4}\bar{F} & 0 & 0 \end{bmatrix} \tag{5.25}$$

It is evident in Eq. (5.25) that the force is applied on the top surface by the term that multiplies the $w^{(1)}$ nodal dof.

Moreover, the span-to-thickness ratio considered is 4 for both beams, representing a typical value for very thick beam. In Figure 32, the convergence ratios of the L1 (Figure 32-a)) and S1 beam (Figure 32-b)) are shown.

After some solution oscillations, when the structure is discretized with few elements, both proposed elements converge to the solution. For the L1 beam case, the error induced by the approximated solution for 4096 beam elements is 0.05%. Whereas for the S1 beam case, the error induced is 2.78. This different behaviour is due to the different transverse normal deformability, which is more pronounced in the sandwich beam.

For the static analysis and free vibration problem, to guarantee the accuracy of the approximated solutions, 4096 elements are used to study the beams. As a result, the computational cost involved by high-fidelity FE Nastran model consists of 242002 nodal dof's, whereas considering 4096 elements are involved, only 24582 dof's, which is a remarkable advantage.

In addition, the convergence results show that for the considered discretization, both 2B-RZT$^{(m)}_{\{3,2\}}$ and 2Bc-RZT$^{(m)}_{\{3,2\}}$ elements give the same results. Therefore, the following numerical analysis is focused only on 2B-RZT$^{(m)}_{\{3,2\}}$ elements.

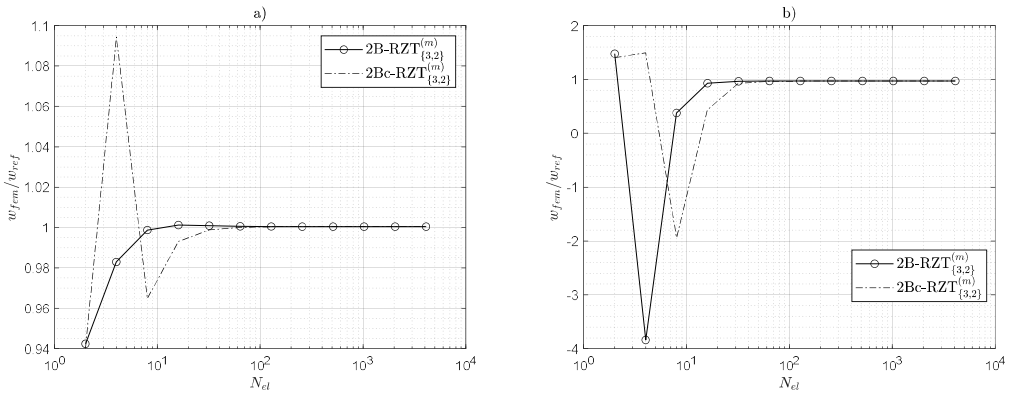

Figure 32: Convergence analysis for the maximum displacement of a) cross-ply (L1) and b)sandwich (S1) simply-supported beams under a concentrated force in the mid-span.

5.4.2 Linear bending

In this Section, the linear bending problem using the 2B-RZT$^{(m)}_{\{3,2\}}$ element is numerically assessed. After the convergence analysis, the converged solution is obtained using 4096 beam elements for both laminations. The beams are simply-supported on the two end edges, according to the definition provided earlier, and a concentrated force of intensity $-10N$ is applied at the mid-span length of the beam on the top external surface.

In Figure 33 and Figure 34 are reported the results for the through-the-thickness distributions of in-plane displacement at the supported edge (a), and the transverse displacements at the beam mid-span (b). The in-plane distribution is in very good agreement with the reference solution, especially for the values assumed at the top and bottom beam surfaces. The transverse displacements evaluated at the top, bottom and on the axis in the beam mid-span point are close to the Nastran solution, especially for the L1 beam. Whereas for the sandwich S1 beam, the effect of transverse normal deformability is more pronounced. In fact, the assumed parabolic function for the transverse displacement cannot follow exactly the through-the-thickness variation of the transverse displacement. Moreover, in the applied force point, the effect of transverse normal deformability is sensible higher, and the assumed transverse normal stress could not correctly represent the correct through-the-thickness variation. This effect is also noticeable in the transverse shear stresses, showing more discrepancies in the through-the-thickness patterns, especially in the middle layer.

In Figure 33 and Figure 34 (c), the distributions of the top and bottom transverse displacements along the axis are reported. As expected, the transverse displacement results are in good agreement with the reference solution, except for the area near the applied force. Furthermore, in Figure 33 and Figure 34 (d), the distributions of the axial strains evaluated at the bottom and top interfaces of the internal layer are displayed. The results provided by $2\text{B-RZT}^{(m)}_{\{3,2\}}$ element are able to predict the variation of the axial strains at the interfaces along the longitudinal direction, except for the area closer to the applied force in which the reference strain field is more complex to follow. However, for the first time, a model based on the RZT kinematics has reached this accuracy has been reached for the value of the span-to-thickness ratio considered.

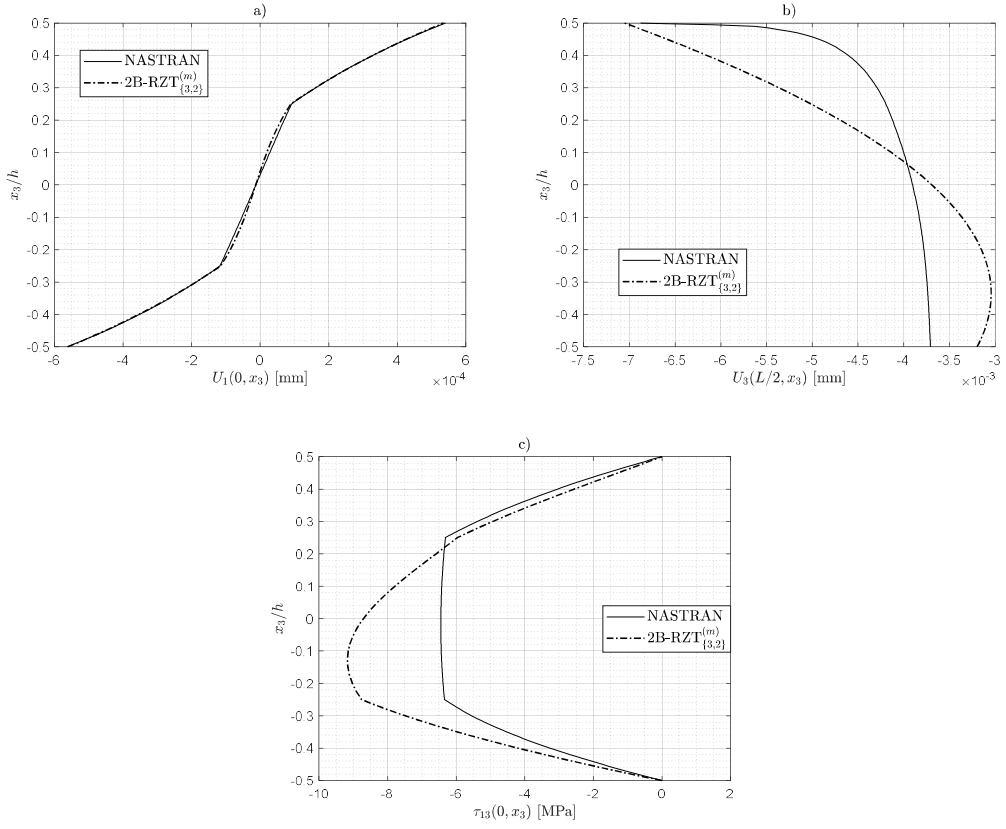

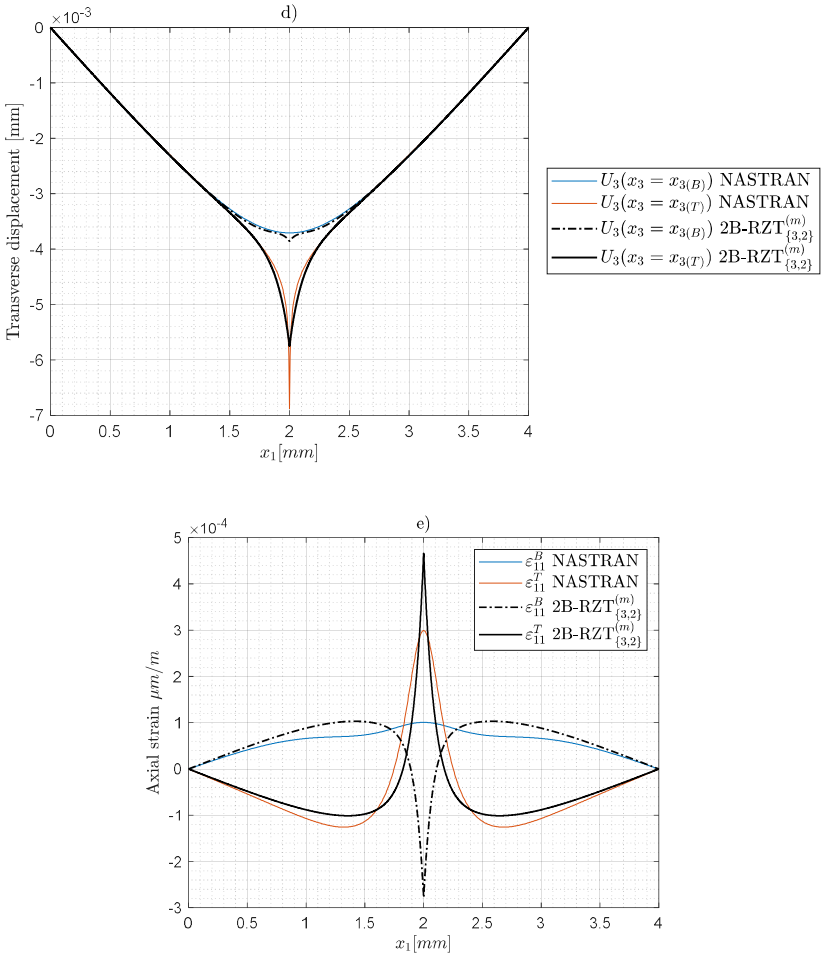

Figure 33: Through-the-thickness in-plane and transverse displacements a)-b) and transverse shear stress c). Distribution of the bottom and top transverse displacements d) and axial deformations at the internal layer interfaces e) for cross-ply L1.

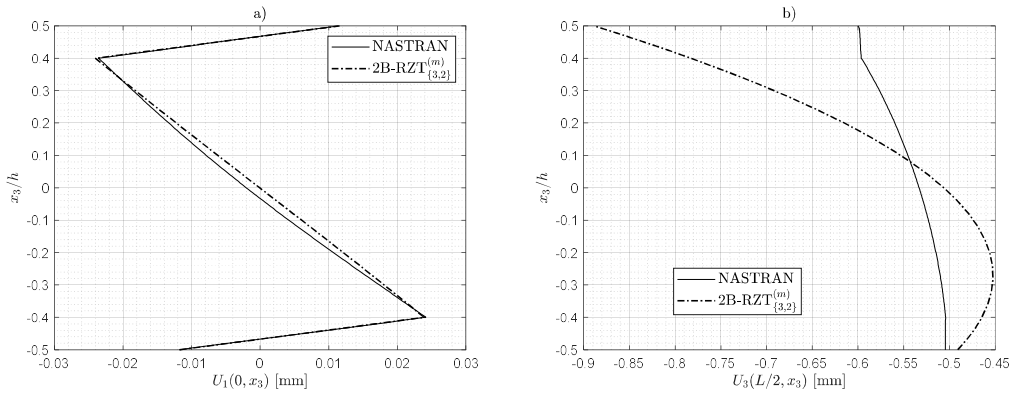

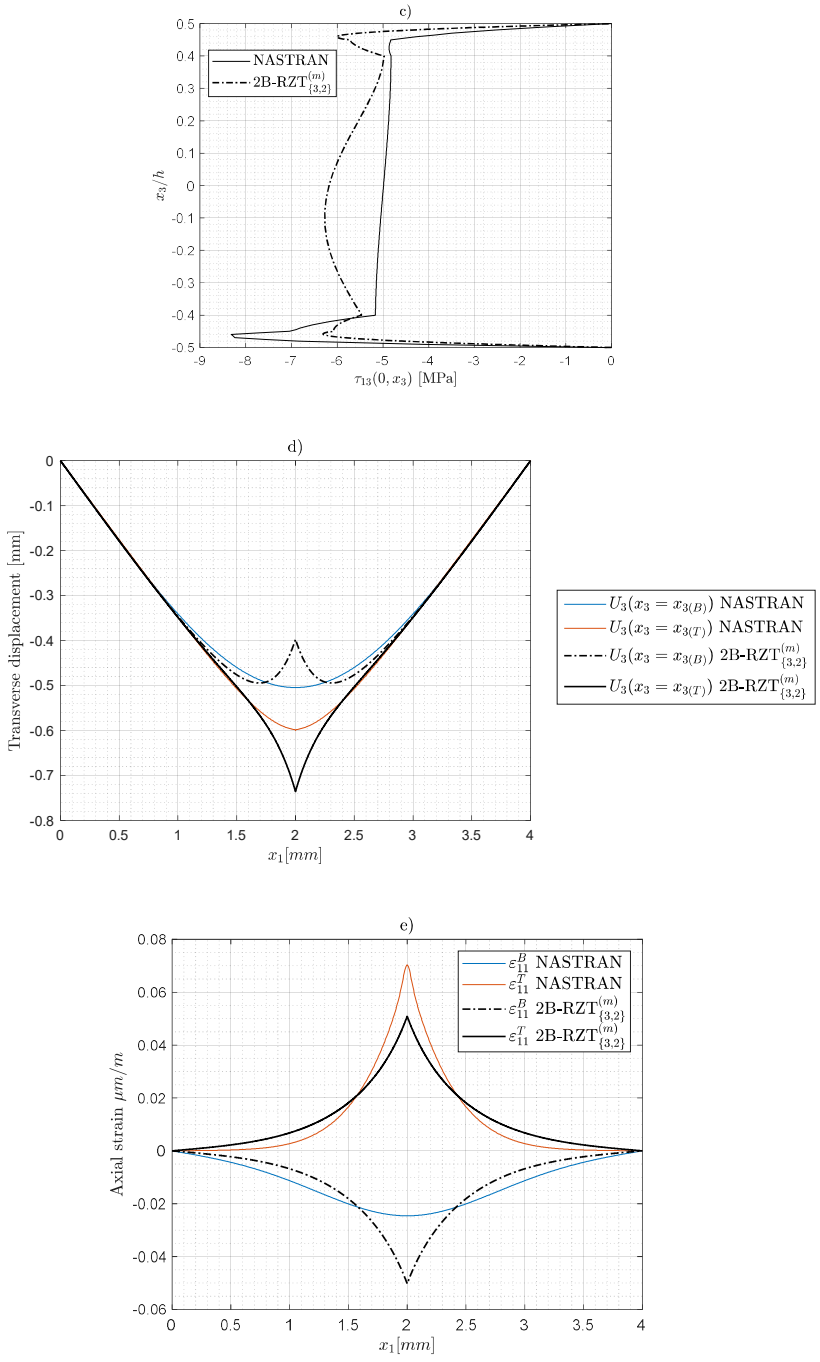

Figure 34: Through-the-thickness in-plane and transverse displacements a)-b) and transverse shear stress c). Distribution of the bottom and top transverse displacements d) and axial deformation at the internal layer interfaces e) for sandwich S1.

5.4.3 Free vibrations

In this section, the free vibration analysis of simply-supported multilayered cross-ply and sandwich beams is assessed using the 2B-RZT$^{(m)}_{\{3,2\}}$ elements. As anticipated, the results for the dynamic analysis involve 4096 beam elements. Also, in this dynamic assessment, the span-to-thickness is typical for very thick structures, i.e. *L/h=4*. The constraint conditions on the nodal dof's are those reported by Eq. (5.24). Such as been done for the static bending analysis, the reference model is a 2D high-fidelity FE model using 40000 membrane QUAD8 Nastran elements. Only the frequencies corresponding to the flexural modes in the high-fidelity FE model are compared with the results provided by the 2B-RZT$^{(m)}_{\{3,2\}}$ elements.

Table 21 and Table 22 report the normalized natural frequencies of the flexural modes corresponding to the cross-ply L1 and cross-ply sandwich S1 beams. The results agree with those obtained by the high-fidelity FE model taken as reference. With respect to the investigated bending case, in this analysis, the effect of applied forces is not considered; thus, the assumed transverse normal stress and transverse displacement patterns are sufficiently accurate to describe the exact three-dimensional behaviour.

Furthermore, the accuracy of the 2B-RZT$^{(m)}_{\{3,2\}}$ is also shown in the low error values for the sandwich beam frequency predictions, where the highest is for the third transversal symmetric mode is less than 1%, which is a remarkable result.

Table 21: Normalized circular frequencies and percent errors of simply-supported cross-ply L1 beam (*L/h=4*), discretized with 4096 2B-RZT$^{(m)}_{\{3,2\}}$ elements.

Mode	**NASTRAN®**	**2B-RZT$^{(m)}_{\{3,2\}}$**	**err%**
1	968.8	968.7	-0.05
2	2278.7	2277.6	-0.09
3	3622.7	3618.1	-0.15
4	4991.6	4980.5	-0.23
5	6369.6	6349.8	-0.31

6	7746.6	7717.7	-0.37
7	9116.0	9080.3	-0.39
8	10473.0	10436.1	-0.36
9	11813.0	11784.2	-0.27
10	13131.7	13123.6	-0.12

Table 22: Normalized circular frequencies and percent errors of simply-supported cross-ply sandwich S1 beam (*L/h=4*) discretized with 4096 $\text{2B-RZT}^{(m)}_{\{3,2\}}$ elements

Mode	**NASTRAN®**	**2B-RZT$^{(m)}_{\{3,2\}}$**	**err%**
1	177.0	176.9	-0.09
2	430.9	430.8	-0.08
3	796.2	796.8	0.05
4	1276.2	1272.7	-0.28
5	1853.0	1815.2	0.97
6	2474.7	2304.1	-0.04

Chapter 6

Experimental validations: static and dynamic analysis

In this Chapter, a static and dynamic experimental assessment is performed to investigate displacements, strains and natural frequencies of sandwich structures. This experimental campaign aims to provide a set of experimental results that can be used to validate statically and dynamically the numerical models. The experiments are focused on evaluating displacements and strains of sandwich beam specimens by using three- and four-point bending tests and natural frequencies and modal shapes in free boundary conditions.

The sandwich beams specimens are made of EN-AW 7075T6 Aluminium alloy (Ergal) and Rohacell® foam cores. The specimens have been divided into two groups due to the different core materials and test purposes. The first is represented by the beam specimens tested statically, whose cores are made of Rohacell® IG-31 soft foam, whereas the second is tested dynamically, and the core material is of Rohacell® WF110 rigid foam.

The experimental results for static and dynamic problems are compared with the new B-RZT$^{(m)}_{\{3,2\}}$ model. Due to the boundary conditions and load case, the formulated beam finite elements have been used.

The experimental campaign has been conducted at the LAQ-AERMEC laboratory of the Department of Mechanical and Aerospace Engineering

(DIMEAS) of the Politecnico di Torino. The specimens have been manufactured by the Department of Science and Aerospace Technology of Politecnico di Milano.

6.1 Specimens properties

As introduced, the beam specimens present a typical sandwich lamination scheme used for aeronautical applications, two face-sheets of 7075 Aluminium alloy separated by a thick core made of Rohacell® polymethacrylamide foam.

In order to investigate the effect of foam material, length-to-thickness ratio and core-to-face thickness ratio, different specimens have been manufactured.

A first group of beam sandwich specimens was tested via three- and four-point bending tests. The group is represented by four specimens beams made with IG-31 foam core with different length-to-thickness ratios. Each beam has a 3 mm face-sheet thickness bonded to the core layer with 0.25 mm 3M™ Scotch-Weld™ Structural Adhesive Film AF 163-2K.

A second group of four sandwich beam specimens was tested dynamically to obtain the experimental natural frequencies and corresponding modal shapes. The beams' cores are made of WF-110 foam. Different face-to-core thickness and length-to-thickness ratios have been considered in these specimens. Two beams have a 2 mm face-sheet of 7075 Aluminium alloy bonded to the core layer with 0.25 mm 3M™ Scotch-Weld™ Structural Adhesive Film AF 163-2K.

The sandwich beam specimens were designed by considering nominal values for the geometry and materials. Therefore, it is evident that in the design phase, the manufacturing process to produce the specimens has not been considered. Thus, it is necessary to measure and characterize the mechanical properties of the constituent materials of the specimens.

The nomenclature and geometries of the sandwich beam specimens, statically and dynamically investigated, are reported in Table 23. The reported dimensions refer to the quantities shown in Figure 35. In addition, for the group of specimens considered for bending analysis (e.g. B01, B02, B03 and B04), the effective bending length $\left(L_{eff}\right)$ related to the distance between the supports is also reported in Table 23. The same distance is not reported for the sandwich beam specimens of the dynamic analysis (e.g. D01, D02, D03 and D04).

A third group of specimens is made to experimentally determine the mechanical characteristics of the beam constituent materials, except for the adhesive layer, whose properties have been assumed from the producer datasheets. Table 24 presents the list of the specimens considered for the material characterization. Moreover, the Rohacell® IG-31 and WF-110 foam specimens (e.g. P07, P08, P09, P10 and P11), and Ergal specimen (e.g. P12) are also tested statically. The effective bending length of the beam specimens is also reported in Table 24.

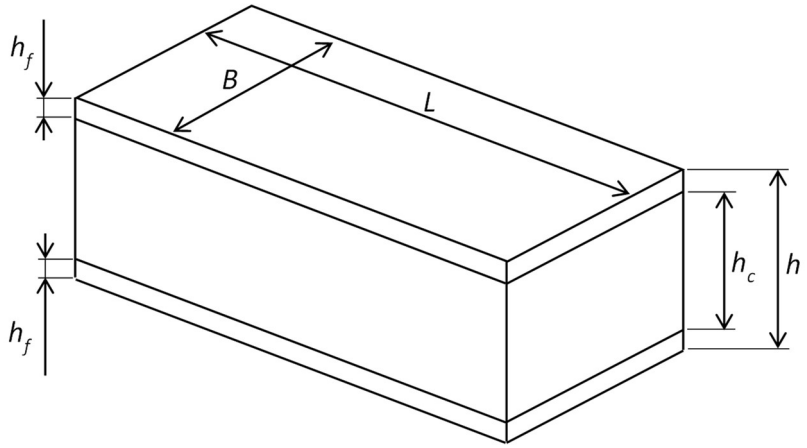

Figure 35: Geometry of the sandwich beam specimens

Table 23: Sandwich beam specimens nomenclature and dimensions (in mm).

Specimen ID	Core Material	L	L_{eff}	B	h	h_f	L/h	h_c/h_f
B01	IG-31	640.00	600.00	90.00	44.60	3.00	14.35	12.87
B02	IG-31	490.00	450.00	90.00	43.30	3.00	11.32	12.40
B03	IG-31	340.00	300.00	90.00	43.50	3.00	7.82	12.50
B04	IG-31	280.00	240.00	90.00	43.10	3.00	6.50	12.37
D01	WF-110	500.00	-	80.00	43.32	2.00	11.54	19.66
D02	WF-110	500.00	-	80.00	41.18	1.00	12.14	39.18
D03	WF-110	500.00	-	80.00	33.53	2.00	14.91	14.77
D04	WF-110	500.00	-	80.00	31.54	1.00	15.85	29.54

Table 24: Nomenclature and specimens' dimensions for material characterization (values are given in mm).

Specimen ID	Material	L	L_{eff}	B	h
P01	WF-110	80.50	-	50.25	27.10
P02	WF-110	80.53	-	50.20	18.28
P03	WF-110	95.25	-	80.402	39.63
P04	WF-110	179.75	-	80.45	49.99
P05	IG-31	89.70	-	40.21	35.33
P06	IG-31	107.17	-	89.90	40.17
P07	IG-31	587.00	540.00	80.04	40.12
P08	IG-31	427.67	400.00	64.74	40.10
P09	IG-31	603.00	560.00	89.59	40.14
P10	WF-110	1105.00	1000.00	80.36	39.83
P11	WF-110	1105.00	1000.00	80.38	39.93
P12	EN AW 7075 T6	1017.500	400.00	40.13	3.00

6.2 Material characterization

In this section, the procedure adopted to characterize the mechanical properties of the 7075 Aluminium alloy (Ergal) and the Rohacell® IG-31 and WF-110 foams is reported. It is evident that material characterization is necessary to determine the effective properties of the specimens to make the proper comparisons between the numerical models and the experimental tests.

Table 25 reports the nominal values of the material mechanical properties as given by the corresponding producers' datasheets. The mass density of the adhesive layer has given for 0.25 mm thickness.

Table 25: Material mechanical properties: nominal values, the Young's and shear modulus are in MPa, and the mass density is in kg/m^3.

Material	E	G	ρ
EN-AW 7075 T6 (Ergal)	73000	28007	2700
Rohacell® IG-31	36	13	32
Rohacell® WF-110	180	70	110
AF-163-2K	1110	414.2	1210

6.2.1 Mass density

The material mass densities of Rohacell® foams are estimated by averaging each density mass of the P01, P02, P03 and P04 for the WF-110 and P05, P06 and P07 for the IG-31. The measured weights of each specimen are then divided by the corresponding specimens' volume. In the same way, the material mass density of the 7075 Aluminium alloy (Ergal) is obtained by considering specimen P12. The obtained experimental results are reported in Table 26.

Table 26: Experimentally measured material mass density in kg/m^3.

	EN AW 7075 T6 (Ergal)	Rohacell® IG-31	Rohacell® WF-110
ρ	2750.6	36.5	109.5

6.2.2 Young's and shear moduli evaluation

In this section, the mechanical properties are estimated experimentally. The Young's modulus of the Rohacell® WF-110 and IG-31 foams are characterized by following the standard test method described by the ASTM D790 [174]. A three-point bending test has been performed on simply-supported beam specimens to determine the maximum central deflection and the deflection at a quarter of the effective bending length. The beam specimens tested to determine Young's modulus are P07, P08 and P09 for the IG-31 foam and P10 and P11 for the WF-110. A load cell (HBM – strain gauge load cell, 200 kg) measures the load applied to the beam specimens. In Figure 36, the experimental set-up used for the three-point bending test on the Rohacell® foam specimens is shown: A rigid support; B displacement control system; F load cell; W1, W2, W3 and $W_{L/4}$ Linear Variable Transducer Displacements (LVDTs).

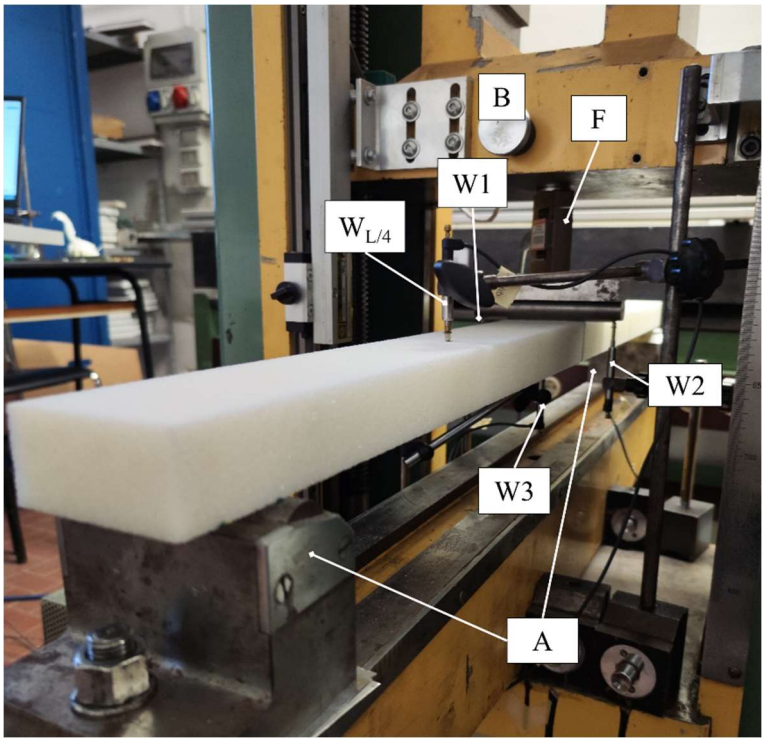

Figure 36: Rohacell® three-point bending test: sensor disposal and configuration.

Two LVDTs (e.g. W1 and W2) have been positioned directly in contact with the load cylinder to measure the deflection at the top surface of the foam specimen. From the two measures, an average value, i.e. w_T, is calculated. The third LVDT, i.e. W3=w_B, measures the deflection at the bottom surface of the foam beam specimen. The three LVDTs, (e.g. W1, W2 and W2) are positioned at the mid-span length of the foam specimens. The maximum central deflection is then obtained by averaging the w_T and w_B measures. A fourth LVDT ($W_{L/4}$) is placed on the top surface at the point corresponding to the quarter effective beam length. A simplified scheme of the experimental set-up for the foam specimens is reported in Figure 37.

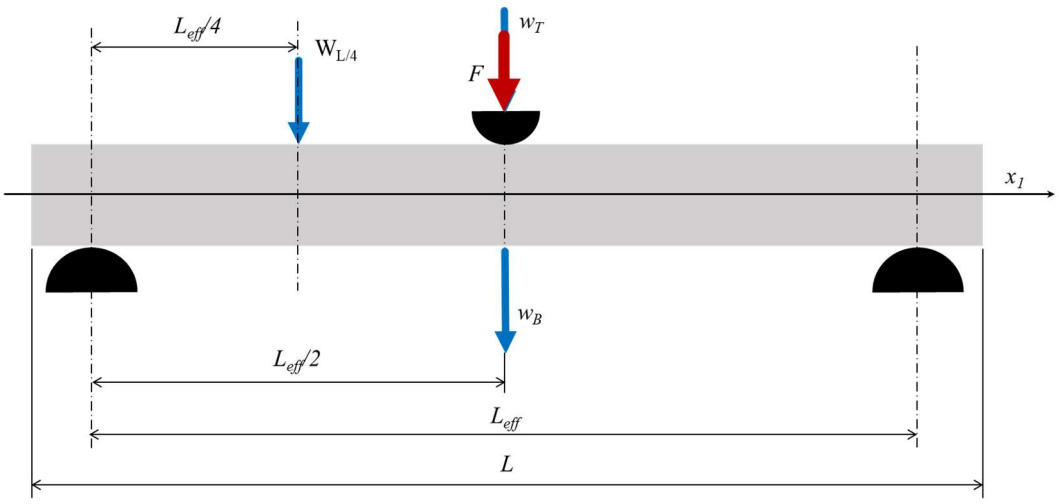

Figure 37: Three-point bending test on foam specimens and nomenclature for displacements.

A high-fidelity 2D FE model with QUAD8 membrane Nastran® elements has been made for each tested beam specimen. In addition, a preliminary numerical analysis has been performed using the nominal values for isotropic materials.

The effect of the transverse shear deformability is considered in the high-fidelity 2D model, although its influence is almost negligible. However, a more simplified beam model, Timoshenko beam theory, which includes the effect of transverse deformability, can be used to estimate deflections. They read:

$$w_{L/2} = \frac{FL_{eff}^3}{48EI} + \frac{FL_{eff}}{4k^2GBh}$$
$$w_{L/4} = \frac{11FL_{eff}^3}{768EI} + \frac{FL_{eff}}{8k^2GBh} \quad (6.1)$$

where G and E the shear and Young's modulus, respectively, k^2 the shear correction factor (equal to 5/6), F the applied force, L_{eff} the effective bending length and I the inertia of the beam section. Considering the beam specimens' lengths and section areas, the contribution due to the shear deformability to the central deflection is less than 3.4%, whereas for the quarter-length beam deflection is negligible. Thus, using as inputs the measured deflections to determine at the same time both Young's and shear moduli using the Eq. (6.1) leads to an erroneous evaluation of the shear moduli. In fact, in literature, the

same issue has been encountered in Iurlaro's work [140], where similar beam specimens were used.

Based on these considerations and the high-fidelity 2D results on the models using the nominal material's values, the beam bending behaviour can be approximated as the Bernoulli-Euler beam model, in which only the elastic modulus is considered. According to the Bernoulli-Euler model, the maximum deflection and the deflection at a quarter of the effective bending length are obtained by the following formulas:

$$w_{L/2} = \frac{FL_{eff}^3}{48EI}$$
$$w_{L/4} = \frac{11FL_{eff}^3}{768EI} \tag{6.2}$$

It can be seen from Eq. (6.2) that, for a beam geometry known, Young's modulus is a function only of the force-to-transverse displacement ratio for both displacements. Based on this consideration, for each beam foam specimen statically assessed (e.g. P07, P08, P09, P10 and P11), the elastic modulus is determined using the linear regression method on the experimental data. The experimental force-displacement curves of Rohacell® IG-31 and WF-110 are shown in Figure 38 - Figure 42 and are used to determine the corresponding Young's modulus. The linear fitting curves for central and quarter-length displacements have been determined for each beam foam specimen; from the computed curves, the elastic modulus is then obtained using Eq. (6.2). Based on these results, Table 27 shows the results of the Rohacell® IG-31 and WF-110 experimental Young's moduli in terms of mean value and standard deviation.

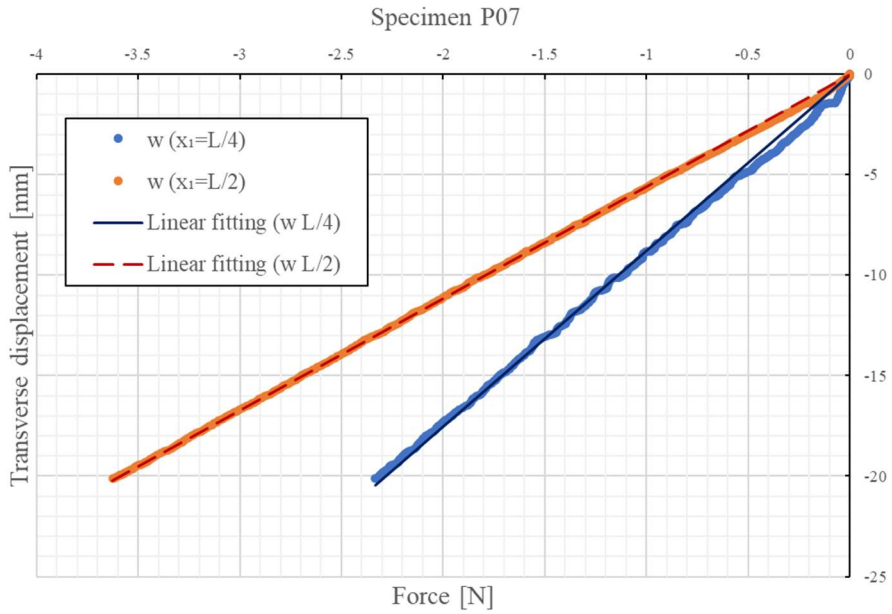

Figure 38: Three-point bending test on specimen P07 (Rohacell® IG-31), force-displacement curve.

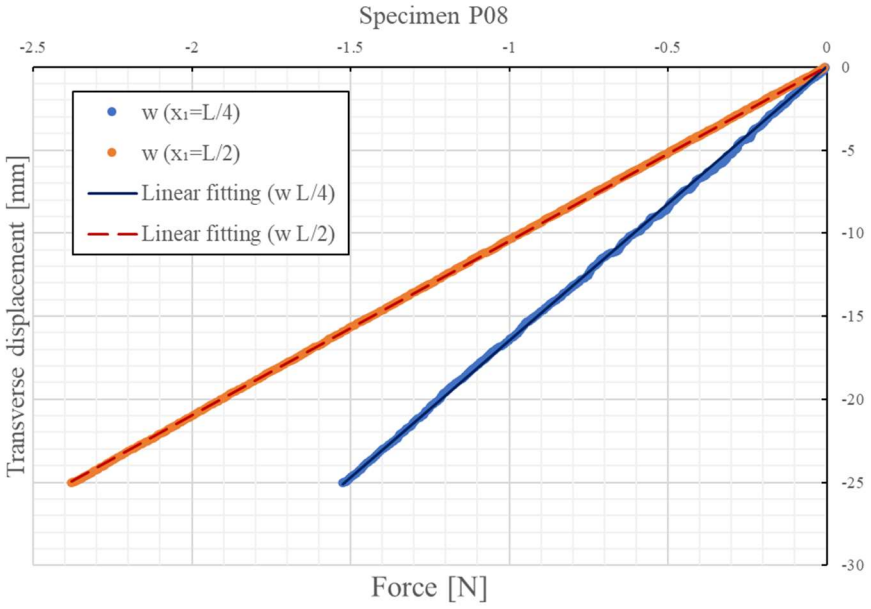

Figure 39: Three-point bending test on specimen P08 (Rohacell® IG-31), force-displacement curve.

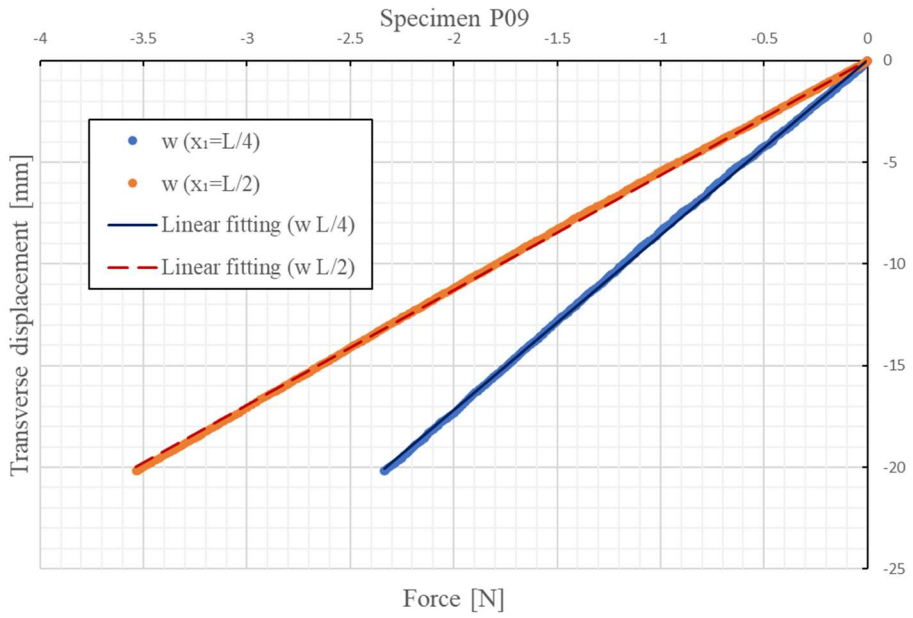

Figure 40: Three-point bending test on specimen P09 (Rohacell® IG-31), force-displacement curve.

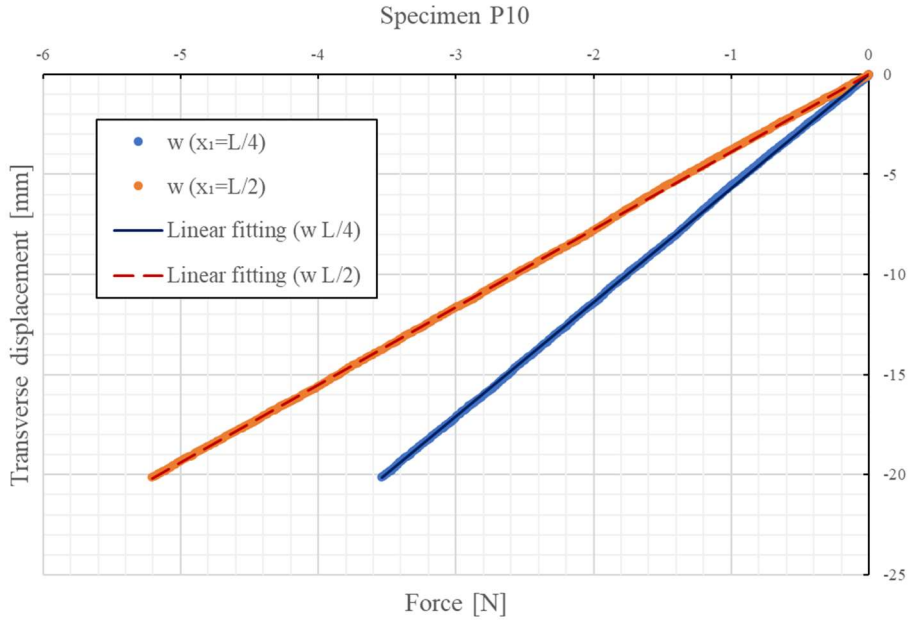

Figure 41: Three-point bending test on specimen P10 (Rohacell® WF-110), force-displacement curve.

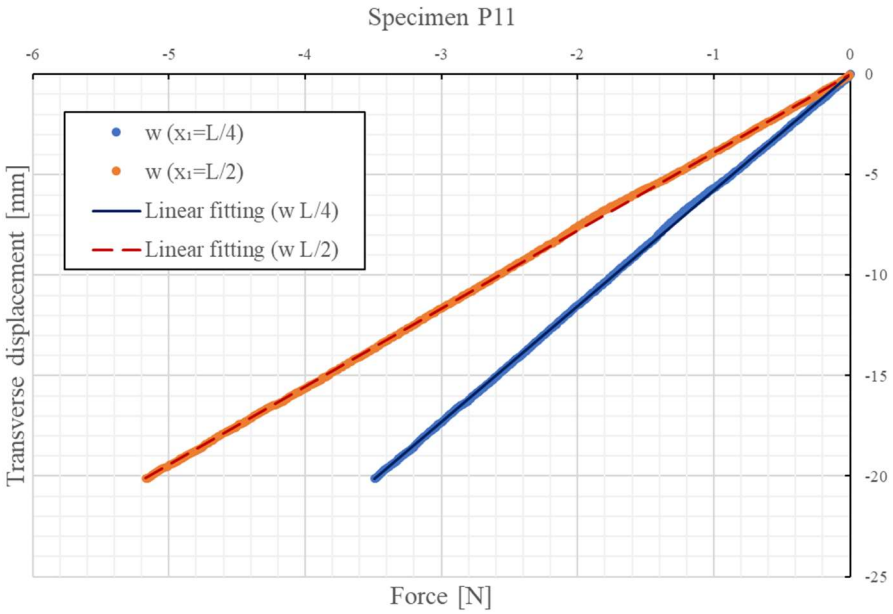

Figure 42: Three-point bending test on specimen P11 (Rohacell® WF-110), force-displacement curve.

The elastic modulus of the Aluminium alloy (Ergal) has been determined by evaluating the maximum deflection at the end of the beam specimen P12. The beam specimen has been clamped to one edge, whereas a concentrated force has been applied to the other, as shown in Figure 43. The deflection has been measured from the reference position using a ruler positioned next to the beam end, as reported in Figure 43. The maximum beam deflections have been measured for the following value of the applied forces 0.5 kg, 1.0 kg and 1.5kg, considering an effective bending length (L_{eff}) of 400.00 mm. Three tests on the beam specimens are conducted. The tests results are reported in Figure 44.

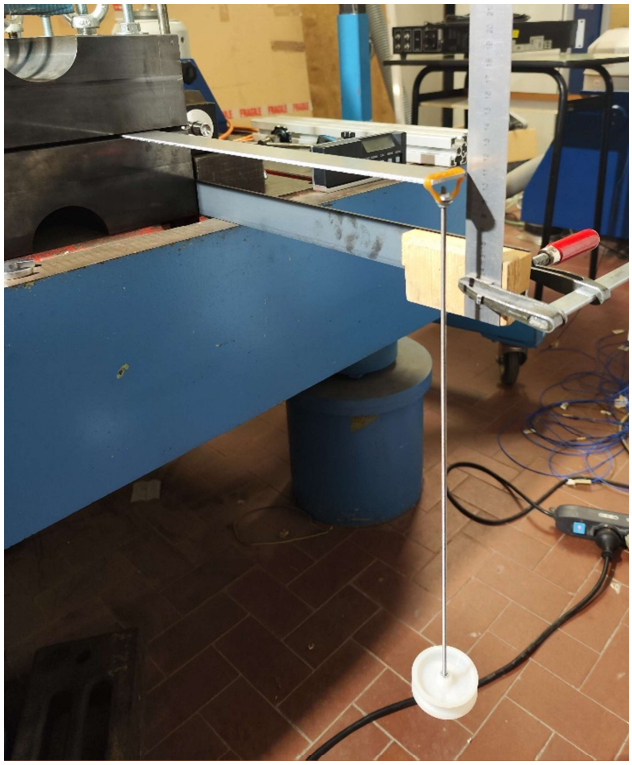

Figure 43: Aluminium alloy specimen P12 tested for Young's modulus evaluation, clamped boundary condition and concentrated tip force.

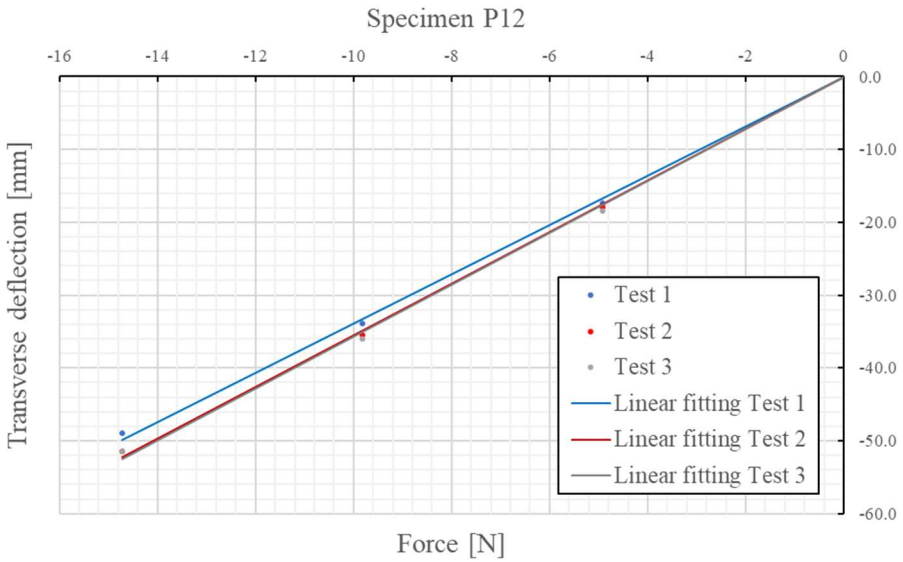

Figure 44: Maximum deflection vs the applied force of specimen P12 (Aluminium alloy, Ergal).

Taking into account the Bernoulli-Euler beam model, the transverse displacement can be computed as follows:

$$w_L = \frac{FL_{eff}^3}{3EI} \tag{6.3}$$

From Eq. (6.3), the elastic modulus can be easily obtained, and the result is reported in Table 27. Due to the material property of the 7075 Aluminium alloy, the typical Poisson's ratio has a value of 0.33 and assuming the isotropic behaviour, the corresponding shear modulus is obtained.

The second step is dedicated to determining the transverse shear moduli of the foam specimens. It is evident from the previous results that testing a homogeneous isotropic material cannot provide an accurate value for the shear modulus. It should be addressed in a structure in which the effect of transverse shear deformability is pronounced. A typical example of such structure is represented by sandwich-like structures where the core takes the most shear deformability.

Two sandwich beam specimens were considered to determine the shear modulus of Rohacell® IG-31 and WF-110. A three-point bending test has been performed on specimens B01 and D01 using the same LVDT configuration considered for pure foam specimen tests. The experimental deflection results have been compared with a 2D high-fidelity model using membrane QUAD4 NASTRAN® elements representative of the B01 and D01 beam specimens to evaluate the value of shear moduli numerically. Due to the symmetry of the problem, only half of the beam is discretized in the FE model, using 227840 QUAD4 elements, taking advantage of computational cost save. In the FE model, the material mechanical properties for Ergal face-sheets and Young's moduli of the Rohacell® foams are those determined experimentally in the former step; for the adhesive layer, instead, are considered those given by the producer (the adhesive thickness is considered 0.25mm). In the NASTRAN® elements, the Ergal and the adhesive material are modelled as isotropic materials.

A parametric analysis is performed to determine the shear modulus values that match better the experimental and numerical deflections with less than 1% of errors. The shear modulus, instead, assumes different values in the range

$[0.8G_n : G_n]$, since the expected values are below the nominal ones. The corresponding values have been obtained for the three measured displacements, top and bottom central beam and a quarter of the beam length. In this case, due to the possibility of having G values that could not satisfy the Poisson's relation for isotropic materials, the core material properties are assumed as 2D orthotropic where the Poisson's ratio value is nominal. Figure 45 and Figure 46 report the percent errors for IG-31 and WF-110 between the FEM and experimental results for central top and bottom deflection and top deflection at a quarter of the effective beam length. It is worth noting that for the IG-31 foam, the numerical shear moduli that give an error below 1 % are not almost identical for the bottom and quarter-length deflections, see Figure 45. Whereas, for WF-110 foam, a shear modulus is obtainable if the quarter-length and central bottom deflection are the only displacement considered. It is important to note that for both cases, the experimental central displacement at the top surface is always greater than the bottom one. Although the Rohacell® foams are made of the same plastic material, Polymethacrylamide (PMI), the differences in the material properties are due to the foam manufacturing process.

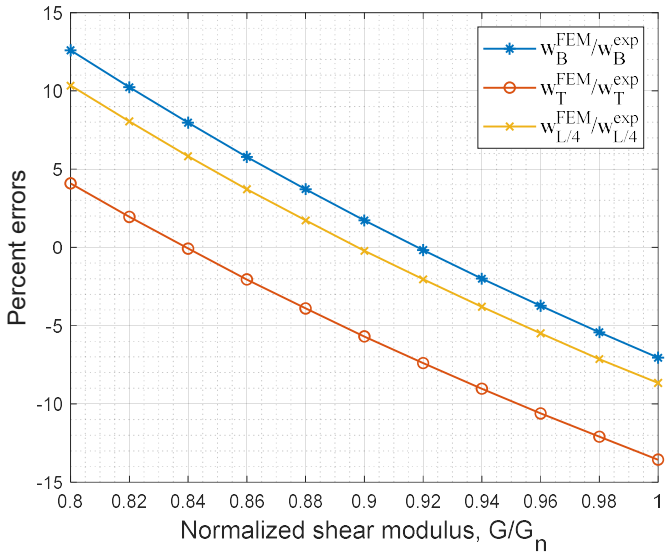

Figure 45: Percent errors of numerical displacements versus the normalized shear modulus (B01).

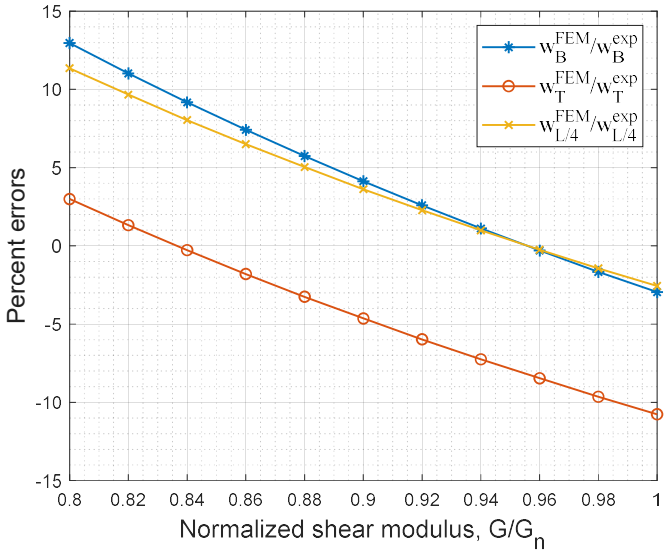

Figure 46: Percent errors of numerical displacements versus the normalized shear modulus (D01).

It is interesting to note from the datasheets of the material properties given for the IG-31 foam that two values of Young's modulus have been given, one related to the traction case and the other for compression, which is sensibly lower than the first one. It can be seen that the traction elastic modulus is very close to those determined experimentally. However, this thesis's work does not consider a different definition of the value for elastic modulus if the material is in traction or compression condition, nor is it included in the high-fidelity FE model. However, considering the high-fidelity FE model of B01 with nominal values for the material properties, it can be easily seen from the transverse normal stress plot Figure 47 that the core in the transverse thickness direction is mostly in compression or has very low-stress values. A similar effect is expected to be reproduced for the D01 beam, as reported in Ref. [175], where the core has been made of WF-110. However, from the producer datasheet for WF-110 foam, an elastic modulus for compression has not been given. It is reasonable that the top displacement where the load is applied produces a local nonlinear effect that is not noticeable with the current models. Thus, the shear modulus of the WF-110 foam is determined only by considering the bottom central and quarter-length deflections.

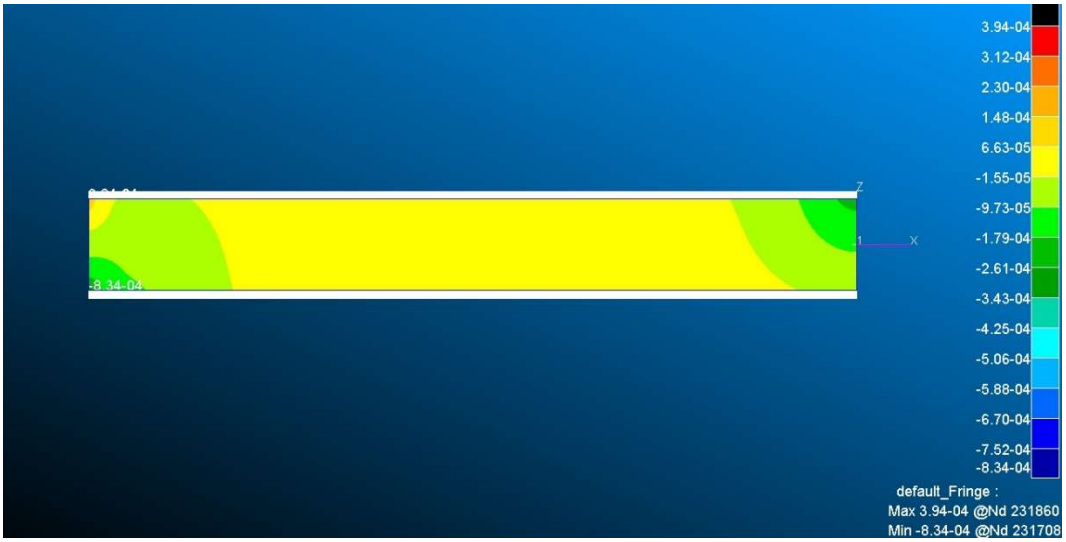

Figure 47: Normal transverse stress distribution σ_{33} in core layer for beam B01 considering nominal material properties of Rohacell® IG-31.

For the IG-31 foam, based on this numerical consideration, it seems appropriate to consider the value of Young's modulus in the transverse direction as the corresponding compression modulus. Therefore, taking advantage of the 2D orthotropic material definition in the NASTRAN® model, a new parametric analysis has been performed to determine the shear modulus that better matches the displacements, considering the compressive modulus for the transverse mechanical property. The numerical results of the displacements, in terms of percent errors with the experimental results, are shown in Figure 48.

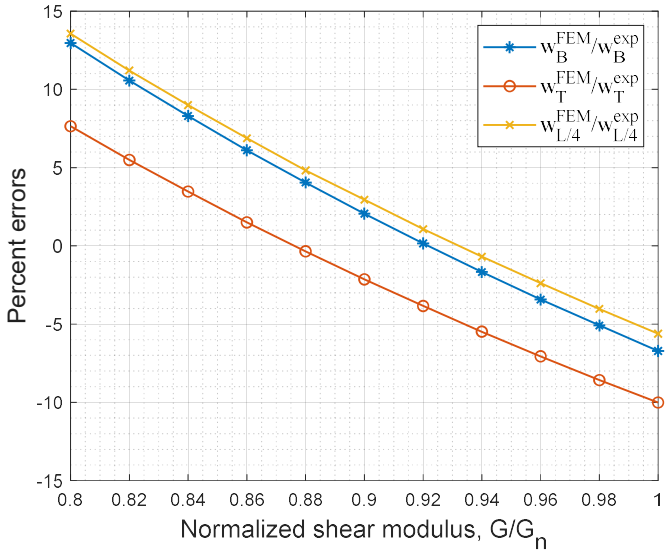

Figure 48: Percent errors of numerical displacements versus the normalized shear modulus (B01), considering the compressive elastic modulus in the transverse direction.

The central bottom and quarter-length displacement error curves shown in Figure 43 are closer than those in Figure 45. Thus, it is possible to obtain a value for the shear modulus that can ensure an error for these displacements of less than 1%. However, considering a compressive value for Young's modulus in the transverse direction guarantees a lower error also for the central top displacement. For the assumed value of the shear modulus of IG-31 foam, the error on top central deflection is less than 5% for beam B01. It should be noted that the central top deflection is very sensible to Young's modulus in the transverse direction. It is expected that for other beam specimens, the error could be greater due to the more pronounced compression of the core given by the manufacturing process (the nominal thickness of the core has been reduced by 3 mm).

The results of the experimental characterization are reported in Table 27. In addition, these values are used in the following numerical comparisons between the experimental and the new model results.

Table 27: Experimental material mechanical properties. Young's and shear modulus are in MPa.

Material	E	G
EN-AW 7075 T6 (Ergal)	67545.6 ± 1947.9	25393.1
Rohacell® IG-31*	43.2 ± 2.0	12.1
Rohacell® WF-110	194.1 ± 4.8	66.9

* for the transverse direction, the compressive modulus is considered (E=17 MPa).

6.3 Static assessment

In this Section, the experimental static responses of three- and four-point bending tests on sandwich beams (B01, B02, B03 and B04) are shown and compared with the new RZT mixed model.

The novelty aspect of this static analysis is the experimental evaluation of the strain quantities at the interfaces between IG-31 core and Ergal face-sheets. The optical fibre sensors have been made by Politecnico di Milano and embedded in the sandwich during the manufacturing layup before the curing process. The sensors, of different lengths, are placed parallel to the beam's longitudinal axis. The sensor placement scheme is reported in Figure 49.

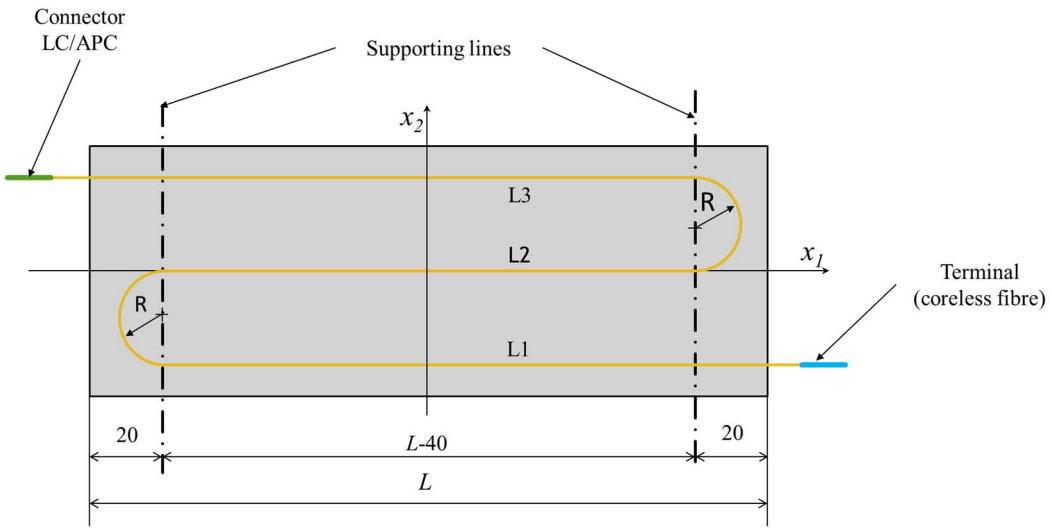

Figure 49: View from above of the optical fibre sensor positioning at the layer interface, the radius R=15 mm (data in mm).

Moreover, a groove guide on the Ergal face-sheet has been done to keep the sensor in position during the curing process, and the adhesive layer is placed, as shown in Figure 50. Finally, the bonding process and the following cure process have been done in the autoclave. Then, the sandwich beams were placed in a mechanical press to restore the planarity between the Ergal face-sheets, modified as a consequence of the protecting supports for the optical fibre sensors, see Figure 51.

The optical fibre sensors are connected to the acquisition system (Luna Inc. ODISI 610x series) through the remote modules to the first two channels, see Figure 52.

In addition to the optical fibre sensors, some strain gauges were placed on the beams. Four strain gauges (E1, E2, E3 and E4) were placed for each beam, two on top and two on bottom surfaces, to measure the axial deformations. Moreover, a further strain gauge (E5) has been placed to verify the symmetry of the boundary and applied load condition during the test. The transverse displacements at the top and bottom surfaces have been measured using three LVDTs. Two have been positioned in the corresponding point of applied force (W1 and W2), and the third is positioned on the bottom surface at the centre of the beam (W3).

The load cell, LVDTs and strain gauges positioned on the beam specimen are, respectively, shown in Figure 53, Figure 54 and Figure 55.

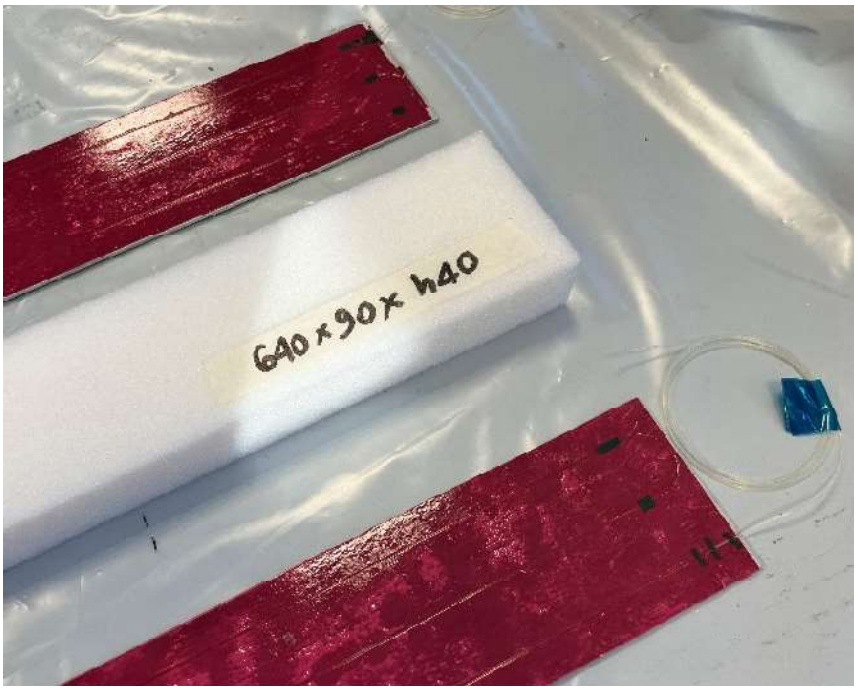

Figure 50: fibre optic sensors placed on the Ergal face-sheets, adhesive layer (in red) and Rohacell® IG-31 foam.

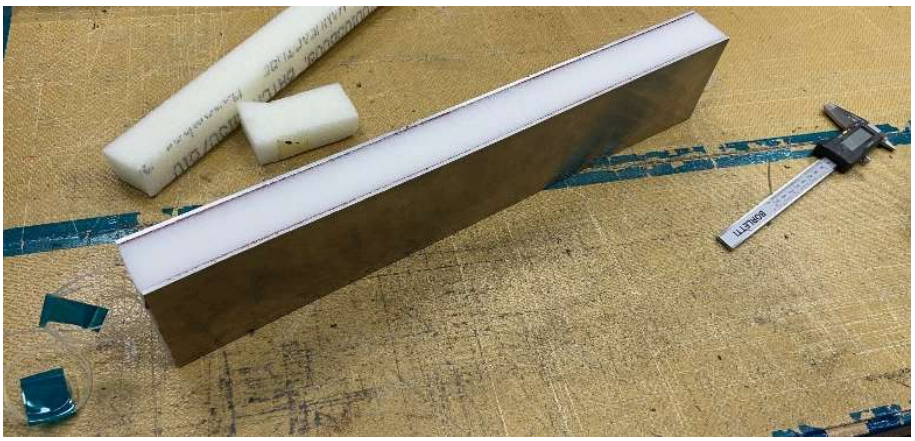

Figure 51: manufactured beam specimen (B02) after mechanical pressing.

Figure 52: Luna Inc. ODISI 610x optical fibre acquisition system.

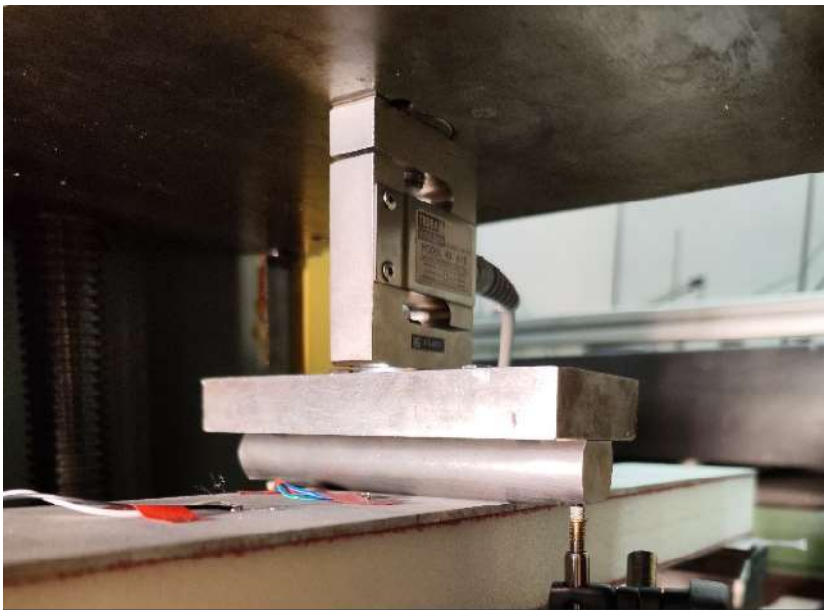

Figure 53: HBM strain gauge load cell (200kg)

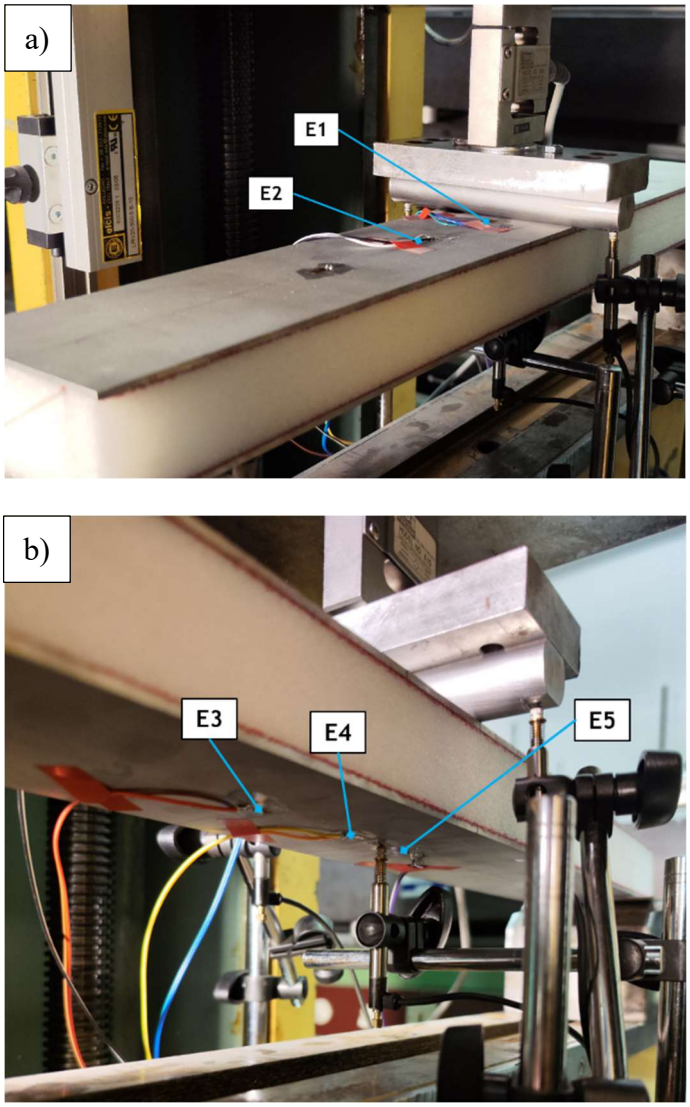

Figure 54: strain gauges embedded on beam top (a) and bottom (b) surfaces.

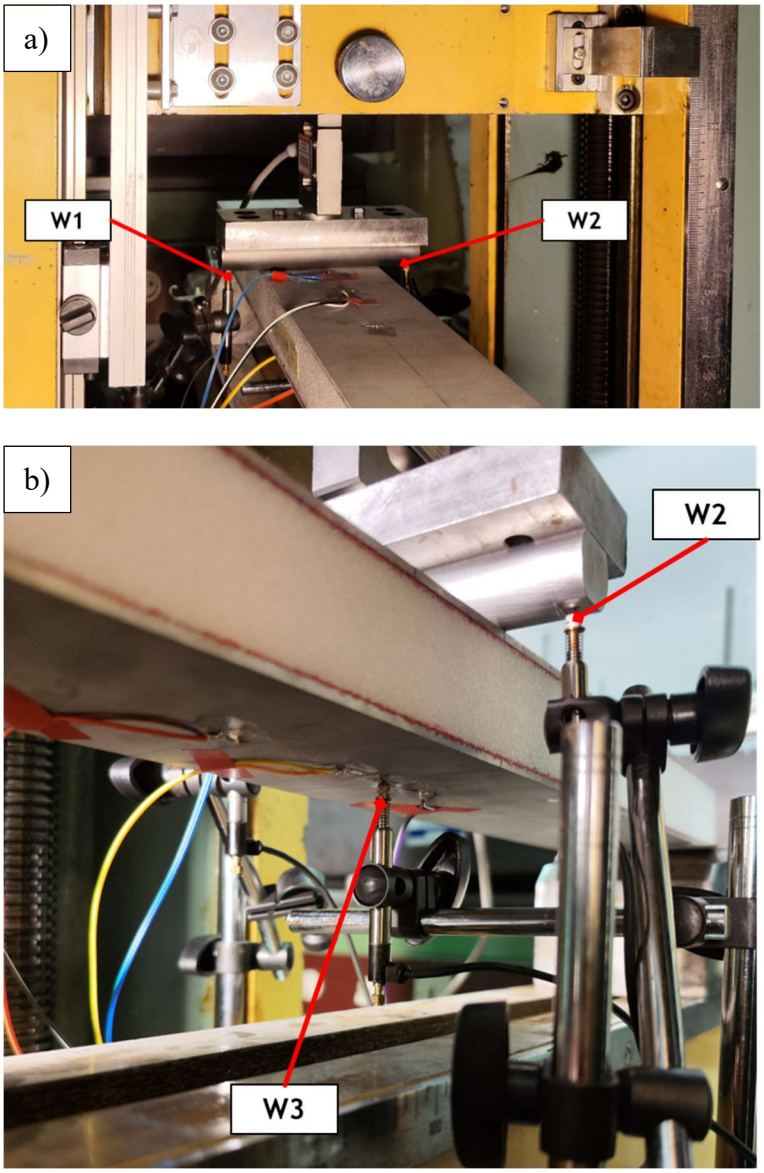

Figure 55: LVDTs positioning and nomenclature for the top (a) and bottom (b) displacements.

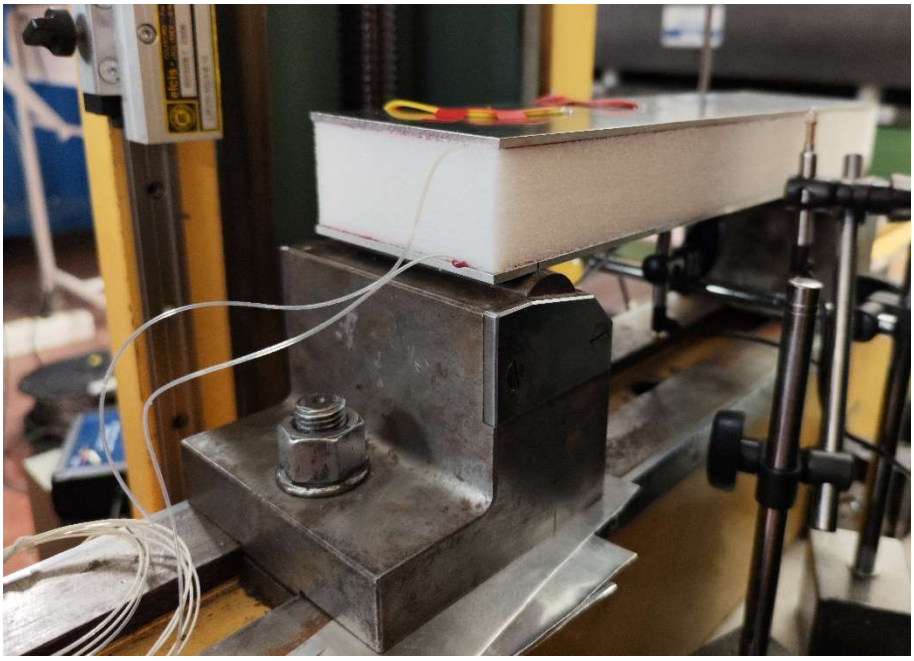

Figure 56: Supported condition on the sandwich beam specimens.

The supported edge of the beam specimens is shown in Figure 56. For the numerical model, the transverse displacement of the contact point between the supporting cylinder and the beam specimen is prescribed to be null.

In the numerical comparison of the experimental results with the 2B-RZT$^{(m)}_{\{3,2\}}$ elements, differently from how it has been done for the numerical analysis, the simply-supported condition is modelled differently. In this case, the constraint on the transverse displacement has been enforced only on the contact point on the bottom beam surface. The constraint conditions are:

$$\begin{aligned} &@\, x_1 = -L_{eff}/2, +L_{eff}/2 \qquad && U_3(x_3 = x_{3(B)}) = 0 \\ &@\, x_1 = 0 && U_1^{(k)}(x_3) = 0 \rightarrow u = 0,\ \theta = 0,\ \psi = 0 \end{aligned} \tag{6.4}$$

A discretization using 2B-RZT$^{(m)}_{\{3,2\}}$ beam element of 0.25 mm of length has been used for each beam. Concerning the high-fidelity FE model, the beams are discretised using membrane QUAD4 elements. In Table 28, the number of elements and the corresponding total dof's for the sandwich beam models are reported.

Table 28: Number of elements and dof's in 2B-RZT$^{(m)}_{\{3,2\}}$ and Nastran models for static analysis.

Beam ID	2B-RZT$^{(m)}_{\{3,2\}}$		NASTRAN	
	Number of elements	Dof's	Number of elements	Dof's
B01	2560	30726	227840	458458
B02	1960	23526	169540	341388
B03	1360	16326	118320	236640
B04	1120	13446	96320	194106

6.4.1 Three-point bending tests

The three-point bending test is performed according to the scheme given in Figure 57. The nomenclature for the measured displacements and strains is reported in the same figure. The experimental axial strains are also evaluated across the thickness at the layer interfaces in two sections $x_{S1} = -20mm$ and $x_{S2} = -75mm$. The position of strain gauge E5 is $x = +20mm$.

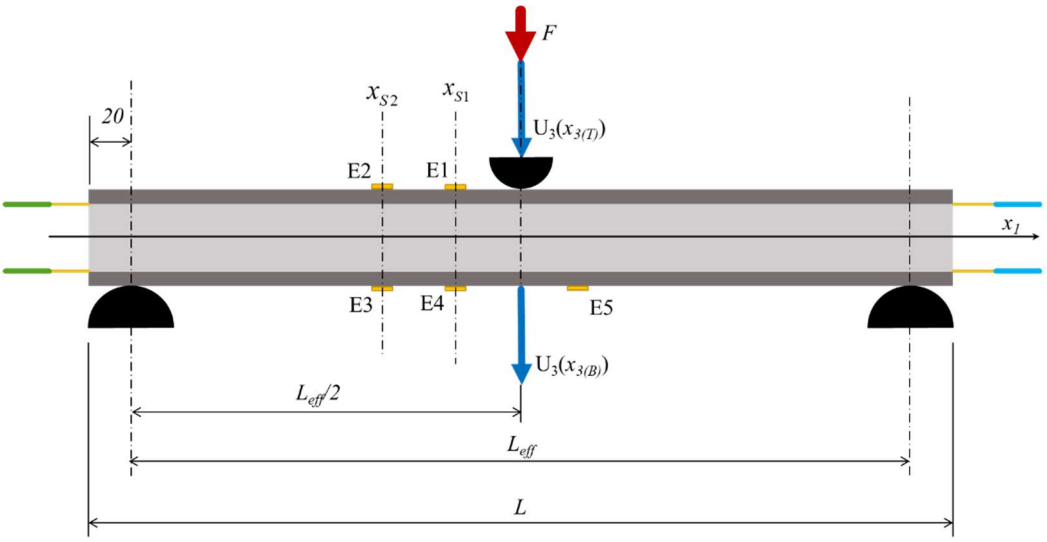

Figure 57: Scheme for three-point bending test and nomenclature for strain gauges and displacements (in mm).

The measured axial strains along the axis coordinate of the three rectilinear lines are averaged to obtain a single strain function representative of the beam behaviour. The reason is dictated by the high resolution of the optical fibre sensors that are very sensitive to geometry imperfections.

The experimental results are compared with those from the mixed RZT beam finite element model and those obtained by the high-fidelity FE Nastran model. The test was performed by increasing the applied load and reaching four different load levels to measure the quantities appropriately.

In Table 29, the experimental and numerical normalized displacements and corresponding percent errors are compared. Figure 58, Figure 60, Figure 62 and Figure 64 show the axial strain distributions along the longitudinal axis for each beam specimen at the bottom and top interfaces between the Ergal face-sheets and the IG-31 foam core. Moreover, in Figure 59, Figure 61, Figure 63 and Figure 65, the trough-the-thickness distributions of the axial strains at the prescribed sections x_{S1} and x_{S2} are reported for each beam specimen. The Nastran solution is reported only for half-beam length since the symmetry of the problem has been considered to save computational costs.

Table 29: Comparison of normalized displacements for three-point bending test between numerical and experimental, in brackets the percent errors.

Beam specimen ID	**Transverse displacement**	**Experimental**	**2B-RZT$^{(\mathbf{m})}_{\{\mathbf{3,2}\}}$**
B01	$U_3(z_{(T)})$	3.354E-03	3.601E-03 (7.4)
	$U_3(z_{(B)})$	3.009E-03	2.913E-03 (-3.2)
B02	$U_3(z_{(T)})$	2.891E-03	2.737E-03 (-5.3)
	$U_3(z_{(B)})$	2.269E-03	2.051E-03 (-9.6)
B03	$U_3(z_{(T)})$	2.283E-03	1.865E-03 (-18.3)
	$U_3(z_{(B)})$	1.713E-03	1.178E-03 (-31.2)
B04	$U_3(z_{(T)})$	1.589E-03	1.544E-03 (-2.9)
	$U_3(z_{(B)})$	1.062E-03	8.571E-04 (-19.3)

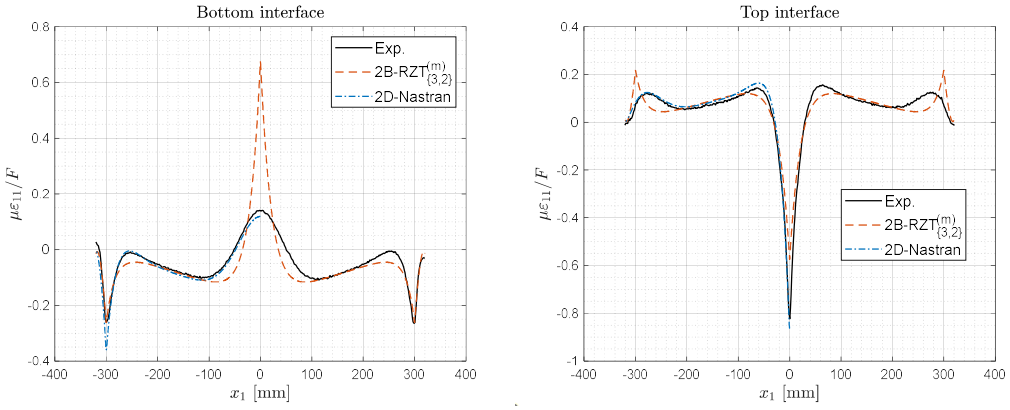

Figure 58: Axial strain distributions along the longitudinal axis for beam B01 (three-point bending).

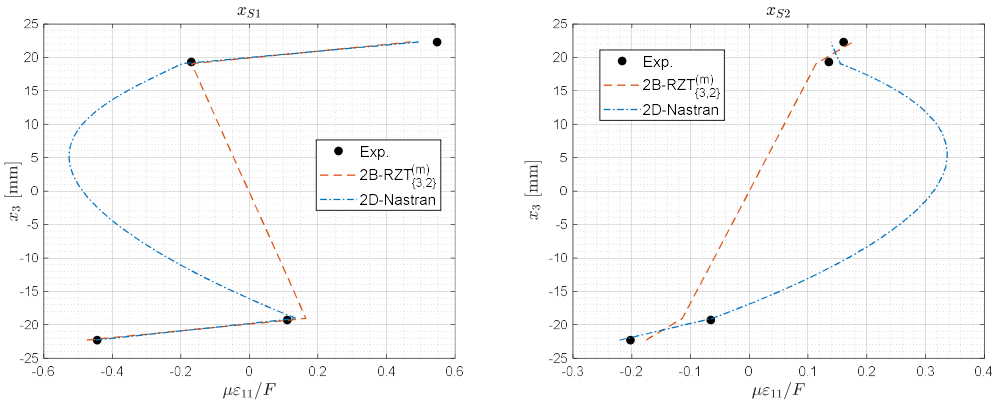

Figure 59: Through-the-thickness distributions of axial strains, beam B01, at $x_{S1} = -20mm$ and $x_{S2} = -75mm$.

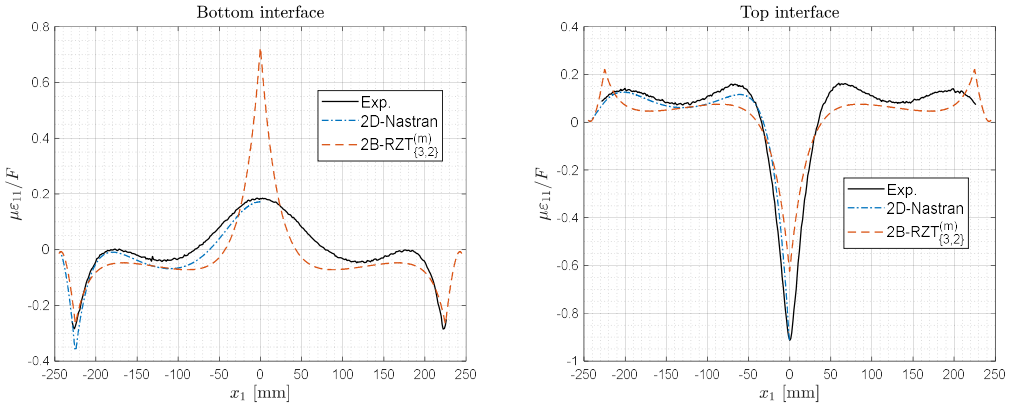

Figure 60: Axial strain distributions along the longitudinal axis for beam B02 (three-point bending).

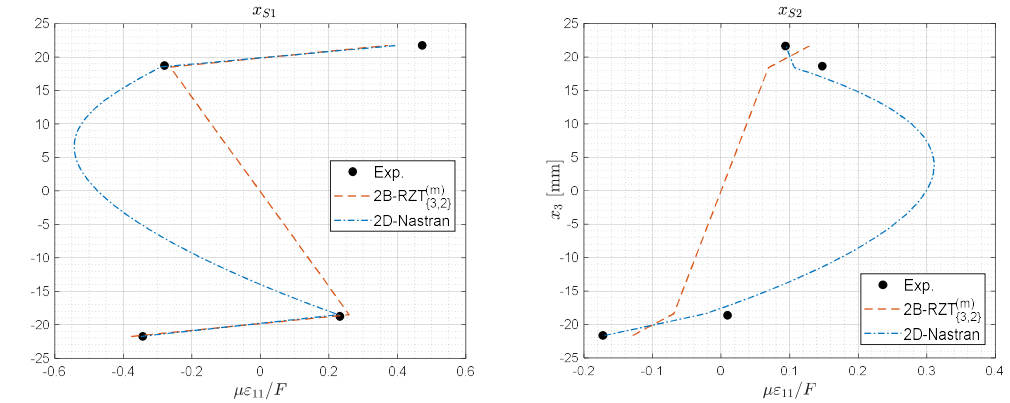

Figure 61: Through-the-thickness distributions of axial strains, beam B02, at $x_{S1} = -20mm$ and $x_{S2} = -75mm$.

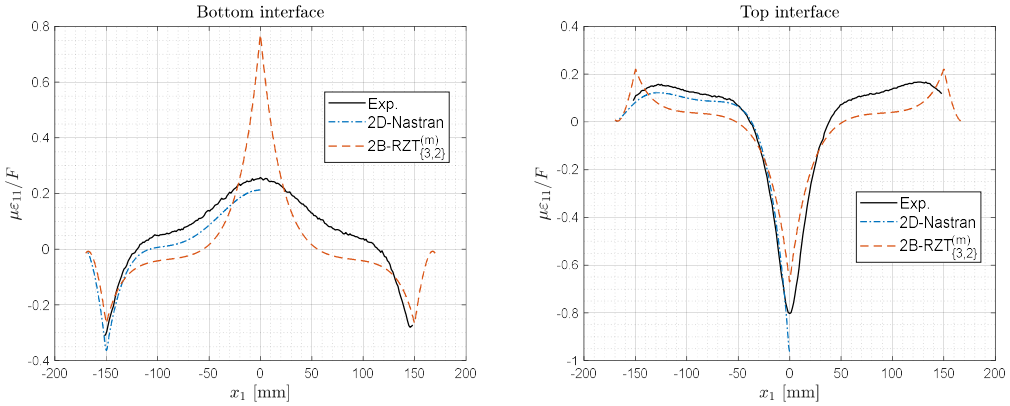

Figure 62: Axial strain distributions along the longitudinal axis for beam B03 (three-point bending).

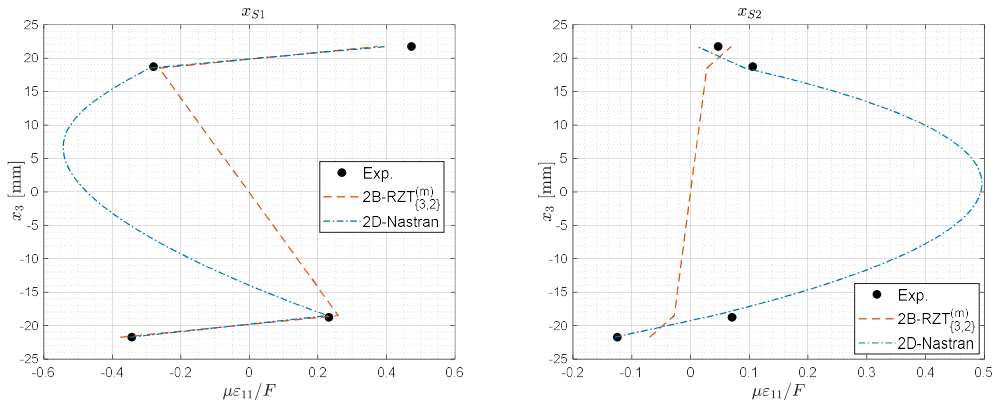

Figure 63: Through-the-thickness distributions of axial strains, beam B03, at $x_{S1} = -20mm$ and $x_{S2} = -75mm$.

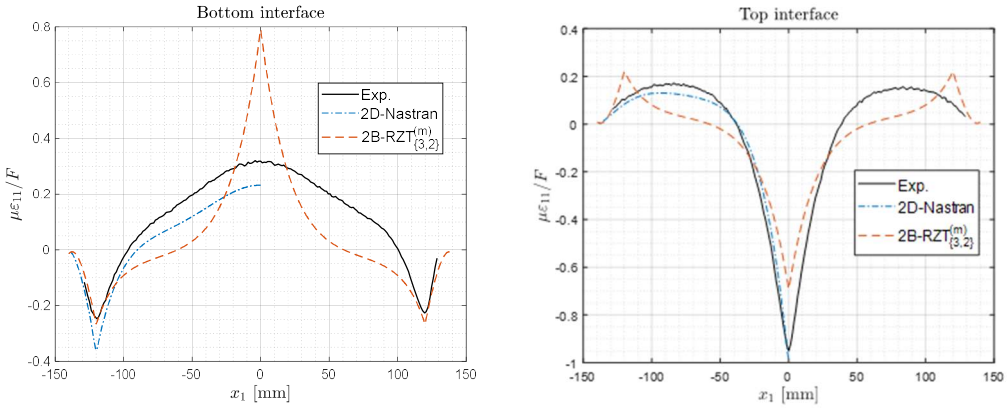

Figure 64: Axial strain distributions along the longitudinal axis for beam B04 (three-point bending).

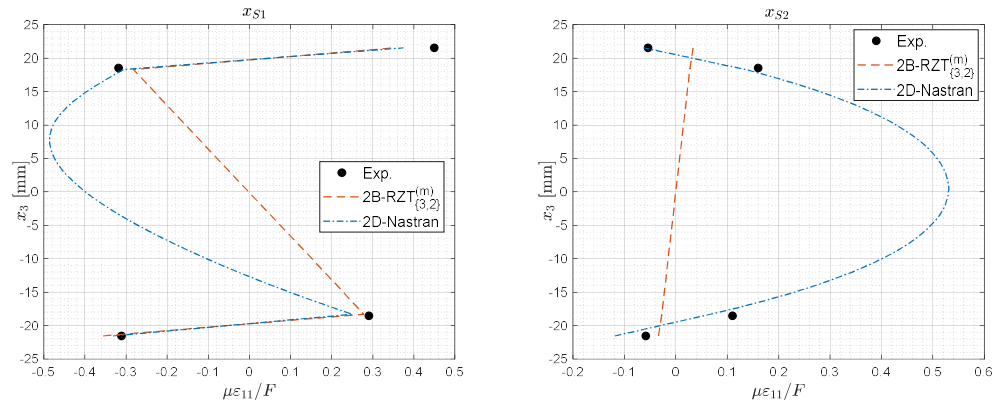

Figure 65: Through-the-thickness distributions of axial strains, beam B04, at $x_{S1} = -20mm$ and $x_{S2} = -75mm$.

For three-point bending, the 2B-RZT$^{(m)}_{\{3,2\}}$ elements are able to estimate the top and bottom central deflection with errors in some cases lower than 5%. However, the discrepancies are due to the geometry imperfections in the thickness and the material characterization uncertainties, i.e. Young's modulus in the transverse direction. However, for the first time, the longitudinal axial strains at the sandwich interfaces are evaluated and compared with the numerical models. Both Nastran and 2B-RZT$^{(m)}_{\{3,2\}}$ elements are able to predict the strain variations at the bottom and top interfaces. In particular, the 2B-RZT$^{(m)}_{\{3,2\}}$ elements are able to predict the strains in the corresponding point of the supported cylinder at the bottom interface with remarkable precision. Moreover, the zigzag effect along the transverse direction has been experimentally observed. Finally, it is important to highlight the low computational cost given by the 2B-RZT$^{(m)}_{\{3,2\}}$ elements with respect to the high-fidelity FE model.

6.4.2 Four-point bending tests

The four-point bending test is performed according to the scheme reported in Figure 66, where the strain gauges and displacements have been considered. Note that the two sections where are evaluated the axial strains at the sandwich interfaces are $x_{S1} = -20mm$ and $x_{S2} = -75mm$. Whereas, the strain gauge E5 that controls the symmetry of the loads and supported conditions is at $x = +20mm$.

As done for the three-point bending test, the average axial strain is representative of the beam behaviour.

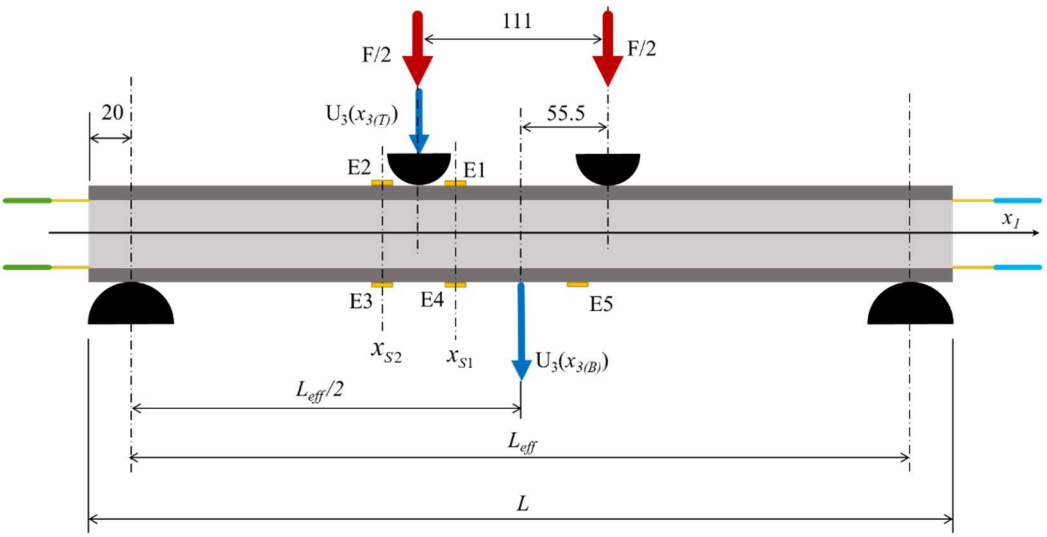

Figure 66: Scheme for four-point bending test and nomenclature for strain gauges and displacements (in mm).

The experimental results are compared with those from the mixed RZT beam finite element model and those obtained by the high-fidelity FE Nastran model. The discretizations and dof's of both 2B-RZT$^{(m)}_{\{3,2\}}$ and Nastran elements are reported in Table 28.

In Table 30, the experimental and numerical normalized displacements and corresponding percent errors are compared.

Table 30: Comparison of normalized displacements for four-point bending test between numerical and experimental, in brackets the percent errors.

Beam specimen ID	**Transverse displacement**	**Experimental**	**2B-RZT$^{(m)}_{\{3,2\}}$**
B01	$U_3(z_{(T)})$	2.881E-03	2.938E-03 (2.0)
	$U_3(z_{(B)})$	2.886E-03	2.858E-03 (-1.0)
B02	$U_3(z_{(T)})$	2.238E-03	2.070E-03 (-7.5)
	$U_3(z_{(B)})$	2.050E-03	1.991E-03 (-2.9)
B03	$U_3(z_{(T)})$	1.334E-03	1.209E-03 (-9.4)
	$U_3(z_{(B)})$	1.226E-03	1.125E-03 (-8.2)
B04	$U_3(z_{(T)})$	9.176E-04	8.907E-04 (-2.9)
	$U_3(z_{(B)})$	7.857E-04	8.047E-04 (2.4)

Figure 67, Figure 69, Figure 71 and Figure 73 report the axial strain distributions along the longitudinal beam axis at the interfaces between the IG-31 foam core layer and the Ergal face-sheets. Moreover, the through-the-thickness distributions of numerical axial strains at the two sections are compared with the experimental results provided by the optical fibre sensors and the strain gauge are shown in Figure 70, Figure 68, Figure 72 and Figure 74.

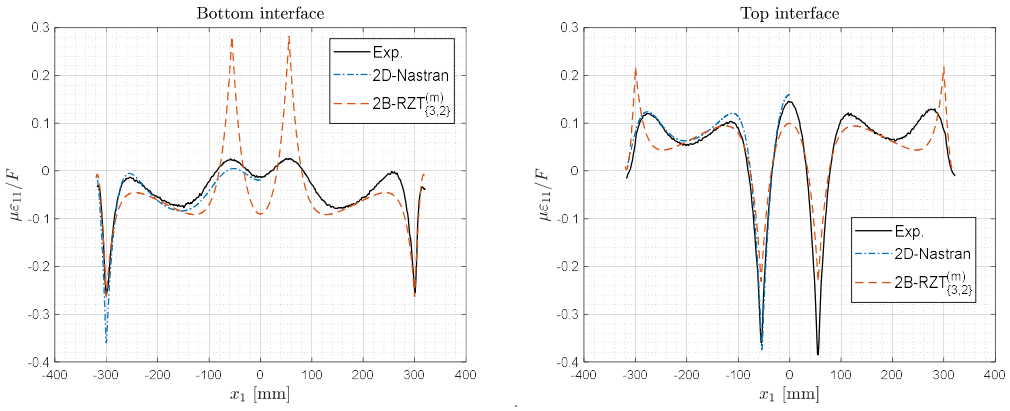

Figure 67: Axial strain distributions along the longitudinal axis for beam B01 (four-point bending).

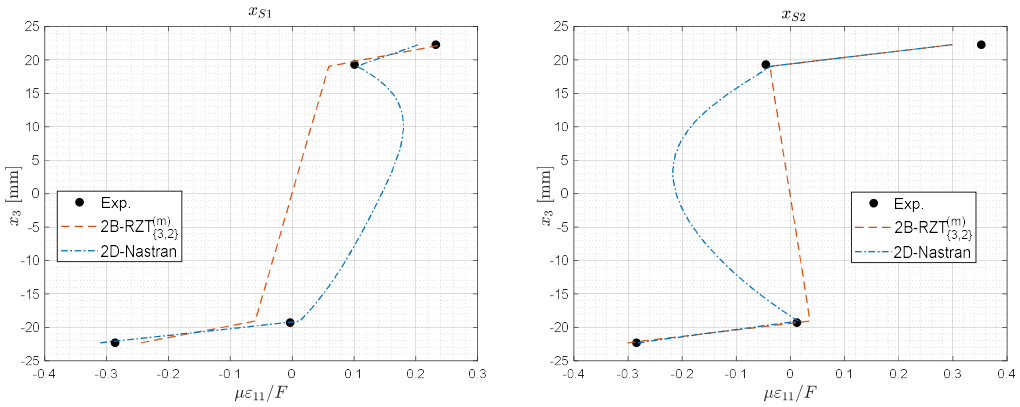

Figure 68: Through-the-thickness distributions of axial strains, beam B01, at $x_{S1} = -20mm$ and $x_{S2} = -75mm$.

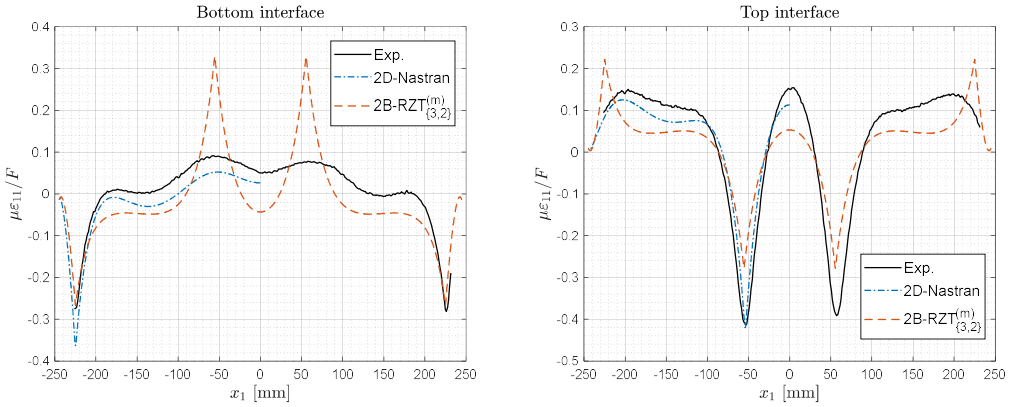

Figure 69: Axial strain distributions along the longitudinal axis for beam B02 (four-point bending).

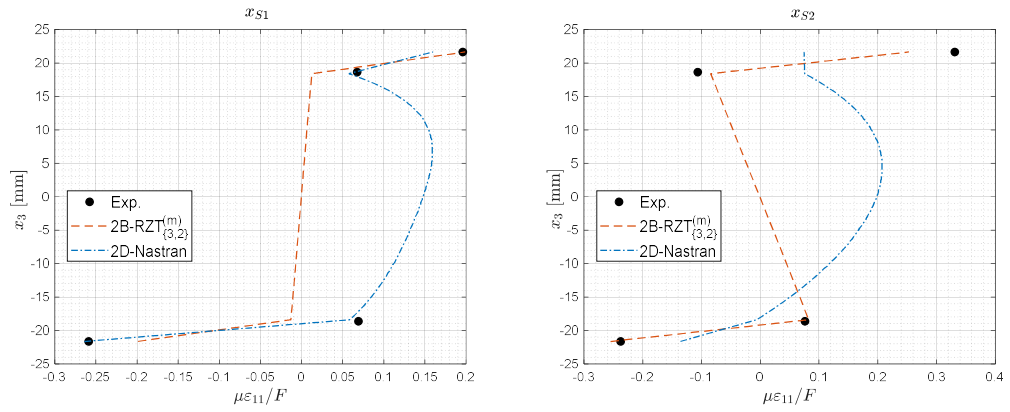

Figure 70: Through-the-thickness distributions of axial strains, beam B02, at $x_{S1} = -20mm$ and $x_{S2} = -75mm$.

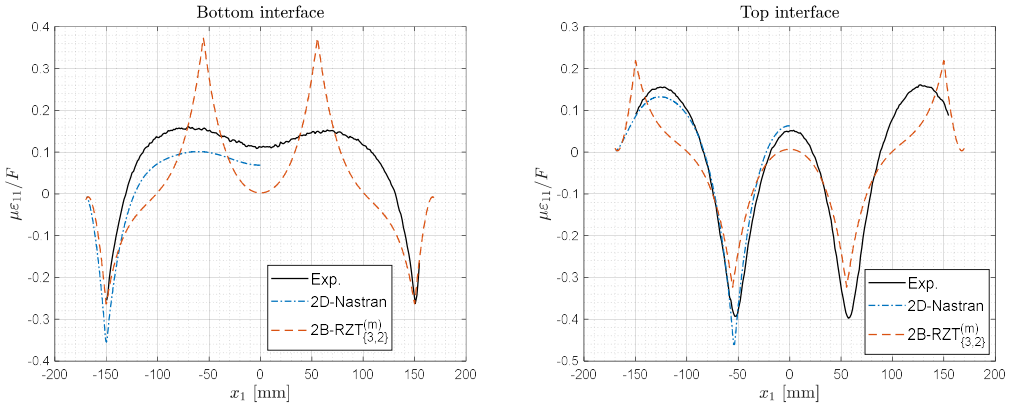

Figure 71: Axial strain distributions along the longitudinal axis for beam B03 (four-point bending).

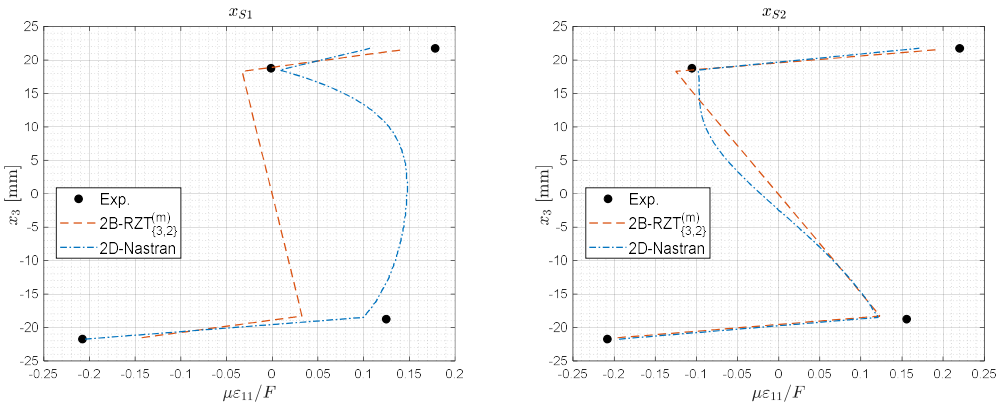

Figure 72: Through-the-thickness distributions of axial strains, beam B03, at $x_{S1} = -20mm$ and $x_{S2} = -75mm$.

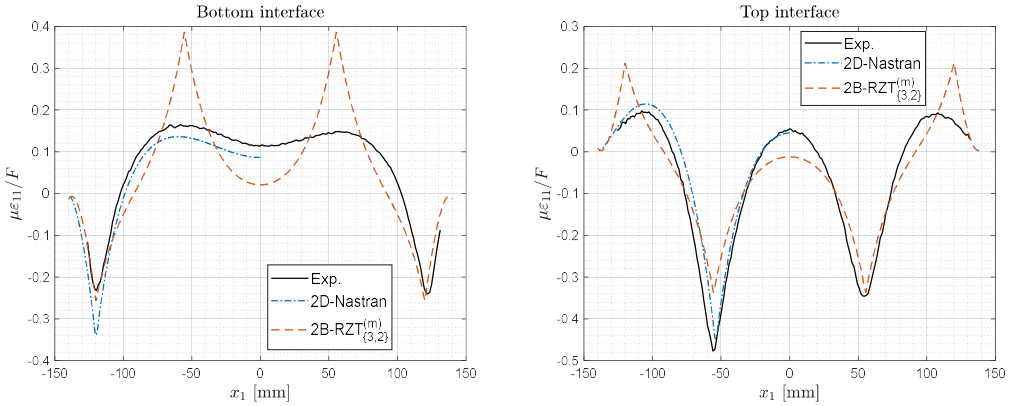

Figure 73: Axial strain distributions along the longitudinal axis for beam B04 (four-point bending).

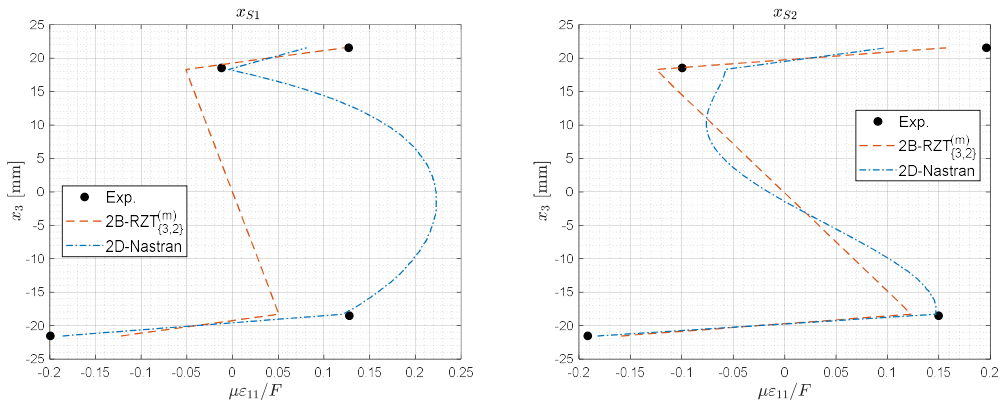

Figure 74: Through-the-thickness distributions of axial strains, beam B04, at $x_{S1} = -20mm$ and $x_{S2} = -75mm$.

The four-point bending tests' results confirm the ability of 2B-RZT$^{(m)}_{\{3,2\}}$ elements to follow the experimental deformations along the axis direction for all the beam specimens. Moreover, the errors between the experimental and numerical displacements are lower than those of the three-point bending tests. This effect is due to the lower local value of the applied force on the top beam surface. Furthermore, the ability of 2B-RZT$^{(m)}_{\{3,2\}}$ elements to predict the bottom interface strains in the area closer to the boundaries confirms the accuracy of the zigzag model with an affordable computational cost lower than the high-fidelity FE model. Finally, the numerical results provided by the through-the-thickness values of the axial strains at the two considered sections are in good agreement with the experimental ones. The discrepancies between 2B-RZT$^{(m)}_{\{3,2\}}$ elements and the experimental axial distributions at top and bottom interfaces are probably due to the symmetry distributions of the third-order zigzag functions that are only dependent on the transverse shear material properties and are insensitive to the effect of the transverse normal stress induced by the applied load as also shown for the three-point bending case.

6.5 Dynamic assessments

In this Section, the experimental results regarding the natural frequencies and the corresponding modal shapes are presented. The beam specimens D01, D02, D03 and D04 have been tested for free-free boundary conditions. The experimental modal analysis has been performed using the Laser Doppler Vibrometer (LVD) methodology. A Polytec PSV-500 scanning laser head and its frontend equipment have been used to measure the velocity responses of the

relevant scanning points without using accelerometers. The excitation force was applied using an electrodynamic shaker (K2007E01 – up to 9kHz and up to 67 N of applied force). Moreover, an impedance head (PCB Piezotronics, Inc. – model 288D01) has been glued on the beam at the excitation point to measure the force intensity and the corresponding response acceleration.

The specimens were hanged to the support system made of steel using cable ties and rubber bands to simulate the free-free boundary conditions, see Figure 75. The impedance head was glued to the beam structure and, due to the support system of the shaker, was able to excite both torsional and flexural modes. The experimental modal analysis to determine the modal parameter has been conducted on both kinds of deformation modes; however, only the results for the flexural frequencies and Frequency Response Functions (FRFs) have been considered in this assessment.

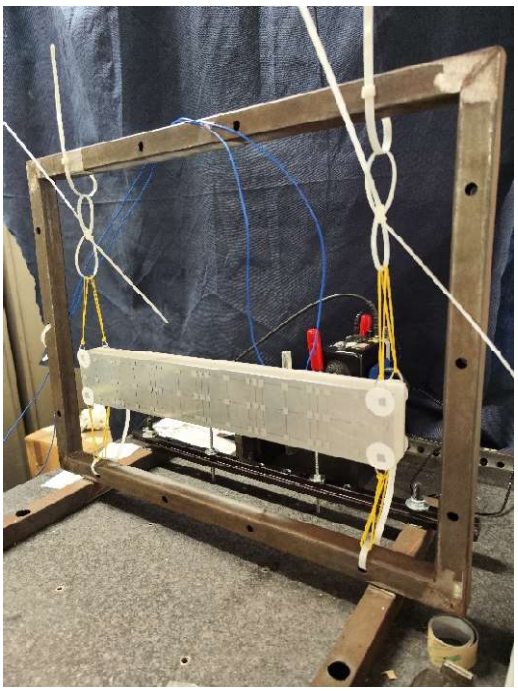

Figure 75: Experimental set-up for dynamic analysis of sandwich beams.

The scanning points are preliminary selected by a numerical modal analysis on a high-fidelity FE model using membrane QUAD4 Nastran elements. The high-fidelity FE models of the sandwich beam specimens considered for the dynamic experimental assessment (e.g. D01, D02, D03 and D04) model the entire beam length since the aim is to observe both symmetric and anti-symmetric

flexural modes. The effect of the adhesive layer is taken in consideration in the finite element models. In the Nastran model, the QUAD4 membrane elements reproduce the plane-stress condition typical of the beam structures. In the Nastran model, the coupled mass matrix has been considered in the modal analysis. In Table 31 are reported the number of 2B-RZT$^{(m)}_{\{3,2\}}$ and NASTRAN® elements considered in the dynamic assessment for each beam specimen.

Table 31: Number of elements and dof's in 2B-RZT$^{(m)}_{\{3,2\}}$ and NASTRAN® models for dynamic analysis.

	2B-RZT$^{(m)}_{\{3,2\}}$		**NASTRAN**	
Beam ID	**Number of elements**	**Dof's**	**Number of elements**	**Dof's**
D01	4096	24576	87000	175350
D02	4096	24576	41500	84344
D03	4096	24576	34000	69314
D04	4096	24576	32000	66162

The position of the scanning points along the (x_1, x_2) coordinate reference system is reported in Table 32, whereas the graphical representation is reported in Figure 76. All the points are positioned on the external top surface of the beam, i.e. $x_3 = +h/2$. The reference point 0, where the force is applied, is on the bottom surface at the coordinates $x_1 = 350mm$, $x_2 = -15mm$ and $x_3 = -h/2$.

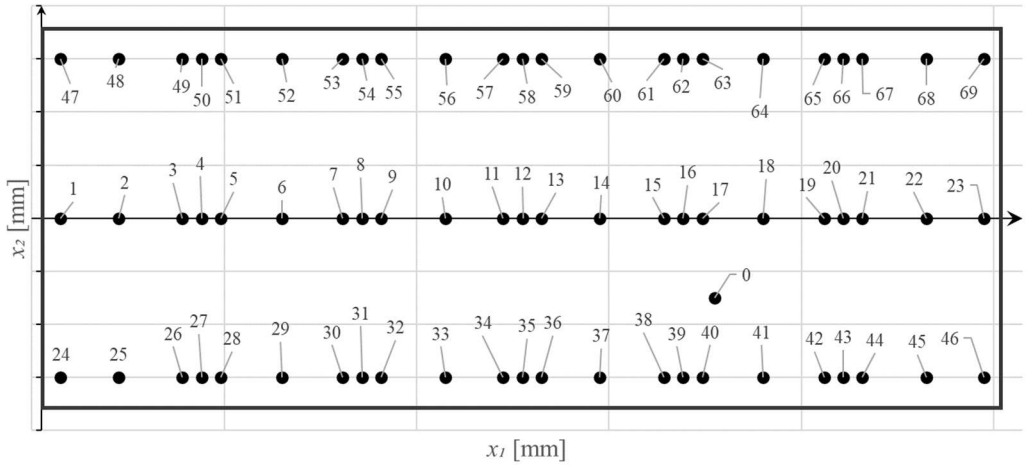

Figure 76: Scanning points representation in (x_1, x_2) plane.

Table 32: Scanning points, data are in mm.

Point ID	x_1	x_2	Point ID	x_1	x_2	Point ID	x_1	x_2
1	10	0	**24**	10	-30	**47**	10	30
2	40	0	**25**	40	-30	**48**	40	30
3	73.3	0	**26**	73.3	-30	**49**	73.3	30
4	83.3	0	**27**	83.3	-30	**50**	83.3	30
5	93.3	0	**28**	93.3	-30	**51**	93.3	30
6	125	0	**29**	125	-30	**52**	125	30
7	156.6	0	**30**	156.6	-30	**53**	156.6	30
8	166.6	0	**31**	166.6	-30	**54**	166.6	30
9	176.6	0	**32**	176.6	-30	**55**	176.6	30
10	210	0	**33**	210	-30	**56**	210	30
11	240	0	**34**	240	-30	**57**	240	30
12	250	0	**35**	250	-30	**58**	250	30
13	260	0	**36**	260	-30	**59**	260	30
14	290	0	**37**	290	-30	**60**	290	30
15	323.4	0	**38**	323.4	-30	**61**	323.4	30
16	333.4	0	**39**	333.4	-30	**62**	333.4	30
17	343.4	0	**40**	343.4	-30	**63**	343.4	30
18	375	0	**41**	375	-30	**64**	375	30
19	406.7	0	**42**	406.7	-30	**65**	406.7	30
20	416.7	0	**43**	416.7	-30	**66**	416.7	30
21	426.7	0	**44**	426.7	-30	**67**	426.7	30
22	460	0	**45**	460	-30	**68**	460	30
23	490	0	**46**	490	-30	**69**	490	30

Due to the material reflection, the quality of the laser measurements in the scanning point has been increased using reflectors. The frequency bandwidth investigated starts from 400 Hz to 4kHz since no frequencies were expected below this value. The excitation force signal is a periodic chirp function of constant amplitude. The amplitudes and the laser sensibilities have been chosen differently due to the different beam specimens. Both input force and output acceleration and velocities have been measured to compute the experimental FRFs. A complex base averaging of forty FRF scan measurements has been done to guarantee the accuracy response signal for each scanning point.

The experimental FRFs of the whole scanning points have been processed by LSM-Siemens Test.Lab. The Polymax algorithm implemented in Test.Lab and based on the least square complex exponential algorithm was performed to estimate the modal parameters. In Table 33, Table 34, Table 35 and Table 36, the experimental natural frequencies of the flexural modes up to 4kHz and those computed with 2B-RZT$^{(m)}_{\{3,2\}}$ elements are reported. The Polymax algorithm has been able to compute also the torsional modes due to the distribution of the scanning points. However, they are not considered since the numerical model cannot include the torsional modal shapes. In addition, the corresponding experimental modal damping computed using the Polymax algorithm has been reported for each flexural mode. The relative errors with the experimental results are shown in brackets, and from Figure 77 to Figure 80 are reported some of the experimental FRFs of the four beam specimens considered for the modal parameter estimation.

The new mixed-RZT beam results appear more flexible than the experimental ones. An explanation of this aspect is due to the dispersion of the material properties (Young's moduli and shear moduli) experimentally determined, which affects the numerical results. A further contribution in higher experimental frequencies than the numerical one is due to the effect of the stiffness induced by the shaker stinger. In fact, the application force point is a circular surface area of 10 mm in diameter, which constrains displacements of that point. Moreover, the cable ties and rubber bands contribute to increasing the experimental frequencies, although their mechanical properties have a minor effect. However, these effects could affect the experimental results due to their uncertainties in modelling, and mechanical characterizations are not considered in the mixed-RZT model. A further explanation is the coupling between some torsional and flexural modes observed experimentally, which could affect the experimental frequency estimation. As highlighted in Chapter 5, the numerical frequencies computed

using the 2B-RZT$^{(m)}_{\{3,2\}}$ elements are very accurate if compared with the high-fidelity FE model, with a maximum error of 2.5% for the highest flexural mode of beam D04; for this reason, the results using Nastran 2D elements are not reported. As expected, the errors between numerical and experimental results increase with flexural mode number. However, the maximum error values for higher modes do not exceed 15%, which is a remarkable result considering the large frequency range considered.

Table 33: Experimental and numerical frequencies (in Hz) of the D01 sandwich beam (in brackets, the percent errors).

Mode	**Experimental**	ζ_n	**2B-RZT$^{(m)}_{\{3,2\}}$**
1	764.95	0.68	703.67 (-8.0)
2	1277.75	1.71	1148.85 (-10.1)
3	1859.23	1.68	1635.65 (-12.0)
4	2368.74	1.81	2050.93 (-13.4)
5	2881.96	2.19	2514.79 (-12.7)
6	3348.54	1.65	2902.10 (-13.3)
7	3931.40	1.14	3374.78 (-14.2)

Table 34: Experimental and numerical frequencies (in Hz) of the D02 sandwich beam (in brackets, the percent errors).

Mode	**Experimental**	ζ_n	**2B-RZT$^{(m)}_{\{3,2\}}$**
1	794.30	1.15	734.12 (-7.6)
2	1434.06	1.66	1309.77 (-8.7)
3	2120.12	1.84	1894.03 (-10.7)
4	2768.03	1.94	2416.09 (-12.7)
5	3315.51	1.92	2956.34 (-10.8)
6	3800.49	1.92	3440.83 (-9.5)

Table 35: Experimental and numerical frequencies (in Hz) of the D03 sandwich beam (in brackets, the percent errors).

Mode	**Experimental**	ζ_n	**2B-RZT**$^{(\mathbf{m})}_{\{3,2\}}$
1	662.34	0.84	610.60 (-7.8)
2	1160.15	1.57	1035.37 (-10.8)
3	1688.45	2.08	1484.22 (-12.1)
4	2198.60	1.54	1885.44 (-14.2)
5	2659.24	1.87	2316.86 (-12.9)
6	3107.86	2.16	2713.92 (-12.7)
7	3678.10	0.84	3151.30 (-14.3)

Table 36: Experimental and numerical frequencies (in Hz) of the D04 sandwich beam (in brackets, the percent errors).

Mode	**Experimental**	ζ_n	**2B-RZT**$^{(\mathbf{m})}_{\{3,2\}}$
1	654.10	1.33	629.75 (-3.7)
2	1287.40	1.42	1175.62 (-8.7)
3	1942.27	1.79	1721.04 (-11.4)
4	2568.28	1.97	2222.18 (-13.5)
5	3094.25	1.98	2727.28 (-11.9)
6	3683.74	1.92	3203.43 (-13.0)

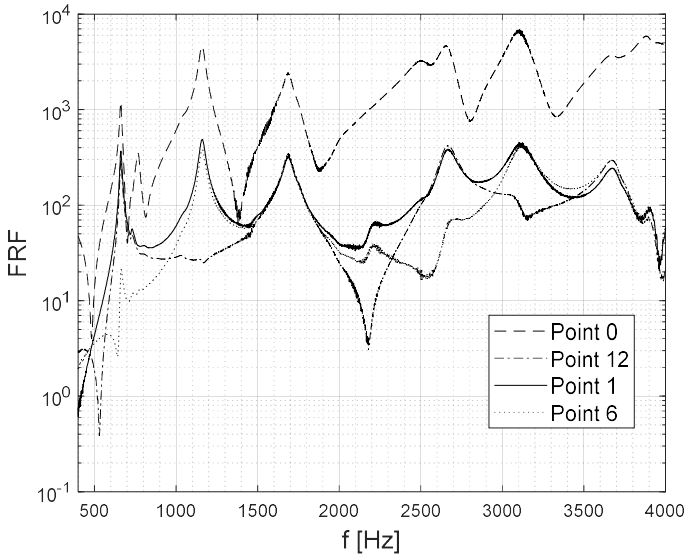

Figure 77: Experimental Frequency Response Functions (FRFs) of beam specimen D01.

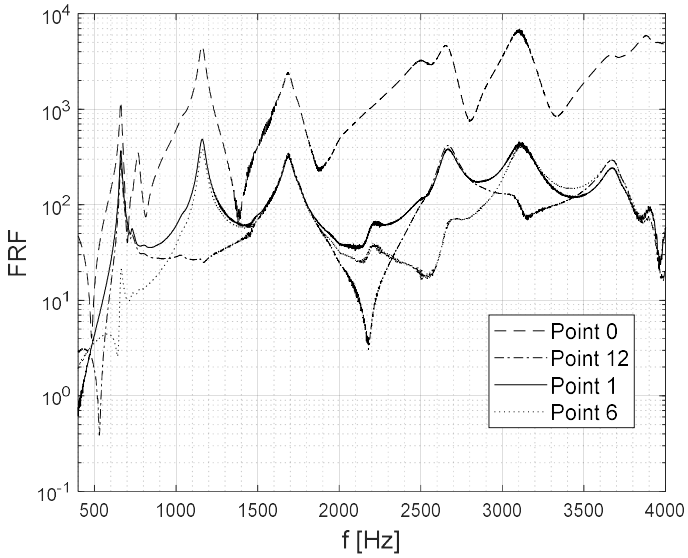

Figure 78: Experimental Frequency Response Functions (FRFs) of beam specimen D02.

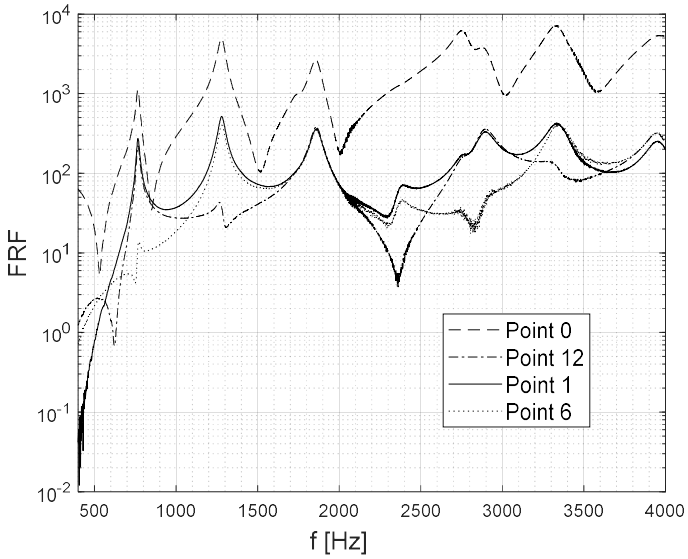

Figure 79: Experimental Frequency Response Functions (FRFs) of beam specimen D03.

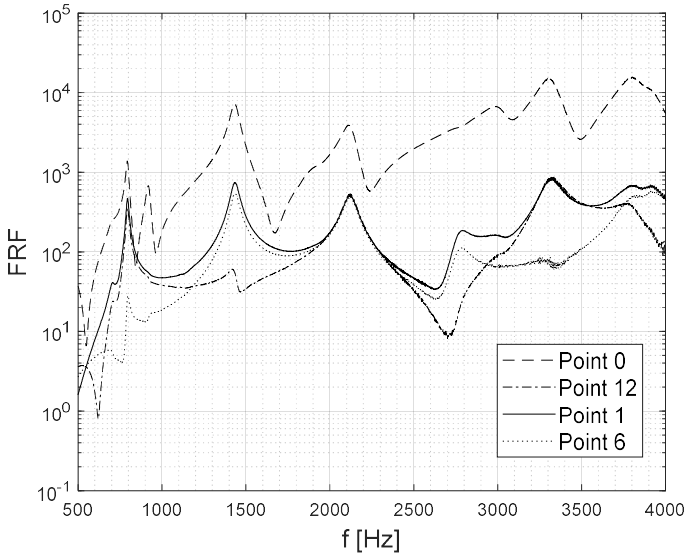

Figure 80: Experimental Frequency Response Functions (FRFs) of beam specimen D04.

Chapter 7

Concluding remarks

The research work presented in this Thesis is devoted to the refined zigzag model formulations, numerical assessments and experimental validations. The theoretical zigzag models formulated in Chapters 2-4 are numerically assessed in Chapter 5 for various problems, static and dynamic. In Chapter 6, an experimental campaign is conducted to evaluate global and local quantities responses to compare with the numerical results provided by the newly formulated models.

The starting point of this research activity has been represented by the structural models available in the current literature. In Chapter 1, a detailed overview of the existing structural theories for structural analysis in the aerospace engineering field has been presented. Among them, the zigzag models represent an interesting field of investigation thanks to their accuracy compared to the reduced computational cost.

In the recent literature, the Refined Zigzag Theory (RZT) has represented a valuable alternative in the structural analysis of multilayered composite and sandwich structures. Thanks to its formulation, the global first-order kinematics have been improved with appropriate zigzag functions, allowing a layer-wise description of the in-plane displacements and more accurate in-plane strain and stress distributions. The through-the-thickness piecewise constant distribution with jumps at the interfaces of the shear stress is able to predict the global response of the multilayered structure without involving any shear correction factor. Moreover, if computed by integrating Cauchy's equations and compared

with the three-dimensional elasticity solution, the obtained shear stress distributions have demonstrated to describe the transverse shear deformability with higher precision than the FSDT. Moreover, thanks to the partial fulfilment of transverse shear stress continuities at the layer interfaces, the RZT do not encounter the same inconsistencies as the ZZT in transverse shear stress evaluation at the clamped edge. From the provided literature, the transverse stresses (shear and normal) of the RZT could be improved by using the mixed formulation. With particular attention to Reissner's Mixed Variational Theorem (RMVT), some mixed versions of the RZT have been developed and applied to the analysis of the multilayered cross-ply and sandwich beam/plates.

However, it has been highlighted that a class of laminates, the angle-ply multilayered structures, in which the lamination angles assume the same absolute value for each layer, cannot be investigated by the RZT. In fact, the RZT standard formulation of the zigzag function is not able to predict the transverse shear coupling induced by the material anisotropy of the lamination scheme. As a result, the RZT degenerates into the FSDT model. The generally adopted procedure to make the RZT useable is to slightly modify the lamination angle of each layer; however, this numerical strategy does not solve a problem insight in the model formulation.

Taking inspiration from the literature on the previously developed zigzag models and from the works on the transverse shear coupling in anisotropic multilayered structures, in Chapter 2, the Refined Zigzag Theory has been enriched with two additional zigzag functions able to couple the in-plane local displacement refinement. The new enhanced zigzag functions are formulated according to the standard procedure that defines their zigzag slopes through the partial enforcement of the transverse shear stress continuity at the layer interfaces and the vanishing condition at the top and bottom external surfaces. The governing equations and consistent boundary conditions have been formulated for the static and dynamic analysis of more general laminated plates. In Chapter 5, the new enhanced-Refined Zigzag Theory (en-RZT) is assessed for the static bending, stability and free vibration problems to investigate the benefits and relative limitations. The numerical comparisons on the evaluation of the enhanced zigzag function reveal that the new enhanced model is a generalization of the standard RZT. In fact, for multilayered cross-ply and sandwich plates, the standard RZT kinematics is re-obtained since the new coupling zigzag functions are null. This result should not be surprising since, for such cases, the transverse shear coupling induced by the material anisotropy is not present, and the enhanced formulation is

capable of including the particular one. The numerical results also reveal the accuracy of the en-RZT model in displacement and stress predictions for multilayered symmetric and anti-symmetric angle-ply structures. The analytical solutions provided for the simply-supported cases are considered benchmark solutions enriching the list of cases treated in literature and possible comparisons. With respect to other zigzag or higher-order models, the en-RZT is able to provide the same degree of accuracy in predicting global quantities and through-the-thickness distributions. From the results provided in Chapter 5, the en-RZT provides superior prediction capabilities over the FSDT and the TSDT.

Consistent with the en-RZT assumptions, the transverse shear stress distribution computed using the constitutive material relation is a piecewise constant function with jumps at the interfaces. In an average sense, it provides an accurate global description of the transverse shear deformability, but it is not able to ensure the transverse shear stress continuity. Moreover, the model assumes a transverse displacement that is uniform along the whole laminate thickness, which is not able to describe the transverse normal deformability typical of thick multilayered and sandwich structures. As anticipated, a mixed version of the RZT has been formulated in conjunction with using the RMVT to analyse multilayered composite and sandwich thick structures. However, the hypothesis of cylindrical bending is necessary to avoid inconsistencies in transverse shear stress predictions due to the weak enforcement of transverse shear strain compatibilities. This hypothesis to determine the expression of the assumed transverse shear stresses cannot be applied to the multilayered anisotropic plates in which the effect of transverse shear coupling is not negligible. Therefore, it has been necessary to formulate a new mixed model based on the enhanced zigzag kinematics.

In Chapter 3, a novel higher-order zigzag model is proposed. Among the aims of this research activity, one represents the inclusion of the non-linear trough-the-thickness distribution of the displacement field. This nonlinearity is typically encountered for thick multilayered composite and sandwich structures. Starting from the en-RZT kinematics, the displacement field is enriched with through-the-thickness parabolic and cubic contributions for the in-plane displacement and linear and parabolic contributions for the transverse displacement. The total number of kinematic variables is reduced by taking advantage of the partial fulfilment of the transverse shear stress continuity at the layer interfaces and a further condition on the partial null in-plane traction conditions at the top and bottom surfaces. The resulting displacement field has a new set of third-order enhanced zigzag functions. The transverse normal and shear

stresses are assumed independently from the displacement field. More specifically, the transverse normal stress is assumed as a smeared cubic through-the-thickness continuous function that satisfies the traction condition at the top and bottom external surfaces. The assumed transverse shear stresses are obtained from integrating Cauchy's equations without any simplifications. The variational statement involves the Hellinger-Reissner principle since a new set of strain variables is used to interpolate the assumed transverse shear stresses. In addition, a new penalty term is added to the governing functional to enforce the compatibility conditions with the strains derived from the displacement field. Finally, the governing equations and consistent boundary conditions of the new $\text{en-RZT}^{(m)}_{\{3,2\}}$ model are derived and specialized for the static bending and free vibration problems. In Chapter 5, the governing equations of $\text{en-RZT}^{(m)}_{\{3,2\}}$ model are solved analytically for simply-supported multilayered cross-ply/angle-ply and sandwich plates. The provided results show the accuracy of the newly mixed model in displacements and through-the-thickness stress predictions if compared with the available three-dimensional solutions. More specifically, the transverse shear and normal stress distributions are very accurate, even for very thick multilayered plates and, for the first time, also for multilayered angle-ply plates. Furthermore, the accuracy in dynamic analysis has been confirmed by the results on the natural frequencies that agree with three-dimensional results.

In Chapter 4, the $\text{en-RZT}^{(m)}_{\{3,2\}}$ model has been restricted to the analysis of beam structures. The obtained displacement field is formally equivalent to Iurlaro's third-order RZT kinematics; however, the variational statement is the same as the new $\text{en-RZT}^{(m)}_{\{3,2\}}$ model, including the Hellinger-Reissner and penalty terms for the weak strain compatibilities. In addition, the governing equations and consistent boundary conditions are specified for the beam problems and solved for some numerical examples in Chapter 5. The results confirm the predictivity capabilities and transverse normal and shear stress distributions due to the mixed formulation via the HR principle. Furthermore, remarkably accurate results have also been obtained for the free vibration problems.

A finite element formulation is proposed in Chapter 4 to investigate multilayered thick beam structures under the action of concentrated forces on the top surface. Two beam elements are formulated, $\text{2B-RZT}^{(m)}_{\{3,2\}}$ and $\text{2Bc-RZT}^{(m)}_{\{3,2\}}$, with different interpolation strategies for the kinematic and strain variables. The linear Lagrangian shape functions have been used for $\text{2B-RZT}^{(m)}_{\{3,2\}}$ element,

whereas an anisotropic-constrained strategy with Serendipity shape functions has been considered for the $2\text{Bc-RZT}^{(m)}_{\{3,2\}}$ element. Both elements have been assessed in Chapter 5. They are able to give the same results in terms of displacements, natural frequencies and strain distributions for the investigated numerical cases. The free vibration study on the element behaviours reveals the accuracy of frequency prediction when the model is compared with other high-fidelity FE models. However, it has also been revealed that for static problems, the effect of transverse normal deformability induced by concentrated loads is more complex to investigate. However, the solution regarding displacements and axial strains is quite accurate except for the area next to the applied force.

Finally, in Chapter 6, an experimental campaign is conducted on a different series of thick sandwich beams considering different length-to-thickness ratios, foam core materials and boundary conditions. For the first time, the results of the axial strains at the interfaces between the sandwich core and face-sheets are measured and compared with the newly zigzag elements. Thanks to the fibre optic sensors, the axial deformation can be measured along the longitudinal beam axis. Three- and four-point bending tests have been performed to evaluate deflections and strains. The provided results highlight the ability of the new RZT mixed model to predict accurately at the bottom interfaces the axial deformations in the boundary area and the top interface axial deformations close to the applied force. It is a remarkable result since the number of dof's involved in using the $2\text{B-RZT}^{(m)}_{\{3,2\}}$ elements is fifteen times lower than the high-fidelity FE models. An experimental modal analysis has been conducted using the Laser-Doppler-Vibrometer to evaluate the natural frequencies of another set of thick sandwich beam specimens. The experimental results have revealed that the beam exhibits a stiffer behaviour with respect to the $2\text{B-RZT}^{(m)}_{\{3,2\}}$ elements; however, due to the accuracy of the dynamic analysis presented in Chapter 5, the discrepancies are due to the standard variation of the mechanical properties of the beam and the disturbed induced by boundary conditions adopted in the experimental tests. The provided numerical results agree with the experimental ones for a wide range of frequencies investigated with limited errors on the wide range of frequencies investigated.

The research activity herein presented, supported by the numerical and experimental results, wants to offer a more general and complete methodology based on the refined zigzag models to investigate multilayered composite and sandwich structures. In particular, the newly formulated models could be used to

analyse structures in which the material transverse anisotropy is not negligible. Moreover, the mixed formulation of the new models could be used to investigate even thick multilayered structures. The formulated elements make these new mixed models appealing in their predictivity capabilities and affordable low computational cost compared to other available models.

References

[1] Reddy JN. Mechanics of Laminated Composite Plates and Shells : Theory and Analysis. 2nd ed. CRC Press; 2003. https://doi.org/10.1201/b12409.

[2] Jones RM. Mechanics of Composite Materials. CRC Press; 1999. https://doi.org/10.1201/9781498711067.

[3] Pagano NJ. Exact Solutions for Composite Laminates in Cylindrical Bending. Journal of Composite Materials 1969;3:398–411. https://doi.org/10.1177/002199836900300304.

[4] Pagano NJ. Exact Solutions for Rectangular Bidirectional Composites and Sandwich Plates. Journal of Composite Materials 1970;4:20–34. https://doi.org/10.1177/002199837000400102.

[5] Pagano NJ. Influence of Shear Coupling in Cylindrical Bending of Anisotropic Laminates. Journal of Composite Materials 1970;4:330–43. https://doi.org/10.1177/002199837000400305.

[6] Pagano N j., Hatfield HJ. Elastic Behavior of Multilayered Bidirectional Composites. AIAA Journal 1972;10:931–3. https://doi.org/10.2514/3.50249.

[7] Zenkour AM. Three-dimensional Elasticity Solution for Uniformly Loaded Cross-ply Laminates and Sandwich Plates. Journal of Sandwich Structures & Materials 2007;9:213–38. https://doi.org/10.1177/1099636207065675.

[8] Srinivas S, Joga Rao CV, Rao AK. An exact analysis for vibration of simply-supported homogeneous and laminated thick rectangular plates. Journal of Sound and Vibration 1970;12:187–99. https://doi.org/10.1016/0022-460X(70)90089-1.

[9] Srinivas S, Rao AK. Bending, vibration and buckling of simply supported thick orthotropic rectangular plates and laminates. International Journal of Solids and Structures 1970;6:1463–81. https://doi.org/10.1016/0020-7683(70)90076-4.

[10] Srinivas S, Joga Rao CV, Rao AK. Some Results From an Exact Analysis of Thick Laminates in Vibration and Buckling. Journal of Applied Mechanics 1970;37:868–70. https://doi.org/10.1115/1.3408626.

[11] Srinivas S, Rao AK. A three-dimensional solution for plates and laminates. Journal of the Franklin Institute 1971;291:469–81. https://doi.org/10.1016/0016-0032(71)90004-4.

[12] Noor AK, Burton WS. Three-Dimensional Solutions for Antisymmetrically Laminated Anisotropic Plates. J Appl Mech 1990;57:182–8. https://doi.org/10.1115/1.2888300.

[13] Savoia M, Reddy JN. A Variational Approach to Three-Dimensional Elasticity Solutions of Laminated Composite Plates. J Appl Mech 1992;59:S166–75. https://doi.org/10.1115/1.2899483.

[14] Brischetto S. Exact three-dimensional static analysis of single- and multi-layered plates and shells. Composites Part B: Engineering 2017;119:230–52. https://doi.org/10.1016/j.compositesb.2017.03.010.

[15] Brischetto S. A general exact elastic shell solution for bending analysis of functionally graded structures. Composite Structures 2017;175:70–85. https://doi.org/10.1016/j.compstruct.2017.04.002.

[16] Washizu K. Variational methods in elasticity and plasticity. Second. Pergamon Press; 1975.

[17] Yunhua L, Eriksson A. An alternative assumed strain method. Computer Methods in Applied Mechanics and Engineering 1999;178:23–37. https://doi.org/10.1016/S0045-7825(99)00002-X.

[18] Wisniewski K, Turska E. Four-node mixed Hu–Washizu shell element with drilling rotation. International Journal for Numerical Methods in Engineering 2012;90:506–36. https://doi.org/10.1002/nme.3335.

[19] Zhen W, Wanji C. A global higher-order zig-zag model in terms of the HW variational theorem for multilayered composite beams. Composite Structures 2016;158:128–36. https://doi.org/10.1016/j.compstruct.2016.09.021.

[20] Icardi U, Urraci A. Novel HW mixed zig-zag theory accounting for transverse normal deformability and lower-order counterparts assessed by old and new elastostatic benchmarks. Aerospace Science and Technology 2018;80:541–71. https://doi.org/10.1016/j.ast.2018.07.040.

[21] Icardi U, Urraci A. Elastostatic assessment of several mixed/displacement-based laminated plate theories, differently accounting for transverse normal deformability. Aerospace Science and Technology 2020;98:105651. https://doi.org/10.1016/j.ast.2019.105651.

[22] Urraci A. Development of accurate and efficient structural models for analysis of multilayered and sandwich structures of industrial interest. PhD Thesis. Politecnico di Torino, 2020.

[23] Reissner E. On a Variational Theorem in Elasticity. Journal of Mathematics and Physics 1950;29:90–5. https://doi.org/10.1002/sapm195029190.

[24] Reissner E. On a mixed variational theorem and on shear deformable plate theory. International Journal for Numerical Methods in Engineering 1986;23:193–8. https://doi.org/10.1002/nme.1620230203.

[25] Reissner E. On a Certain Mixed Variational Theorem and on Laminated Elastic Shell Theory. In: Elishakoff I, Irretier H, editors. Refined Dynamical Theories of Beams, Plates and Shells and Their Applications, Berlin, Heidelberg: Springer; 1987, p. 17–27. https://doi.org/10.1007/978-3-642-83040-2_2.

[26] Auricchio F, Sacco E. Refined First-Order Shear Deformation Theory Models for Composite Laminates. J Appl Mech 2003;70:381–90. https://doi.org/10.1115/1.1572901.

[27] Abrate S, Di Sciuva M. Equivalent single layer theories for composite and sandwich structures: A review. Composite Structures 2017;179:482–94. https://doi.org/10.1016/j.compstruct.2017.07.090.

[28] Sayyad AS, Ghugal YM. Bending, buckling and free vibration of laminated composite and sandwich beams: A critical review of literature. Composite Structures 2017;C:486–504. https://doi.org/10.1016/j.compstruct.2017.03.053.

[29] Reissner E. The Effect of Transverse Shear Deformation on the Bending of Elastic Plates. ASME Journal of Applied Mechanics 1945;12:A69–77.

[30] Cowper GR. The Shear Coefficient in Timoshenko's Beam Theory. J Appl Mech 1966;33:335–40. https://doi.org/10.1115/1.3625046.

[31] Whitney JM. Shear Correction Factors for Orthotropic Laminates Under Static Load. J Appl Mech 1973;40:302–4. https://doi.org/10.1115/1.3422950.

[32] Hutchinson JR. Shear Coefficients for Timoshenko Beam Theory. Journal of Applied Mechanics 2000;68:87–92. https://doi.org/10.1115/1.1349417.

[33] Madabhusi-Raman P, Davalos JF. Static shear correction factor for laminated rectangular beams. Composites Part B: Engineering 1996;27:285–93. https://doi.org/10.1016/1359-8368(95)00014-3.

[34] Oñate E. Structural Analysis with the Finite Element Method. Linear Statics: Volume 2: Beams, Plates and Shells. Springer Netherlands; 2013.

[35] Zienkiewicz OC, Taylor RL, Too JM. Reduced integration technique in general analysis of plates and shells. International Journal for Numerical Methods in Engineering 1971;3:275–90. https://doi.org/10.1002/nme.1620030211.

[36] Hughes TJR, Taylor RL, Kanoknukulchai W. A simple and efficient finite element for plate bending. International Journal for Numerical Methods in Engineering 1977;11:1529–43. https://doi.org/10.1002/nme.1620111005.

[37] Hughes TJR, Cohen M, Haroun M. Reduced and selective integration techniques in the finite element analysis of plates. Nuclear Engineering and Design 1978;46:203–22. https://doi.org/10.1016/0029-5493(78)90184-X.

[38] Pugh EDL, Hinton E, Zienkiewicz OC. A study of quadrilateral plate bending elements with 'reduced' integration. International Journal for Numerical Methods in Engineering 1978;12:1059–79. https://doi.org/10.1002/nme.1620120702.

[39] Belytschko T, Jame Shau-Jen Ong, Wing Kam Liu. A consistent control of spurious singular modes in the 9-node Lagrange element for the laplace and Mindlin plate equations. Computer Methods in Applied Mechanics and Engineering 1984;44:269–95. https://doi.org/10.1016/0045-7825(84)90133-6.

[40] Belytschko T, Leviathan I. Physical stabilization of the 4-node shell element with one point quadrature. Computer Methods in Applied Mechanics and Engineering 1994;113:321–50. https://doi.org/10.1016/0045-7825(94)90052-3.

[41] Katili I. A new discrete Kirchhoff-Mindlin element based on Mindlin-Reissner plate theory and assumed shear strain fields—part I: An extended DKT element for thick-plate bending analysis. International Journal for Numerical Methods in Engineering 1993;36:1859–83. https://doi.org/10.1002/nme.1620361106.

[42] Batoz J-L, Bathe K-Jür, Ho L-W. A study of three-node triangular plate bending elements. International Journal for Numerical Methods in Engineering 1980;15:1771–812. https://doi.org/10.1002/nme.1620151205.

[43] Bathe K-J, Dvorkin EN. A formulation of general shell elements—the use of mixed interpolation of tensorial components. International Journal for Numerical Methods in Engineering 1986;22:697–722. https://doi.org/10.1002/nme.1620220312.

[44] Bathe K, Luiz Bucalem M, Brezzi F. Displacement and stress convergence of our MITC plate bending elements. Engineering Computations 1990;7:291–302. https://doi.org/10.1108/eb023816.

[45] Bathe K-J. Finite element procedures. 2nd ed. Englewood Cliffs, N.J: Prentice-Hall; 1996.

[46] Bathe K-J, Iosilevich A, Chapelle D. An evaluation of the MITC shell elements. Computers & Structures 2000;75:1–30. https://doi.org/10.1016/S0045-7949(99)00214-X.

[47] Simo JC, Rifai MS. A class of mixed assumed strain methods and the method of incompatible modes. International Journal for Numerical Methods in Engineering 1990;29:1595–638. https://doi.org/10.1002/nme.1620290802.

[48] Tessler A, Dong SB. On a hierarchy of conforming timoshenko beam elements. Computers & Structures 1981;14:335–44. https://doi.org/10.1016/0045-7949(81)90017-1.

[49] Tessler A, Hughes TJR. An improved treatment of transverse shear in the Mindlin-type four-node quadrilateral element. Computer Methods in Applied Mechanics and Engineering 1983;39:311–35. https://doi.org/10.1016/0045-7825(83)90096-8.

[50] Tessler A, Hughes TJR. A three-node Mindlin plate element with improved transverse shear. Computer Methods in Applied Mechanics and Engineering 1985;50:71–101. https://doi.org/10.1016/0045-7825(85)90114-8.

[51] Tessler A, Spiridigliozzi L. Curved beam elements with penalty relaxation. International Journal for Numerical Methods in Engineering 1986;23:2245–62. https://doi.org/10.1002/nme.1620231207.

[52] Tessler A, Spiridigliozzi L. Resolving membrane and shear locking phenomena in curved shear-deformable axisymmetric shell elements. International Journal for Numerical Methods in Engineering 1988;26:1071–86. https://doi.org/10.1002/nme.1620260506.

[53] Auricchio F, Sacco E. Partial-mixed formulation and refined models for the analysis of composite laminates within an FSDT. Composite Structures 1999;46:103–13. https://doi.org/10.1016/S0263-8223(99)00035-5.

[54] Reddy JN. A Simple Higher-Order Theory for Laminated Composite Plates. J Appl Mech 1984;51:745–52. https://doi.org/10.1115/1.3167719.

[55] Reddy JN. A refined nonlinear theory of plates with transverse shear deformation. International Journal of Solids and Structures 1984;20:881–96. https://doi.org/10.1016/0020-7683(84)90056-8.

[56] Groh RMJ, Weaver PM. Static inconsistencies in certain axiomatic higher-order shear deformation theories for beams, plates and shells. Composite Structures 2015;120:231–45. https://doi.org/10.1016/j.compstruct.2014.10.006.

[57] Di Sciuva M. On the Equivalence of Displacement-Based Third-Order Shear Deformation Plate Theories. Journal of Engineering Mechanics 2019;145:04019044. https://doi.org/10.1061/(ASCE)EM.1943-7889.0001616.

[58] Touratier M. An efficient standard plate theory. International Journal of Engineering Science 1991;29:901–16. https://doi.org/10.1016/0020-7225(91)90165-Y.

[59] Soldatos KP. A transverse shear deformation theory for homogeneous monoclinic plates. Acta Mechanica 1992;94:195–220. https://doi.org/10.1007/BF01176650.

[60] Karama M, Afaq KS, Mistou S. A new theory for laminated composite plates. Proceedings of the IMechE 2009;223:53–62. https://doi.org/10.1243/14644207JMDA189.

[61] Sarangan S, Singh BN. Higher-order closed-form solution for the analysis of laminated composite and sandwich plates based on new shear deformation theories. Composite Structures 2016;138:391–403. https://doi.org/10.1016/j.compstruct.2015.11.049.

[62] Carrera E. Theories and Finite Elements for Multilayered Plates and Shells:A Unified compact formulation with numerical assessment and benchmarking. ARCO 2003;10:215–96. https://doi.org/10.1007/BF02736224.

[63] Carrera E, Giunta G. Refined beam theories based on a unified formulation. Int J Appl Mechanics 2010;02:117–43. https://doi.org/10.1142/S1758825110000500.

[64] Neves AMA, Ferreira AJM, Carrera E, Roque CMC, Cinefra M, Jorge RMN, et al. A quasi-3D sinusoidal shear deformation theory for the static and free vibration analysis of functionally graded plates. Composites Part B: Engineering 2012;43:711–25. https://doi.org/10.1016/j.compositesb.2011.08.009.

[65] Fazzolari FA, Carrera E. Free vibration analysis of sandwich plates with anisotropic face sheets in thermal environment by using the hierarchical trigonometric Ritz formulation. Composites Part B: Engineering 2013;50:67–81. https://doi.org/10.1016/j.compositesb.2013.01.020.

[66] Tornabene F, Fantuzzi N, Viola E, Carrera E. Static analysis of doubly-curved anisotropic shells and panels using CUF approach, differential geometry and differential quadrature method. Composite Structures 2014;107:675–97. https://doi.org/10.1016/j.compstruct.2013.08.038.

[67] Alesadi A, Galehdari M, Shojaee S. Free vibration and buckling analysis of composite laminated plates using layerwise models based on isogeometric approach and Carrera unified formulation. Mechanics of Advanced Materials and Structures 2018;25:1018–32. https://doi.org/10.1080/15376494.2017.1342883.

[68] Carrera E, Cinefra M, Li G. Refined finite element solutions for anisotropic laminated plates. Composite Structures 2018;183:63–76. https://doi.org/10.1016/j.compstruct.2017.01.014.

[69] Pagani A, Carrera E. Unified formulation of geometrically nonlinear refined beam theories. Mechanics of Advanced Materials and Structures 2018;25:15–31. https://doi.org/10.1080/15376494.2016.1232458.

[70] Carrera E, Zozulya VV. Carrera unified formulation (CUF) for shells of revolution. I. Higher-order theory. Acta Mech 2023;234:109–36. https://doi.org/10.1007/s00707-022-03372-7.

[71] Demasi L. ∞^3 Hierarchy plate theories for thick and thin composite plates: The generalized unified formulation. Composite Structures 2008;84:256–70. https://doi.org/10.1016/j.compstruct.2007.08.004.

[72] Demasi L. ∞^6 Mixed plate theories based on the Generalized Unified Formulation. Part I: Governing equations. Composite Structures 2009;87:1–11. https://doi.org/10.1016/j.compstruct.2008.07.013.

[73] Demasi L. ∞^6 Mixed plate theories based on the Generalized Unified Formulation. Part V: Results. Composite Structures 2009;88:1–16. https://doi.org/10.1016/j.compstruct.2008.07.009.

[74] Petrolo M, Carrera E, Cinefra M, Zappino E. Finite Element Analysis of Structures through Unified Formulation. John Wiley & Sons; 2014.

[75] Abrate S, Di Sciuva M. Multilayer Models for Composite and Sandwich Structures. In: Beaumont PWR, Zweben CH, editors. Comprehensive Composite Materials II, Elsevier; 2018, p. 399–425. https://doi.org/10.1016/B978-0-12-803581-8.09885-4.

[76] Li D. Layerwise Theories of Laminated Composite Structures and Their Applications: A Review. Arch Computat Methods Eng 2021;28:577–600. https://doi.org/10.1007/s11831-019-09392-2.

[77] Ambartsumyan SA. On a general theory of anisotropic shells. Journal of Applied Mathematics and Mechanics 1958;22:305–19. https://doi.org/10.1016/0021-8928(58)90108-4.

[78] Whitney JM. The Effect of Transverse Shear Deformation on the Bending of Laminated Plates. Journal of Composite Materials 1969;3:534–47. https://doi.org/10.1177/002199836900300316.

[79] Di Sciuva M. A refinement of the transverse shear deformation theory for multilayered orthotropic plates. Proc. of AIDAA VII National Conference, vol. I, Napoli: 1983, p. 83–95.

[80] Di Sciuva M. A refined transverse shear deformation theory for multilayered anisotropic plates. Atti Accademia Delle Scienze Di Torino 1984;118:279–95.

[81] Di Sciuva M. Development of an anisotropic, multilayered, shear-deformable rectangular plate element. Computers & Structures 1985;21:789–96. https://doi.org/10.1016/0045-7949(85)90155-5.

[82] Di Sciuva M, Cicorello A, Dalle Mura V. A class of multilayered anisotropic plate elements including the effects of transverse shear deformability. vol. II, Torino: 1985, p. 877–92.

[83] Di Sciuva M. Bending, vibration and buckling of simply supported thick multilayered orthotropic plates: An evaluation of a new displacement model. Journal of Sound and Vibration 1986;105:425–42. https://doi.org/10.1016/0022-460X(86)90169-0.

[84] Di Sciuva M. Multilayered anisotropic plate models with continuous interlaminar stresses. Composite Structures 1992;22:149–67. https://doi.org/10.1016/0263-8223(92)90003-U.

[85] Cho M, Parmerter RR. An efficient higher-order plate theory for laminated composites. Composite Structures 1992;20:113–23. https://doi.org/10.1016/0263-8223(92)90067-M.

[86] Cho M, Parmerter R. Efficient higher order composite plate theory for general lamination configurations. AIAA Journal 1993;31:1299–306. https://doi.org/10.2514/3.11767.

[87] Di Sciuva M. A general quadrilateral multilayered plate element with continuous interlaminar stresses. Computers & Structures 1993;47:91–105. https://doi.org/10.1016/0045-7949(93)90282-I.

[88] Di Sciuva M. An Improved Shear-Deformation Theory for Moderately Thick Multilayered Anisotropic Shells and Plates. J Appl Mech 1987;54:589–96. https://doi.org/10.1115/1.3173074.

[89] Di Sciuva M. Geometrically nonlinear theory of multilayered plates with interlayer slips. AIAA Journal 1997;35:1753–9.

[90] Icardi U. Higher-order zig-zag model for analysis of thick composite beams with inclusion of transverse normal stress and sublaminates approximations. Composites Part B: Engineering 2001;32:343–54. https://doi.org/10.1016/S1359-8368(01)00016-6.

[91] Icardi U. A three-dimensional zig-zag theory for analysis of thick laminated beams. Composite Structures 2001;52:123–35. https://doi.org/10.1016/S0263-8223(00)00189-6.

[92] Murakami H. Laminated Composite Plate Theory With Improved In-Plane Responses. J Appl Mech 1986;53:661–6. https://doi.org/10.1115/1.3171828.

[93] Toledano A, Murakami H. A Composite Plate Theory for Arbitrary Laminate Configurations. J Appl Mech 1987;54:181–9. https://doi.org/10.1115/1.3172955.

[94] Gherlone M. On the Use of Zigzag Functions in Equivalent Single Layer Theories for Laminated Composite and Sandwich Beams: A Comparative Study and Some Observations on External Weak Layers. J Appl Mech 2013;80:1–19. https://doi.org/10.1115/1.4023690.

[95] Averill RC. Static and dynamic response of moderately thick laminated beams with damage. Composites Engineering 1994;4:381–95. https://doi.org/10.1016/S0961-9526(09)80013-0.

[96] Averill RC, Yip YC. Development of simple, robust finite elements based on refined theories for thick laminated beams. Computers & Structures 1996;59:529–46. https://doi.org/10.1016/0045-7949(95)00269-3.

[97] Cho Y-B, Averill RC. An improved theory and finite-element model for laminated composite and sandwich beams using first-order zig-zag sublaminate approximations. Composite Structures 1997;37:281–98. https://doi.org/10.1016/S0263-8223(96)00004-9.

[98] Icardi U, Sola F. Development of an Efficient Zigzag Model with Variable Representation of Displacements across the Thickness. Journal of Engineering Mechanics 2014;140:531–41. https://doi.org/10.1061/(ASCE)EM.1943-7889.0000673.

[99] Icardi U, Sola F. C^0 Fixed Degrees of Freedom Zigzag Model with Variable In-Plane and Out-of-Plane Kinematics and Quadrilateral Plate Element. J Aerosp Eng 2015;28:04014135. https://doi.org/10.1061/(ASCE)AS.1943-5525.0000472.

[100] Sola F. Simulation of Local Effects, Energy Absorption and Failure Mechanism in Multilayered and Sandwich Structures. PhD Thesis. Politecnico di Torino, 2016.

[101] Icardi U, Urraci A. Free and Forced Vibration of Laminated and Sandwich Plates by Zig-Zag Theories Differently Accounting for Transverse Shear and Normal Deformability. Aerospace 2018;5:108. https://doi.org/10.3390/aerospace5040108.

[102] Tessler A, Di Sciuva M, Gherlone M. Refinement of Timoshenko Beam Theory for Composite and Sandwich Beams using Zigzag Kinematics. NASA/TP-2007-215086 2007:1–45.

[103] Tessler A, Di Sciuva M, Gherlone M. Refined Zigzag Theory for Laminated Composite and Sandwich Plates. NASA/TP-2009-215561 2009:1–53.

[104] Di Sciuva M, Gherlone M, Tessler A. A Robust and Consistent First-Order Zigzag Theory for Multilayered Beams. In: Gilat R, Banks-Sills L, editors. Advances in Mathematical Modeling and Experimental Methods for Materials and Structures: The Jacob Aboudi Volume, Dordrecht: Springer Netherlands; 2009, p. 255–68. https://doi.org/10.1007/978-90-481-3467-0_20.

[105] Tessler A, Di Sciuva M, Gherlone M. Refined Zigzag Theory for Homogeneous, Laminated Composite, and Sandwich Plates: A Homogeneous Limit Methodology for Zigzag Function Selection. NASA/TP-2010-216214 2010:34.

[106] Iurlaro L, Gherlone M, Di Sciuva M. Bending and free vibration analysis of functionally graded sandwich plates using the Refined Zigzag Theory. Jnl of Sandwich Structures & Materials 2014;16:669–99. https://doi.org/10.1177/1099636214548618.

[107] Gherlone M, Tessler A, Di Sciuva M. C^0 beam elements based on the Refined Zigzag Theory for multilayered composite and sandwich laminates. Composite Structures 2011;93:2882–94. https://doi.org/10.1016/j.compstruct.2011.05.015.

[108] Di Sciuva M, Gherlone M, Iurlaro L, Tessler A. A class of higher-order C^0 composite and sandwich beam elements based on the Refined Zigzag Theory. Composite Structures 2015;132:784–803. https://doi.org/10.1016/j.compstruct.2015.06.071.

[109] Oñate E, Eijo A, Oller S. Simple and accurate two-noded beam element for composite laminated beams using a refined zigzag theory. Computer Methods in Applied Mechanics and Engineering 2012;213–216:362–82. https://doi.org/10.1016/j.cma.2011.11.023.

[110] Eijo A, Oñate E, Oller S. A four-noded quadrilateral element for composite laminated plates/shells using the refined zigzag theory. International Journal for Numerical Methods in Engineering 2013;95:631–60. https://doi.org/10.1002/nme.4503.

[111] Versino D, Gherlone M, Mattone MC, Di Sciuva M, Tessler A. C^0 triangular elements based on the Refined Zigzag Theory for multilayered composite and sandwich plates. Composites Part B: Engineering 2013;44:218–30. https://doi.org/10.1016/j.compositesb.2012.05.026.

[112] Versino D, Gherlone M, Di Sciuva M. Four-node shell element for doubly curved multilayered composites based on the Refined Zigzag Theory. Composite Structures 2014;118:392–402. https://doi.org/10.1016/j.compstruct.2014.08.018.

[113] Dorduncu M. Stress analysis of laminated composite beams using refined zigzag theory and peridynamic differential operator. Composite Structures 2019;218:193–203. https://doi.org/10.1016/j.compstruct.2019.03.035.

[114] Dorduncu M. Stress analysis of sandwich plates with functionally graded cores using peridynamic differential operator and refined zigzag theory. Thin-Walled Structures 2020;146:106468. https://doi.org/10.1016/j.tws.2019.106468.

[115] Tessler A. Refined zigzag theory for homogeneous, laminated composite, and sandwich beams derived from Reissner's mixed variational principle. Meccanica 2015;50:2621–48. https://doi.org/10.1007/s11012-015-0222-0.

[116] Iurlaro L, Gherlone M, Di Sciuva M, Tessler A. Refined Zigzag Theory for laminated composite and sandwich plates derived from Reissner's Mixed Variational Theorem. Composite Structures 2015;133:809–17. https://doi.org/10.1016/j.compstruct.2015.08.004.

[117] Gherlone M. Static Analysis of Sandwich Beams Including the Effect of Adhesive Layers by Using the Mixed Refined Zigzag Theory. 14th U.S. National Congress on Computational Mechanics, Montreal, Quebec, Canada: 2017.

[118] Gherlone M. Tria and quad plate finite elements based on RZT(m) for the analysis of multilayered sandwich structures. Composite Structures 2019;220:510–20. https://doi.org/10.1016/j.compstruct.2019.04.032.

[119] Kefal A, Hasim KA, Yildiz M. A novel isogeometric beam element based on mixed form of refined zigzag theory for thick sandwich and multilayered composite beams. Composites Part B: Engineering 2019;167:100–21. https://doi.org/10.1016/j.compositesb.2018.11.102.

[120] Kutlu A. Mixed finite element formulation for bending of laminated beams using the refined zigzag theory. Proceedings of the Institution of Mechanical Engineers, Part L: Journal of Materials: Design and Applications 2021;235:1712–22. https://doi.org/10.1177/14644207211018839.

[121] Kutlu A, Dorduncu M, Rabczuk T. A novel mixed finite element formulation based on the refined zigzag theory for the stress analysis of laminated composite plates. Composite Structures 2021;267:113886. https://doi.org/10.1016/j.compstruct.2021.113886.

[122] Groh RM, Weaver PM, Tessler A. Application of the Refined Zigzag Theory to the Modeling of Delaminations in Laminated Composites. NASA/TM-2015-218808 2015:1–22.

[123] Groh RMJ, Tessler A. Computationally efficient beam elements for accurate stresses in sandwich laminates and laminated composites with

delaminations. Computer Methods in Applied Mechanics and Engineering 2017;320:369–95. https://doi.org/10.1016/j.cma.2017.03.035.

[124] Barut A, Madenci E, Tessler A. A Refined Zigzag Theory for Laminated Composite and Sandwich Plates Incorporating Thickness Stretch Deformation. 53rd AIAA/ASME/ASCE/AHS/ASC Structures, Structural Dynamics and Materials Conference, American Institute of Aeronautics and Astronautics; 2012. https://doi.org/doi.org/10.2514/6.2012-1705.

[125] Barut A, Madenci E, Tessler A. C0-continuous triangular plate element for laminated composite and sandwich plates using the {2,2} – Refined Zigzag Theory. Composite Structures 2013;106:835–53. https://doi.org/10.1016/j.compstruct.2013.07.024.

[126] Dorduncu M, Kutlu A, Madenci E. Triangular C0 continuous finite elements based on refined zigzag theory {2,2} for free and forced vibration analyses of laminated plates. Composite Structures 2021:115058. https://doi.org/10.1016/j.compstruct.2021.115058.

[127] Groh RMJ, Weaver PM. On displacement-based and mixed-variational equivalent single layer theories for modelling highly heterogeneous laminated beams. International Journal of Solids and Structures 2015;59:147–70. https://doi.org/10.1016/j.ijsolstr.2015.01.020.

[128] Groh RMJ, Weaver PM. A computationally efficient 2D model for inherently equilibrated 3D stress predictions in heterogeneous laminated plates. Part I: Model formulation. Composite Structures 2016;156:171–85. https://doi.org/10.1016/j.compstruct.2015.11.078.

[129] Groh RMJ, Weaver PM. A computationally efficient 2D model for inherently equilibrated 3D stress predictions in heterogeneous laminated plates. Part II: Model validation. Composite Structures 2016;156:186–217. https://doi.org/10.1016/j.compstruct.2015.11.077.

[130] Iurlaro L, Gherlone M, Di Sciuva M. A mixed cubic zigzag model for multilayered composite and sandwich plates including transverse normal deformability. Proceedings of the 11th World Conference on Computational Methods, Barcelona, Spain: 2014, p. 2.

[131] Iurlaro L, Gherlone M, Di Sciuva M. The (3,2)-Mixed Refined Zigzag Theory for generally laminated beams: Theoretical development and C^0 finite element formulation. International Journal of Solids and Structures 2015;73–74:1–19. https://doi.org/10.1016/j.ijsolstr.2015.07.028.

[132] Iurlaro L. Development of refined models for multilayered composite and sandwich structures: analytical formulation, FEM implementation and experimental assessment. PhD Thesis. Politecnico di Torino, 2015.

[133] Kreja I, Sabik A. Equivalent single-layer models in deformation analysis of laminated multilayered plates. Acta Mech 2019;230:2827–51. https://doi.org/10.1007/s00707-019-02434-7.

[134] Tessler A, Di Sciuva M, Gherlone M. A homogeneous limit methodology and refinements of computationally efficient zigzag theory for homogeneous, laminated composite, and sandwich plates. Numerical Methods for Partial Differential Equations 2011;27:208–29. https://doi.org/10.1002/num.20646.

[135] Tessler A, Di Sciuva M, Gherlone M. Refined Zigzag Theory for Laminated Composite and Sandwich Plates. NASA/TP-2009-215561 2009:1–53.

[136] Sorrenti M, Di Sciuva M. An enhancement of the warping shear functions of Refined Zigzag Theory. Journal of Applied Mechanics 2021;88:7. https://doi.org/10.1115/1.4050908.

[137] Sorrenti M, Gherlone M, Di Sciuva M. Buckling analysis of angle-ply multilayered and sandwich plates using the enhanced Refined Zigzag Theory. PEAS 2022;71:84. https://doi.org/10.3176/proc.2022.1.08.

[138] Di Sciuva M. Evaluation of some multilayered, shear-deformable plate elements. Computers & Structures 1986;24:845–54. https://doi.org/10.1016/0045-7949(86)90293-2.

[139] Shu X-P, Soldatos KP. Cylindrical bending of angle-ply laminates subjected to different sets of edge boundary conditions. International Journal of Solids and Structures 2000:19.

[140] Messina A, Soldatos KP. A general vibration model of angle-ply laminated plates that accounts for the continuity of interlaminar stresses. International Journal of Solids and Structures 2002;39:617–35. https://doi.org/10.1016/S0020-7683(01)00169-X.

[141] Kim J-S, Cho M. Enhanced modeling of laminated and sandwich plates via strain energy transformation. Composites Science and Technology 2006;66:1575–87. https://doi.org/10.1016/j.compscitech.2005.11.018.

[142] Loredo A. Transverse shear warping functions for anisotropic multilayered plates. Classical Physics 2012:1–19.

[143] Loredo A, Castel A. Two multilayered plate models with transverse shear warping functions issued from three dimensional elasticity equations. Composite Structures 2014;117:382–95. https://doi.org/10.1016/j.compstruct.2014.07.001.

[144] Loredo A. A multilayered plate theory with transverse shear and normal warping functions. Composite Structures 2016;156:361–74. https://doi.org/10.1016/j.compstruct.2015.08.084.

[145] Loredo A, D'Ottavio M, Vidal P, Polit O. A family of higher-order single layer plate models meeting C_z^0-requirements for arbitrary laminates. Composite Structures 2019;225:14. https://doi.org/10.1016/j.compstruct.2019.111146.

[146] Leissa AW. Conditions for laminated plates to remain flat under inplane loading. Composite Structures 1986;6:261–70. https://doi.org/10.1016/0263-8223(86)90022-X.

[147] Whitney JM. Structural Analysis of Laminated Anisotropic Plates. 1° edizione. Lancaster, Pa., U.S.A: CRC Press; 1987.

[148] Loughlan J. The influence of mechanical couplings on the compressive stability of anti-symmetric angle-ply laminates. Composite Structures 2002;57:473–82. https://doi.org/10.1016/S0263-8223(02)00116-2.

[149] Sorrenti M, Gherlone M. A new mixed model based on the enhanced-Refined Zigzag Theory for the analysis of thick multilayered composite plates. Proceedings of the 25th International Conference on Composite Structures, Faculty of Engineering, University of Porto (Portugal): 2022, p. 237.

[150] Sorrenti M, Gherlone M. A new mixed model based on the enhanced-Refined Zigzag Theory for the analysis of thick multilayered composite plates. Composite Structures 2023;311:116787. https://doi.org/10.1016/j.compstruct.2023.116787.

[151] Tessler A. An improved plate theory of {1,2}-order for thick composite laminates. International Journal of Solids and Structures 1993;30:981–1000. https://doi.org/10.1016/0020-7683(93)90022-Y.

[152] Cook GM, Tessler A. A {3,2}-order bending theory for laminated composite and sandwich beams. Composites Part B: Engineering 1998;29:565–76. https://doi.org/10.1016/S1359-8368(98)00011-0.

[153] Barut A, Madenci E, Heinrich J, Tessler A. Analysis of thick sandwich construction by a {3,2}-order theory. International Journal of Solids and Structures 2001;38:6063–77. https://doi.org/10.1016/S0020-7683(00)00367-X.

[154] Di Sciuva M, Gherlone M. A global/local third-order Hermitian displacement field with damaged interfaces and transverse extensibility: analytical formulation. Composite Structures 2003;59:419–31. https://doi.org/10.1016/S0263-8223(02)00168-X.

[155] Di Sciuva M, Gherlone M. A global/local third-order Hermitian displacement field with damaged interfaces and transverse extensibility: FEM formulation. Composite Structures 2003;59:433–44. https://doi.org/10.1016/S0263-8223(02)00169-1.

[156] Di Sciuva M, Gherlone M. Quasi-3D Static and Dynamic Analysis of Undamaged and Damaged Sandwich Beams. Jnl of Sandwich Structures & Materials 2005;7:31–52. https://doi.org/10.1177/1099636205043821.

[157] Gherlone M, Di Sciuva M. Thermo-mechanics of undamaged and damaged multilayered composite plates: a sub-laminates finite element approach. Composite Structures 2007;81:125–36. https://doi.org/10.1016/j.compstruct.2006.08.004.

[158] Gherlone M, Di Sciuva M. Thermo-mechanics of undamaged and damaged multilayered composite plates: assessment of the FEM sub-laminates approach. Composite Structures 2007;81:137–55. https://doi.org/10.1016/j.compstruct.2006.08.005.

[159] Thurnherr C, Groh RMJ, Ermanni P, Weaver PM. Higher-order beam model for stress predictions in curved beams made from anisotropic materials. International Journal of Solids and Structures 2016;97–98:16–28. https://doi.org/10.1016/j.ijsolstr.2016.08.004.

[160] Eijo A, Oñate E, Oller S. A numerical model of delamination in composite laminated beams using the LRZ beam element based on the refined zigzag theory. Composite Structures 2013;104:270–80. https://doi.org/10.1016/j.compstruct.2013.04.035.

[161] Nallim LG, Oller S, Oñate E, Flores FG. A hierarchical finite element for composite laminated beams using a refined zigzag theory. Composite Structures 2017;163:168–84. https://doi.org/10.1016/j.compstruct.2016.12.031.

[162] Wimmer H, Nachbagauer K. Exact transfer- and stiffness matrix for the composite beam-column with Refined Zigzag kinematics. Composite Structures 2018;189:700–6. https://doi.org/10.1016/j.compstruct.2018.01.022.

[163] Ascione A, Orifici AC, Gherlone M. Experimental and Numerical Investigation of the Refined Zigzag Theory for Accurate Buckling Analysis of Highly Heterogeneous Sandwich Beams. Int J Str Stab Dyn 2020;20:2050078. https://doi.org/10.1142/S0219455420500789.

[164] Ascione A, Gherlone M, Orifici AC. Nonlinear static analysis of composite beams with piezoelectric actuator patches using the Refined Zigzag Theory. Composite Structures 2021:115018. https://doi.org/10.1016/j.compstruct.2021.115018.

[165] Flores FG, Oller S, Nallim LG. On the analysis of non-homogeneous laminates using the refined zigzag theory. Composite Structures 2018;204:791–802. https://doi.org/10.1016/j.compstruct.2018.08.018.

[166] Tessler A. A two-node beam element including transverse shear and transverse normal deformations. International Journal for Numerical

Methods in Engineering 1991;32:1027–39. https://doi.org/10.1002/nme.1620320507.

[167] Sorrenti M, Gherlone M. Dynamic analysis of sandwich beams with adhesive layers using the mixed Refined Zigzag Theory. 19th International Conference of numerical analysis and applied mechanics, Rhodes, Greece: 2021.

[168] Sorrenti M, Gherlone M, Di Sciuva M. Free vibration analysis of angle-ply laminated and sandwich plates using enhanced Refined Zigzag Theory. 19th International Conference of numerical analysis and applied mechanics, Rhodes, Greece: 2021.

[169] Di Sciuva M, Sorrenti M. Bending and free vibration analysis of functionally graded sandwich plates: An assessment of the Refined Zigzag Theory. Journal of Sandwich Structures & Materials 2019:1–43. https://doi.org/10.1177/1099636219843970.

[170] Kirchhoff G. Über das Gleichgewicht und die Bewegung einer elastischen Scheibe. Journal Für Die Reine Und Angewandte Mathematik (Crelles Journal) 1850:51–88. https://doi.org/10.1515/crll.1850.40.51.

[171] Matsunaga H. Vibration and stability of angle-ply laminated composite plates subjected to in-plane stresses. International Journal of Mechanical Sciences 2001;43:1925–44. https://doi.org/10.1016/S0020-7403(01)00002-9.

[172] Di Sciuva M, Icardi U. Numerical studies on bending, free vibration and buckling of multilayered anisotropic plates. Aerotecnica Missili & Spazio 1993;72:21–36.

[173] Swaminathan K, Patil SS. Analytical solutions using a higher order refined computational model with 12 degrees of freedom for the free vibration analysis of antisymmetric angle-ply plates. Composite Structures 2008;82:209–16. https://doi.org/10.1016/j.compstruct.2007.01.001.

[174] Standard Test Methods for Flexural properties of Unreinforced and Reinforced plastics and electrical Insulating Materials 2017.

[175] Zenkert D, Burman M. Tension, Compression and Shear Fatigue of a closed cell foam, Kyoto, Japan: 2007.

Appendix A

Derivation of the assumed transverse normal stress

In this appendix, the details are given for the solution of the weak form of the compatibility constraint between the transverse normal strain derived from the kinematic field and that derived from the assumed transverse normal stress. The procedure adopted here takes inspiration from those addressed by Iurlaro et al. [131]. However, in this newly developed model, a more general lamination scheme is considered that involves the enhanced higher-order zigzag functions.

Due to the arbitrary variation of the unknown stress vector $\mathbf{q}_{\boldsymbol{\sigma}}(\mathbf{x})$, the Eq. (3.34) can be solved as follows:

$$\int_V \delta\sigma_{33}^a \left(\varepsilon_{33} - \varepsilon_{33}^a\right) dV = \left\langle \delta\sigma_{33}^a \left(\varepsilon_{33} - \varepsilon_{33}^{a(k)}\right)\right\rangle = 0 \tag{A.1}$$

where the symbol $\langle ... \rangle$ denotes the integration over all the plate thickness.

Using the material constitutive relation for the transverse normal strain, it reads:

$$\varepsilon_{33}^a(\mathbf{x}, x_3) = S_{33}^{(k)} \sigma_{33}^a(\mathbf{x}, x_3) - \mathbf{R}^{(k)} \boldsymbol{\varepsilon}_p^{(k)}(\mathbf{x}, x_3) \tag{A.2}$$

where $\mathbf{R}^{(k)} = \begin{bmatrix} R_{13}^{(k)} & R_{23}^{(k)} & R_{63}^{(k)} \end{bmatrix}$.

Performing the virtual variation of the transverse normal stress and substituting the expression of Eq. (A.2) into Eq. (A.1), it follows:

$$\left\langle \delta \mathbf{q}_{\boldsymbol{\sigma}}{}^{T} \mathbf{P}_{\sigma}{}^{T} \left(\mathbf{H}_{,3}^{z} \mathbf{w} - S_{33}^{(k)} \left(\mathbf{L} \overline{\mathbf{q}}_{z} + \mathbf{P}_{\sigma} \mathbf{q}_{\boldsymbol{\sigma}} - \mathbf{R}^{(k)} \boldsymbol{\varepsilon}_{p}^{(k)} \right) \right) \right\rangle = 0 \tag{A.3}$$

Substituting the expression for in-plane strain quantities, as defined by Eq. (3.8), yields the following expression:

$$\begin{aligned} &\left\langle \mathbf{P}_{\sigma}{}^{T} \mathbf{H}_{,3}^{z} \right\rangle \mathbf{w} - \left\langle S_{33}^{(k)} \mathbf{P}_{\sigma}{}^{T} \mathbf{L} \right\rangle \overline{\mathbf{q}}_{z} - \left\langle S_{33}^{(k)} \mathbf{P}_{\sigma}{}^{T} \mathbf{P}_{\sigma} \right\rangle \mathbf{q}_{\boldsymbol{\sigma}} + \\ &+ \left\langle \mathbf{P}_{\sigma}{}^{T} \mathbf{R}^{(k)} \right\rangle \boldsymbol{\varepsilon}_{m} + \left\langle \mathbf{P}_{\sigma}{}^{T} \mathbf{R}^{(k)} x_{3} \right\rangle \boldsymbol{\varepsilon}_{\theta} + \left\langle \mathbf{P}_{\sigma}{}^{T} \mathbf{R}^{(k)} \mathbf{M}^{(k)} \right\rangle \boldsymbol{\varepsilon}_{\psi} = 0 \end{aligned} \tag{A.4}$$

From which it is possible to solve in terms of the vector $\mathbf{q}_{\boldsymbol{\sigma}}(\mathbf{x})$ that contains the unknown stress quantities:

$$\begin{aligned} \mathbf{q}_{\boldsymbol{\sigma}}(\mathbf{x}) = &\left\langle S_{33}^{(k)} \mathbf{P}_{\sigma}{}^{T} \mathbf{P}_{\sigma} \right\rangle^{-1} \left\langle \mathbf{P}_{\sigma}{}^{T} \mathbf{H}_{,3}^{z} \right\rangle \mathbf{w}(\mathbf{x}) - \left\langle S_{33}^{(k)} \mathbf{P}_{\sigma}{}^{T} \mathbf{P}_{\sigma} \right\rangle^{-1} \left\langle S_{33}^{(k)} \mathbf{P}_{\sigma}{}^{T} \mathbf{L} \right\rangle \overline{\mathbf{q}}_{z}(\mathbf{x}) + \\ &+ \left\langle S_{33}^{(k)} \mathbf{P}_{\sigma}{}^{T} \mathbf{P}_{\sigma} \right\rangle^{-1} \left\langle \mathbf{P}_{\sigma}{}^{T} \mathbf{R}^{(k)} \right\rangle \boldsymbol{\varepsilon}_{m}(\mathbf{x}) + \\ &+ \left\langle S_{33}^{(k)} \mathbf{P}_{\sigma}{}^{T} \mathbf{P}_{\sigma} \right\rangle^{-1} \left\langle \mathbf{P}_{\sigma}{}^{T} \mathbf{R}^{(k)} z \right\rangle \boldsymbol{\varepsilon}_{\theta}(\mathbf{x}) + \\ &+ \left\langle S_{33}^{(k)} \mathbf{P}_{\sigma}{}^{T} \mathbf{P}_{\sigma} \right\rangle^{-1} \left\langle \mathbf{P}_{\sigma}{}^{T} \mathbf{R}^{(k)} \mathbf{M}^{(k)} \right\rangle \boldsymbol{\varepsilon}_{\psi}(\mathbf{x}) \end{aligned} \tag{A.5}$$

Substituting expression (A.5) into Eq. (3.23), after some mathematics, the final expression reads:

$$\begin{aligned} \sigma_{33}^{a}(\mathbf{x}, x_3) = &\mathbf{A}_{\sigma}^{u}(x_3) \boldsymbol{\varepsilon}_{m}(\mathbf{x}) + \mathbf{A}_{\sigma}^{\theta}(x_3) \boldsymbol{\varepsilon}_{\theta}(\mathbf{x}) + \\ &+ \mathbf{A}_{\sigma}^{\psi}(x_3) \boldsymbol{\varepsilon}_{\psi}(\mathbf{x}) + \mathbf{A}_{\sigma}^{w}(x_3) \mathbf{w}(\mathbf{x}) + \mathbf{A}_{\sigma}^{q_z}(x_3) \overline{\mathbf{q}}_{z}(\mathbf{x}) \end{aligned} \tag{A.6}$$

where

$$
\begin{aligned}
&\mathbf{A}_{\sigma}^{u}(x_3)=\mathbf{P}_{\sigma}(x_3)\left\langle S_{33}^{(k)}\mathbf{P}_{\sigma}(x_3)^{T}\mathbf{P}_{\sigma}(x_3)\right\rangle^{-1}\left\langle \mathbf{P}_{\sigma}(x_3)^{T}\mathbf{R}^{(k)}\right\rangle;\\
&\mathbf{A}_{\sigma}^{\theta}(x_3)=\mathbf{P}_{\sigma}(x_3)\left\langle S_{33}^{(k)}\mathbf{P}_{\sigma}(x_3)^{T}\mathbf{P}_{\sigma}(x_3)\right\rangle^{-1}\left\langle \mathbf{P}_{\sigma}(x_3)^{T}\mathbf{R}^{(k)}x_3\right\rangle;\\
&\mathbf{A}_{\sigma}^{\psi}(x_3)=\mathbf{P}_{\sigma}(x_3)\left\langle S_{33}^{(k)}\mathbf{P}_{\sigma}{}^{T}\mathbf{P}_{\sigma}\right\rangle^{-1}\left\langle \mathbf{P}_{\sigma}(x_3)^{T}\mathbf{R}^{(k)}\mathbf{M}^{(k)}(x_3)\right\rangle;\\
&\mathbf{A}_{\sigma}^{w}(x_3)=\mathbf{P}_{\sigma}(x_3)\left\langle S_{33}^{(k)}\mathbf{P}_{\sigma}{}^{T}\mathbf{P}_{\sigma}\right\rangle^{-1}\left\langle \mathbf{P}_{\sigma}{}^{T}\mathbf{H}_{,3}^{z}\right\rangle;\\
&\mathbf{A}_{\sigma}^{q_z}(x_3)=\left[\mathbf{L}(x_3)-\mathbf{P}_{\sigma}(x_3)\left\langle S_{33}^{(k)}\mathbf{P}_{\sigma}(x_3)^{T}\mathbf{P}_{\sigma}(x_3)\right\rangle^{-1}\left\langle S_{33}^{(k)}\mathbf{P}_{\sigma}(x_3)^{T}\mathbf{L}(x_3)\right\rangle\right]
\end{aligned}
\tag{A.7}
$$

are the shape functions of the thickness coordinate for the transverse normal stress.

Appendix B

Derivation of the assumed transverse shear stresses

In this appendix, the mathematical passages to obtain the full expression of the transverse shear stress are reported.

Using the assumed transverse normal stress expression defined by Eq. (3.36) and substituting into the mixed material constitutive relations, the in-plane stress quantities are here defined in a compact matrix form:

$$\begin{aligned}
&\begin{Bmatrix} \sigma_{11}^{(k)}(\mathbf{x},x_3) \\ \sigma_{22}^{(k)}(\mathbf{x},x_3) \\ \tau_{12}^{(k)}(\mathbf{x},x_3) \end{Bmatrix} = \boldsymbol{\sigma}_p^{(k)} = \breve{\mathbf{C}}_p^{(k)}\boldsymbol{\varepsilon}_p^{(k)}(\mathbf{x},x_3) + \mathbf{R}^{(k)}\sigma_{33}^{a}(\mathbf{x},x_3) = \\
&= \left(\breve{\mathbf{C}}_p^{(k)} + \mathbf{R}^{(k)}\mathbf{A}_\sigma^{u}(x_3)\right)\boldsymbol{\varepsilon}_m(\mathbf{x}) + \left(x_3\breve{\mathbf{C}}_p^{(k)} + \mathbf{R}^{(k)}\mathbf{A}_\sigma^{\theta}(x_3)\right)\boldsymbol{\varepsilon}_\theta(\mathbf{x}) + \\
&+ \left(\breve{\mathbf{C}}_p^{(k)}\mathbf{M}^{(k)} + \mathbf{R}^{(k)}\mathbf{A}_\sigma^{\psi}(x_3)\right)\boldsymbol{\varepsilon}_\psi(\mathbf{x}) + \mathbf{R}^{(k)}\mathbf{A}_\sigma^{w}(x_3)\mathbf{w}(\mathbf{x}) + \mathbf{R}^{(k)}\mathbf{A}_\sigma^{q_z}(x_3)\overline{\mathbf{q}}_z(\mathbf{x})
\end{aligned} \tag{B.1}$$

Before substituting into the expression of local equilibrium equations defined by Eq. (3.25), it will be performed the substitution of the strain quantities with the new set of independent variables as defined by Eq. (3.26). This procedure results in the following:

$$\begin{aligned}\boldsymbol{\sigma}_p^{(k)} &= \left(\breve{\mathbf{C}}_p^{(k)} + \mathbf{R}^{(k)}\mathbf{A}_\sigma^u(x_3)\right)\mathbf{e}(\mathbf{x}) + \left(x_3\breve{\mathbf{C}}_p^{(k)} + \mathbf{R}^{(k)}\mathbf{A}_\sigma^\theta(x_3)\right)\mathbf{k}(\mathbf{x}) + \\ &+\left(\breve{\mathbf{C}}_p^{(k)}\mathbf{M}^{(k)} + \mathbf{R}^{(k)}\mathbf{A}_\sigma^\psi(x_3)\right)\mathbf{k}^\psi(\mathbf{x}) + \\ &+\mathbf{R}^{(k)}\mathbf{A}_\sigma^w(x_3)\mathbf{w}(\mathbf{x}) + \mathbf{R}^{(k)}\mathbf{A}_\sigma^{q_z}(x_3)\overline{\mathbf{q}}_z(\mathbf{x})\end{aligned} \tag{B.2}$$

Deriving the expression of Eq. (B.2) with respect to x_1 and x_2 directions and substituting into Eq. (3.25) the integration along the thickness direction is performed, resulting in the following expression:

$$\begin{aligned}\boldsymbol{\tau}_t^a(\mathbf{x},x_3) = -\overline{\mathbf{p}}^{(B)}(\mathbf{x}) + \mathbf{A}^{\mathbf{z}}(x_3)\partial\mathbf{e}(\mathbf{x}) + \mathbf{B}^{\mathbf{z}}(x_3)\partial\mathbf{k}(\mathbf{x}) + \\ +\mathbf{D}^{\mathbf{z}}(x_3)\partial\mathbf{k}^\psi(\mathbf{x}) + \mathbf{E}^{\mathbf{z}}(x_3)\partial\mathbf{w}(\mathbf{x}) + \mathbf{F}^{\mathbf{z}}(x_3)\partial\overline{\mathbf{q}}_z(\mathbf{x})\end{aligned} \tag{B.3}$$

where $\mathbf{A}^{\mathbf{z}}(x_3)$, $\mathbf{B}^{\mathbf{z}}(x_3)$, $\mathbf{D}^{\mathbf{z}}(x_3)$, $\mathbf{E}^{\mathbf{z}}(x_3)$, $\mathbf{F}^{\mathbf{z}}(x_3)$ are the shape functions in the transverse direction, and the derivative of the independent strain variables are defined as follows:

$$\begin{aligned}\partial\mathbf{e}(\mathbf{x})^T &= \left[e_{11,1} \quad e_{22,1} \quad e_{12,1} \quad e_{11,2} \quad e_{22,2} \quad e_{12,2}\right]; \\ \partial\mathbf{k}(\mathbf{x})^T &= \left[k_{11,1} \quad k_{22,1} \quad k_{12,1} \quad k_{11,2} \quad k_{22,2} \quad k_{12,2}\right]; \\ \partial\mathbf{k}^\psi(\mathbf{x})^T &= \left[k^\psi_{11,1} \quad k^\psi_{22,1} \quad k^\psi_{12,1} \quad k^\psi_{21,1} \quad k^\psi_{11,2} \quad k^\psi_{22,2} \quad k^\psi_{12,2} \quad k^\psi_{21,2}\right]; \\ \partial\mathbf{w}(\mathbf{x})^T &= \left[w^{(0)}_{,1} \quad w^{(1)}_{,1} \quad w^{(2)}_{,1} \quad w^{(0)}_{,2} \quad w^{(1)}_{,2} \quad w^{(2)}_{,2}\right]; \\ \partial\overline{\mathbf{q}}_z(\mathbf{x})^T &= \left[\overline{p}_{3(B),1} \quad \overline{p}_{3(T),1} \quad \overline{p}_{3(B),2} \quad \overline{p}_{3(T),2}\right]\end{aligned} \tag{B.4}$$

The shape functions are expressed as follows:

$$\mathbf{A}^{\mathbf{z}}(x_3)^T = \begin{bmatrix} -\left[\int_{-h/2}^{x_3}\left(\breve{C}_{11}^{(k)} + R_{13}^{(k)}A_{\sigma 11}^{u}\right)dx_3\right] & -\left[\int_{-h/2}^{x_3}\left(\breve{C}_{16}^{(k)} + R_{63}^{(k)}A_{\sigma 11}^{u}\right)dx_3\right] \\ -\left[\int_{-h/2}^{x_3}\left(\breve{C}_{12}^{(k)} + R_{13}^{(k)}A_{\sigma 12}^{u}\right)dx_3\right] & -\left[\int_{-h/2}^{x_3}\left(\breve{C}_{26}^{(k)} + R_{63}^{(k)}A_{\sigma 12}^{u}\right)dx_3\right] \\ -\left[\int_{-h/2}^{x_3}\left(\breve{C}_{16}^{(k)} + R_{13}^{(k)}A_{\sigma 13}^{u}\right)dx_3\right] & -\left[\int_{-h/2}^{x_3}\left(\breve{C}_{66}^{(k)} + R_{63}^{(k)}A_{\sigma 13}^{u}\right)dx_3\right] \\ -\left[\int_{-h/2}^{x_3}\left(\breve{C}_{16}^{(k)} + R_{63}^{(k)}A_{\sigma 11}^{u}\right)dx_3\right] & -\left[\int_{-h/2}^{x_3}\left(\breve{C}_{12}^{(k)} + R_{23}^{(k)}A_{\sigma 11}^{u}\right)dx_3\right] \\ -\left[\int_{-h/2}^{x_3}\left(\breve{C}_{26}^{(k)} + R_{63}^{(k)}A_{\sigma 12}^{u}\right)dx_3\right] & -\left[\int_{-h/2}^{x_3}\left(\breve{C}_{22}^{(k)} + R_{23}^{(k)}A_{\sigma 12}^{u}\right)dx_3\right] \\ -\left[\int_{-h/2}^{x_3}\left(\breve{C}_{66}^{(k)} + R_{63}^{(k)}A_{\sigma 13}^{u}\right)dx_3\right] & -\left[\int_{-h/2}^{x_3}\left(\breve{C}_{26}^{(k)} + R_{23}^{(k)}A_{\sigma 13}^{u}\right)dx_3\right] \end{bmatrix} \tag{B.5}$$

$$\mathbf{B}^{\mathbf{z}}(x_3)^T = \begin{bmatrix} -\left[\int_{-h/2}^{x_3}\left(x_3\breve{C}_{11}^{(k)} + R_{13}^{(k)}A_{\sigma 11}^{\theta}\right)dx_3\right] & -\left[\int_{-h/2}^{x_3}\left(x_3\breve{C}_{16}^{(k)} + R_{63}^{(k)}A_{\sigma 11}^{\theta}\right)dx_3\right] \\ -\left[\int_{-h/2}^{x_3}\left(x_3\breve{C}_{12}^{(k)} + R_{13}^{(k)}A_{\sigma 12}^{\theta}\right)dx_3\right] & -\left[\int_{-h/2}^{x_3}\left(x_3\breve{C}_{26}^{(k)} + R_{63}^{(k)}A_{\sigma 12}^{\theta}\right)dx_3\right] \\ -\left[\int_{-h/2}^{x_3}\left(x_3\breve{C}_{16}^{(k)} + R_{13}^{(k)}A_{\sigma 13}^{\theta}\right)dx_3\right] & -\left[\int_{-h/2}^{x_3}\left(x_3\breve{C}_{66}^{(k)} + R_{63}^{(k)}A_{\sigma 13}^{\theta}\right)dx_3\right] \\ -\left[\int_{-h/2}^{x_3}\left(x_3\breve{C}_{16}^{(k)} + R_{63}^{(k)}A_{\sigma 11}^{\theta}\right)dx_3\right] & -\left[\int_{-h/2}^{x_3}\left(x_3\breve{C}_{12}^{(k)} + R_{23}^{(k)}A_{\sigma 11}^{\theta}\right)dx_3\right] \\ -\left[\int_{-h/2}^{x_3}\left(x_3\breve{C}_{26}^{(k)} + R_{63}^{(k)}A_{\sigma 12}^{\theta}\right)dx_3\right] & -\left[\int_{-h/2}^{x_3}\left(x_3\breve{C}_{22}^{(k)} + R_{23}^{(k)}A_{\sigma 12}^{\theta}\right)dx_3\right] \\ -\left[\int_{-h/2}^{x_3}\left(x_3\breve{C}_{66}^{(k)} + R_{63}^{(k)}A_{\sigma 13}^{\theta}\right)dx_3\right] & -\left[\int_{-h/2}^{x_3}\left(x_3\breve{C}_{26}^{(k)} + R_{23}^{(k)}A_{\sigma 13}^{\theta}\right)dx_3\right] \end{bmatrix} \tag{B.6}$$

$$\mathbf{D}^{\mathbf{z}}(x_3)^T = \begin{bmatrix} -\left[\int_{-h/2}^{x_3}\left(Q_{11}^{(k)}\mu_{11}^{(k)} + Q_{16}^{(k)}\mu_{21}^{(k)} + R_{13}^{(k)}A_{\sigma 11}^{\psi}\right)dx_3\right] & -\left[\int_{-h/2}^{x_3}\left(Q_{16}^{(k)}\mu_{11}^{(k)} + Q_{66}^{(k)}\mu_{21}^{(k)} + R_{63}^{(k)}A_{\sigma 11}^{\psi}\right)dx_3\right] \\ -\left[\int_{-h/2}^{x_3}\left(Q_{12}^{(k)}\mu_{22}^{(k)} + Q_{16}^{(k)}\mu_{12}^{(k)} + R_{13}^{(k)}A_{\sigma 12}^{\psi}\right)dx_3\right] & -\left[\int_{-h/2}^{x_3}\left(Q_{26}^{(k)}\mu_{22}^{(k)} + C_{66}^{(k)}\mu_{12}^{(k)} + R_{63}^{(k)}A_{\sigma 12}^{\psi}\right)dx_3\right] \\ -\left[\int_{-h/2}^{x_3}\left(Q_{12}^{(k)}\mu_{21}^{(k)} + Q_{16}^{(k)}\mu_{11}^{(k)} + R_{13}^{(k)}A_{\sigma 13}^{\psi}\right)dx_3\right] & -\left[\int_{-h/2}^{x_3}\left(Q_{26}^{(k)}\mu_{21}^{(k)} + Q_{66}^{(k)}\mu_{11}^{(k)} + R_{63}^{(k)}A_{\sigma 13}^{\psi}\right)dx_3\right] \\ -\left[\int_{-h/2}^{x_3}\left(Q_{11}^{(k)}\mu_{12}^{(k)} + Q_{16}^{(k)}\mu_{22}^{(k)} + R_{13}^{(k)}A_{\sigma 14}^{\psi}\right)dx_3\right] & -\left[\int_{-h/2}^{x_3}\left(Q_{16}^{(k)}\mu_{12}^{(k)} + Q_{66}^{(k)}\mu_{22}^{(k)} + R_{63}^{(k)}A_{\sigma 14}^{\psi}\right)dx_3\right] \\ -\left[\int_{-h/2}^{x_3}\left(Q_{16}^{(k)}\mu_{11}^{(k)} + Q_{66}^{(k)}\mu_{21}^{(k)} + R_{63}^{(k)}A_{\sigma 11}^{\psi}\right)dx_3\right] & -\left[\int_{-h/2}^{x_3}\left(Q_{12}^{(k)}\mu_{11}^{(k)} + Q_{26}^{(k)}\mu_{21}^{(k)} + R_{23}^{(k)}A_{\sigma 11}^{\psi}\right)dx_3\right] \\ -\left[\int_{-h/2}^{x_3}\left(Q_{26}^{(k)}\mu_{22}^{(k)} + Q_{66}^{(k)}\mu_{12}^{(k)} + R_{63}^{(k)}A_{\sigma 12}^{\psi}\right)dx_3\right] & -\left[\int_{-h/2}^{x_3}\left(Q_{22}^{(k)}\mu_{22}^{(k)} + Q_{26}^{(k)}\mu_{12}^{(k)} + R_{23}^{(k)}A_{\sigma 12}^{\psi}\right)dx_3\right] \\ -\left[\int_{-h/2}^{x_3}\left(Q_{26}^{(k)}\mu_{21}^{(k)} + Q_{66}^{(k)}\mu_{11}^{(k)} + R_{63}^{(k)}A_{\sigma 13}^{\psi}\right)dx_3\right] & -\left[\int_{-h/2}^{x_3}\left(Q_{22}^{(k)}\mu_{21}^{(k)} + Q_{26}^{(k)}\mu_{11}^{(k)} + R_{23}^{(k)}A_{\sigma 13}^{\psi}\right)dx_3\right] \\ -\left[\int_{-h/2}^{x_3}\left(Q_{16}^{(k)}\mu_{12}^{(k)} + Q_{66}^{(k)}\mu_{22}^{(k)} + R_{63}^{(k)}A_{\sigma 14}^{\psi}\right)dx_3\right] & -\left[\int_{-h/2}^{x_3}\left(Q_{12}^{(k)}\mu_{12}^{(k)} + Q_{26}^{(k)}\mu_{22}^{(k)} + R_{23}^{(k)}A_{\sigma 14}^{\psi}\right)dx_3\right] \end{bmatrix} \quad \text{(B.7)}$$

$$\mathbf{E}^{\mathbf{z}}(x_3)^T = \begin{bmatrix} -\left[\int_{-h/2}^{x_3} R_{13}^{(k)}A_{\sigma 11}^{w}dx_3\right] & -\left[\int_{-h/2}^{x_3} R_{63}^{(k)}A_{\sigma 11}^{w}dx_3\right] \\ -\left[\int_{-h/2}^{x_3} R_{13}^{(k)}A_{\sigma 12}^{w}dx_3\right] & -\left[\int_{-h/2}^{x_3} R_{63}^{(k)}A_{\sigma 12}^{w}dx_3\right] \\ -\left[\int_{-h/2}^{x_3} R_{13}^{(k)}A_{\sigma 13}^{w}dx_3\right] & -\left[\int_{-h/2}^{x_3} R_{63}^{(k)}A_{\sigma 13}^{w}dx_3\right] \\ -\left[\int_{-h/2}^{x_3} R_{63}^{(k)}A_{\sigma 11}^{w}dx_3\right] & -\left[\int_{-h/2}^{x_3} R_{23}^{(k)}A_{\sigma 11}^{w}dx_3\right] \\ -\left[\int_{-h/2}^{x_3} R_{63}^{(k)}A_{\sigma 12}^{w}dx_3\right] & -\left[\int_{-h/2}^{x_3} R_{23}^{(k)}A_{\sigma 12}^{w}dx_3\right] \\ -\left[\int_{-h/2}^{x_3} R_{63}^{(k)}A_{\sigma 13}^{w}dx_3\right] & -\left[\int_{-h/2}^{x_3} R_{23}^{(k)}A_{\sigma 13}^{w}dx_3\right] \end{bmatrix} \quad \text{(B.8)}$$

$$\mathbf{F}^{\mathbf{z}}(x_3)^T = \begin{bmatrix} -\left[\int_{-h/2}^{x_3} R_{13}^{(k)} A_{\sigma 11}^{q_z} dx_3\right] & -\left[\int_{-h/2}^{x_3} R_{63}^{(k)} A_{\sigma 11}^{q_z} dx_3\right] \\ -\left[\int_{-h/2}^{x_3} R_{13}^{(k)} A_{\sigma 12}^{q_z} dx_3\right] & -\left[\int_{-h/2}^{x_3} R_{63}^{(k)} A_{\sigma 12}^{q_z} dx_3\right] \\ -\left[\int_{-h/2}^{x_3} R_{63}^{(k)} A_{\sigma 11}^{q_z} dx_3\right] & -\left[\int_{-h/2}^{x_3} R_{23}^{(k)} A_{\sigma 11}^{q_z} dx_3\right] \\ -\left[\int_{-h/2}^{x_3} R_{63}^{(k)} A_{\sigma 12}^{q_z} dx_3\right] & -\left[\int_{-h/2}^{x_3} R_{23}^{(k)} A_{\sigma 12}^{q_z} dx_3\right] \end{bmatrix} \tag{B.9}$$

Since the expression (B.3) is not able to satisfy the traction condition at the top surface, a further term is added:

$$\begin{aligned} \boldsymbol{\tau}_t^a(\mathbf{x}, x_3) = &-\overline{\mathbf{p}}^{(B)}(\mathbf{x}) + \mathbf{A}^{\mathbf{z}}(x_3)\partial\mathbf{e}(\mathbf{x}) + \mathbf{B}^{\mathbf{z}}(x_3)\partial\mathbf{k}(\mathbf{x}) + \\ &+\mathbf{D}^{\mathbf{z}}(x_3)\partial\mathbf{k}^{\psi}(\mathbf{x}) + \mathbf{E}^{\mathbf{z}}(x_3)\partial\mathbf{w}(\mathbf{x}) + \mathbf{F}^{\mathbf{z}}(x_3)\partial\overline{\mathbf{q}}_z(\mathbf{x}) + \mathbf{a}(x_3 + h/2) \end{aligned} \tag{B.10}$$

The expression of **a** is obtained by integrating the transverse shear stresses along the whole laminate thickness and enforcing the traction conditions in both directions at the top surface. It reads:

$$\begin{aligned} \mathbf{a} = &-\frac{1}{h}\left(\overline{\mathbf{p}}^{(T)} + \overline{\mathbf{p}}^{(B)}\right) - \frac{1}{h}\left\langle \mathbf{A}^{\mathbf{z}} \right\rangle \partial\mathbf{e} - \frac{1}{h}\left\langle \mathbf{B}^{\mathbf{z}} \right\rangle \partial\mathbf{k} + \\ &-\frac{1}{h}\left\langle \mathbf{D}^{\mathbf{z}} \right\rangle \partial\mathbf{k}^{\psi} + \frac{1}{h}\left\langle \mathbf{E}^{\mathbf{z}} \right\rangle \partial\mathbf{w} + \frac{1}{h}\left\langle \mathbf{F}^{\mathbf{z}} \right\rangle \partial\overline{\mathbf{q}}_z \end{aligned} \tag{B.11}$$

Substituting the expression of Eq. (B.11) into (B.10) yields:

$$\begin{aligned} \boldsymbol{\tau}_t^a(\mathbf{x}, x_3) = &\overline{\mathbf{p}}^{(B)}(\mathbf{x})\left(-1 - \frac{1}{h}(x_3 + h/2)\right) - \frac{1}{h}(x_3 + h/2)\overline{\mathbf{p}}^{(T)}(\mathbf{x}) + \widehat{\mathbf{A}}^{z}(x_3)\partial\mathbf{e}(\mathbf{x}) + \\ &+\widehat{\mathbf{B}}^{z}(x_3)\partial\mathbf{k}(\mathbf{x}) + \widehat{\mathbf{D}}^{z}(x_3)\partial\mathbf{k}^{\psi}(\mathbf{x}) + \widehat{\mathbf{E}}^{z}(x_3)\partial\mathbf{w}(\mathbf{x}) + \widehat{\mathbf{F}}^{z}(x_3)\partial\overline{\mathbf{q}}_z(\mathbf{x}) = \\ &= \mathbf{Z}_p(x_3)\overline{\mathbf{q}}_{\mathbf{p}}(\mathbf{x}) + \mathbf{Z}_t(x_3)\mathbf{q}_t(\mathbf{x}) + \mathbf{Z}_{qz}(x_3)\partial\overline{\mathbf{q}}_z(\mathbf{x}) \end{aligned} \tag{B.12}$$

where, the terms of Eq. (B.12) and Eq. (3.37) are defined as follows:

$$
\begin{aligned}
&\widehat{\mathbf{A}}^{z}(x_3)=\mathbf{A}^{\mathbf{z}}(x_3)-(x_3+h/2)\frac{1}{h}\left\langle \mathbf{A}^{\mathbf{z}}\right\rangle \\
&\widehat{\mathbf{B}}^{z}(x_3)=\mathbf{B}^{\mathbf{z}}(x_3)-(x_3+h/2)\frac{1}{h}\left\langle \mathbf{B}^{\mathbf{z}}\right\rangle \\
&\widehat{\mathbf{D}}^{z}(x_3)=\mathbf{D}^{\mathbf{z}}(x_3)-(x_3+h/2)\frac{1}{h}\left\langle \mathbf{D}^{\mathbf{z}}\right\rangle \\
&\widehat{\mathbf{E}}^{z}(x_3)=\mathbf{E}^{\mathbf{z}}(x_3)-(x_3+h/2)\frac{1}{h}\left\langle \mathbf{E}^{\mathbf{z}}\right\rangle \\
&\widehat{\mathbf{F}}^{z}(x_3)=\mathbf{F}^{\mathbf{z}}(x_3)-(x_3+h/2)\frac{1}{h}\left\langle \mathbf{F}^{\mathbf{z}}\right\rangle \\
&\mathbf{Z}_{p}(x_3)=\left[\left(-1-\frac{1}{h}(x_3+h/2)\right)\quad -\frac{1}{h}(x_3+h/2)\right] \\
&\mathbf{Z}_{t}(x_3)=\left[\widehat{\mathbf{A}}^{z}(x_3)\quad \widehat{\mathbf{B}}^{z}(x_3)\quad \widehat{\mathbf{D}}^{z}(x_3)\quad \widehat{\mathbf{E}}^{z}(x_3)\right] \\
&\mathbf{Z}_{qz}(x_3)=\widehat{\mathbf{F}}^{z}(x_3) \\
&\overline{\mathbf{q}}_{\mathbf{p}}(\mathbf{x})^{T}=\left[\overline{\mathbf{p}}^{(B)}\quad \overline{\mathbf{p}}^{(T)}\right]=\left[p_{1(B)}\quad p_{2(B)}\quad p_{1(T)}\quad p_{2(T)}\right] \\
&\mathbf{q}_{t}(\mathbf{x})^{T}=\left[\partial\mathbf{e}^{T}\quad \partial\mathbf{k}^{T}\quad \partial\mathbf{k}^{\psi T}\quad \partial\mathbf{w}^{T}\right]
\end{aligned}
\tag{B.13}
$$

Appendix C

Full expressions of the equilibrium equation and boundary conditions terms

In this appendix, the full expressions of the terms that appeared in the en-RZT$^{(m)}_{\{3,2\}}$ equilibrium equations, i.e. Eqs. (3.40) - (3.56) are expressed as follows:

$$
\begin{aligned}
\widehat{Q}^{w0} = &-\left(\hat{D}^{w}_{11}w^{(0)}_{,11} + \hat{D}^{w}_{12}w^{(1)}_{,11} + \hat{D}^{w}_{13}w^{(2)}_{,11} + \hat{D}^{w}_{14}w^{(0)}_{,12} + \hat{D}^{w}_{15}w^{(1)}_{,12} + \hat{D}^{w}_{16}w^{(2)}_{,12} + \hat{D}^{\theta}_{11}\theta_{1,1} + \hat{D}^{\theta}_{12}\theta_{2,1} + \hat{D}^{\psi}_{11}\psi_{1,1} + \hat{D}^{\psi}_{12}\psi_{2,1}\right) + \\
&-\left(\hat{D}^{w}_{41}w^{(0)}_{,12} + \hat{D}^{w}_{42}w^{(1)}_{,12} + \hat{D}^{w}_{43}w^{(2)}_{,12} + \hat{D}^{w}_{44}w^{(0)}_{,22} + \hat{D}^{w}_{45}w^{(1)}_{,22} + \hat{D}^{w}_{46}w^{(2)}_{,22} + \hat{D}^{\theta}_{41}\theta_{1,2} + \hat{D}^{\theta}_{42}\theta_{2,2} + \hat{D}^{\psi}_{41}\psi_{1,2} + \hat{D}^{\psi}_{42}\psi_{2,2}\right) + \\
&+\hat{A}^{kw}_{11}e_{11,11} + \hat{A}^{kw}_{21}e_{22,11} + \hat{A}^{kw}_{31}e_{12,11} + \hat{A}^{kw}_{41}e_{11,12} + \hat{A}^{kw}_{51}e_{22,12} + \hat{A}^{kw}_{61}e_{12,12} + \\
&+\hat{B}^{kw}_{11}k_{11,11} + \hat{B}^{kw}_{21}k_{22,11} + \hat{B}^{kw}_{31}k_{12,11} + \hat{B}^{kw}_{41}k_{11,12} + \hat{B}^{kw}_{51}k_{22,12} + \hat{B}^{kw}_{61}k_{12,12} + \hat{C}^{kw}_{11}k^{\psi}_{11,11} + \hat{C}^{kw}_{21}k^{\psi}_{22,11} + \hat{C}^{kw}_{31}k^{\psi}_{12,11} + \hat{C}^{kw}_{41}k^{\psi}_{21,11} + \\
&+\hat{C}^{kw}_{51}k^{\psi}_{11,12} + \hat{C}^{kw}_{61}k^{\psi}_{22,12} + \hat{C}^{kw}_{71}k^{\psi}_{12,12} + \hat{C}^{kw}_{81}k^{\psi}_{21,12} + \hat{D}^{kw}_{11}w^{(0)}_{,11} + \hat{D}^{kw}_{12}w^{(1)}_{,11} + \hat{D}^{kw}_{13}w^{(2)}_{,11} + \hat{D}^{kw}_{14}w^{(0)}_{,12} + \hat{D}^{kw}_{15}w^{(1)}_{,12} + \hat{D}^{kw}_{16}w^{(2)}_{,12} + \\
&\hat{A}^{kw}_{14}e_{11,12} + \hat{A}^{kw}_{24}e_{22,12} + \hat{A}^{kw}_{34}e_{12,12} + \hat{A}^{kw}_{44}e_{11,22} + \hat{A}^{kw}_{54}e_{22,22} + \hat{A}^{kw}_{64}e_{12,22} + \\
&+\hat{B}^{kw}_{14}k_{11,12} + \hat{B}^{kw}_{24}k_{22,12} + \hat{B}^{kw}_{34}k_{12,12} + \hat{B}^{kw}_{44}k_{11,22} + \hat{B}^{kw}_{54}k_{22,22} + \hat{B}^{kw}_{64}k_{12,22}\hat{C}^{kw}_{14}k^{\psi}_{11,12} + \hat{C}^{kw}_{24}k^{\psi}_{22,12} + \hat{C}^{kw}_{34}k^{\psi}_{12,12} + \hat{C}^{kw}_{44}k^{\psi}_{21,12} + \\
&+\hat{C}^{kw}_{54}k^{\psi}_{11,22} + \hat{C}^{kw}_{64}k^{\psi}_{22,22} + \hat{C}^{kw}_{74}k^{\psi}_{12,22} + \hat{C}^{kw}_{84}k^{\psi}_{21,22} + \hat{D}^{kw}_{41}w^{(0)}_{,12} + \hat{D}^{kw}_{42}w^{(1)}_{,12} + \hat{D}^{kw}_{43}w^{(2)}_{,12} + \hat{D}^{kw}_{44}w^{(0)}_{,22} + \hat{D}^{kw}_{45}w^{(1)}_{,22} + \hat{D}^{kw}_{46}w^{(2)}_{,22} +
\end{aligned}
\tag{C.1}
$$

$$\begin{aligned}\widehat{Q}^{w1} = &-\left(\hat{D}_{11}^{w}w_{,11}^{(0)} + \hat{D}_{12}^{w}w_{,11}^{(1)} + \hat{D}_{13}^{w}w_{,11}^{(2)} + \hat{D}_{14}^{w}w_{,12}^{(0)} + \hat{D}_{15}^{w}w_{,12}^{(1)} + \hat{D}_{16}^{w}w_{,12}^{(2)} + \hat{D}_{11}^{\theta}\theta_{1,1} + \hat{D}_{12}^{\theta}\theta_{2,1} + \hat{D}_{11}^{\psi}\psi_{1,1} + \hat{D}_{12}^{\psi}\psi_{2,1}\right) + \\ &-\left(\hat{D}_{51}^{w}w_{,12}^{(0)} + \hat{D}_{52}^{w}w_{,12}^{(1)} + \hat{D}_{53}^{w}w_{,12}^{(2)} + \hat{D}_{54}^{w}w_{,22}^{(0)} + \hat{D}_{55}^{w}w_{,22}^{(1)} + \hat{D}_{56}^{w}w_{,22}^{(2)} + \hat{D}_{51}^{\theta}\theta_{1,2} + \hat{D}_{52}^{\theta}\theta_{2,2} + \hat{D}_{51}^{\psi}\psi_{1,2} + \hat{D}_{52}^{\psi}\psi_{2,2}\right) + \\ &+\hat{A}_{12}^{kw}e_{11,11} + \hat{A}_{22}^{kw}e_{22,11} + \hat{A}_{32}^{kw}e_{12,11} + \hat{A}_{42}^{kw}e_{11,12} + \hat{A}_{52}^{kw}e_{22,12} + \hat{A}_{62}^{kw}e_{12,12} + \\ &+\hat{B}_{12}^{kw}k_{11,11} + \hat{B}_{22}^{kw}k_{22,11} + \hat{B}_{32}^{kw}k_{12,11} + \hat{B}_{42}^{kw}k_{11,12} + \hat{B}_{52}^{kw}k_{22,12} + \hat{B}_{62}^{kw}k_{12,12} + \\ &+\hat{C}_{12}^{kw}k_{11,11}^{\psi} + \hat{C}_{22}^{kw}k_{22,11}^{\psi} + \hat{C}_{32}^{kw}k_{12,11}^{\psi} + \hat{C}_{41}^{kw}k_{22,11}^{\psi} + \hat{C}_{52}^{kw}k_{11,12}^{\psi} + \hat{C}_{62}^{kw}k_{22,12}^{\psi} + \hat{C}_{72}^{kw}k_{12,12}^{\psi} + \hat{C}_{82}^{kw}k_{21,12}^{\psi} + \\ &+\hat{D}_{21}^{kw}w_{,11}^{(0)} + \hat{D}_{22}^{kw}w_{,11}^{(1)} + \hat{D}_{23}^{kw}w_{,11}^{(2)} + \hat{D}_{24}^{kw}w_{,12}^{(0)} + \hat{D}_{25}^{kw}w_{,12}^{(1)} + \hat{D}_{26}^{kw}w_{,12}^{(2)} + \\ &+\hat{A}_{15}^{kw}e_{11,12} + \hat{A}_{25}^{kw}e_{22,12} + \hat{A}_{35}^{kw}e_{12,12} + \hat{A}_{45}^{kw}e_{11,22} + \hat{A}_{55}^{kw}e_{22,22} + \hat{A}_{65}^{kw}e_{12,22} + \\ &+\hat{B}_{15}^{kw}k_{11,12} + \hat{B}_{25}^{kw}k_{22,12} + \hat{B}_{35}^{kw}k_{12,12} + \hat{B}_{45}^{kw}k_{11,22} + \hat{B}_{55}^{kw}k_{22,22} + \hat{B}_{65}^{kw}k_{12,22} + \\ &+\hat{C}_{15}^{kw}k_{11,12}^{\psi} + \hat{C}_{25}^{kw}k_{22,12}^{\psi} + \hat{C}_{35}^{kw}k_{12,12}^{\psi} + \hat{C}_{45}^{kw}k_{21,12}^{\psi} + \hat{C}_{55}^{kw}k_{11,22}^{\psi} + \hat{C}_{65}^{kw}k_{22,22}^{\psi} + \hat{C}_{75}^{kw}k_{12,22}^{\psi} + \hat{C}_{85}^{kw}k_{21,22}^{\psi} + \\ &+\hat{D}_{51}^{kw}w_{,12}^{(0)} + \hat{D}_{52}^{kw}w_{,12}^{(1)} + \hat{D}_{53}^{kw}w_{,12}^{(2)} + \hat{D}_{54}^{kw}w_{,22}^{(0)} + \hat{D}_{55}^{kw}w_{,22}^{(1)} + \hat{D}_{56}^{kw}w_{,22}^{(2)} + \end{aligned} \tag{C.2}$$

$$\begin{aligned}\widehat{Q}^{w2} = &-\left(\hat{D}_{31}^{w}w_{,11}^{(0)} + \hat{D}_{32}^{w}w_{,11}^{(1)} + \hat{D}_{33}^{w}w_{,11}^{(2)} + \hat{D}_{34}^{w}w_{,12}^{(0)} + \hat{D}_{35}^{w}w_{,12}^{(1)} + \hat{D}_{36}^{w}w_{,12}^{(2)} + \hat{D}_{31}^{\theta}\theta_{1,1} + \hat{D}_{32}^{\theta}\theta_{2,1} + \hat{D}_{31}^{\psi}\psi_{1,1} + \hat{D}_{32}^{\psi}\psi_{2,1}\right) + \\ &-\left(\hat{D}_{61}^{w}w_{,12}^{(0)} + \hat{D}_{62}^{w}w_{,12}^{(1)} + \hat{D}_{63}^{w}w_{,12}^{(2)} + \hat{D}_{64}^{w}w_{,22}^{(0)} + \hat{D}_{65}^{w}w_{,22}^{(1)} + \hat{D}_{66}^{w}w_{,22}^{(2)} + \hat{D}_{61}^{\theta}\theta_{1,2} + \hat{B}_{62}^{\theta}\theta_{2,2} + \hat{D}_{61}^{\psi}\psi_{1,2} + \hat{D}_{62}^{\psi}\psi_{2,2}\right) + \\ &+\hat{A}_{13}^{kw}e_{11,11} + \hat{A}_{23}^{kw}e_{22,11} + \hat{A}_{33}^{kw}e_{12,11} + \hat{A}_{43}^{kw}e_{11,12} + \hat{A}_{53}^{kw}e_{22,12} + \hat{A}_{63}^{kw}e_{12,12} + \\ &+\hat{B}_{13}^{kw}k_{11,11} + \hat{B}_{23}^{kw}k_{22,11} + \hat{B}_{33}^{kw}k_{12,11} + \hat{B}_{43}^{kw}k_{11,12} + \hat{B}_{53}^{kw}k_{22,12} + \hat{B}_{63}^{kw}k_{12,12} + \\ &+\hat{C}_{13}^{kw}k_{11,11}^{\psi} + \hat{C}_{23}^{kw}k_{22,11}^{\psi} + \hat{C}_{33}^{kw}k_{12,11}^{\psi} + \hat{C}_{43}^{kw}k_{21,11}^{\psi} + \hat{C}_{53}^{kw}k_{11,12}^{\psi} + \hat{C}_{63}^{kw}k_{22,12}^{\psi} + \hat{C}_{73}^{kw}k_{12,12}^{\psi} + \hat{C}_{83}^{kw}k_{21,12}^{\psi} + \\ &+\hat{D}_{31}^{kw}w_{,11}^{(0)} + \hat{D}_{32}^{kw}w_{,11}^{(1)} + \hat{D}_{33}^{kw}w_{,11}^{(2)} + \hat{D}_{34}^{kw}w_{,12}^{(0)} + \hat{D}_{35}^{kw}w_{,12}^{(1)} + \hat{D}_{36}^{kw}w_{,12}^{(2)} + \\ &+\hat{A}_{16}^{kw}e_{11,12} + \hat{A}_{26}^{kw}e_{22,12} + \hat{A}_{36}^{kw}e_{12,12} + \hat{A}_{46}^{kw}e_{11,22} + \hat{A}_{56}^{kw}e_{22,22} + \hat{A}_{66}^{kw}e_{12,22} + \\ &+\hat{B}_{16}^{kw}k_{11,12} + \hat{B}_{26}^{kw}k_{22,12} + \hat{B}_{36}^{kw}k_{12,12} + \hat{B}_{46}^{kw}k_{11,22} + \hat{B}_{56}^{kw}k_{22,22} + \hat{B}_{66}^{kw}k_{12,22} + \\ &+\hat{C}_{16}^{kw}k_{11,12}^{\psi} + \hat{C}_{26}^{kw}k_{22,12}^{\psi} + \hat{C}_{36}^{kw}k_{12,12}^{\psi} + \hat{C}_{46}^{kw}k_{21,12}^{\psi} + \hat{C}_{56}^{kw}k_{11,22}^{\psi} + \hat{C}_{66}^{kw}k_{22,22}^{\psi} + \hat{C}_{76}^{kw}k_{12,22}^{\psi} + \hat{C}_{86}^{kw}k_{21,22}^{\psi} + \\ &+\hat{D}_{61}^{kw}w_{,12}^{(0)} + \hat{D}_{62}^{kw}w_{,12}^{(1)} + \hat{D}_{63}^{kw}w_{,12}^{(2)} + \hat{D}_{64}^{kw}w_{,22}^{(0)} + \hat{D}_{65}^{kw}w_{,22}^{(1)} + \hat{D}_{66}^{kw}w_{,22}^{(2)} + \end{aligned} \tag{C.3}$$

$$\begin{aligned}E_{11}^{HR} = &\hat{A}_{11}^{w}w_{,11}^{(0)} + \hat{A}_{12}^{w}w_{,11}^{(1)} + \hat{A}_{13}^{w}w_{,11}^{(2)} + \hat{A}_{14}^{w}w_{,12}^{(0)} + \hat{A}_{15}^{w}w_{,12}^{(1)} + \hat{A}_{16}^{w}w_{,12}^{(2)} + \hat{A}_{11}^{\theta}\theta_{1,1} + \hat{A}_{12}^{\theta}\theta_{2,1} + \hat{A}_{11}^{\psi}\psi_{1,1} + \hat{A}_{12}^{\psi}\psi_{2,1} + \\ &+\hat{A}_{41}^{w}w_{,12}^{(0)} + \hat{A}_{42}^{w}w_{,12}^{(1)} + \hat{A}_{43}^{w}w_{,12}^{(2)} + \hat{A}_{44}^{w}w_{,22}^{(0)} + \hat{A}_{45}^{w}w_{,22}^{(1)} + \hat{A}_{46}^{w}w_{,22}^{(2)} + \hat{A}_{41}^{\theta}\theta_{1,2} + \hat{A}_{42}^{\theta}\theta_{2,2} + \hat{A}_{41}^{\psi}\psi_{1,2} + \hat{A}_{42}^{\psi}\psi_{2,2} + \\ &-\begin{pmatrix} \hat{A}_{11}^{p}\overline{p}_{1(B),1} + \hat{A}_{12}^{p}\overline{p}_{2(B),1} + \hat{A}_{13}^{p}\overline{p}_{1(T),1} + \hat{A}_{14}^{p}\overline{p}_{2(T),1} + \hat{A}_{11}^{e}e_{11,11} + \hat{A}_{12}^{e}e_{22,11} + \hat{A}_{13}^{e}e_{12,11} + \hat{A}_{14}^{e}e_{11,12} + \hat{A}_{15}^{e}e_{22,12} + \hat{A}_{16}^{e}e_{12,12} + \\ +\hat{A}_{11}^{k}k_{11,11} + \hat{A}_{12}^{k}k_{22,11} + \hat{A}_{13}^{k}k_{12,11} + \hat{A}_{14}^{k}k_{11,12} + \hat{A}_{15}^{k}k_{22,12} + \hat{A}_{16}^{k}k_{12,12} + \\ +\hat{A}_{11}^{k\psi}k_{11,11}^{\psi} + \hat{A}_{12}^{k\psi}k_{22,11}^{\psi} + \hat{A}_{13}^{k\psi}k_{12,11}^{\psi} + \hat{A}_{14}^{k\psi}k_{21,11}^{\psi} + \hat{A}_{15}^{k\psi}k_{11,12}^{\psi} + \hat{A}_{16}^{k\psi}k_{22,12}^{\psi} + \hat{A}_{17}^{k\psi}k_{12,12}^{\psi} + \hat{A}_{18}^{k\psi}k_{21,12}^{\psi} + \\ +\hat{A}_{11}^{kw}w_{,11}^{(0)} + \hat{A}_{12}^{kw}w_{,11}^{(1)} + \hat{A}_{13}^{kw}w_{,11}^{(2)} + \hat{A}_{14}^{kw}w_{,12}^{(0)} + \hat{A}_{15}^{kw}w_{,12}^{(1)} + \hat{A}_{16}^{kw}w_{,12}^{(2)} + \\ +\hat{A}_{41}^{p}\overline{p}_{1(B),2} + \hat{A}_{42}^{p}\overline{p}_{2(B),2} + \hat{A}_{43}^{p}\overline{p}_{1(T),2} + \hat{A}_{44}^{p}\overline{p}_{2(T),2} + \hat{A}_{41}^{e}e_{11,12} + \hat{A}_{42}^{e}e_{22,12} + \hat{A}_{43}^{e}e_{12,12} + \hat{A}_{44}^{e}e_{11,22} + \hat{A}_{45}^{e}e_{22,22} + \hat{A}_{46}^{e}e_{12,22} + \\ +\hat{A}_{41}^{k}k_{11,12} + \hat{A}_{42}^{k}k_{22,12} + \hat{A}_{43}^{k}k_{12,12} + \hat{A}_{44}^{k}k_{11,22} + \hat{A}_{45}^{k}k_{22,22} + \hat{A}_{46}^{k}k_{12,22} + \\ +\hat{A}_{41}^{k\psi}k_{11,12}^{\psi} + \hat{A}_{42}^{k\psi}k_{22,12}^{\psi} + \hat{A}_{43}^{k\psi}k_{12,12}^{\psi} + \hat{A}_{44}^{k\psi}k_{21,12}^{\psi} + \hat{A}_{45}^{k\psi}k_{11,22}^{\psi} + \hat{A}_{46}^{k\psi}k_{22,22}^{\psi} + \hat{A}_{47}^{k\psi}k_{12,22}^{\psi} + \hat{A}_{48}^{k\psi}k_{21,22}^{\psi} + \\ +\hat{A}_{41}^{kw}w_{,12}^{(0)} + \hat{A}_{42}^{kw}w_{,12}^{(1)} + \hat{A}_{43}^{kw}w_{,12}^{(2)} + \hat{A}_{44}^{kw}w_{,22}^{(0)} + \hat{A}_{45}^{kw}w_{,22}^{(1)} + \hat{A}_{46}^{kw}w_{,22}^{(2)} + \\ +\hat{A}_{11}^{q}\overline{p}_{3(B),11} + \hat{A}_{12}^{q}\overline{p}_{3(T),11} + \hat{A}_{13}^{q}\overline{p}_{3(B),12} + \hat{A}_{14}^{q}\overline{p}_{3(T),12} + \hat{A}_{41}^{q}\overline{p}_{3(B),12} + \hat{A}_{42}^{q}\overline{p}_{3(T),12} + \hat{A}_{43}^{q}\overline{p}_{3(B),22} + \hat{A}_{44}^{q}\overline{p}_{3(T),22} \end{pmatrix} \end{aligned} \tag{C.4}$$

$$
\begin{aligned}
E_{22}^{HR} = {} & \hat{A}_{21}^{w} w_{,11}^{(0)} + \hat{A}_{22}^{w} w_{,11}^{(1)} + \hat{A}_{23}^{w} w_{,11}^{(2)} + \hat{A}_{24}^{w} w_{,12}^{(0)} + \hat{A}_{25}^{w} w_{,12}^{(1)} + \hat{A}_{26}^{w} w_{,12}^{(2)} + \hat{A}_{21}^{\theta} \theta_{1,1} + \hat{A}_{22}^{\theta} \theta_{2,1} + \hat{A}_{21}^{\psi} \psi_{1,1} + \hat{A}_{22}^{\psi} \psi_{2,1} + \\
& + \hat{A}_{51}^{w} w_{,12}^{(0)} + \hat{A}_{52}^{w} w_{,12}^{(1)} + \hat{A}_{53}^{w} w_{,12}^{(2)} + \hat{A}_{54}^{w} w_{,22}^{(0)} + \hat{A}_{55}^{w} w_{,22}^{(1)} + \hat{A}_{56}^{w} w_{,22}^{(2)} + \hat{A}_{51}^{\theta} \theta_{1,2} + \hat{A}_{52}^{\theta} \theta_{2,2} + \hat{A}_{51}^{\psi} \psi_{1,2} + \hat{A}_{52}^{\psi} \psi_{2,2} + \\
& \left(\begin{array}{l}
\hat{A}_{21}^{p} \overline{p}_{1(B),1} + \hat{A}_{22}^{p} \overline{p}_{2(B),1} + \hat{A}_{23}^{p} \overline{p}_{1(T),1} + \hat{A}_{24}^{p} \overline{p}_{2(T),1} + \hat{A}_{21}^{e} e_{11,11} + \hat{A}_{22}^{e} e_{22,11} + \hat{A}_{23}^{e} e_{12,11} + \hat{A}_{24}^{e} e_{11,12} + \hat{A}_{25}^{e} e_{22,12} + \hat{A}_{26}^{e} e_{12,12} + \\
+ \hat{A}_{21}^{k} k_{11,11} + \hat{A}_{22}^{k} k_{22,11} + \hat{A}_{23}^{k} k_{12,11} + \hat{A}_{24}^{k} k_{11,12} + \hat{A}_{25}^{k} k_{22,12} + \hat{A}_{26}^{k} k_{12,12} + \\
+ \hat{A}_{21}^{k\psi} k_{11,11}^{\psi} + \hat{A}_{22}^{k\psi} k_{22,11}^{\psi} + \hat{A}_{23}^{k\psi} k_{12,11}^{\psi} + \hat{A}_{24}^{k\psi} k_{21,11}^{\psi} + \hat{A}_{25}^{k\psi} k_{11,12}^{\psi} + \hat{A}_{26}^{k\psi} k_{22,12}^{\psi} + \hat{A}_{27}^{k\psi} k_{12,12}^{\psi} + \hat{A}_{28}^{k\psi} k_{21,12}^{\psi} + \\
+ \hat{A}_{21}^{kw} w_{,11}^{(0)} + \hat{A}_{22}^{kw} w_{,11}^{(1)} + \hat{A}_{23}^{kw} w_{,11}^{(2)} + \hat{A}_{24}^{kw} w_{,12}^{(0)} + \hat{A}_{25}^{kw} w_{,12}^{(1)} + \hat{A}_{26}^{kw} w_{,12}^{(2)} + \\
- \hat{A}_{51}^{p} \overline{p}_{1(B),2} + \hat{A}_{52}^{p} \overline{p}_{2(B),2} + \hat{A}_{53}^{p} \overline{p}_{1(T),2} + \hat{A}_{54}^{p} \overline{p}_{2(T),2} + \hat{A}_{51}^{e} e_{11,12} + \hat{A}_{52}^{e} e_{22,12} + \hat{A}_{53}^{e} e_{12,12} + \hat{A}_{54}^{e} e_{11,22} + \hat{A}_{55}^{e} e_{22,22} + \hat{A}_{56}^{e} e_{12,22} + \\
+ \hat{A}_{51}^{k} k_{11,12} + \hat{A}_{52}^{k} k_{22,12} + \hat{A}_{53}^{k} k_{12,12} + \hat{A}_{54}^{k} k_{11,22} + \hat{A}_{55}^{k} k_{22,22} + \hat{A}_{56}^{k} k_{12,22} + \\
+ \hat{A}_{51}^{k\psi} k_{11,12}^{\psi} + \hat{A}_{52}^{k\psi} k_{22,12}^{\psi} + \hat{A}_{53}^{k\psi} k_{12,12}^{\psi} + \hat{A}_{54}^{k\psi} k_{21,12}^{\psi} + \hat{A}_{55}^{k\psi} k_{11,22}^{\psi} + \hat{A}_{56}^{k\psi} k_{22,22}^{\psi} + \hat{A}_{57}^{k\psi} k_{12,22}^{\psi} + \hat{A}_{58}^{k\psi} k_{21,22}^{\psi} + \\
+ \hat{A}_{51}^{kw} w_{,12}^{(0)} + \hat{A}_{52}^{kw} w_{,12}^{(1)} + \hat{A}_{53}^{kw} w_{,12}^{(2)} + \hat{A}_{54}^{kw} w_{,22}^{(0)} + \hat{A}_{55}^{kw} w_{,22}^{(1)} + \hat{A}_{56}^{kw} w_{,22}^{(2)} + \\
+ \hat{A}_{21}^{q} \overline{p}_{3(B),11} + \hat{A}_{22}^{q} \overline{p}_{3(T),11} + \hat{A}_{23}^{q} \overline{p}_{3(B),12} + \hat{A}_{24}^{q} \overline{p}_{3(T),12} + \hat{A}_{51}^{q} \overline{p}_{3(B),12} + \hat{A}_{52}^{q} \overline{p}_{3(T),12} + \hat{A}_{53}^{q} \overline{p}_{3(B),22} + \hat{A}_{54}^{q} \overline{p}_{3(T),22}
\end{array} \right)
\end{aligned}
\tag{C.5}
$$

$$
\begin{aligned}
E_{12}^{HR} = {} & \hat{A}_{31}^{w} w_{,11}^{(0)} + \hat{A}_{32}^{w} w_{,11}^{(1)} + \hat{A}_{33}^{w} w_{,11}^{(2)} + \hat{A}_{34}^{w} w_{,12}^{(0)} + \hat{A}_{35}^{w} w_{,12}^{(1)} + \hat{A}_{36}^{w} w_{,12}^{(2)} + \hat{A}_{31}^{\theta} \theta_{1,1} + \hat{A}_{32}^{\theta} \theta_{2,1} + \hat{A}_{31}^{\psi} \psi_{1,1} + \hat{A}_{32}^{\psi} \psi_{2,1} + \\
& + \hat{A}_{61}^{w} w_{,12}^{(0)} + \hat{A}_{62}^{w} w_{,12}^{(1)} + \hat{A}_{63}^{w} w_{,12}^{(2)} + \hat{A}_{64}^{w} w_{,22}^{(0)} + \hat{A}_{65}^{w} w_{,22}^{(1)} + \hat{A}_{66}^{w} w_{,22}^{(2)} + \hat{A}_{61}^{\theta} \theta_{1,2} + \hat{A}_{62}^{\theta} \theta_{2,2} + \hat{A}_{61}^{\psi} \psi_{1,2} + \hat{A}_{62}^{\psi} \psi_{2,2} + \\
& \left(\begin{array}{l}
\hat{A}_{31}^{p} \overline{p}_{1(B),1} + \hat{A}_{32}^{p} \overline{p}_{2(B),1} + \hat{A}_{33}^{p} \overline{p}_{1(T),1} + \hat{A}_{34}^{p} \overline{p}_{2(T),1} + \hat{A}_{31}^{e} e_{11,11} + \hat{A}_{32}^{e} e_{22,11} + \hat{A}_{33}^{e} e_{12,11} + \hat{A}_{34}^{e} e_{11,12} + \hat{A}_{35}^{e} e_{22,12} + \hat{A}_{36}^{e} e_{12,12} + \\
+ \hat{A}_{31}^{k} k_{11,11} + \hat{A}_{32}^{k} k_{22,11} + \hat{A}_{33}^{k} k_{12,11} + \hat{A}_{34}^{k} k_{11,12} + \hat{A}_{35}^{k} k_{22,12} + \hat{A}_{36}^{k} k_{12,12} + \\
+ \hat{A}_{31}^{k\psi} k_{11,11}^{\psi} + \hat{A}_{32}^{k\psi} k_{22,11}^{\psi} + \hat{A}_{33}^{k\psi} k_{12,11}^{\psi} + \hat{A}_{34}^{k\psi} k_{21,11}^{\psi} + \hat{A}_{35}^{k\psi} k_{11,12}^{\psi} + \hat{A}_{36}^{k\psi} k_{22,12}^{\psi} + \hat{A}_{37}^{k\psi} k_{12,12}^{\psi} + \hat{A}_{38}^{k\psi} k_{21,12}^{\psi} + \\
+ \hat{A}_{31}^{kw} w_{,11}^{(0)} + \hat{A}_{32}^{kw} w_{,11}^{(1)} + \hat{A}_{33}^{kw} w_{,11}^{(2)} + \hat{A}_{34}^{kw} w_{,12}^{(0)} + \hat{A}_{35}^{kw} w_{,12}^{(1)} + \hat{A}_{36}^{kw} w_{,12}^{(2)} + \\
- \hat{A}_{61}^{p} \overline{p}_{1(B),2} + \hat{A}_{62}^{p} \overline{p}_{2(B),2} + \hat{A}_{63}^{p} \overline{p}_{1(T),2} + \hat{A}_{64}^{p} \overline{p}_{2(T),2} + \hat{A}_{61}^{e} e_{11,12} + \hat{A}_{62}^{e} e_{22,12} + \hat{A}_{63}^{e} e_{12,12} + \hat{A}_{64}^{e} e_{11,22} + \hat{A}_{65}^{e} e_{22,22} + \hat{A}_{66}^{e} e_{12,22} + \\
+ \hat{A}_{61}^{k} k_{11,12} + \hat{A}_{62}^{k} k_{22,12} + \hat{A}_{63}^{k} k_{12,12} + \hat{A}_{64}^{k} k_{11,22} + \hat{A}_{65}^{k} k_{22,22} + \hat{A}_{66}^{k} k_{12,22} + \\
+ \hat{A}_{61}^{k\psi} k_{11,12}^{\psi} + \hat{A}_{62}^{k\psi} k_{22,12}^{\psi} + \hat{A}_{63}^{k\psi} k_{12,12}^{\psi} + \hat{A}_{64}^{k\psi} k_{21,12}^{\psi} + \hat{A}_{65}^{k\psi} k_{11,22}^{\psi} + \hat{A}_{66}^{k\psi} k_{22,22}^{\psi} + \hat{A}_{67}^{k\psi} k_{12,22}^{\psi} + \hat{A}_{68}^{k\psi} k_{21,22}^{\psi} + \\
+ \hat{A}_{61}^{kw} w_{,12}^{(0)} + \hat{A}_{62}^{kw} w_{,12}^{(1)} + \hat{A}_{63}^{kw} w_{,12}^{(2)} + \hat{A}_{64}^{kw} w_{,22}^{(0)} + \hat{A}_{65}^{kw} w_{,22}^{(1)} + \hat{A}_{66}^{kw} w_{,22}^{(2)} + \\
+ \hat{A}_{31}^{q} \overline{p}_{3(B),11} + \hat{A}_{32}^{q} \overline{p}_{3(T),11} + \hat{A}_{33}^{q} \overline{p}_{3(B),12} + \hat{A}_{34}^{q} \overline{p}_{3(T),12} + \hat{A}_{61}^{q} \overline{p}_{3(B),12} + \hat{A}_{62}^{q} \overline{p}_{3(T),12} + \hat{A}_{63}^{q} \overline{p}_{3(B),22} + \hat{A}_{64}^{q} \overline{p}_{3(T),22}
\end{array} \right)
\end{aligned}
\tag{C.6}
$$

$$
\begin{aligned}
K_{11}^{HR} = {} & \hat{B}_{11}^{w} w_{,11}^{(0)} + \hat{B}_{12}^{w} w_{,11}^{(1)} + \hat{B}_{13}^{w} w_{,11}^{(2)} + \hat{B}_{14}^{w} w_{,12}^{(0)} + \hat{B}_{15}^{w} w_{,12}^{(1)} + \hat{B}_{16}^{w} w_{,12}^{(2)} + \hat{B}_{11}^{\theta} \theta_{1,1} + \hat{B}_{12}^{\theta} \theta_{2,1} + \hat{B}_{11}^{\psi} \psi_{1,1} + \hat{B}_{12}^{\psi} \psi_{2,1} + \\
& + \hat{B}_{41}^{w} w_{,12}^{(0)} + \hat{B}_{42}^{w} w_{,12}^{(1)} + \hat{B}_{43}^{w} w_{,12}^{(2)} + \hat{B}_{44}^{w} w_{,22}^{(0)} + \hat{B}_{45}^{w} w_{,22}^{(1)} + \hat{B}_{46}^{w} w_{,22}^{(2)} + \hat{B}_{41}^{\theta} \theta_{1,2} + \hat{B}_{42}^{\theta} \theta_{2,2} + \hat{B}_{41}^{\psi} \psi_{1,2} + \hat{B}_{42}^{\psi} \psi_{2,2} + \\
& \left(\begin{array}{l}
\hat{B}_{11}^{p} \overline{p}_{1(B),1} + \hat{B}_{12}^{p} \overline{p}_{2(B),1} + \hat{B}_{13}^{p} \overline{p}_{1(T),1} + \hat{B}_{14}^{p} \overline{p}_{2(T),1} + \hat{A}_{11}^{k} e_{11,11} + \hat{A}_{21}^{k} e_{22,11} + \hat{A}_{31}^{k} e_{12,11} + \hat{A}_{41}^{k} e_{11,12} + \hat{A}_{51}^{k} e_{22,12} + \hat{A}_{61}^{k} e_{12,12} + \\
+ \hat{B}_{11}^{k} k_{11,11} + \hat{B}_{12}^{k} k_{22,11} + \hat{B}_{13}^{k} k_{12,11} + \hat{B}_{14}^{k} k_{11,12} + \hat{B}_{15}^{k} k_{22,12} + \hat{B}_{16}^{k} k_{12,12} + \\
+ \hat{B}_{11}^{k\psi} k_{11,11}^{\psi} + \hat{B}_{12}^{k\psi} k_{22,11}^{\psi} + \hat{B}_{13}^{k\psi} k_{12,11}^{\psi} + \hat{B}_{14}^{k\psi} k_{21,11}^{\psi} + \hat{B}_{15}^{k\psi} k_{11,12}^{\psi} + \hat{B}_{16}^{k\psi} k_{22,12}^{\psi} + \hat{B}_{17}^{k\psi} k_{12,12}^{\psi} + \hat{B}_{18}^{k\psi} k_{21,12}^{\psi} + \\
+ \hat{B}_{11}^{kw} w_{,11}^{(0)} + \hat{B}_{12}^{kw} w_{,11}^{(1)} + \hat{B}_{13}^{kw} w_{,11}^{(2)} + \hat{B}_{14}^{kw} w_{,12}^{(0)} + \hat{B}_{15}^{kw} w_{,12}^{(1)} + \hat{B}_{16}^{kw} w_{,12}^{(2)} + \\
- \hat{B}_{41}^{p} \overline{p}_{1(B),2} + \hat{B}_{42}^{p} \overline{p}_{2(B),2} + \hat{B}_{43}^{p} \overline{p}_{1(T),2} + \hat{B}_{44}^{p} \overline{p}_{2(T),2} + \hat{A}_{14}^{k} e_{11,12} + \hat{A}_{24}^{k} e_{22,12} + \hat{A}_{34}^{k} e_{12,12} + \hat{A}_{44}^{k} e_{11,22} + \hat{A}_{54}^{k} e_{22,22} + \hat{A}_{64}^{k} e_{12,22} + \\
+ \hat{B}_{41}^{k} k_{11,12} + \hat{B}_{42}^{k} k_{22,12} + \hat{B}_{43}^{k} k_{12,12} + \hat{B}_{44}^{k} k_{11,22} + \hat{B}_{45}^{k} k_{22,22} + \hat{B}_{46}^{k} k_{12,22} + \\
+ \hat{B}_{41}^{k\psi} k_{11,12}^{\psi} + \hat{B}_{42}^{k\psi} k_{22,12}^{\psi} + \hat{B}_{43}^{k\psi} k_{12,12}^{\psi} + \hat{B}_{44}^{k\psi} k_{21,12}^{\psi} + \hat{B}_{45}^{k\psi} k_{11,22}^{\psi} + \hat{B}_{46}^{k\psi} k_{22,22}^{\psi} + \hat{B}_{47}^{k\psi} k_{12,22}^{\psi} + \hat{B}_{48}^{k\psi} k_{21,22}^{\psi} + \\
+ \hat{B}_{41}^{kw} w_{,12}^{(0)} + \hat{B}_{42}^{kw} w_{,12}^{(1)} + \hat{B}_{43}^{kw} w_{,12}^{(2)} + \hat{B}_{44}^{kw} w_{,22}^{(0)} + \hat{B}_{45}^{kw} w_{,22}^{(1)} + \hat{B}_{46}^{kw} w_{,22}^{(2)} + \\
+ \hat{B}_{11}^{q} \overline{p}_{3(B),11} + \hat{B}_{12}^{q} \overline{p}_{3(T),11} + \hat{B}_{13}^{q} \overline{p}_{3(B),12} + \hat{B}_{14}^{q} \overline{p}_{3(T),12} + \hat{B}_{41}^{q} \overline{p}_{3(B),12} + \hat{B}_{42}^{q} \overline{p}_{3(T),12} + \hat{B}_{43}^{q} \overline{p}_{3(B),22} + \hat{B}_{44}^{q} \overline{p}_{3(T),22}
\end{array} \right)
\end{aligned}
\tag{C.7}
$$

$$
\begin{aligned}
K_{22}^{HR} = {} & \hat{B}_{21}^{w} w_{,11}^{(0)} + \hat{B}_{22}^{w} w_{,11}^{(1)} + \hat{B}_{23}^{w} w_{,11}^{(2)} + \hat{B}_{24}^{w} w_{,12}^{(0)} + \hat{B}_{25}^{w} w_{,12}^{(1)} + \hat{B}_{26}^{w} w_{,12}^{(2)} + \hat{B}_{21}^{\theta} \theta_{,1} + \hat{B}_{22}^{\theta} \theta_{2,1} + \hat{B}_{21}^{\psi} \psi_{1,1} + \hat{B}_{22}^{\psi} \psi_{2,1} + \\
& + \hat{B}_{51}^{w} w_{,12}^{(0)} + \hat{B}_{52}^{w} w_{,12}^{(1)} + \hat{B}_{53}^{w} w_{,12}^{(2)} + \hat{B}_{54}^{w} w_{,22}^{(0)} + \hat{B}_{55}^{w} w_{,22}^{(1)} + \hat{B}_{56}^{w} w_{,22}^{(2)} + \hat{B}_{51}^{\theta} \theta_{1,2} + \hat{B}_{52}^{\theta} \theta_{2,2} + \hat{B}_{51}^{\psi} \psi_{1,2} + \hat{B}_{52}^{\psi} \psi_{2,2} + \\
& \left(\begin{array}{l}
\hat{B}_{21}^{p} \overline{p}_{1(B),1} + \hat{B}_{22}^{p} \overline{p}_{2(B),1} + \hat{B}_{23}^{p} \overline{p}_{1(T),1} + \hat{B}_{24}^{p} \overline{p}_{2(T),1} + \hat{A}_{12}^{k} e_{11,11} + \hat{A}_{22}^{k} e_{22,11} + \hat{A}_{32}^{k} e_{12,11} + \hat{A}_{42}^{k} e_{11,12} + \hat{A}_{52}^{k} e_{22,12} + \hat{A}_{62}^{k} e_{12,12} + \\
+ \hat{B}_{21}^{k} k_{11,11} + \hat{B}_{22}^{k} k_{22,11} + \hat{B}_{23}^{k} k_{12,11} + \hat{B}_{24}^{k} k_{11,12} + \hat{B}_{25}^{k} k_{22,12} + \hat{B}_{26}^{k} k_{12,12} + \\
+ \hat{B}_{21}^{k\psi} k_{11,11}^{\psi} + \hat{B}_{22}^{k\psi} k_{22,11}^{\psi} + \hat{B}_{23}^{k\psi} k_{12,11}^{\psi} + \hat{B}_{24}^{k\psi} k_{21,11}^{\psi} + \hat{B}_{25}^{k\psi} k_{11,12}^{\psi} + \hat{B}_{26}^{k\psi} k_{22,12}^{\psi} + \hat{B}_{27}^{k\psi} k_{12,12}^{\psi} + \hat{B}_{28}^{k\psi} k_{21,12}^{\psi} + \\
+ \hat{B}_{21}^{kw} w_{,11}^{(0)} + \hat{B}_{22}^{kw} w_{,11}^{(1)} + \hat{B}_{23}^{kw} w_{,11}^{(2)} + \hat{B}_{24}^{kw} w_{,12}^{(0)} + \hat{B}_{25}^{kw} w_{,12}^{(1)} + \hat{B}_{26}^{kw} w_{,12}^{(2)} + \\
- \hat{B}_{51}^{p} \overline{p}_{1(B),2} + \hat{B}_{52}^{p} \overline{p}_{2(B),2} + \hat{B}_{53}^{p} \overline{p}_{1(T),2} + \hat{B}_{54}^{p} \overline{p}_{2(T),2} + \hat{A}_{15}^{k} e_{11,12} + \hat{A}_{25}^{k} e_{22,12} + \hat{A}_{35}^{k} e_{12,12} + \hat{A}_{45}^{k} e_{11,22} + \hat{A}_{55}^{k} e_{22,22} + \hat{A}_{65}^{k} e_{12,22} + \\
+ \hat{B}_{51}^{k} k_{11,12} + \hat{B}_{52}^{k} k_{22,12} + \hat{B}_{53}^{k} k_{12,12} + \hat{B}_{54}^{k} k_{11,22} + \hat{B}_{55}^{k} k_{22,22} + \hat{B}_{56}^{k} k_{12,22} + \\
+ \hat{B}_{51}^{k\psi} k_{11,12}^{\psi} + \hat{B}_{52}^{k\psi} k_{22,12}^{\psi} + \hat{B}_{53}^{k\psi} k_{12,12}^{\psi} + \hat{B}_{54}^{k\psi} k_{21,12}^{\psi} + \hat{B}_{55}^{k\psi} k_{11,22}^{\psi} + \hat{B}_{56}^{k\psi} k_{22,22}^{\psi} + \hat{B}_{57}^{k\psi} k_{12,22}^{\psi} + \hat{B}_{58}^{k\psi} k_{21,22}^{\psi} + \\
+ \hat{B}_{51}^{kw} w_{,12}^{(0)} + \hat{B}_{52}^{kw} w_{,12}^{(1)} + \hat{B}_{53}^{kw} w_{,12}^{(2)} + \hat{B}_{54}^{kw} w_{,22}^{(0)} + \hat{B}_{55}^{kw} w_{,22}^{(1)} + \hat{B}_{56}^{kw} w_{,22}^{(2)} + \\
+ \hat{B}_{21}^{q} \overline{p}_{3(B),11} + \hat{B}_{22}^{q} \overline{p}_{3(T),11} + \hat{B}_{23}^{q} \overline{p}_{3(B),12} + \hat{B}_{24}^{q} \overline{p}_{3(T),12} + \hat{B}_{51}^{q} \overline{p}_{3(B),12} + \hat{B}_{52}^{q} \overline{p}_{3(T),12} + \hat{B}_{53}^{q} \overline{p}_{3(B),22} + \hat{B}_{54}^{q} \overline{p}_{3(T),22}
\end{array} \right) \qquad \text{(C.8)}
\end{aligned}
$$

$$
\begin{aligned}
K_{12}^{HR} = {} & \hat{B}_{31}^{w} w_{,11}^{(0)} + \hat{B}_{32}^{w} w_{,11}^{(1)} + \hat{B}_{33}^{w} w_{,11}^{(2)} + \hat{B}_{34}^{w} w_{,12}^{(0)} + \hat{B}_{35}^{w} w_{,12}^{(1)} + \hat{B}_{36}^{w} w_{,12}^{(2)} + \hat{B}_{31}^{\theta} \theta_{,1} + \hat{B}_{32}^{\theta} \theta_{2,1} + \hat{B}_{31}^{\psi} \psi_{1,1} + \hat{B}_{32}^{\psi} \psi_{2,1} + \\
& + \hat{B}_{61}^{w} w_{,12}^{(0)} + \hat{B}_{62}^{w} w_{,12}^{(1)} + \hat{B}_{63}^{w} w_{,12}^{(2)} + \hat{B}_{64}^{w} w_{,22}^{(0)} + \hat{B}_{65}^{w} w_{,22}^{(1)} + \hat{B}_{66}^{w} w_{,22}^{(2)} + \hat{B}_{61}^{\theta} \theta_{,2} + \hat{B}_{62}^{\theta} \theta_{2,2} + \hat{B}_{61}^{\psi} \psi_{1,2} + \hat{B}_{62}^{\psi} \psi_{2,2} + \\
& \left(\begin{array}{l}
\hat{B}_{31}^{p} \overline{p}_{1(B),1} + \hat{B}_{32}^{p} \overline{p}_{2(B),1} + \hat{B}_{33}^{p} \overline{p}_{1(T),1} + \hat{B}_{34}^{p} \overline{p}_{2(T),1} + \hat{A}_{13}^{k} e_{11,11} + \hat{A}_{23}^{k} e_{22,11} + \hat{A}_{33}^{k} e_{12,11} + \hat{A}_{43}^{k} e_{11,12} + \hat{A}_{53}^{k} e_{22,12} + \hat{A}_{63}^{k} e_{12,12} + \\
+ \hat{B}_{31}^{k} k_{11,11} + \hat{B}_{32}^{k} k_{22,11} + \hat{B}_{33}^{k} k_{12,11} + \hat{B}_{34}^{k} k_{11,12} + \hat{B}_{35}^{k} k_{22,12} + \hat{B}_{36}^{k} k_{12,12} + \\
+ \hat{B}_{31}^{k\psi} k_{11,11}^{\psi} + \hat{B}_{32}^{k\psi} k_{22,11}^{\psi} + \hat{B}_{33}^{k\psi} k_{12,11}^{\psi} + \hat{B}_{34}^{k\psi} k_{21,11}^{\psi} + \hat{B}_{35}^{k\psi} k_{11,12}^{\psi} + \hat{B}_{36}^{k\psi} k_{22,12}^{\psi} + \hat{B}_{37}^{k\psi} k_{12,12}^{\psi} + \hat{B}_{38}^{k\psi} k_{21,12}^{\psi} + \\
+ \hat{B}_{31}^{kw} w_{,11}^{(0)} + \hat{B}_{32}^{kw} w_{,11}^{(1)} + \hat{B}_{33}^{kw} w_{,11}^{(2)} + \hat{B}_{34}^{kw} w_{,12}^{(0)} + \hat{B}_{35}^{kw} w_{,12}^{(1)} + \hat{B}_{36}^{kw} w_{,12}^{(2)} + \\
- \hat{B}_{61}^{p} \overline{p}_{1(B),2} + \hat{B}_{62}^{p} \overline{p}_{2(B),2} + \hat{B}_{63}^{p} \overline{p}_{1(T),2} + \hat{B}_{64}^{p} \overline{p}_{2(T),2} + \hat{A}_{16}^{k} e_{11,12} + \hat{A}_{26}^{k} e_{22,12} + \hat{A}_{36}^{k} e_{12,12} + \hat{A}_{46}^{k} e_{11,22} + \hat{A}_{56}^{k} e_{22,22} + \hat{A}_{66}^{k} e_{12,22} + \\
+ \hat{B}_{61}^{k} k_{11,12} + \hat{B}_{62}^{k} k_{22,12} + \hat{B}_{63}^{k} k_{12,12} + \hat{B}_{64}^{k} k_{11,22} + \hat{B}_{65}^{k} k_{22,22} + \hat{B}_{66}^{k} k_{12,22} + \\
+ \hat{B}_{61}^{k\psi} k_{11,12}^{\psi} + \hat{B}_{62}^{k\psi} k_{22,12}^{\psi} + \hat{B}_{63}^{k\psi} k_{12,12}^{\psi} + \hat{B}_{64}^{k\psi} k_{21,12}^{\psi} + \hat{B}_{65}^{k\psi} k_{11,22}^{\psi} + \hat{B}_{66}^{k\psi} k_{22,22}^{\psi} + \hat{B}_{67}^{k\psi} k_{12,22}^{\psi} + \hat{B}_{68}^{k\psi} k_{21,22}^{\psi} + \\
+ \hat{B}_{61}^{kw} w_{,12}^{(0)} + \hat{B}_{62}^{kw} w_{,12}^{(1)} + \hat{B}_{63}^{kw} w_{,12}^{(2)} + \hat{B}_{64}^{kw} w_{,22}^{(0)} + \hat{B}_{65}^{kw} w_{,22}^{(1)} + \hat{B}_{66}^{kw} w_{,22}^{(2)} + \\
+ \hat{B}_{31}^{q} \overline{p}_{3(B),11} + \hat{B}_{32}^{q} \overline{p}_{3(T),11} + \hat{B}_{33}^{q} \overline{p}_{3(B),12} + \hat{B}_{34}^{q} \overline{p}_{3(T),12} + \hat{B}_{61}^{q} \overline{p}_{3(B),12} + \hat{B}_{62}^{q} \overline{p}_{3(T),12} + \hat{B}_{63}^{q} \overline{p}_{3(B),22} + \hat{B}_{64}^{q} \overline{p}_{3(T),22}
\end{array} \right) \qquad \text{(C.9)}
\end{aligned}
$$

$$
\begin{aligned}
K_{\psi 11}^{HR} = {} & \hat{C}_{11}^{w} w_{,11}^{(0)} + \hat{C}_{12}^{w} w_{,11}^{(1)} + \hat{C}_{13}^{w} w_{,11}^{(2)} + \hat{C}_{14}^{w} w_{,12}^{(0)} + \hat{C}_{15}^{w} w_{,12}^{(1)} + \hat{C}_{16}^{w} w_{,12}^{(2)} + \hat{C}_{11}^{\theta} \theta_{,1} + \hat{C}_{12}^{\theta} \theta_{2,1} + \hat{C}_{11}^{\psi} \psi_{1,1} + \hat{C}_{12}^{\psi} \psi_{2,1} + \\
& + \hat{C}_{51}^{w} w_{,12}^{(0)} + \hat{C}_{52}^{w} w_{,12}^{(1)} + \hat{C}_{53}^{w} w_{,12}^{(2)} + \hat{C}_{54}^{w} w_{,22}^{(0)} + \hat{C}_{55}^{w} w_{,22}^{(1)} + \hat{C}_{56}^{w} w_{,22}^{(2)} + \hat{C}_{51}^{\theta} \theta_{1,2} + \hat{C}_{52}^{\theta} \theta_{2,2} + \hat{C}_{51}^{\psi} \psi_{1,2} + \hat{C}_{52}^{\psi} \psi_{2,2} + \\
& \left(\begin{array}{l}
\hat{C}_{11}^{p} \overline{p}_{1(B),1} + \hat{C}_{12}^{p} \overline{p}_{2(B),1} + \hat{C}_{13}^{p} \overline{p}_{1(T),1} + \hat{C}_{14}^{p} \overline{p}_{2(T),1} + \hat{A}_{11}^{k\psi} e_{11,11} + \hat{A}_{21}^{k\psi} e_{22,11} + \hat{A}_{31}^{k\psi} e_{12,11} + \hat{A}_{41}^{k\psi} e_{11,12} + \hat{A}_{51}^{k\psi} e_{22,12} + \hat{A}_{61}^{k\psi} e_{12,12} + \\
+ \hat{B}_{11}^{k\psi} k_{11,11} + \hat{B}_{21}^{k\psi} k_{22,11} + \hat{B}_{31}^{k\psi} k_{12,11} + \hat{B}_{41}^{k\psi} k_{11,12} + \hat{B}_{51}^{k\psi} k_{22,12} + \hat{B}_{61}^{k\psi} k_{12,12} + \\
+ \hat{C}_{11}^{k\psi} k_{11,11}^{\psi} + \hat{C}_{12}^{k\psi} k_{22,11}^{\psi} + \hat{C}_{13}^{k\psi} k_{12,11}^{\psi} + \hat{C}_{14}^{k\psi} k_{21,11}^{\psi} + \hat{C}_{15}^{k\psi} k_{11,12}^{\psi} + \hat{C}_{16}^{k\psi} k_{22,12}^{\psi} + \hat{C}_{17}^{k\psi} k_{12,12}^{\psi} + \hat{C}_{18}^{k\psi} k_{21,12}^{\psi} + \\
+ \hat{C}_{11}^{kw} w_{,11}^{(0)} + \hat{C}_{12}^{kw} w_{,11}^{(1)} + \hat{C}_{13}^{kw} w_{,11}^{(2)} + \hat{C}_{14}^{kw} w_{,12}^{(0)} + \hat{C}_{15}^{kw} w_{,12}^{(1)} + \hat{C}_{16}^{kw} w_{,12}^{(2)} + \\
- \hat{C}_{51}^{p} \overline{p}_{1(B),2} + \hat{C}_{52}^{p} \overline{p}_{2(B),2} + \hat{C}_{53}^{p} \overline{p}_{1(T),2} + \hat{C}_{54}^{p} \overline{p}_{2(T),2} + \hat{A}_{15}^{k\psi} e_{11,12} + \hat{A}_{25}^{k\psi} e_{22,12} + \hat{A}_{35}^{k\psi} e_{12,12} + \hat{A}_{45}^{k\psi} e_{11,22} + \hat{A}_{55}^{k\psi} e_{22,22} + \hat{A}_{65}^{k\psi} e_{12,22} + \\
+ \hat{B}_{15}^{k\psi} k_{11,12} + \hat{B}_{25}^{k\psi} k_{22,12} + \hat{B}_{35}^{k\psi} k_{12,12} + \hat{B}_{45}^{k\psi} k_{11,22} + \hat{B}_{55}^{k\psi} k_{22,22} + \hat{B}_{65}^{k\psi} k_{12,22} + \\
+ \hat{C}_{51}^{k\psi} k_{11,12}^{\psi} + \hat{C}_{52}^{k\psi} k_{22,12}^{\psi} + \hat{C}_{53}^{k\psi} k_{12,12}^{\psi} + \hat{C}_{54}^{k\psi} k_{21,12}^{\psi} + \hat{C}_{55}^{k\psi} k_{11,22}^{\psi} + \hat{C}_{56}^{k\psi} k_{22,22}^{\psi} + \hat{C}_{57}^{k\psi} k_{12,22}^{\psi} + \hat{C}_{58}^{k\psi} k_{21,22}^{\psi} + \\
+ \hat{C}_{51}^{kw} w_{,12}^{(0)} + \hat{C}_{52}^{kw} w_{,12}^{(1)} + \hat{C}_{53}^{kw} w_{,12}^{(2)} + \hat{C}_{54}^{kw} w_{,22}^{(0)} + \hat{C}_{55}^{kw} w_{,22}^{(1)} + \hat{C}_{56}^{kw} w_{,22}^{(2)} + \\
+ \hat{C}_{11}^{q} \overline{p}_{3(B),11} + \hat{C}_{12}^{q} \overline{p}_{3(T),11} + \hat{C}_{13}^{q} \overline{p}_{3(B),12} + \hat{C}_{14}^{q} \overline{p}_{3(T),12} + \hat{C}_{51}^{q} \overline{p}_{3(B),12} + \hat{C}_{52}^{q} \overline{p}_{3(T),12} + \hat{C}_{53}^{q} \overline{p}_{3(B),22} + \hat{C}_{54}^{q} \overline{p}_{3(T),22}
\end{array} \right) \qquad \text{(C.10)}
\end{aligned}
$$

$$
\begin{aligned}
K_{\psi 22}^{HR} = {} & \hat{C}_{21}^{w} w_{,11}^{(0)} + \hat{C}_{22}^{w} w_{,11}^{(1)} + \hat{C}_{23}^{w} w_{,11}^{(2)} + \hat{C}_{24}^{w} w_{,12}^{(0)} + \hat{C}_{25}^{w} w_{,12}^{(1)} + \hat{C}_{26}^{w} w_{,12}^{(2)} + \hat{C}_{21}^{\theta} \theta_{1,1} + \hat{C}_{22}^{\theta} \theta_{2,1} + \hat{C}_{21}^{\psi} \psi_{1,1} + \hat{C}_{22}^{\psi} \psi_{2,1} + \\
& + \hat{C}_{61}^{w} w_{,12}^{(0)} + \hat{C}_{62}^{w} w_{,12}^{(1)} + \hat{C}_{63}^{w} w_{,12}^{(2)} + \hat{C}_{64}^{w} w_{,22}^{(0)} + \hat{C}_{65}^{w} w_{,22}^{(1)} + \hat{C}_{66}^{w} w_{,22}^{(2)} + \hat{C}_{61}^{\theta} \theta_{1,2} + \hat{C}_{62}^{\theta} \theta_{2,2} + \hat{C}_{61}^{\psi} \psi_{1,2} + \hat{C}_{62}^{\psi} \psi_{2,2} + \\
& \left(\begin{array}{l}
\hat{C}_{21}^{p} \overline{p}_{1(B),1} + \hat{C}_{22}^{p} \overline{p}_{2(B),1} + \hat{C}_{23}^{p} \overline{p}_{1(T),1} + \hat{C}_{24}^{p} \overline{p}_{2(T),1} + \hat{A}_{12}^{k\psi} e_{11,11} + \hat{A}_{22}^{k\psi} e_{22,11} + \hat{A}_{32}^{k\psi} e_{12,11} + \hat{A}_{42}^{k\psi} e_{11,12} + \hat{A}_{52}^{k\psi} e_{22,12} + \hat{A}_{62}^{k\psi} e_{12,12} + \\
+ \hat{B}_{12}^{k\psi} k_{11,11} + \hat{B}_{22}^{k\psi} k_{22,11} + \hat{B}_{32}^{k\psi} k_{12,11} + \hat{B}_{42}^{k\psi} k_{11,12} + \hat{B}_{52}^{k\psi} k_{22,12} + \hat{B}_{62}^{k\psi} k_{12,12} + \\
+ \hat{C}_{21}^{k\psi} k_{11,11}^{\psi} + \hat{C}_{22}^{k\psi} k_{22,11}^{\psi} + \hat{C}_{23}^{k\psi} k_{12,11}^{\psi} + \hat{C}_{24}^{k\psi} k_{21,11}^{\psi} + \hat{C}_{25}^{k\psi} k_{11,12}^{\psi} + \hat{C}_{26}^{k\psi} k_{22,12}^{\psi} + \hat{C}_{27}^{k\psi} k_{12,12}^{\psi} + \hat{C}_{28}^{k\psi} k_{21,12}^{\psi} + \\
+ \hat{C}_{21}^{kw} w_{,11}^{(0)} + \hat{C}_{22}^{kw} w_{,11}^{(1)} + \hat{C}_{23}^{kw} w_{,11}^{(2)} + \hat{C}_{24}^{kw} w_{,12}^{(0)} + \hat{C}_{25}^{kw} w_{,12}^{(1)} + \hat{C}_{26}^{kw} w_{,12}^{(2)} + \\
- \hat{C}_{61}^{p} \overline{p}_{1(B),2} + \hat{C}_{62}^{p} \overline{p}_{2(B),2} + \hat{C}_{63}^{p} \overline{p}_{1(T),2} + \hat{C}_{64}^{p} \overline{p}_{2(T),2} + \hat{A}_{16}^{k\psi} e_{11,12} + \hat{A}_{26}^{k\psi} e_{22,12} + \hat{A}_{36}^{k\psi} e_{12,12} + \hat{A}_{46}^{k\psi} e_{11,22} + \hat{A}_{56}^{k\psi} e_{22,22} + \hat{A}_{66}^{k\psi} e_{12,22} + \\
+ \hat{B}_{16}^{k\psi} k_{11,12} + \hat{B}_{26}^{k\psi} k_{22,12} + \hat{B}_{36}^{k\psi} k_{12,12} + \hat{B}_{46}^{k\psi} k_{11,22} + \hat{B}_{56}^{k\psi} k_{22,22} + \hat{B}_{66}^{k\psi} k_{12,22} + \\
+ \hat{C}_{61}^{k\psi} k_{11,12}^{\psi} + \hat{C}_{62}^{k\psi} k_{22,12}^{\psi} + \hat{C}_{63}^{k\psi} k_{12,12}^{\psi} + \hat{C}_{64}^{k\psi} k_{21,12}^{\psi} + \hat{C}_{65}^{k\psi} k_{11,22}^{\psi} + \hat{C}_{66}^{k\psi} k_{22,22}^{\psi} + \hat{C}_{67}^{k\psi} k_{12,22}^{\psi} + \hat{C}_{68}^{k\psi} k_{21,22}^{\psi} + \\
+ \hat{C}_{61}^{kw} w_{,12}^{(0)} + \hat{C}_{62}^{kw} w_{,12}^{(1)} + \hat{C}_{63}^{kw} w_{,12}^{(2)} + \hat{C}_{64}^{kw} w_{,22}^{(0)} + \hat{C}_{65}^{kw} w_{,22}^{(1)} + \hat{C}_{66}^{kw} w_{,22}^{(2)} + \\
+ \hat{C}_{21}^{q} \overline{p}_{3(B),11} + \hat{C}_{22}^{q} \overline{p}_{3(T),11} + \hat{C}_{23}^{q} \overline{p}_{3(B),12} + \hat{C}_{24}^{q} \overline{p}_{3(T),12} + \hat{C}_{61}^{q} \overline{p}_{3(B),12} + \hat{C}_{62}^{q} \overline{p}_{3(T),12} + \hat{C}_{63}^{q} \overline{p}_{3(B),22} + \hat{C}_{64}^{q} \overline{p}_{3(T),22}
\end{array} \right)
\end{aligned}
\tag{C.11}
$$

$$
\begin{aligned}
K_{\psi 12}^{HR} = {} & \hat{C}_{31}^{w} w_{,11}^{(0)} + \hat{C}_{32}^{w} w_{,11}^{(1)} + \hat{C}_{33}^{w} w_{,11}^{(2)} + \hat{C}_{34}^{w} w_{,12}^{(0)} + \hat{C}_{35}^{w} w_{,12}^{(1)} + \hat{C}_{36}^{w} w_{,12}^{(2)} + \hat{C}_{31}^{\theta} \theta_{1,1} + \hat{C}_{32}^{\theta} \theta_{2,1} + \hat{C}_{31}^{\psi} \psi_{1,1} + \hat{C}_{32}^{\psi} \psi_{2,1} + \\
& + \hat{C}_{71}^{w} w_{,12}^{(0)} + \hat{C}_{72}^{w} w_{,12}^{(1)} + \hat{C}_{73}^{w} w_{,12}^{(2)} + \hat{C}_{74}^{w} w_{,22}^{(0)} + \hat{C}_{75}^{w} w_{,22}^{(1)} + \hat{C}_{76}^{w} w_{,22}^{(2)} + \hat{C}_{71}^{\theta} \theta_{1,2} + \hat{C}_{72}^{\theta} \theta_{2,2} + \hat{C}_{71}^{\psi} \psi_{1,2} + \hat{C}_{72}^{\psi} \psi_{2,2} + \\
& \left(\begin{array}{l}
\hat{C}_{31}^{p} \overline{p}_{1(B),1} + \hat{C}_{32}^{p} \overline{p}_{2(B),1} + \hat{C}_{33}^{p} \overline{p}_{1(T),1} + \hat{C}_{34}^{p} \overline{p}_{2(T),1} + \hat{A}_{13}^{k\psi} e_{11,11} + \hat{A}_{23}^{k\psi} e_{22,11} + \hat{A}_{33}^{k\psi} e_{12,11} + \hat{A}_{43}^{k\psi} e_{11,12} + \hat{A}_{53}^{k\psi} e_{22,12} + \hat{A}_{63}^{k\psi} e_{12,12} + \\
+ \hat{B}_{13}^{k\psi} k_{11,11} + \hat{B}_{23}^{k\psi} k_{22,11} + \hat{B}_{33}^{k\psi} k_{12,11} + \hat{B}_{43}^{k\psi} k_{11,12} + \hat{B}_{53}^{k\psi} k_{22,12} + \hat{B}_{63}^{k\psi} k_{12,12} + \\
+ \hat{C}_{31}^{k\psi} k_{11,11}^{\psi} + \hat{C}_{32}^{k\psi} k_{22,11}^{\psi} + \hat{C}_{33}^{k\psi} k_{12,11}^{\psi} + \hat{C}_{34}^{k\psi} k_{21,11}^{\psi} + \hat{C}_{35}^{k\psi} k_{11,12}^{\psi} + \hat{C}_{36}^{k\psi} k_{22,12}^{\psi} + \hat{C}_{37}^{k\psi} k_{12,12}^{\psi} + \hat{C}_{38}^{k\psi} k_{21,12}^{\psi} + \\
+ \hat{C}_{31}^{kw} w_{,11}^{(0)} + \hat{C}_{32}^{kw} w_{,11}^{(1)} + \hat{C}_{33}^{kw} w_{,11}^{(2)} + \hat{C}_{34}^{kw} w_{,12}^{(0)} + \hat{C}_{35}^{kw} w_{,12}^{(1)} + \hat{C}_{36}^{kw} w_{,12}^{(2)} + \\
- \hat{C}_{71}^{p} \overline{p}_{1(B),2} + \hat{C}_{72}^{p} \overline{p}_{2(B),2} + \hat{C}_{73}^{p} \overline{p}_{1(T),2} + \hat{C}_{74}^{p} \overline{p}_{2(T),2} + \hat{A}_{17}^{k\psi} e_{11,12} + \hat{A}_{27}^{k\psi} e_{22,12} + \hat{A}_{37}^{k\psi} e_{12,12} + \hat{A}_{47}^{k\psi} e_{11,22} + \hat{A}_{57}^{k\psi} e_{22,22} + \hat{A}_{67}^{k\psi} e_{12,22} + \\
+ \hat{B}_{17}^{k\psi} k_{11,12} + \hat{B}_{27}^{k\psi} k_{22,12} + \hat{B}_{37}^{k\psi} k_{12,12} + \hat{B}_{47}^{k\psi} k_{11,22} + \hat{B}_{57}^{k\psi} k_{22,22} + \hat{B}_{67}^{k\psi} k_{12,22} + \\
+ \hat{C}_{71}^{k\psi} k_{11,12}^{\psi} + \hat{C}_{72}^{k\psi} k_{22,12}^{\psi} + \hat{C}_{73}^{k\psi} k_{12,12}^{\psi} + \hat{C}_{74}^{k\psi} k_{21,12}^{\psi} + \hat{C}_{75}^{k\psi} k_{11,22}^{\psi} + \hat{C}_{76}^{k\psi} k_{22,22}^{\psi} + \hat{C}_{77}^{k\psi} k_{12,22}^{\psi} + \hat{C}_{78}^{k\psi} k_{21,22}^{\psi} + \\
+ \hat{C}_{71}^{kw} w_{,12}^{(0)} + \hat{C}_{72}^{kw} w_{,12}^{(1)} + \hat{C}_{73}^{kw} w_{,12}^{(2)} + \hat{C}_{74}^{kw} w_{,22}^{(0)} + \hat{C}_{75}^{kw} w_{,22}^{(1)} + \hat{C}_{76}^{kw} w_{,22}^{(2)} + \\
\hat{C}_{31}^{q} \overline{p}_{3(B),11} + \hat{C}_{32}^{q} \overline{p}_{3(T),11} + \hat{C}_{33}^{q} \overline{p}_{3(B),12} + \hat{C}_{34}^{q} \overline{p}_{3(T),12} + \hat{C}_{71}^{q} \overline{p}_{3(B),12} + \hat{C}_{72}^{q} \overline{p}_{3(T),12} + \hat{C}_{73}^{q} \overline{p}_{3(B),22} + \hat{C}_{74}^{q} \overline{p}_{3(T),22}
\end{array} \right)
\end{aligned}
\tag{C.12}
$$

$$
\begin{aligned}
K_{\psi 21}^{HR} = {} & \hat{C}_{41}^{w} w_{,11}^{(0)} + \hat{C}_{42}^{w} w_{,11}^{(1)} + \hat{C}_{43}^{w} w_{,11}^{(2)} + \hat{C}_{44}^{w} w_{,12}^{(0)} + \hat{C}_{45}^{w} w_{,12}^{(1)} + \hat{C}_{46}^{w} w_{,12}^{(2)} + \hat{C}_{41}^{\theta} \theta_{1,1} + \hat{C}_{42}^{\theta} \theta_{2,1} + \hat{C}_{41}^{\psi} \psi_{1,1} + \hat{C}_{42}^{\psi} \psi_{2,1} + \\
& + \hat{C}_{81}^{w} w_{,12}^{(0)} + \hat{C}_{82}^{w} w_{,12}^{(1)} + \hat{C}_{83}^{w} w_{,12}^{(2)} + \hat{C}_{84}^{w} w_{,22}^{(0)} + \hat{C}_{85}^{w} w_{,22}^{(1)} + \hat{C}_{86}^{w} w_{,22}^{(2)} + \hat{C}_{81}^{\theta} \theta_{1,2} + \hat{C}_{82}^{\theta} \theta_{2,2} + \hat{C}_{81}^{\psi} \psi_{1,2} + \hat{C}_{82}^{\psi} \psi_{2,2} + \\
& \left(\begin{array}{l}
\hat{C}_{41}^{p} \overline{p}_{1(B),1} + \hat{C}_{42}^{p} \overline{p}_{2(B),1} + \hat{C}_{43}^{p} \overline{p}_{1(T),1} + \hat{C}_{44}^{p} \overline{p}_{2(T),1} + \hat{A}_{14}^{k\psi} e_{11,11} + \hat{A}_{24}^{k\psi} e_{22,11} + \hat{A}_{34}^{k\psi} e_{12,11} + \hat{A}_{44}^{k\psi} e_{11,12} + \hat{A}_{54}^{k\psi} e_{22,12} + \hat{A}_{64}^{k\psi} e_{12,12} + \\
+ \hat{B}_{14}^{k\psi} k_{11,11} + \hat{B}_{24}^{k\psi} k_{22,11} + \hat{B}_{34}^{k\psi} k_{12,11} + \hat{B}_{44}^{k\psi} k_{11,12} + \hat{B}_{54}^{k\psi} k_{22,12} + \hat{B}_{64}^{k\psi} k_{12,12} + \\
+ \hat{C}_{41}^{k\psi} k_{11,11}^{\psi} + \hat{C}_{42}^{k\psi} k_{22,11}^{\psi} + \hat{C}_{43}^{k\psi} k_{12,11}^{\psi} + \hat{C}_{44}^{k\psi} k_{21,11}^{\psi} + \hat{C}_{45}^{k\psi} k_{11,12}^{\psi} + \hat{C}_{46}^{k\psi} k_{22,12}^{\psi} + \hat{C}_{47}^{k\psi} k_{12,12}^{\psi} + \hat{C}_{48}^{k\psi} k_{21,12}^{\psi} + \\
+ \hat{C}_{41}^{kw} w_{,11}^{(0)} + \hat{C}_{42}^{kw} w_{,11}^{(1)} + \hat{C}_{43}^{kw} w_{,11}^{(2)} + \hat{C}_{44}^{kw} w_{,12}^{(0)} + \hat{C}_{45}^{kw} w_{,12}^{(1)} + \hat{C}_{46}^{kw} w_{,12}^{(2)} + \\
- \hat{C}_{81}^{p} \overline{p}_{1(B),2} + \hat{C}_{82}^{p} \overline{p}_{2(B),2} + \hat{C}_{83}^{p} \overline{p}_{1(T),2} + \hat{C}_{84}^{p} \overline{p}_{2(T),2} + \hat{A}_{18}^{k\psi} e_{11,12} + \hat{A}_{28}^{k\psi} e_{22,12} + \hat{A}_{38}^{k\psi} e_{12,12} + \hat{A}_{48}^{k\psi} e_{11,22} + \hat{A}_{58}^{k\psi} e_{22,22} + \hat{A}_{68}^{k\psi} e_{12,22} + \\
+ \hat{B}_{18}^{k\psi} k_{11,12} + \hat{B}_{28}^{k\psi} k_{22,12} + \hat{B}_{38}^{k\psi} k_{12,12} + \hat{B}_{48}^{k\psi} k_{11,22} + \hat{B}_{58}^{k\psi} k_{22,22} + \hat{B}_{68}^{k\psi} k_{12,22} + \\
+ \hat{C}_{81}^{k\psi} k_{11,12}^{\psi} + \hat{C}_{82}^{k\psi} k_{22,12}^{\psi} + \hat{C}_{83}^{k\psi} k_{12,12}^{\psi} + \hat{C}_{84}^{k\psi} k_{21,12}^{\psi} + \hat{C}_{85}^{k\psi} k_{11,22}^{\psi} + \hat{C}_{86}^{k\psi} k_{22,22}^{\psi} + \hat{C}_{87}^{k\psi} k_{12,22}^{\psi} + \hat{C}_{88}^{k\psi} k_{21,22}^{\psi} + \\
+ \hat{C}_{81}^{kw} w_{,12}^{(0)} + \hat{C}_{82}^{kw} w_{,12}^{(1)} + \hat{C}_{83}^{kw} w_{,12}^{(2)} + \hat{C}_{84}^{kw} w_{,22}^{(0)} + \hat{C}_{85}^{kw} w_{,22}^{(1)} + \hat{C}_{86}^{kw} w_{,22}^{(2)} + \\
+ \hat{C}_{41}^{q} \overline{p}_{3(B),11} + \hat{C}_{42}^{q} \overline{p}_{3(T),11} + \hat{C}_{43}^{q} \overline{p}_{3(B),12} + \hat{C}_{44}^{q} \overline{p}_{3(T),12} + \hat{C}_{81}^{q} \overline{p}_{3(B),12} + \hat{C}_{82}^{q} \overline{p}_{3(T),12} + \hat{C}_{83}^{q} \overline{p}_{3(B),22} + \hat{C}_{84}^{q} \overline{p}_{3(T),22}
\end{array} \right)
\end{aligned}
\tag{C.13}
$$

Furthermore, the terms shown in the boundary condition expression, i.e. Eq. (3.76), can read:

$$
\begin{aligned}
{}^{HR}\overline{\mathbf{E}} &= \hat{\mathbf{A}}^{w} \partial \mathbf{w} + \hat{\mathbf{A}}^{\theta} \boldsymbol{\theta} + \hat{\mathbf{A}}^{\psi} \boldsymbol{\psi} - \left(\hat{\mathbf{A}}^{p} \overline{\mathbf{p}} + \hat{\mathbf{A}}^{e} \partial \mathbf{e} + \hat{\mathbf{A}}^{k} \partial \mathbf{k} + \hat{\mathbf{A}}^{k\psi} \partial \mathbf{k}^{\psi} + \hat{\mathbf{A}}^{kw} \partial \mathbf{w} + \hat{\mathbf{A}}^{q} \partial \overline{\mathbf{q}}_{z} \right) \\
{}^{HR}\overline{\mathbf{K}} &= \hat{\mathbf{B}}^{w} \partial \mathbf{w} + \hat{\mathbf{B}}^{\theta} \boldsymbol{\theta} + \hat{\mathbf{B}}^{\psi} \boldsymbol{\psi} - \left(\hat{\mathbf{B}}^{p} \overline{\mathbf{p}} + \hat{\mathbf{A}}^{kT} \partial \mathbf{e} + \hat{\mathbf{B}}^{k} \partial \mathbf{k} + \hat{\mathbf{B}}^{k\psi} \partial \mathbf{k}^{\psi} + \hat{\mathbf{B}}^{kw} \partial \mathbf{w} + \hat{\mathbf{B}}^{q} \partial \overline{\mathbf{q}}_{z} \right) \\
{}^{HR}\overline{\mathbf{K}}^{\psi} &= \hat{\mathbf{C}}^{w} \partial \mathbf{w} + \hat{\mathbf{C}}^{\theta} \boldsymbol{\theta} + \hat{\mathbf{C}}^{\psi} \boldsymbol{\psi} - \left(\hat{\mathbf{C}}^{p} \overline{\mathbf{p}} + \hat{\mathbf{A}}^{k\psi T} \partial \mathbf{e} + \hat{\mathbf{B}}^{k\psi T} \partial \mathbf{k} + \hat{\mathbf{C}}^{k\psi} \partial \mathbf{k}^{\psi} + \hat{\mathbf{C}}^{kw} \partial \mathbf{w} + \hat{\mathbf{C}}^{q} \partial \overline{\mathbf{q}}_{z} \right) \\
{}^{HR}\overline{\mathbf{Q}} &= \hat{\mathbf{D}}^{w} \partial \mathbf{w} + \hat{\mathbf{D}}^{\theta} \boldsymbol{\theta} + \hat{\mathbf{D}}^{\psi} \boldsymbol{\psi} - \left(\hat{\mathbf{D}}^{p} \overline{\mathbf{p}} + \hat{\mathbf{A}}^{kwT} \partial \mathbf{e} + \hat{\mathbf{B}}^{kwT} \partial \mathbf{k} + \hat{\mathbf{C}}^{kwT} \partial \mathbf{k}^{\psi} + \hat{\mathbf{D}}^{kw} \partial \mathbf{w} + \hat{\mathbf{D}}^{q} \partial \overline{\mathbf{q}}_{z} \right)
\end{aligned}
\tag{C.14}
$$

where

$$
\begin{aligned}
{}^{HR}\overline{\mathbf{E}}^{T} &= \left[{}^{HR}\overline{E}_1^{e11} \quad {}^{HR}\overline{E}_1^{e22} \quad {}^{HR}\overline{E}_1^{e12} \quad {}^{HR}\overline{E}_2^{e11} \quad {}^{HR}\overline{E}_2^{e22} \quad {}^{HR}\overline{E}_2^{e12} \right]; \\
{}^{HR}\overline{\mathbf{K}}^{T} &= \left[{}^{HR}\overline{K}_1^{k11} \quad {}^{HR}\overline{K}_1^{k22} \quad {}^{HR}\overline{K}_1^{k12} \quad {}^{HR}\overline{K}_2^{k11} \quad {}^{HR}\overline{K}_2^{k22} \quad {}^{HR}\overline{K}_2^{k12} \right]; \\
{}^{HR}\overline{\mathbf{K}}^{\psi T} &= \left[{}^{HR}\overline{K}_1^{k11\psi} \quad {}^{HR}\overline{K}_1^{k22\psi} \quad {}^{HR}\overline{K}_1^{k12\psi} \quad {}^{HR}\overline{K}_1^{k21\psi} \quad {}^{HR}\overline{K}_2^{k11\psi} \quad {}^{HR}\overline{K}_2^{k22\psi} \quad {}^{HR}\overline{K}_2^{k12\psi} \quad {}^{HR}\overline{K}_2^{k21\psi} \right]; \\
{}^{HR}\overline{\mathbf{Q}}^{T} &= \left[{}^{HR}\overline{Q}_1^{w0} \quad {}^{HR}\overline{Q}_1^{w1} \quad {}^{HR}\overline{Q}_1^{w2} \quad {}^{HR}\overline{Q}_2^{w0} \quad {}^{HR}\overline{Q}_2^{w1} \quad {}^{HR}\overline{Q}_2^{w2} \right]
\end{aligned}
\tag{C.15}
$$

Appendix D

Matrix definitions of the en-RZT$^{(m)}_{\{3,2\}}$ constitutive relations

In this appendix are resumed the matrices definitions of the constitutive relations for resultants of forces and moments:

$$
\begin{aligned}
&\tilde{\mathbf{A}} = \left\langle \breve{\mathbf{C}}_p^{(k)} + \mathbf{R}^{(k)T}\mathbf{A}_{\boldsymbol{\sigma}}^{u} \right\rangle; \quad \tilde{\mathbf{B}} = \left\langle x_3\breve{\mathbf{C}}_p^{(k)} + \mathbf{R}^{(k)T}\mathbf{A}_{\boldsymbol{\sigma}}^{\boldsymbol{\theta}} \right\rangle; \quad \tilde{\mathbf{A}}^{\boldsymbol{\phi}} = \left\langle \breve{\mathbf{C}}_p^{(k)}\mathbf{M}^{(k)} + \mathbf{R}^{(k)T}\mathbf{A}_{\boldsymbol{\sigma}}^{\boldsymbol{\psi}} \right\rangle; \\
&\tilde{\mathbf{A}}^{w} = \left\langle \mathbf{R}^{(k)T}\mathbf{A}_{\boldsymbol{\sigma}}^{w} \right\rangle; \quad \tilde{\mathbf{A}}^{qz} = \left\langle \mathbf{R}^{(k)T}\mathbf{A}_{\boldsymbol{\sigma}}^{q_z} \right\rangle; \\
&\tilde{\mathbf{C}} = \left\langle x_3\breve{\mathbf{C}}_p^{(k)} + x_3\mathbf{R}^{(k)T}\mathbf{A}_{\boldsymbol{\sigma}}^{u} \right\rangle; \quad \tilde{\mathbf{D}} = \left\langle x_3^{\,2}\breve{\mathbf{C}}_p^{(k)} + x_3\mathbf{R}^{(k)T}\mathbf{A}_{\boldsymbol{\sigma}}^{\boldsymbol{\theta}} \right\rangle; \quad \tilde{\mathbf{B}}^{\boldsymbol{\phi}} = \left\langle x_3\breve{\mathbf{C}}_p^{(k)}\mathbf{M}^{(k)} + x_3\mathbf{R}^{(k)T}\mathbf{A}_{\boldsymbol{\sigma}}^{\boldsymbol{\psi}} \right\rangle; \\
&\tilde{\mathbf{B}}^{w} = \left\langle x_3\mathbf{R}^{(k)T}\mathbf{A}_{\boldsymbol{\sigma}}^{w} \right\rangle; \quad \tilde{\mathbf{B}}^{qz} = \left\langle x_3\mathbf{R}^{(k)T}\mathbf{A}_{\boldsymbol{\sigma}}^{q_z} \right\rangle; \\
&\tilde{\mathbf{E}}^{\boldsymbol{\phi}} = \left\langle \mathbf{M}^{(k)T}\breve{\mathbf{C}}_p^{(k)} + \mathbf{M}^{(k)T}\mathbf{R}^{(k)T}\mathbf{A}_{\boldsymbol{\sigma}}^{u} \right\rangle; \quad \tilde{\mathbf{F}}^{\boldsymbol{\phi}} = \left\langle x_3\mathbf{M}^{(k)T}\breve{\mathbf{C}}_p^{(k)} + \mathbf{M}^{(k)T}\mathbf{R}^{(k)T}\mathbf{A}_{\boldsymbol{\sigma}}^{\boldsymbol{\theta}} \right\rangle; \\
&\tilde{\mathbf{G}}^{\boldsymbol{\phi}} = \left\langle \mathbf{M}^{(k)T}\breve{\mathbf{C}}_p^{(k)}\mathbf{M}^{(k)} + \mathbf{M}^{(k)T}\mathbf{R}^{(k)T}\mathbf{A}_{\boldsymbol{\sigma}}^{\boldsymbol{\psi}} \right\rangle; \\
&\tilde{\mathbf{C}}^{w} = \left\langle \mathbf{M}^{(k)T}\mathbf{R}^{(k)T}\mathbf{A}_{\boldsymbol{\sigma}}^{w} \right\rangle; \quad \tilde{\mathbf{C}}^{qz} = \left\langle \mathbf{M}^{(k)T}\mathbf{R}^{(k)T}\mathbf{A}_{\boldsymbol{\sigma}}^{q_z} \right\rangle \\
&\mathbf{A}^{Nz} = \left\langle \mathbf{H}_{,3}^{z\,T}\mathbf{A}_{\boldsymbol{\sigma}}^{u} \right\rangle; \quad \mathbf{B}^{Nz} = \left\langle \mathbf{H}_{,3}^{z\,T}\mathbf{A}_{\boldsymbol{\sigma}}^{\boldsymbol{\theta}} \right\rangle; \quad \mathbf{C}^{Nz} = \left\langle \mathbf{H}_{,3}^{z\,T}\mathbf{A}_{\boldsymbol{\sigma}}^{\boldsymbol{\psi}} \right\rangle; \quad \mathbf{D}^{Nz} = \left\langle \mathbf{H}_{,3}^{z\,T}\mathbf{A}_{\boldsymbol{\sigma}}^{w} \right\rangle; \quad \mathbf{E}^{Nz} = \left\langle \mathbf{H}_{,3}^{z\,T}\mathbf{A}_{\boldsymbol{\sigma}}^{q_z} \right\rangle
\end{aligned}
\tag{D.1}
$$

From the HR statement related to the transverse shear strain compatibility, the constitutive matrices have the following expressions:

$$
\begin{aligned}
&\hat{\mathbf{A}}^{w}=\left\langle \widehat{\mathbf{A}}^{zT}\mathbf{H}^{z}\right\rangle;\quad \hat{\mathbf{A}}^{\theta}=\left\langle \widehat{\mathbf{A}}^{zT}\right\rangle;\quad \hat{\mathbf{A}}^{\psi}=\left\langle \widehat{\mathbf{A}}^{zT}\partial_{z}\boldsymbol{\mu}^{(k)}\right\rangle;\quad \hat{\mathbf{A}}^{p}=\left\langle \widehat{\mathbf{A}}^{zT}\mathbf{S}_{t}^{(k)}\mathbf{Z}_{p}\right\rangle;\quad \hat{\mathbf{A}}^{e}=\left\langle \widehat{\mathbf{A}}^{zT}\mathbf{S}_{t}^{(k)}\widehat{\mathbf{A}}^{z}\right\rangle;\\
&\hat{\mathbf{A}}^{k}=\left\langle \widehat{\mathbf{A}}^{zT}\mathbf{S}_{t}^{(k)}\widehat{\mathbf{B}}^{z}\right\rangle;\quad \hat{\mathbf{A}}^{k\psi}=\left\langle \widehat{\mathbf{A}}^{zT}\mathbf{S}_{t}^{(k)}\widehat{\mathbf{D}}^{z}\right\rangle;\quad \hat{\mathbf{A}}^{kw}=\left\langle \widehat{\mathbf{A}}^{zT}\mathbf{S}_{t}^{(k)}\widehat{\mathbf{E}}^{z}\right\rangle;\quad \hat{\mathbf{A}}^{q}=\left\langle \widehat{\mathbf{A}}^{zT}\mathbf{S}_{t}^{(k)}\widehat{\mathbf{F}}^{z}\right\rangle;\\
&\hat{\mathbf{B}}^{w}=\left\langle \widehat{\mathbf{B}}^{zT}\mathbf{H}^{z}\right\rangle;\quad \hat{\mathbf{B}}^{\theta}=\left\langle \widehat{\mathbf{B}}^{zT}\right\rangle;\quad \hat{\mathbf{B}}^{\psi}=\left\langle \widehat{\mathbf{B}}^{zT}\partial_{3}\boldsymbol{\mu}^{(k)}\right\rangle;\quad \hat{\mathbf{B}}^{p}=\left\langle \widehat{\mathbf{B}}^{zT}\mathbf{S}_{t}^{(k)}\mathbf{Z}_{p}\right\rangle;\quad \hat{\mathbf{B}}^{e}=\hat{\mathbf{A}}^{kT}=\left\langle \widehat{\mathbf{B}}^{zT}\mathbf{S}_{t}^{(k)}\widehat{\mathbf{A}}^{z}\right\rangle;\\
&\hat{\mathbf{B}}^{k}=\left\langle \widehat{\mathbf{B}}^{zT}\mathbf{S}_{t}^{(k)}\widehat{\mathbf{B}}^{z}\right\rangle;\quad \hat{\mathbf{B}}^{k\psi}=\left\langle \widehat{\mathbf{B}}^{zT}\mathbf{S}_{t}^{(k)}\widehat{\mathbf{D}}^{z}\right\rangle;\quad \hat{\mathbf{B}}^{kw}=\left\langle \widehat{\mathbf{B}}^{zT}\mathbf{S}_{t}^{(k)}\widehat{\mathbf{E}}^{z}\right\rangle;\quad \hat{\mathbf{B}}^{q}=\left\langle \widehat{\mathbf{B}}^{zT}\mathbf{S}_{t}^{(k)}\widehat{\mathbf{F}}^{z}\right\rangle;\\
&\hat{\mathbf{C}}^{w}=\left\langle \widehat{\mathbf{D}}^{zT}\mathbf{H}^{z}\right\rangle;\quad \hat{\mathbf{C}}^{\theta}=\left\langle \widehat{\mathbf{D}}^{zT}\right\rangle;\quad \hat{\mathbf{C}}^{\psi}=\left\langle \widehat{\mathbf{D}}^{zT}\partial_{3}\boldsymbol{\mu}^{(k)}\right\rangle;\quad \hat{\mathbf{C}}^{p}=\left\langle \widehat{\mathbf{D}}^{zT}\mathbf{S}_{t}^{(k)}\mathbf{Z}_{p}\right\rangle;\quad \hat{\mathbf{C}}^{e}=\hat{\mathbf{A}}^{k\psi T}=\left\langle \widehat{\mathbf{D}}^{zT}\mathbf{S}_{t}^{(k)}\widehat{\mathbf{A}}^{z}\right\rangle;\\
&\hat{\mathbf{C}}^{k}=\hat{\mathbf{B}}^{k\psi T}=\left\langle \widehat{\mathbf{D}}^{zT}\mathbf{S}_{t}^{(k)}\widehat{\mathbf{B}}^{z}\right\rangle;\quad \hat{\mathbf{C}}^{k\psi}=\left\langle \widehat{\mathbf{D}}^{zT}\mathbf{S}_{t}^{(k)}\widehat{\mathbf{D}}^{z}\right\rangle;\quad \hat{\mathbf{C}}^{kw}=\left\langle \widehat{\mathbf{D}}^{zT}\mathbf{S}_{t}^{(k)}\widehat{\mathbf{E}}^{z}\right\rangle;\quad \hat{\mathbf{C}}^{q}=\left\langle \widehat{\mathbf{D}}^{zT}\mathbf{S}_{t}^{(k)}\widehat{\mathbf{F}}^{z}\right\rangle;\\
&\hat{\mathbf{D}}^{w}=\left\langle \widehat{\mathbf{E}}^{zT}\mathbf{H}^{z}\right\rangle;\quad \hat{\mathbf{D}}^{\theta}=\left\langle \widehat{\mathbf{E}}^{zT}\right\rangle;\quad \hat{\mathbf{D}}^{\psi}=\left\langle \widehat{\mathbf{E}}^{zT}\partial_{3}\boldsymbol{\mu}^{(k)}\right\rangle;\quad \hat{\mathbf{D}}^{p}=\left\langle \widehat{\mathbf{E}}^{zT}\mathbf{S}_{t}^{(k)}\mathbf{Z}_{p}\right\rangle;\quad \hat{\mathbf{D}}^{e}=\hat{\mathbf{A}}^{kwT}=\left\langle \widehat{\mathbf{E}}^{zT}\mathbf{S}_{t}^{(k)}\widehat{\mathbf{A}}^{z}\right\rangle;\\
&\hat{\mathbf{D}}^{k}=\hat{\mathbf{B}}^{kwT}=\left\langle \widehat{\mathbf{E}}^{zT}\mathbf{S}_{t}^{(k)}\widehat{\mathbf{B}}^{z}\right\rangle;\quad \hat{\mathbf{D}}^{k\psi}=\hat{\mathbf{C}}^{kwT}=\left\langle \widehat{\mathbf{E}}^{zT}\mathbf{S}_{t}^{(k)}\widehat{\mathbf{D}}^{z}\right\rangle;\quad \hat{\mathbf{D}}^{kw}=\left\langle \widehat{\mathbf{E}}^{zT}\mathbf{S}_{t}^{(k)}\widehat{\mathbf{E}}^{z}\right\rangle;\quad \hat{\mathbf{D}}^{q}=\left\langle \widehat{\mathbf{E}}^{zT}\mathbf{S}_{t}^{(k)}\widehat{\mathbf{F}}^{z}\right\rangle;\\
&\hat{\mathbf{E}}^{w}=\left\langle \mathbf{H}^{zT}\widehat{\mathbf{F}}^{z}\right\rangle;\quad \hat{\mathbf{E}}^{\theta}=\left\langle \widehat{\mathbf{F}}^{z}\right\rangle;\quad \hat{\mathbf{E}}^{\psi}=\left\langle \partial_{3}\boldsymbol{\mu}^{(k)T}\widehat{\mathbf{F}}^{z}\right\rangle;
\end{aligned}
\tag{D.2}
$$

Appendix E

Full expressions and constitutive relations B-RZT$^{(m)}_{\{3,2\}}$

In this appendix are reported the full expressions of the quantities involved in the governing equations and boundary conditions:

$$\begin{aligned}\widehat{Q}^{w0} = &-\left(\hat{D}^{w}_{11}w^{(0)}_{,11} + \hat{D}^{w}_{12}w^{(1)}_{,11} + \hat{D}^{w}_{13}w^{(2)}_{,11} + \hat{D}^{\theta}_{11}\theta_{,1} + \hat{D}^{\psi}_{11}\psi_{,1}\right) + \\ &+\hat{A}^{kw}_{11}e_{,11} + \hat{B}^{kw}_{11}k_{,11} + \hat{C}^{kw}_{11}k^{\psi}_{,11} + \hat{D}^{kw}_{11}w^{(0)}_{,11} + \hat{D}^{kw}_{12}w^{(1)}_{,11} + \hat{D}^{kw}_{13}w^{(2)}_{,11}\end{aligned} \tag{E.1}$$

$$\begin{aligned}\widehat{Q}^{w1} = &-\left(\hat{D}^{w}_{11}w^{(0)}_{,11} + \hat{D}^{w}_{12}w^{(1)}_{,11} + \hat{D}^{w}_{13}w^{(2)}_{,11} + \hat{D}^{\theta}_{21}\theta_{,1} + \hat{D}^{\psi}_{21}\psi_{,1}\right) + \\ &+\hat{A}^{kw}_{12}e_{,11} + \hat{B}^{kw}_{12}k_{,11} + \hat{C}^{kw}_{12}k^{\psi}_{,11} + \hat{D}^{kw}_{21}w^{(0)}_{,11} + \hat{D}^{kw}_{22}w^{(1)}_{,11} + \hat{D}^{kw}_{23}w^{(2)}_{,11}\end{aligned} \tag{E.2}$$

$$\begin{aligned}\widehat{Q}^{w2} = &-\left(\hat{D}^{w}_{31}w^{(0)}_{,11} + \hat{D}^{w}_{32}w^{(1)}_{,11} + \hat{D}^{w}_{33}w^{(2)}_{,11} + \hat{D}^{\theta}_{31}\theta_{,1} + \hat{D}^{\psi}_{31}\psi_{,1}\right) \\ &+\hat{A}^{kw}_{13}e_{,11} + \hat{B}^{kw}_{13}k_{,11} + \hat{C}^{kw}_{13}k^{\psi}_{,11} + \hat{D}^{kw}_{31}w^{(0)}_{,11} + \hat{D}^{kw}_{32}w^{(1)}_{,11} + \hat{D}^{kw}_{33}w^{(2)}_{,11}\end{aligned} \tag{E.3}$$

$$\begin{aligned}E^{HR} = &\hat{A}^{w}_{11}w^{(0)}_{,11} + \hat{A}^{w}_{12}w^{(1)}_{,11} + \hat{A}^{w}_{13}w^{(2)}_{,11} + \hat{A}^{\theta}_{11}\theta_{,1} + \hat{A}^{\psi}_{11}\psi_{,1} + \\ &-\left(\begin{array}{l}\hat{A}^{p}_{11}\overline{p}_{1(B),1} + \hat{A}^{p}_{13}\overline{p}_{1(T),1} + \hat{A}^{e}_{11}e_{,11} + \hat{A}^{k}_{11}k_{,11} + \hat{A}^{k\psi}_{11}k^{\psi}_{,11} + \\ +\hat{A}^{kw}_{11}w^{(0)}_{,11} + \hat{A}^{kw}_{12}w^{(1)}_{,11} + \hat{A}^{kw}_{13}w^{(2)}_{,11} + \hat{A}^{q}_{11}\overline{p}_{3(B),11} + \hat{A}^{q}_{12}\overline{p}_{3(T),11}\end{array}\right)\end{aligned} \tag{E.4}$$

$$
\begin{aligned}
K^{HR} = {} & \hat{B}^{w}_{11} w^{(0)}_{,11} + \hat{B}^{w}_{12} w^{(1)}_{,11} + \hat{B}^{w}_{13} w^{(2)}_{,11} + \hat{B}^{\theta}_{11} \theta_{,1} + \hat{B}^{\psi}_{11} \psi_{,1} + \\
& - \begin{pmatrix} \hat{B}^{p}_{11} \overline{p}_{1(B),1} + \hat{B}^{p}_{13} \overline{p}_{1(T),1} + \hat{A}^{k}_{11} e_{,11} + \hat{B}^{k}_{11} k_{,11} + \hat{B}^{k\psi}_{11} k^{\psi}_{,11} \\ + \hat{B}^{kw}_{11} w^{(0)}_{,11} + \hat{B}^{kw}_{12} w^{(1)}_{,11} + \hat{B}^{kw}_{13} w^{(2)}_{,11} + \hat{B}^{q}_{11} \overline{p}_{3(B),11} + \hat{B}^{q}_{12} \overline{p}_{3(T),11} \end{pmatrix}
\end{aligned}
\tag{E.5}
$$

$$
\begin{aligned}
K^{HR}_{\psi} = {} & \hat{C}^{w}_{11} w^{(0)}_{,11} + \hat{C}^{w}_{12} w^{(1)}_{,11} + \hat{C}^{w}_{13} w^{(2)}_{,11} + \hat{C}^{\theta}_{11} \theta_{,1} + \hat{C}^{\psi}_{11} \psi_{,1} + \\
& - \begin{pmatrix} \hat{C}^{p}_{11} \overline{p}_{1(B),1} + \hat{C}^{p}_{13} \overline{p}_{1(T),1} + \hat{A}^{k\psi}_{11} e_{,11} + \hat{B}^{k\psi}_{11} k_{,11} + \hat{C}^{k\psi}_{11} k^{\psi}_{,11} + \\ + \hat{C}^{kw}_{11} w^{(0)}_{,11} + \hat{C}^{kw}_{12} w^{(1)}_{,11} + \hat{C}^{kw}_{13} w^{(2)}_{,11} + \hat{C}^{q}_{11} \overline{p}_{3(B),11} + \hat{C}^{q}_{12} \overline{p}_{3(T),11} \end{pmatrix}
\end{aligned}
\tag{E.6}
$$

Furthermore, the terms shown in the boundary condition expression, i.e. Eq. (4.37), can read:

$$
\begin{aligned}
{}^{HR}\overline{E}^{e} = {} & \hat{\mathbf{A}}^{w} \partial \mathbf{w} + \hat{A}^{\theta} \theta + \hat{A}^{\psi} \psi + \\
& - \left(\hat{\mathbf{A}}^{p} \overline{\mathbf{p}} + \hat{A}^{e} e_{,1} + \hat{A}^{k} k_{,1} + \hat{\mathbf{A}}^{k\psi} k^{\psi}_{,1} + \hat{\mathbf{A}}^{kw} \partial \mathbf{w} + \hat{\mathbf{A}}^{q} \partial \overline{\mathbf{q}}_{z} \right) \\
{}^{HR}\overline{K}^{k} = {} & \hat{\mathbf{B}}^{w} \partial \mathbf{w} + \hat{B}^{\theta} \theta + \hat{B}^{\psi} \psi + \\
& - \left(\hat{\mathbf{B}}^{p} \overline{\mathbf{p}} + \hat{B}^{e} e_{,1} + \hat{B}^{k} k_{,1} + \hat{B}^{k\psi} k^{\psi}_{,1} + \hat{\mathbf{B}}^{kw} \partial \mathbf{w} + \hat{\mathbf{B}}^{q} \partial \overline{\mathbf{q}}_{z} \right) \\
{}^{HR}\overline{K}^{k\psi} = {} & \hat{\mathbf{C}}^{w} \partial \mathbf{w} + \hat{C}^{\theta} \theta_{1} + \hat{C}^{\psi} \psi_{1} + \\
& - \left(\hat{\mathbf{C}}^{p} \overline{\mathbf{p}} + \hat{C}^{e} e_{,1} + \hat{C}^{k} k_{,1} + \hat{C}^{k\psi} k^{\psi}_{,1} + \hat{\mathbf{C}}^{kw} \partial \mathbf{w} + \hat{\mathbf{C}}^{q} \partial \overline{\mathbf{q}}_{z} \right) \\
{}^{HR}\overline{\mathbf{Q}} = {} & \left\lfloor {}^{HR}\overline{Q}^{w0}_{1} \quad {}^{HR}\overline{Q}^{w1}_{1} \quad {}^{HR}\overline{Q}^{w2}_{1} \right\rfloor = \\
& = \hat{\mathbf{D}}^{w} \partial \mathbf{w} + \hat{\mathbf{D}}^{\theta} \theta + \hat{\mathbf{D}}^{\psi} \psi + \\
& - \left(\hat{\mathbf{D}}^{p} \overline{\mathbf{p}} + \hat{\mathbf{A}}^{kwT} e_{,1} + \hat{\mathbf{B}}^{kwT} \partial \mathbf{k} + \hat{\mathbf{C}}^{kwT} \partial \mathbf{k}^{\psi} + \hat{\mathbf{D}}^{kw} \partial \mathbf{w} + \hat{\mathbf{D}}^{q} \partial \overline{\mathbf{q}}_{z} \right)
\end{aligned}
\tag{E.7}
$$